

Texte

52
04

ISSN
0722-186X

Manual on methodologies and criteria for Modelling and Mapping Critical Loads & Levels and Air Pollution Effects, Risks and Trends

**Umwelt
Bundes
Amt** 

Für Mensch und Umwelt



**Manual on methodologies
and criteria for Modelling
and Mapping Critical
Loads & Levels and Air
Pollution Effects, Risks
and Trends**

On behalf of the Federal Environmental Agency

This Publication is also available as Download under
<http://www.umweltbundesamt.de>

The publisher does not accept responsibility for the correctness, accuracy or completeness of the information, or for the observance of the private rights of third parties. The contents of this publication do not necessarily reflect the official opinions.

Publisher: Federal Environmental Agency (Umweltbundesamt)
Postfach 33 00 22
14191 Berlin
Tel.: +49/30/8903-0
Telex: 183 756
Telefax: +49/30/8903 2285
Internet: <http://www.umweltbundesamt.de>

Edited by: Section II 4.4
Dr. Till Spranger (Chairman ICP Modelling & Mapping)
Ullrich Lorenz
Dr. Heinz-Detlef Gregor (Head of Section)

Layout: Dr. Hans-Dieter Nagel
Öko-Data GmbH, Strausberg

Berlin, December 2004

This Manual is the basic guideline for modelling and mapping critical levels and loads and their exceedances, and for dynamic modelling of acidification. It helps Parties to the UNECE Convention on Long-range Transboundary Air Pollution (CLRTAP) to fulfil their obligations to use harmonized methods to derive data for effects and risk assessments. This happens in the framework of the International Cooperative Programme on Modelling and Mapping Critical Loads&Levels and Air Pollution Effects, Risks and Trends (ICP M&M). This programme was established in 1988 under the leadership of Germany; it was chaired from the beginning until 2002 by Heinz Gregor who strongly influenced the development of critical levels and loads, and the role they play in European emission abatement policy.

The new and completely revised version of this Manual was mostly discussed and adopted by the 19th meeting of the ICP M&M Task Force in Tartu, Estonia (May 2003); some additional parts were discussed and adopted by the 20th meeting in Laxenburg, Austria (May 2004). The Working Group on Effects in 2003 appreciated the Manual review and revision and recommended its future use to Parties. This version replaces the previous (1996) Manual, its interim updates, and all other guidelines published in the context of the modelling and mapping work.

This update contains new scientific information and methods developed in the course of the modelling and mapping exercise, coordinated by the Coordination Center for Effects (CCE), and from recent UNECE workshops. The scientific background and relevant sources of additional information to the methods described in the manual are mentioned or included in the respective chapter or annex.

National Focal Centres have strongly contributed to the method development and tested their application on a national level. The complete revision of the Manual itself has only been possible due to numerous contributions by many scientists. The main authors/editors are

- Till Spranger for Ch. 1;
- a revision group led by Ron Smith and David Fowler for Ch. 2;
- an ICP Vegetation revision group led by Gina Mills for Ch. 3;
- ICP Materials for Ch. 4;
- Maximilian Posch for Chapters 5.1 – 5.4 (together with Jane Hall and many others);
- the Expert Panel on Critical Loads of Heavy Metals led by Gudrun Schütze for Ch. 5.5;
- Maximilian Posch, Jean-Paul Hettelingh and Jaap Slootweg for Chapter 6;
- Maximilian Posch for Ch.s 7 and 8

The attractive new layout and the internet presentation has been developed by Hans-Dieter Nagel and his team. The main pathway of distribution is meant to be the internet; revisions and extensions are available at <http://www.icpmapping.org> .

Thanks to all contributors!

(Till Spranger, Chairman of the Task Force on Modelling and Mapping)

1 Introduction		I-1
1.1	THE CRITICAL LOAD AND LEVEL CONCEPT IN THE UNECE CONVENTION ON LONGRANGE TRANSBOUNDARY AIR POLLUTION	I-1
1.2	AIMS OF THE ICP ON MODELLING AND MAPPING	I-5
1.3.	DIVISION OF TASKS WITHIN THE PROGRAMME	I-6
1.3.1	<i>Mandate for the Task Force of the ICP on Modelling and Mapping</i>	I-6
1.3.2	<i>Mandate for the Coordination Center for Effects</i>	I-6
1.3.3	<i>Responsibilities of the National Focal Centres</i>	I-7
1.4.	OBJECTIVES OF THE MANUAL	I-7
1.5.	STRUCTURE AND SCOPE OF THE MANUAL	I-8
	REFERENCES	I-9
2 Guidance on Mapping Concentration Levels and Deposition Loads		II-1
2.1	GENERAL REMARKS AND OBJECTIVES	II-1
2.1.1	<i>Mapping resolution and application of Critical Loads</i>	II-2
2.2	MAPPED ITEMS	II-2
2.3	METHODS OF MAPPING, THEIR UNDERLYING ASSUMPTIONS AND DATA REQUIREMENTS	II-3
2.3.1	<i>Linkage to emission inventories</i>	II-3
2.3.2	<i>Quantification and mapping methods: Scales of time and space</i>	II-3
2.3.3	<i>Mapping meteorological parameters</i>	II-7
2.3.4	<i>Mapping ozone (O₃) concentrations and deposition</i>	II-8
2.3.5	<i>Mapping sulfur dioxide (SO₂) concentrations and oxidised sulfur (SO_x) deposition</i>	II-10
2.3.6	<i>Mapping nitrogen oxides (NO_x) concentrations and oxidised nitrogen (NO_y) deposition</i>	II-12
2.3.7	<i>Mapping ammonia (NH₃) concentration, reduced nitrogen (NH_x) deposition and total nitrogen deposition</i>	II-13
2.3.8	<i>Mapping base cation and chloride deposition</i>	II-15
2.3.9	<i>Mapping total potential acid deposition</i>	II-15
2.3.10	<i>Uncertainties of quantification and mapping methods</i>	II-16
2.4	USE OF DEPOSITION LOAD AND CONCENTRATION MAPS	II-19
	REFERENCES	II-22
3 Mapping Critical Levels for Vegetation		III-1
3.1	GENERAL REMARKS AND OBJECTIVES	III-1
3.2	CRITICAL LEVELS FOR SO₂, NO_x, NH₃ AND O₃	III-2
3.2.1	<i>SO₂</i>	III-2
3.2.2	<i>NO_x</i>	III-2
3.2.3	<i>NH₃</i>	III-3
3.2.4	<i>O₃</i>	III-3
3.3	SCIENTIFIC BASES OF THE CRITICAL LEVELS FOR OZONE	III-9
3.3.1	<i>Crops</i>	III-9
3.3.1.1	<i>Crop sensitivity to ozone</i>	III-9
3.3.1.2	<i>Stomatal flux-based critical levels for yield reduction in wheat and potato</i>	III-9
3.3.1.3	<i>AOTX-based critical levels for crop yield reduction</i>	III-12
3.3.1.4	<i>VPD-modified AOT30 - based critical level for visible injury on crops</i>	III-14
3.3.2	<i>(Semi-) natural vegetation</i>	III-16
3.3.3	<i>Forest trees</i>	III-18

	3.3.3.1	<i>Provisional flux-based critical levels</i>	III-18
	3.3.3.2	<i>AOTX-based critical levels for forest trees</i>	III-19
Chapter I	3.4	CALCULATING EXCEEDANCE OF STOMATAL FLUX-BASED CRITICAL LEVELS FOR OZONE	III-21
	3.4.1	<i>Stages in calculating $AF_{st}Y$ and CL_{ef} exceedance</i>	III-21
	3.4.2	<i>Ozone concentrations at the canopy height</i>	III-22
	3.4.3	<i>Accumulation period</i>	III-24
	3.4.4	<i>The stomatal flux algorithm</i>	III-25
	3.4.5	<i>Calculation of $AF_{st}Y$ and exceedance of CL_{ef} for agricultural crops</i>	III-32
Chapter II	3.4.5.1	<i>Ozone concentration at the top of the wheat and potato canopy</i>	III-32
	3.4.5.2	<i>Estimating the time period for ozone flux accumulation for wheat and potato</i>	III-32
	3.4.5.3	<i>Parameterisation of stomatal flux models for wheat and potato</i>	III-36
	3.4.6	<i>Calculation of $AF_{st}Y$ and exceedance of CL_{ef} for forest trees</i>	III-38
	3.4.6.1	<i>Ozone concentration at the top of the forest canopy</i>	III-38
	3.4.6.2	<i>Parameterisation of the stomatal flux models for beech and birch</i>	III-38
Chapter III	3.5	CALCULATING EXCEEDANCE OF CONCENTRATION-BASED CRITICAL LEVELS FOR OZONE	III-40
	3.5.1	<i>Stages in calculating AOTX and CL_{ec} exceedance</i>	III-40
	3.5.2	<i>Calculation of AOTX and CL_{ec} exceedance for agricultural crops</i>	III-41
	3.5.2.1	<i>Ozone concentrations at the canopy height for agricultural crops</i>	III-41
	3.5.2.2	<i>Accumulation period for agricultural crops</i>	III-41
	3.5.3	<i>Calculation of AOTX and CL_{ec} exceedance for horticultural crops</i>	III-42
Chapter IV	3.5.3.1	<i>Ozone concentrations at the canopy height for horticultural crops</i>	III-42
	3.5.3.2	<i>Accumulation period for horticultural crops</i>	III-42
	3.5.4	<i>Calculation of $AOTX_{VPD}$ and exceedance of the short-term critical level for ozone injury</i>	III-42
	3.5.5	<i>Calculation of AOTX and CL_{ec} exceedance for (semi-) natural vegetation</i>	III-43
Chapter V	3.5.5.1	<i>Ozone concentrations at canopy height</i>	III-43
	3.5.5.2	<i>Time-window for calculating AOT40 for (semi-) natural vegetation</i>	III-43
	3.5.5.3	<i>Mapping (semi-) natural vegetation communities at risk from exceedance of the critical level</i>	III-44
	3.5.6	<i>Calculation of AOTX and CL_{ec} exceedance for forest trees</i>	III-44
	3.5.6.1	<i>Ozone concentrations at canopy height</i>	III-44
	3.5.6.2	<i>Time-window for calculating ozone exposure for forest trees</i>	III-44
Chapter VI	ANNEX I	MPOC APPROACH TO RISK ASSESSMENT FOR FOREST TREES	III-45
	ANNEX II	GUIDANCE FOR ASSESSING IMPACTS OF OZONE ON VEGETATION USING THE MODELS DESCRIBED IN THIS CHAPTER	III-46
		REFERENCES	III-48
Chapter VII	4	Mapping of Effects on Materials	IV-1
	4.1	INTRODUCTION - OBJECTIVES, DEFINITIONS AND GENERAL REMARKS	IV-1
	4.2	MAPPING "ACCEPTABLE CORROSION RATES" AND "ACCEPTABLE LEVELS/LOADS" FOR POLLUTANTS	IV-2
	4.2.1	<i>Introduction</i>	IV-2
	4.2.2	<i>Dose-response functions</i>	IV-2
	4.2.3	<i>Calculation and mapping of acceptable levels/loads and their exceedances</i>	IV-4
	4.2.4	<i>Calculations and mapping of costs resulting from corrosion</i>	IV-6
	4.2.5	<i>Sources of uncertainty</i>	IV-7
Chapter VIII	4.3	DIRECT EFFECTS OF OZONE	IV-7

4.4	DATA AND MAPPING PROCEDURE	IV-8
4.4.1	<i>Data and scale of mapping</i>	IV-9
4.4.2	<i>Urban and rural areas</i>	IV-9
	REFERENCES	IV-10

5 Mapping Critical Loads **V-1**

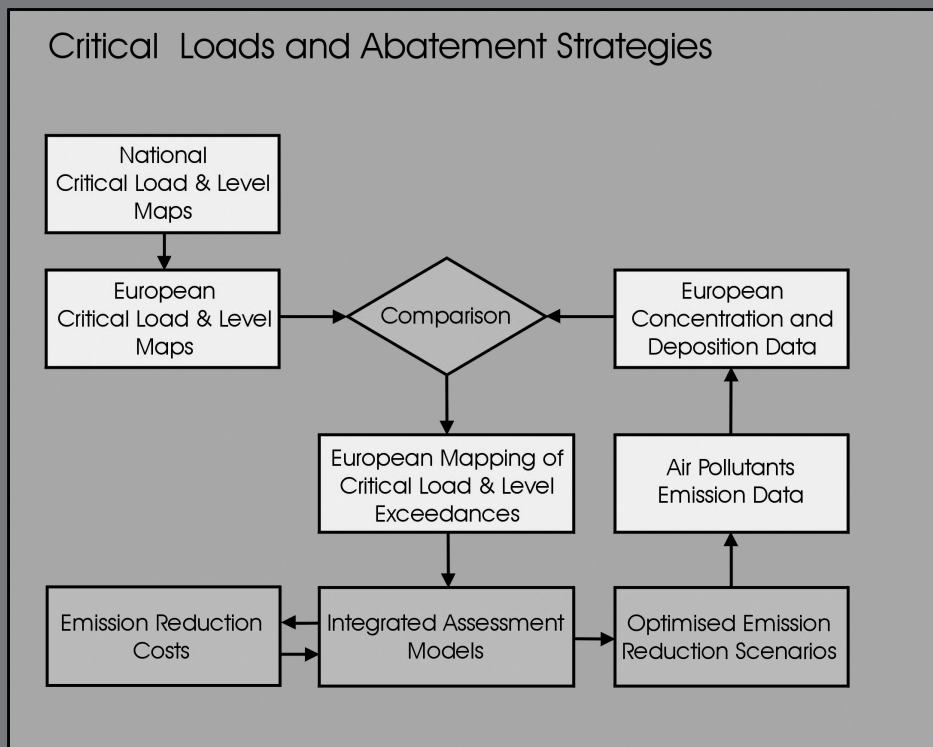
5.1	INTRODUCTION	V-1
5.2	EMPIRICAL CRITICAL LOADS	V-2
5.2.1	<i>Empirical Critical Loads of nutrient nitrogen</i>	V-2
5.2.1.1	<i>Introduction</i>	V-2
5.2.1.2	<i>Data</i>	V-2
5.2.1.3	<i>Ecosystem classification</i>	V-3
5.2.1.4	<i>Use of empirical critical loads</i>	V-6
5.2.1.5	<i>Recommendations</i>	V-6
5.2.2	<i>Empirical Critical Loads of acidity</i>	V-8
5.3	MODELLING CRITICAL LOADS FOR TERRESTRIAL ECOSYSTEMS	V-10
5.3.1	<i>Critical loads of nutrient nitrogen (eutrophication)</i>	V-11
5.3.1.1	<i>Model derivation</i>	V-11
5.3.1.2	<i>The acceptable leaching of nitrogen</i>	V-12
5.3.1.3	<i>Sources and derivation of input data</i>	V-13
5.3.2	<i>Critical loads of acidity</i>	V-15
5.3.2.1	<i>Model derivation: the Simple Mass Balance (SMB) model</i>	V-15
5.3.2.2	<i>Chemical criteria and the critical leaching of Acid Neutralising Capacity</i>	V-18
5.3.2.3	<i>Sources and derivation of input data</i>	V-21
5.3.2.4	<i>Possible extensions to the SMB model</i>	V-24
5.4	CRITICAL LOADS FOR AQUATIC ECOSYSTEMS	V-29
5.4.1	<i>The Steady-State Water Chemistry (SSWC) model</i>	V-29
5.4.1.1	<i>Model derivation</i>	V-29
5.4.1.2	<i>The F-factor</i>	V-30
5.4.1.3	<i>The non-anthropogenic sulphate concentration</i>	V-31
5.4.1.4	<i>The ANC-limit</i>	V-32
5.4.2	<i>The empirical diatom model</i>	V-33
5.4.3	<i>The First-order Acidity Balance (FAB) model</i>	V-34
5.4.3.1	<i>Model derivation</i>	V-34
5.4.3.2	<i>Systems of lakes</i>	V-37
5.4.4	<i>Input data</i>	V-37
5.5	CRITICAL LOADS OF CADMIUM, LEAD AND MERCURY	V-39
5.5.1	<i>General methodological aspects of mapping critical loads of heavy metals</i>	V-39
5.5.1.1	<i>Calculation of different types of critical loads</i>	V-39
5.5.1.2	<i>Limitations in sites that allow critical load calculations</i>	V-41
5.5.1.3	<i>Definitions and symbols/abbreviations used in critical load calculations</i>	V-41
5.5.1.4	<i>Stand-still approach versus calculation of critical limit exceedance</i>	V-43
5.5.2	<i>Terrestrial ecosystems</i>	V-44
5.5.2.1	<i>Simple steady-state mass balance model and related input data</i>	V-44
5.5.2.2	<i>Critical dissolved metal concentrations derived from critical limits in terrestrial ecosystems</i>	V-49

Chapter I
Chapter II
Chapter III
Chapter IV
Chapter V
Chapter VI
Chapter VII
Chapter VIII

5.5.3	<i>Aquatic ecosystems</i>	V-56
5.5.3.1	<i>Critical loads of cadmium and lead</i>	V-56
5.5.3.2	<i>Critical levels of mercury in precipitation</i>	V-60
5.5.4	<i>Limitations in the present approach and possible future refinements</i>	V-63
	REFERENCES	V-65
ANNEX I	TRANSFER FUNCTIONS FOR LEAD AND CADMIUM FOR THE CONVERSION OF METAL CONCENTRATIONS IN DIFFERENT SOIL PHASES	V-A1
ANNEX II	CALCULATION OF TOTAL METAL CONCENTRATION FROM FREE METAL ION CONCENTRATIONS USING THE WHAM MODEL	V-A5
ANNEX III	CALCULATION OF THE CRITICAL TOTAL AQUEOUS CONCENTRATION FROM THE CRITICAL DISSOLVED CONCENTRATION USING THE WHAM MODEL	V-A7
6 Dynamic Modelling		VI-1
6.1	INTRODUCTION	VI-1
6.1.1	<i>Why dynamic modelling?</i>	VI-1
6.1.2	<i>Constraints for dynamic modelling under the LRTAP Convention</i>	VI-3
6.2	BASIC CONCEPTS AND EQUATIONS	VI-3
6.2.1	<i>Charge and mass balances</i>	VI-3
6.2.2	<i>From steady state (critical loads) to dynamic models</i>	VI-4
6.2.3	<i>Finite buffers</i>	VI-5
6.2.3.1	<i>Cation exchange</i>	VI-5
6.2.3.2	<i>Nitrogen immobilisation</i>	VI-6
6.2.3.3	<i>Sulphate adsorption</i>	VI-7
6.2.4	<i>Biological response models</i>	VI-7
6.2.4.1	<i>Terrestrial ecosystems</i>	VI-7
6.2.4.2	<i>Aquatic ecosystems</i>	VI-9
6.3	AVAILABLE DYNAMIC MODELS	VI-10
6.3.1	<i>The VSD model</i>	VI-11
6.3.2	<i>The SMART model</i>	VI-11
6.3.3	<i>The SAFE model</i>	VI-11
6.3.4	<i>The MAGIC model</i>	VI-12
6.4	INPUT DATA AND MODEL CALIBRATION	VI-12
6.4.1	<i>Input data</i>	VI-13
6.4.1.1	<i>Averaging soil properties</i>	VI-14
6.4.1.2	<i>Data that also used for critical load calculations</i>	VI-14
6.4.1.3	<i>Data needed to simulate cation exchange</i>	VI-16
6.4.1.4	<i>Data needed for balances of nitrogen, sulphate and aluminium</i>	VI-20
6.4.2	<i>Model calibration</i>	VI-21
6.5	MODEL CALCULATIONS AND PRESENTATION OF MODEL RESULTS	VI-22
6.5.1	<i>Use of dynamic models in integrated assessment</i>	VI-22
6.5.2	<i>Target load calculations</i>	VI-24
6.5.3	<i>Presentation of model results</i>	VI-28
	REFERENCES	VI-29

7 Exceedance Calculations		VII-1
7.1	BASIC DEFINITIONS	VII-1
7.2	CONDITIONAL CRITICAL LOADS OF <i>N</i> AND <i>S</i>	VII-2
7.3	TWO POLLUTANTS	VII-3
7.4	SURFACE WATERS	VII-7
7.4.1	<i>The SSWC model</i>	VII-7
7.4.2	<i>The empirical diatom model</i>	VII-7
7.4.3	<i>The FAB model</i>	VII-7
7.5	TARGET LOADS	VII-7
	REFERENCES	VII-8
8 General Mapping Issues		VIII-1
8.1	THE EMEP GRID	VIII-1
8.1.1	<i>The polar stereographic projection</i>	VIII-1
8.1.2	<i>The EMEP grid</i>	VIII-2
8.1.3	<i>The area of an EMEP grid cell</i>	VIII-5
8.2	PERCENTILES AND PROTECTION ISOLINES	VIII-6
8.2.1	<i>Cumulative distribution function</i>	VIII-6
8.2.2	<i>Quantiles and percentiles</i>	VIII-7
8.2.3	<i>Percentile functions and protection isolines</i>	VIII-10
8.3	THE AVERAGE ACCUMULATED EXCEEDANCE (AAE)	VIII-12
8.4	CRITICAL LOAD EXCEEDANCE AND GAP CLOSURE METHODS	VIII-12
	REFERENCES	VIII-15

Mapping Manual 2004



Chapter 1 has been edited by Till Spranger (Germany), Chairman of the Task Force on Modelling and Mapping.

The critical loads and levels concept is an effect-based approach that has been used for defining emission reductions aimed protecting ecosystems and other receptors. Sustainability indicators are defined for specific combinations of pollutants, effects, and receptors (see definitions of critical levels in chapter 3, of critical loads in chapter 5.1, and of indicators and criteria used in dynamic models in chapter 6). Critical loads and levels provide a sustainable reference point against which pollution levels can be compared. They can further be used for calculating emission ceilings for individual countries with respect to acceptable air pollution levels (e.g., defined reductions of critical load/level exceedances).

The development of critical loads/levels and their application in an emission reduction policy framework can be seen as an environmental design process, using the same models and methods as causal research but in a reverse sequence (Figure 1).

1.1 The critical load and level concept in the UNECE Convention on Long-range Transboundary Air Pollution

During the 1970s it was recognised that transboundary air pollution has ecological and economic consequences (e.g. for the

forest and fish industries) caused by acidifying air pollutants. In response to this, the countries of the UN Economic Commission for Europe (UNECE) developed a legal, organisational and scientific framework to deal with this problem. The UNECE Convention on Long-range Transboundary Air Pollution (LRTAP) was the first international legally binding instrument to deal with problems of air pollution on a broad regional basis (see www.unece.org/env/lrtap). Signed in 1979, it entered into force in 1983.

The LRTAP Convention requires that its Parties cooperate in research into the effects of sulphur compounds and other major air pollutants on the environment, including agriculture, forestry, natural vegetation, aquatic ecosystems and materials (Article 7(d) of the Convention). The Convention also calls for the exchange of information on the physico-chemical and biological data relating to the effects of LRTAP and the extent of damage which these data indicate can be attributed to LRTAP (Article 8(f) of the Convention). To this end the Executive Body for the Convention established a Working Group on Effects (WGE) that is supported by a number of International Cooperative Programmes (ICPs).

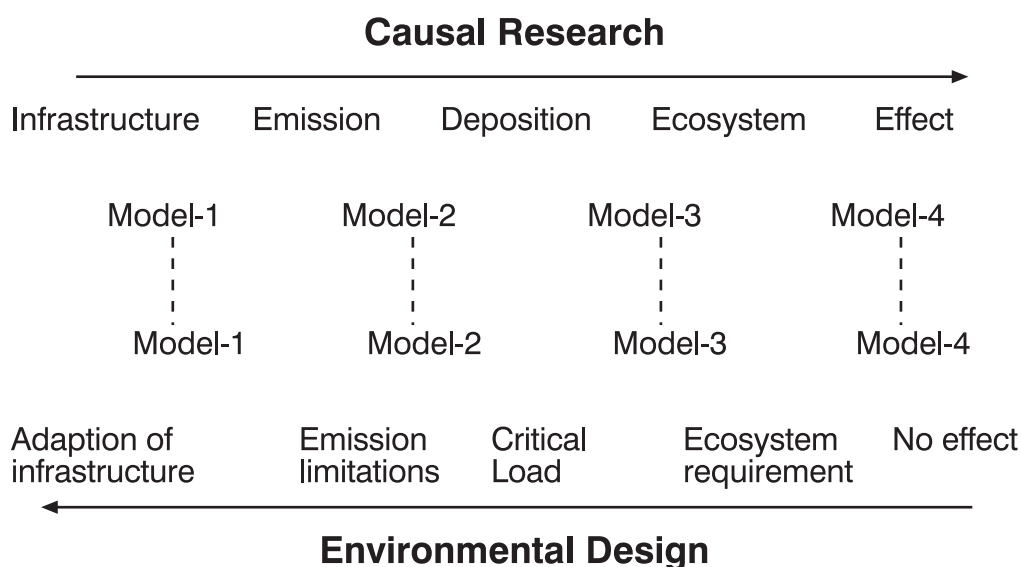


Figure 1: Environmental research vs. environmental design (adapted from Harald Sverdrup)

1 Introduction

In 1986 a work programme under the Nordic Council of Ministers (Nilsson 1986) agreed scientific definitions of critical loads for sulphur and nitrogen. This provided the necessary stimulus to work under the Convention and in March 1988 two Convention workshops were held to further evaluate the critical levels and loads concept and to provide up-to-date figures. The Bad Harzburg (Germany) workshop dealt with critical levels for direct effects of air pollutants on forests, crops, materials and natural vegetation, and the Skokloster (Sweden) workshop (Nilsson and Grennfelt 1988) on critical loads for sulphur and nitrogen compounds. Furthermore, at the Bad Harzburg workshop the first discussions took place on the possible use of critical level/loads maps for defining areas at risk. It was foreseen that these could play an important role in the development of policy.

As a result of these workshops, in 1988 the Executive Body for the Convention approved the establishment of a programme for mapping critical loads and levels (Task Force on

Mapping) under the Working Group for Effects (WGE) with Germany as the lead country (www.icpmapping.org). In 1989 the Executive Body welcomed the offer of the Netherlands to host a Coordination Center for Effects (CCE) that was established at the RIVM in Bilthoven, The Netherlands (www.rivm.nl/cce).

The mandates of the Task Force of the International Cooperative Programme on Modelling and Mapping of Critical Loads and Levels and their Air Pollution Effects, Risks and Trends (ICP M&M)¹, the CCE and the National Focal Centres² are described below.

The structure of the Programme within the Convention is shown in Figure 2.

¹ established by the Executive Body in 1999 to replace the Task Force on Mapping, see chapter. 1.3
² in 2003, 24 National Focal Centres are actively participating in the ICP M&M

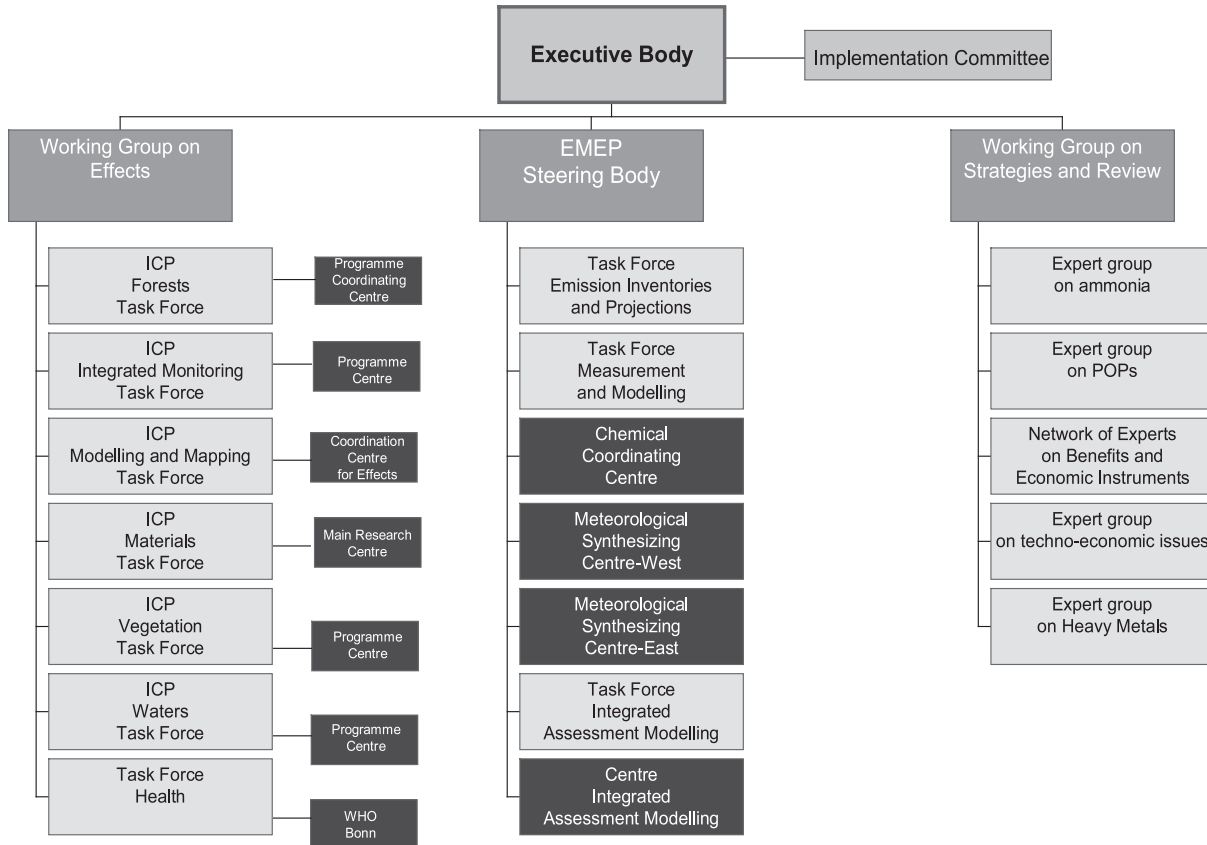


Figure 2: LRTAP Organogram

The Convention has been extended by eight protocols, which identify specific obligations or measures to be taken by Parties. The first substance-specific protocols were negotiated on the basis of economic and technological information (e.g. best available technologies). They set the same emission targets for all Parties, either in terms of a percentage reduction, or as a decrease to an emission level of a former year. They took no direct account of the effects of the emissions.

A second generation of protocols came into being when, in June 1994, a second protocol for reducing sulphur emissions (the 'Oslo protocol') was signed by 30 countries. This identified effects-based, cost-effective abatement measures based on the analysis

of impacts using critical loads. The long-term objective for negotiating national emission reductions was to eliminate the excess sulphur deposition over critical loads for sulphur, i.e. avoid future exceedances. However, cutting sulphur dioxide emissions to achieve deposition levels below critical loads was not feasible for all ecosystems in Europe. Even so, the negotiations were based on the assessment of environmental effects and the protection of ecosystems as well as technical and economic considerations.

The role of critical levels/loads maps for the development and implementation of air pollution control strategies is shown in Figure 3.

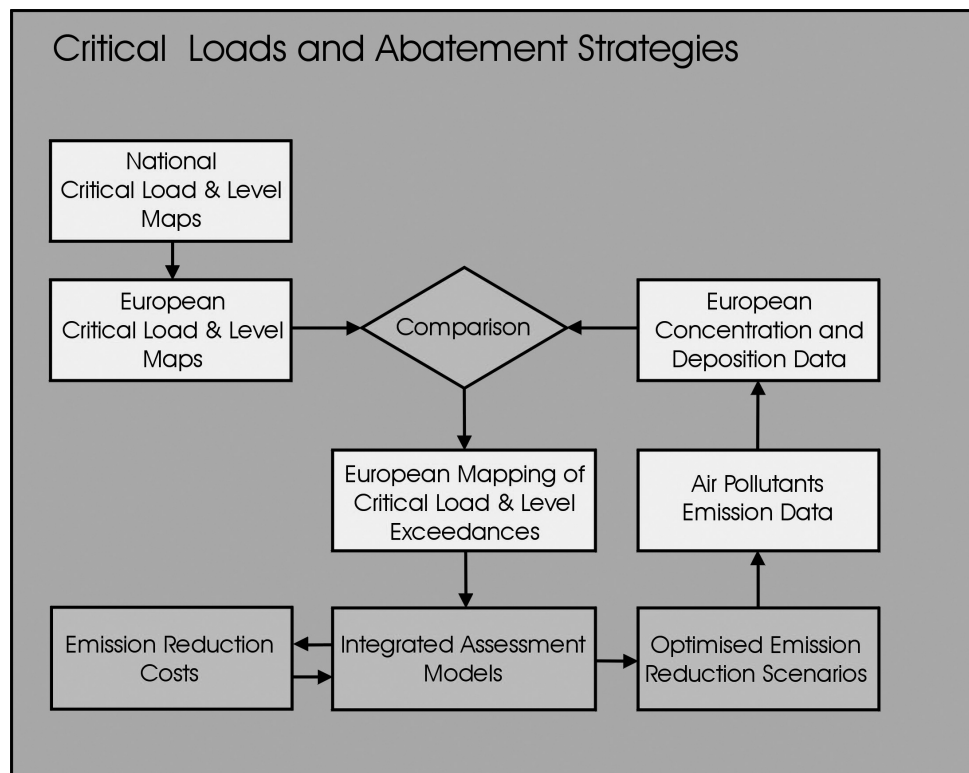


Figure 3: Critical Loads and Abatement strategies

Summarising this figure, the following "crucial steps" are involved:

- Define methods and criteria to determine and map critical loads and levels (Convention workshops);
- Obtain international approval (Working Group on Effects and Executive Body);
- Perform a mapping exercise (based on this Manual and on the proceedings of critical levels/loads and mapping workshops);
- Define excess deposition/concentration per unit area;
- Use the results for developing strategies and negotiating agreements.

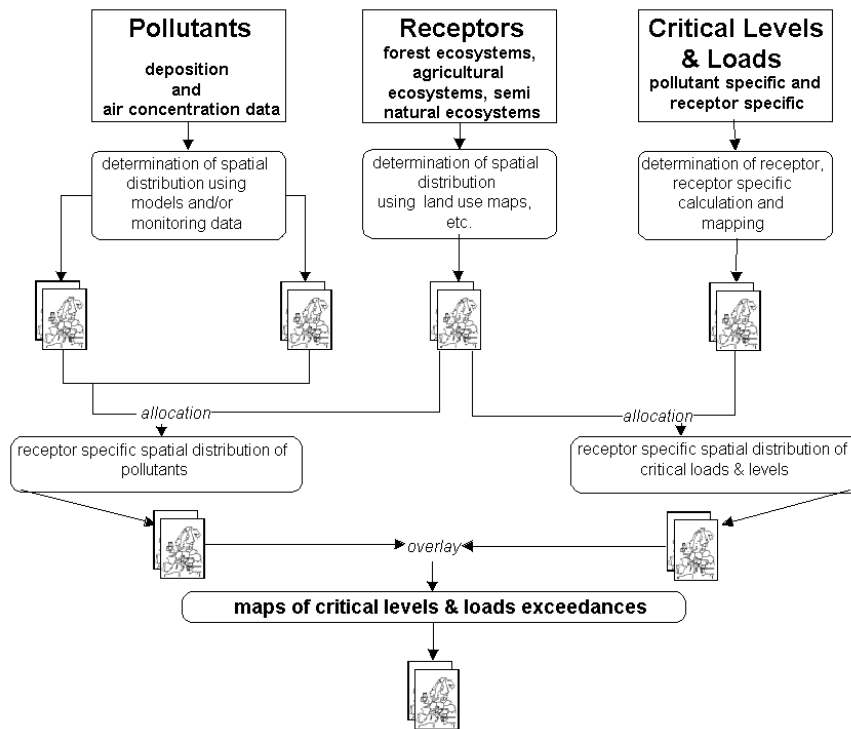


Figure 4: Production of critical levels/loads exceedance maps (adapted from GAUGER et al. 2002)

Figure 4: describes in more detail and on a national level how spatial information on receptors, pollutants and critical levels/loads are combined in the mapping process.

In practice, maps of critical loads have been used as yardsticks to assess the need for reducing depositions in each grid cell of the Co-operative Programme for Monitoring and Evaluation of the Long-Range Transmission of Air Pollutants in Europe (EMEP). An emission scenario may be viewed by comparing a computed European deposition map with the European critical loads map. In support of the Oslo protocol the negotiators started to consider the use of computer models to assess the costs and effectiveness of emission reduction scenarios. One of these "integrated assessment models" is the Regional Acidification INformation and Simulation (RAINS) model. Figure 5 illustrates the modules of the RAINS model. The first module addresses energy use, agricultural and other productive activities, while related emissions and control costs are reflected in the following two modules. The fourth module handles atmospheric dispersion, while the last module addresses environmental effects. The RAINS model can be operated in two distinct

modes. In the scenario analysis mode, the model is run forward: it can predict the regional pattern of concentrations/depositions that will result from the particular combinations of economic activities, along with the costs and environmental benefits of alternative emission control strategies. In optimisation mode, RAINS can determine the least expensive way to arrive at a pre-determined deposition level.

The model user can specify environmental targets in various ways: a certain percentage reduction of excess over critical loads, a deposition pattern of a past year, etc. This mode of RAINS has been used extensively in political negotiations in Europe. Please note that this is a specification and extension of the general concept as shown in Figure 1.

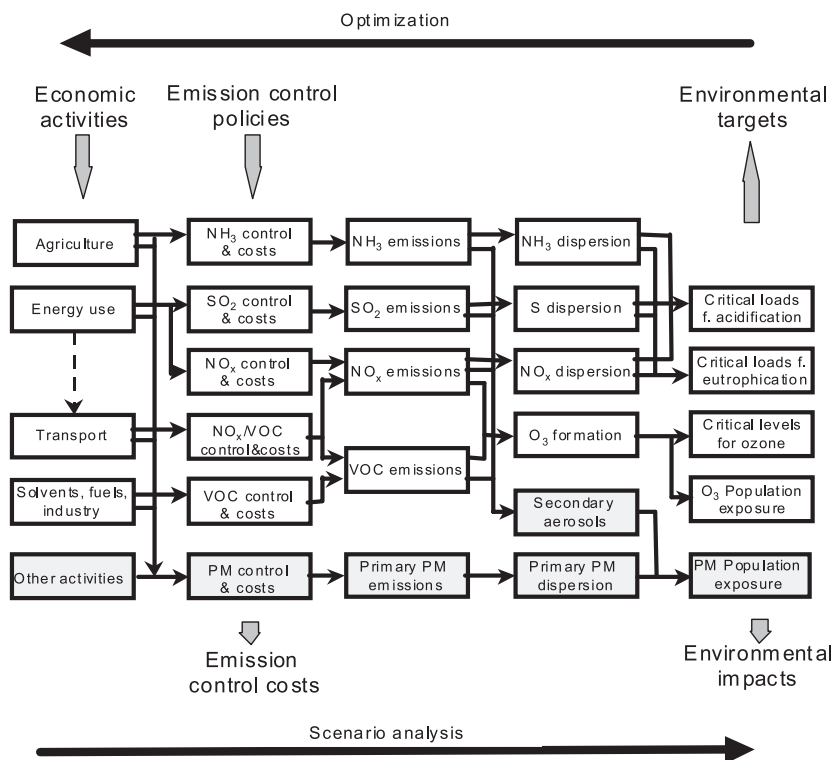


Figure 5: Scheme of the RAINS model (adapted from Amann et al.)

Since the Oslo Protocol negotiations, the complexity of the work under the ICP M&M has increased.

First, a more complex formulation of critical loads was developed and used in support of the 1999 Protocol to Abate Acidification, Eutrophication and Ground-level Ozone (the Gothenburg Protocol). It recognizes that:

- sulphur as well as oxidized and reduced nitrogen contribute to acidification. Therefore, two critical loads for acidity had to be distinguished, the critical load of sulphur-based acidity and the critical load of nitrogen-based acidity (see chapter 5.1 - 5.4).
- both oxidized nitrogen and volatile organic compounds contribute to the formation of tropospheric ozone, for which critical levels are identified for forests, crops and natural vegetation (see chapter 3.2.4).
- a small deposition rate of nitrogen which can be taken up by vegetation or immobilized is essential for ecosystems (see chapter 5.3).
- deposition of both oxidized and reduced nitrogen exceeding the critical

load for nutrient nitrogen contribute to eutrophication (see chapter 5.1 to 5.3).

Second, there have been major activities to develop an effects-based approach also for heavy metals for the preparation of the review and possible revision of the 1998 Århus Protocol on Heavy Metals. Critical limits, transfer functions and methods to determine and apply critical loads of heavy metals are being developed and are listed in chapter 5.5.

1.2 Aims of the ICP on Modelling and Mapping

The aims and objectives of the ICP on Modelling and Mapping were approved by the WGE at its nineteenth session in 2000 (Annex VII of document EB.AIR/WG.1/2000/4):

"To provide the Working Group on Effects and the Executive Body for the Convention and its subsidiary bodies with comprehensive information on critical loads and levels and their exceedances for selected pollutants, on the development and application of other methods for

effect-based approaches, and on the modelling and mapping of the present status and trends in impacts of air pollution."

Short-term and specific aims are agreed annually at sessions of the Working Group and approved by the Executive Body. The reader is invited to view the documents relating to long- and medium-term strategies, and relating to the work-plan of the Executive Body, through the web pages of the Convention (www.unece.org/env/wge/documents and www.unece.org/env/ebrespectively).

1.3 Division of Tasks within the Programme

A network of National Focal Centres (NFCs) under the ICP M&M is responsible for the generation of national data sets. NFCs cooperate with the Coordination Center for Effects to develop modelling methodologies and European databases for critical loads. CCE reports on this work to the Task Force of the ICP M&M.

The Programme's organization and division of tasks between its subsidiary bodies, as approved by the WGE (EB.AIR/WG.1/2000/4) are as follows:

"The International Cooperative Programme on Modelling and Mapping was established in 1999 (ECE/EB.AIR/68, para. 52 (f)) to further develop and expand activities so far carried out by the Task Force on Mapping of Critical Levels and Loads and their Exceedances (led by Germany) and by the Coordination Center for Effects (at the National Institute of Public Health and the Environment at Bilthoven, Netherlands), pursuant to their original mandates (EB.AIR/WG.1/18), amended to reflect the present structure of the Executive Body and the new requirements:

1.3.1 Mandate for the Task Force of the ICP on Modelling and Mapping

(a) The Programme Task Force supports the Working Group on Effects, the

Working Group on Strategies and Review and other subsidiary bodies under the Convention by modelling, mapping, reviewing and assessing the critical loads and levels and their exceedances and by making recommendations on the further development of effect-based approaches, and on future modelling and mapping requirements;

- (b) The Task Force plans, coordinates and evaluates the Programme's activities, it is responsible for updating the Programme Manual, as well as for quality assurance;
- (c) The Task Force prepares regular reports, presenting, and, where appropriate, interpreting Programme data.

1.3.2 Mandate for the Coordination Center for Effects

- (a) The Coordination Center for Effects (CCE) assists the Task Force of the ICP on Modelling and Mapping, and gives scientific and technical support, in collaboration with the Programme Centres under the Convention, to the Working Group on Effects and, as required, to the Working Group on Strategies and Review, as well as to other relevant subsidiary bodies under the Convention, in their work related to the effects of air pollution, including the practical development of methods and models for calculating critical loads and levels and the application of other effect-based approaches;
- (b) In support of the critical loads/levels mapping and modelling exercise, CCE:
 - (i) Provides guidance and documentation on the methodologies and data used in developing critical loads and critical levels of relevant pollutants, and their exceedances;
 - (ii) Collects and assesses national and European data used in the modelling and mapping of critical loads and levels of relevant pollutants. The Center circulates draft maps and modelling methodologies for

review and comment by National Focal Centres, and updates modelling methodologies and maps as appropriate;

- (iii) Produces reports and maps on critical loads/levels documenting mapping and modelling methodologies, with the assistance of the National Focal Centres and in cooperation with the Task Force on ICP on Modelling and Mapping;
 - (iv) Provides, upon request, the Working Group on Effects and the Task Force on ICP on Modelling and Mapping, the Working Group on Strategies and Review and the Task Force on Integrated Assessment Modelling, with scientific advice regarding the use and interpretation of data and modelling methodologies for critical loads and levels;
 - (v) Maintains and updates relevant databases and methodologies, and serves as a clearing house for data collection and exchange regarding critical loads and levels among Parties to the Convention, in consultation with the International Cooperative Programmes and EMEP;
 - (vi) Conducts periodic training sessions and workshops to assist National Focal Centres in their work, and to review activities and develop and refine methodologies used in conjunction with the critical load and critical level mapping exercise;
- (c) While the Coordination Center for Effects reports to the Working Group on Effects and the Task Force of ICP on Modelling and Mapping, and receives guidance and instruction from them concerning tasks, priorities and timetables, it also assists the Working Group on Strategies and Review, the Task Force on Integrated Assessment Modelling, and other bodies under the Convention, when appropriate.

1.3.3 Responsibilities of the National Focal Centres

The tasks of the National Focal Centres have been defined previously in the preceding version of the Mapping Manual:

The National Focal Centres are responsible for:

- (a) the collection and archiving of data needed to obtain maps in accordance with the Manual guidelines and in collaboration with the Coordination Center for Effects,
- (b) the communication of national mapping procedures (data, formats, models, maps) to the Coordination Center for Effects,
- (c) the provision of written reports on the methods and models used to obtain national maps,
- (d) organising training facilities for national experts in collaboration with the Coordination Center for Effects
- (e) making the necessary provisions to obtain national maps in accordance with the resolution and standards (measurement units, periodicity, etc.) described in the Manual,
- (f) collaborating with the Coordination Center for Effects to permit assessment of the methods applied in order to perform multinational mapping exercises (e.g. using GIS) and model comparisons,
- (g) updating the Mapping Manual as appropriate, in collaboration with the Task Force on Mapping and the Coordination Center for Effects.

1.4. Objectives of the Manual

The principal objectives of this Manual are to describe the recommended methods to be used by the Parties to the Convention, represented by their National Focal Centres, to:

- (a) Model and map critical levels and loads in the ECE region;

- (b) Model and map areas with air pollution values exceeding critical levels or loads;
- (c) Develop, harmonize and apply methods and procedures (including dynamic modelling) to assess recovery and risk of future damage;
- (d) Determine and identify sensitive receptors and locations.

Thus it provides a scientific basis for the application of critical levels and loads, their interrelationships, and the consequences for abatement strategies, e.g. for the assessment of optimized allocation of emission reductions.

This Manual includes methodologies used by ICP Materials (chapter 4) and (concerning ozone) ICP Vegetation (chapter 3.2.4). In contrast to manuals (or comparable methodological documents) of other ICPs and EMEP CCC this manual does not contain information on methods of measurement and specific details on data generation. This reflects the aims and tasks of the ICP Modelling and Mapping within the Convention.

Specific technical information as well as detailed results and other information by National Focal Centres can be found in the biannual Status Reports of the CCE (see also chapter 1.6).

1.5. Structure and scope of the Manual

Chapter 2 describes methods to map pollutant concentrations and depositions. These may be used to generate exceedance maps by subtracting critical levels/loads with them. At the European scale, EMEP model results are used to construct such maps. The modelled pollutant concentrations and depositions are derived from national emissions which provide the link to negotiations on emission controls. In addition, NFCs are encouraged to produce high resolution maps which can be used for effects assessments in specific ecosystems at the national and local level. This chapter was produced by experts including those from EMEP.

Chapter 3 describes the methods developed for the quantification and mapping of critical levels / fluxes of gaseous pollutants for vegetation. It is largely based on conclusions and recommendations of Convention workshops and, for ozone, on intensive work coordinated by ICP Vegetation in cooperation with EMEP.

Chapter 4 describes derivation and application of acceptable levels for effects on materials. It constitutes an informal Manual of the ICP on Materials (www.corr-institute.se/ICP-Materials).

Chapter 5 describes how to quantify critical loads of nutrient nitrogen, potential acidity and heavy metals. Since this is still the central task of ICP Modelling and Mapping, this is the most detailed chapter. The structure has been changed from the 1996 Manual in that the main distinction is by method (empirical vs. modelled), and not by effect (eutrophication vs. acidity). The chapter starts with an overview including definitions (5.1), followed by a subchapter on empirical critical loads (5.2) with sections on nutrient N (results of a workshop in Berne in 2002) and acidity. Chapter 5.3 describes methods to model critical loads for terrestrial ecosystems (SMB model), again divided into subchapters on nutrient N (eutrophication) and acidity. Compared to the previous Manual, it has been updated taking into account a.o. the results of workshops in Copenhagen (1999) and York (2000), as well as various CCE workshops. Chapter 5.4 deals with critical loads for surface waters (developed in close cooperation with ICP Waters). Finally, chapter 5.5 describes methods to model and map critical loads of heavy metals⁵.

Chapter 6 describes dynamic models and the use of their results. The authors developed it in cooperation with the Joint Expert Group on dynamic modelling.

Chapter 7 describes how to identify critical load exceedance and parameters derived from exceedance (protection isolines, [average] accumulated exceedances).

Chapter 8 describes procedures needed to produce maps, including map geometry / projections, spatial generalisation and repre-

⁵ to be finalised by 2004 with assistance from the ad hoc WG on critical loads of heavy metals

sentativity, and the estimation of uncertainty and bias.

Annex I lists definitions and descriptions of the most important parameters, processes, indicators and criteria.

Annex II describes land use data and ecosystem classification systems used within the Modelling and Mapping programme.

Annex III gives an overview on unit conversions.

In addition, the ICP M&M website (www.icpmapping.org) lists "related documents" (e.g. on deposition methods, on empirical critical loads for nutrient nitrogen) describing certain methodological aspects in more detail.

References

For historical details on the establishment of the Task Force on Mapping and the mandates of the cooperating partners in the mapping exercise see EB AIR/R.18/Annex IV, Section 3.6 and EB AIR/WG.1/R.18/Annex I.

The historical development of the programme and the approaches used for calculating critical loads and levels can be followed by consulting the following background material:

- (a) Report of the Initial ECE Mapping Workshop, Bad Harzburg 1989, Draft Manual on Methodologies and Criteria for Mapping Critical Loads/Levels 1990 with scientific Annexes I to IV, both available at the Federal Environmental Agency, Berlin, Germany
- (b) Mapping Vademecum 1992, available at the Coordination Center for Effects, Bilthoven, The Netherlands, RIVM Report No. 259101002.
- (c) Manual on Methodologies and Criteria for Mapping Critical Loads/Levels (First Edition); Texte Umweltbundesamt 25/93, Federal Environmental Agency (UBA)(ed.), Berlin, Germany

- (d) Manual on Methodologies and Criteria for Mapping Critical Loads/Levels and Geographical Areas Where They Are Exceeded (fully revised in 1995/1996); Texte Umweltbundesamt 71/96, Federal Environmental Agency (UBA)(ed.), Berlin, Germany

- (e) various interim revisions to (d), e.g. for the mapping of critical levels for ozone

- (f) numerous scientific articles referenced in the following chapters.

Status, results and agenda of the ICP Modelling and Mapping are described in various documents to be found on the Convention's web site (www.unece.org/env/wge/documents). Various aspects concerning technical and scientific background and detailed results also of National Focal Centres can be found in CCE publications,

especially the biannual CCE Status Reports (www.rivm.nl/cce).

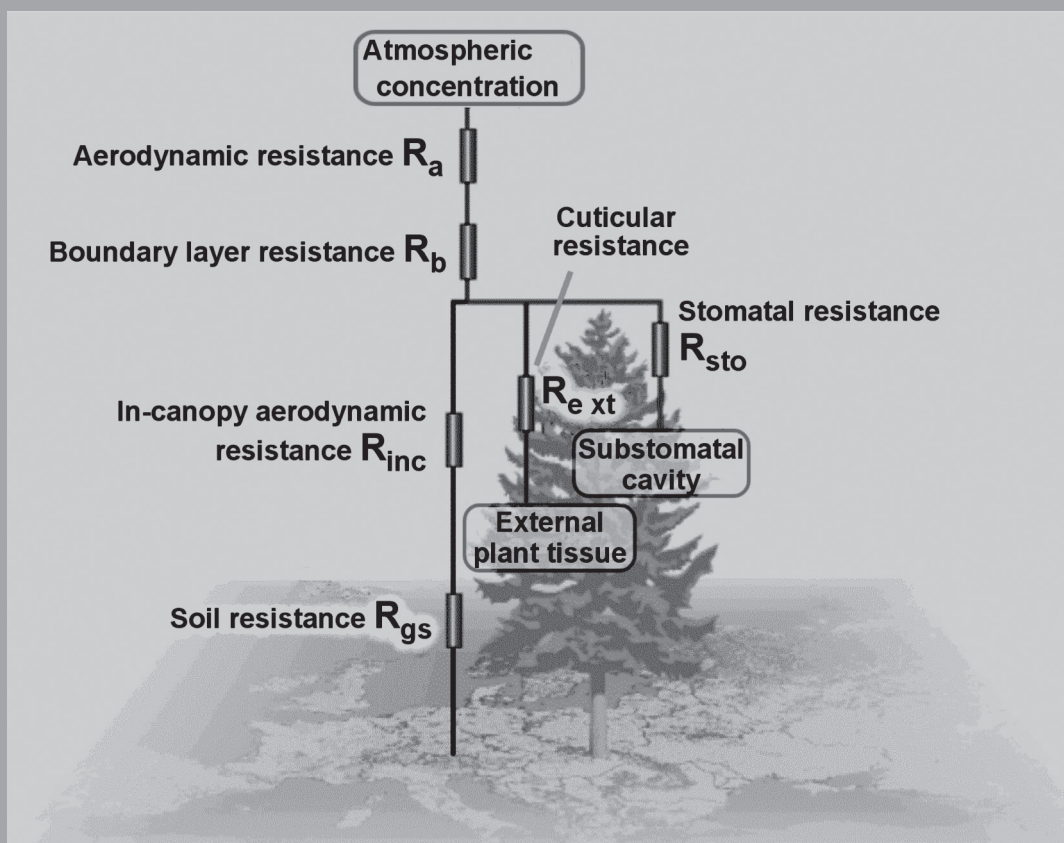
Amann et al. IIASA, The RAINS model, www.iiasa.ac.at/rains

Gauger T, Anshelm F, Schuster H, Erisman JW, Vermeulen AT, Draaijers GPJ, Bleeker A, Nagel HD (2002) Mapping of ecosystem specific long-term trends in deposition loads and concentrations of air pollutants in Germany and their comparison with Critical Loads and Critical Levels, Final Report 299 42 210 Umweltbundesamt Berlin

Nilsson J (ed) (1986) Critical Loads of Nitrogen and Sulphur. Environmental Report 1986:11, Nordic Council of Ministers, Copenhagen, 232 pp.

Nilsson J, Grennfelt P (eds.) (1988) Critical loads for sulphur and nitrogen. Report from a workshop held at Skokloster, Sweden 19-24 March 1988. Miljorapport 15, 1-418.

Mapping Manual 2004



Chapter 2 is an update and extension of the 1996 Mapping Manual. It has been re-edited by a revision group led by David Fowler and Ron Smith.

2.1 General remarks and objectives

The purpose of this chapter is to provide guidance to the participating countries in the generation of concentration level and deposition load maps for a range of pollutants for comparison with critical level/load maps. The document is intended as a general reference, with links into the recent literature. While specific recommendations are provided, the procedures are described in outline and the reader is referred to specialist publications for the measurement and modelling approaches described here.

Total deposition is the sum of dry (turbulent flux of gases and particles to the surface), wet (via rain, snow or hail) and fog and cloud water deposition. All three pathways should be accounted for, but these deposition pathways differ so fundamentally that it is proposed to determine them separately and combine the quantifications to total deposition estimates (Hicks et al. 1993).

There are two main objectives for Europe-wide mapping of concentrations and depositions:

The first aim is to construct exceedance maps relative to critical levels and loads, which are then allocated to emissions in different countries. The thus obtained transfer coefficients between emission in all European countries and exceedances in each grid cell of the Co-operative Programme for Monitoring and Evaluation of the Long-Range Transmission of Air Pollutants in Europe (EMEP) is particularly well suited to provide scientific results for a) implementation of, and compliance with, existing LRTAP Convention protocols and b) their review and extension. Such data are crucial for Integrated Assessment Modelling, and concentration and deposition maps from EMEP model calculations are designed for this purpose. Considering all the uncertainties inherent in the discussions of future emission-deposition relationships, the countries' economies and energy demands, and our knowledge of environmental effects, maps provided at a scale of 150 x 150 km² have proved adequate for the development of international protocols. The new EMEP

Eulerian model provides higher resolution concentration and deposition fields at 50 x 50 km².

The second aim is to map concentrations and depositions which can be used for effects assessments in specific ecosystems. Such data are needed with a much better spatial resolution than required for the Integrated Assessment Modelling. National Focal Centers should aim at a sufficient spatial resolution for the assessment process, making use of national models and measurement networks. EMEP will continue to provide background, long-range transported air components which can be used as boundary conditions for such national models. The chapter provides a range of different techniques for the provision of maps of concentration and deposition, depending on the resources and ambition of the country, with the EMEP values regarded as default data allowing the assessment process to be completed everywhere.

Within the countries of Europe, the expertise and facilities for measurement of concentrations and fluxes of pollutants is very variable. The extent to which the methods presented can be applied is therefore variable and it is necessary to show the range of options available. It is important to stress that involvement in the measurement and modelling activities is highly desirable as a part of the cooperation in the assessment process. The development of satisfactory strategies for control of pollutant emissions requires full participation in the underlying science as well as the political process.

The spatial scale aimed at within the Mapping Programme differs from the site-oriented approach in the ECE International Cooperative Programmes (ICPs) on Integrated Monitoring and on Forests (Level II): what is needed is not data for isolated sites but ecosystem-specific regional estimates for all of Europe. Therefore, the focus of this chapter is on methods that are capable of producing critical level/load exceedance maps for whole countries, using long-range transport models in combination with concentration measurements, small-scale dry deposition modelling and interpolated wet deposition measurement data from

(ICP, EMEP, national, regional) monitoring sites. Site-level measurements of dry deposition and canopy throughfall for example are intended for use for deriving process parametrisations (mainly micrometeorological measurements) and for independent model validation (mainly throughfall measurements; see Chapter 2.3.1, 2.3.2 and 2.3.10).

Consequently, this chapter is much less detailed in its description of field and laboratory methods than the respective sections in these ICPs' Manuals and in the EMEP publications on monitoring methodology (EDC 1993 (ICP Integrated Monitoring); UNECE ICP Forests 1999; EMEP/CCC 1996).

A range of publications is available with detailed descriptions of the underlying theory and methods as well as modelling. These include proceedings from several ECE Workshops dealing with this subject, most notably the 1992 "Workshop on Deposition" in Göteborg, Sweden (Löfblad et al. 1993), the 1993 "Workshop on the Accuracy of Measurements" with WMO sponsored sessions on "Determining the Representativeness of Measured Parameters in a Given Grid Square as Compared to Model Calculations" in Passau, Germany (Berg and Schaug 1994), and in Erisman and Draaijers (1995), Sutton et al. (1998), Slanina (1996), Fowler et al. (1995a, 2001a) and ICP Forests Manual (UNECE 1999). Supplementary information can be found in other workshop proceedings and in scientific journals.

NFCs are strongly advised to ensure that the monitoring and modelling methodologies described in the publications listed above are documented in the development or validation of a database for national concentration and deposition (and critical level and load exceedance) maps. Compatibility of these maps with other national maps within the Mapping Programme as well as with monitoring methods employed within other deposition monitoring programmes under the Convention (ICPs on Forests and on Integrated Monitoring; EMEP) is very important.

2.1.1 Mapping resolution and application of Critical Loads

The use of deposition data with Critical Loads data very often involves different scales of the different datasources. In most cases the Critical Loads data are provided at a finer resolution than the deposition data. To avoid misleading the reader it is essential that the different scales be noted in the legend. However, it is important to note that the application of deposition data at a coarse scale relative to the high resolution Critical Load data usually gives exceedances which are systematically underestimated (see 2.3.2).

2.2 Mapped items

The following items are to be mapped for each country:

For critical level exceedance maps:

- ozone concentration (*AOT40* values) and ozone flux,
- sulfur dioxide concentration,
- nitrogen dioxide concentration,
- ammonia concentration.

As input into deposition and critical load computations:

- precipitation amount and other meteorological parameters (as required),
- wet, dry, cloudwater/fog and aerosol deposition.

For critical load exceedance maps:

- oxidized sulfur (*SO_x*) deposition (total and non-sea-salt),
- oxidized nitrogen (*NO_y*) deposition,
- reduced nitrogen (*NH_x*) deposition,
- base cation and chloride deposition (total and non-sea-salt),
- total nitrogen deposition,
- total potential acid deposition.

Heavy Metal deposition (pending agreement on critical loads):

- aerosol and wet deposition of lead (*Pb*), cadmium (*Cd*), zinc (*Zn*), and copper (*Cu*) (suggested as a minimum),
- total deposition of mercury (*Hg*).

For all maps, the most recent available data should be used, not going further back in time than five years.

The mapping items concerning gaseous pollutant levels to be mapped are listed in detail in Chapter 3 of this manual. The concentrations and averaging periods are based upon the findings of the ECE workshops on critical levels held at Bad Harzburg (Germany) in 1988, in Egham (U.K.) in 1992, Berne (Switzerland) in 1993, St. Gallen (Switzerland) in 1995, Kuopio (Finland) in 1996, Harrogate (UK) in 2002, and Göteborg (Sweden) in 2002.

2.3 Methods of mapping, their underlying assumptions and data requirements

2.3.1 Linkage to emission inventories

Several methods are available to estimate boundary layer atmospheric concentrations and wet, dry, and cloud-water/fog deposition on different scales of time and space.

Only some of these methods are linked to emission inventories (see Table 2.2 / Page II-20): those that are based on emission inventories (*group A*: EMEP and national long-range transport modelling, also combined with small-scale dry deposition models) can be distinguished from those that are independent from emission inventories (*group B*: EMEP and national monitoring of air concentration and wet deposition, site-level micrometeorological and throughfall measurements).

The objectives of methods in *group A* (linked to emissions) are (1) regional present and past situation analysis, and (2) providing a basis for scenario analysis and therefore emission reduction negotiations. The objec-

tives of the measurement activities in *group B* (not linked to emissions) are (1) model evaluation, and (2) site-specific effects analysis (see Chapter 2.1 and Table 2.2).

2.3.2 Quantification and mapping methods: Scales of time and space

For the **time scale**, annual deposition rates are sufficient in order to determine critical load exceedances, whereas for critical level exceedances, short-term information is sometimes needed (see Chapters 3 and 4). However, there can be substantial variability from year to year with deposition, for example with changes in rainfall amount, and it is recommended that a 3 year average deposition is an appropriate time average for calculation of critical load exceedances.

Three groups of methods exist for various **spatial scales**:

Long-range transport models - the most widely used source of deposition data, providing inputs at a range of spatial scales (50 x 50 km² for EMEP, 5 x 5 km² for country scale models)

Nested high-resolution models - are used to provide higher spatial resolution (1 x 1 km²)

Site or catchment specific measurements - providing local deposition estimates (1 to 1000 ha); methods include:

Wet deposition collectors (point or field scale)

Micrometeorology (field scale)

Throughfall methods (canopy scale)

Catchment mass balance (landscape scale).

Long-range transport (LRT) models provide average estimates of concentrations and deposition rates for large grid squares (typically 5 x 5 km² to the EMEP Eulerian model's 50 x 50 km²). They belong to group A as defined above: they are based on emission inventories and are therefore most suitable for scenario analyses and country to country budgets ('blame matrices') used in emission reduction negotiations (if the

model domain is more than one country). Long-range transport model results are available for the European UNECE region from EMEP and can be taken as default or reference model outputs.

Standard multiannual concentrations from EMEP are given as one number per year per component per 50 x 50 km² grid square and deposition fluxes are provided either as average deposition to the 50 x 50 km² grid square or as ecosystem specific deposition estimates. EMEP model output can be provided for shorter time periods, but with the overall constraint that one of the major inputs, the emission inventory, is often provided only as an annual total.

The scale at which critical levels/loads and concentration/deposition are mapped greatly influences the magnitude of exceedance values (Spranger et al. 2001, Bak 2001, Lövblad 1996, Smith et al. 1995). For example, if the average value from a 50 x 50 km² grid square is matched to critical loads on the 250 squares of 1 x 1 km² within the 50 x 50 km² grid square, there will be generally be less critical load exceedance than if the deposition were available at the 1 x 1 km² scale. The only circumstance in which this underestimate would not occur would be if the high deposition locations matched the high critical load locations. Over many areas of Europe, exactly the opposite occurs. In many areas of complex terrain the parts of the landscape receiving the largest deposition, such as the higher areas in the mountains of North-West Europe, are also the most sensitive to the effects of deposition, for example acidification. The same holds true for forested areas, which tend to correlate with poor soils in large parts of Europe. This problem is worse for components with low local sources (NH_3 , NO_x) because the within-grid distribution of sources is not reflected in the grid average estimation from a LRT model, but does markedly increase the within-grid variability of deposition and hence increases the critical load exceedances. As the current deposition estimates from EMEP are provided at a scale which is much larger than the scale of this spatial variability, the critical loads

exceedances for these areas are underestimated.

These effects are minimised by estimating deposition to the smallest spatial scale possible. However, there is an underlying relationship that the critical load exceedances will increase as the spatial resolution of the deposition gets closer to that of the critical loads.

High resolution modelling.

A second group of methods tries to overcome these scale problems by applying smaller-scale “*inferential*” models using large-scale meteorology and concentration fields either obtained from LRT models (see above) or by interpolation of sufficiently dense measurement networks (see below).

Dry deposition is inferred by multiplying the concentration with the deposition velocity of the component of interest (Hicks et al. 1987, 1993). The latter is calculated using a resistance model in which the transport to and absorption or uptake of the component by the surface is described. Resistances are modelled using observations of meteorological parameters and parametrisation of surface exchange processes for different receptor surfaces and pollution climates as described in Erisman et al. (1994a), Smith et al. (2000), Nemitz et al. (2001), Emberson et al. (2000), Grünhage and Haenel (1997), Gauger et al. (2003). The deposition velocities of cloudwater/fog droplets can be similarly estimated by modelling momentum transfer (Fowler et al. 1993) and a similar technique has been used to estimate base cation deposition (Draaijers et al. 1995). Parameters determining the deposition velocity include atmospheric parameters (e.g. wind speed, temperature, radiation, relative humidity, atmospheric stability, cloud and/or fog frequency) and surface conditions (e.g. roughness, wetness, stomatal response, soil water). Unfortunately, up to now no reliable European-wide cloudwater/fog concentration fields are available, hampering cloudwater/fog deposition estimation on a European scale.

The land use maps used for this deposition modelling should be identical to the stock-

at-risk maps used for critical levels/loads mapping (see Chapter 6). In addition to the geographical position of sensitive ecosystems, land use type/vegetation type, vegetation height and crown coverage should be mapped as well on a scale that allows for correct allocation of deposition to all ecosystem types in the model domain.

Uncertainties of inferential deposition models are described in Chapter 2.3.10.

Site or catchment specific measurements.

All methods based on *point measurements* (e.g., wet deposition measurements, micrometeorological dry deposition measurements, throughfall measurements) belong to group B, as they cannot be directly connected to emission inventories. Maps can only be produced directly from these measurements if the network is dense enough to account for spatial (and temporal) variations. This may be the case for networks measuring air concentrations of compounds with little spatial variation or for measurements of wet deposition in areas of simple terrain. Network (point) measurements should be interpolated using the kriging technique and it may be helpful to include monitoring data from neighbouring countries for interpolation. For some air concentrations, such as ammonia, or for rain concentrations in complex terrain, the required density of the measurement network could be too dense for practical application. In these cases, it is recommended that concentrations are obtained from less dense networks and that simple models are used to assist the interpolation, e.g. using altitude dependences. It is preferable to interpolate concentrations in rain or in air and then calculate the deposition at the receptor site using local estimates of rainfall and land-use specific ground-level dry deposition rates (see above).

Additional monitoring of air concentrations of gases in order to create a dense network as a basis for mapping can be made with diffusive samplers. These samplers, can be used for a number of gases (ozone, sulphur dioxide, nitrogen dioxide, nitrogen oxides (NO_x), ammonia, nitric acid, mercury, hydrogen chloride, etc.) The sampler provides average concentrations over a time period,

normally from one week to one month. It is a simple and cheap complementary method, to be used in parallel to other methods providing also the temporal variability (Ferm and Svanberg 1998, Ferm 2001, Sjöberg et al. 2001).

Wet deposition.

In most cases, the long-term spatial variation in wet deposition within regions is determined mostly by variations in precipitation amount and less by variations in concentrations in rain or snow. In addition, precipitation amounts are mostly available from relatively dense meteorological networks. Therefore, if concentration variations are small, maps of annual wet deposition rates should not be drawn by interpolating measured wet deposition rates; it is recommended to interpolate measured solute concentrations and estimate the wet deposition as the product of the mapped solute concentration and the precipitation amount, the latter provided by the meteorological service for the country. This is an important step because the precipitation fields are defined by dense networks of collectors. An additional and very important enhancement of wet deposition occurs in the uplands of Northern Europe, due to wash out of orographic cloud by falling rain or snow. As networks do not generally measure at high elevation in complex terrain, these effects are generally omitted from network measurements. The underlying physical process is well documented and the effects may be modelled using the network data (Dore et al. 1992, Fowler et al. 1995b).

Dry and cloudwater/fog deposition can be estimated from concentration measurements of airborne substances by *micrometeorological measurements* at the process level (for SO_2 : Fowler et al. 2001c; for NH_3 : Flechard and Fowler 1998; for cloud: Beswick et al. 1991). During the last decade it has become possible to make micrometeorologically based long-term flux measurements (i.e. continuous flux measurements over more than a year). This has been demonstrated for O_3 , NO_x and SO_2 (LIFE project, Erisman et al. 1998a) and for CO_2 and H_2O (Aubinet et al. 2000). Such measurements give information about the seasonal

and interannual variability in the fluxes.

These measurements of deposition fluxes have therefore become straightforward and can be applied to all pollutant gases. However, the primary purpose of the measurements is to provide the parameters for modelling as the tool for extrapolation over the landscape as the measurement stations are expensive to operate. Thus the number of dry deposition stations could not realistically be sufficiently large to interpolate fluxes over spatial scales directly. There are low cost micrometeorological methods, such as the Time Averaged Gradient (TAG) system (Fowler et al. 2001b). These will provide the means of obtaining deposition parameters for many more representative terrestrial surfaces in Europe.

The methods mentioned here only work if stringent prerequisites concerning micrometeorological variables (e.g., surface homogeneity) are fulfilled. They cannot be directly extrapolated, but the process knowledge obtained from such measurements can be parametrized in inferential models and fluxes can be mapped using this information (see high resolution modelling above).

Throughfall and stemflow measurements can be used to estimate the site-specific total deposition of sulfur to plant canopies, mainly forests (wet plus dry plus cloudwater/fog). The data are useful for parallel effect studies, in order to estimate deposition rates on the basis of field data available from existing monitoring programmes and to validate other deposition estimates. They will also provide knowledge on the seasonal variation and the trends of deposition. In many cases throughfall monitoring is considered to be sufficient, and stemflow is only measured for some tree species, for which it is known to be of importance (e.g. beech trees) (UNECE 1999). In practice, it is not generally possible to determine the total deposition of substances for which uptake or leaching within the canopy is large relative to the deposited amounts (e.g. nitrate, ammonia, and calcium, potassium and magnesium) from throughfall measurements.

Throughfall measurements are cheaper and generally easier to perform than micromete-

orological measurements. They also give a good overview of the deposition situation in the forest, not only for sulfur but also for nitrogen compounds. Recent Swedish experiences have highlighted the problems with comparing throughfall measurements with wet deposition when the dry deposition contribution to the total is very low (Westling *pers. comm.*), as is now the case for sulphur in many areas of Europe. Large uncertainties in wet deposition at wind-exposed sites have been shown with field intercomparison studies (Draaijers et al. 2001). Even if it is not possible to estimate the total deposition of nitrogen with this method, a lower limit can be set. Sampling considerations (e.g. location of collectors, species composition, spatial variability) are very important for achieving good results and sampling requirements are described in detail in the ICP Forests Manual (UNECE 1999) and in review articles such as Draaijers et al. (1996a) and Erisman et al. (1994b).

In order to interpret the data, the relation between total deposition and throughfall can be expressed:

(2.1)

$$Total\ DEP = DRY + WET + Cl/Fog = THF - CEX$$

where:

THF = Flux in throughfall (plus stemflow)

DRY, WET, Cl/Fog = dry, wet, cloudwater/fog deposition

CEX = canopy exchange; *CEX* > 0 for leaching, *CEX* < 0 for uptake

When *CEX*=0, the dry deposition can be estimated as the difference between total flux in throughfall and independent measurements of wet and cloudwater/fog deposition. If *CEX* differs from 0, dry deposition cannot be distinguished from internal cycling. This method can give large overestimates of the true deposition flux (*CEX*>0), due to canopy leaching (for some base cations), or large underestimates of the true deposition flux (*CEX*<0), due to canopy uptake (e.g., for nitrogen compounds and protons). Therefore, throughfall plus stemflow fluxes

should be interpreted as upper bounds of total base cation deposition and as lower bounds of total nitrogen and proton deposition.

In some cases, the total deposition to plant canopies can be deduced from throughfall and precipitation measurements in the open field using empirical *canopy budget models*. These models are not always applicable and should if used be applied with care. The method by Ulrich (1983), which uses the relation of dry vs. total deposition of sodium as an indicator of dry vs. total deposition of other elements, is used most widely. However, some of its assumptions, such as the constant (in time and with respect to substances) ratio of dry particulate deposition vs. wet deposition rates, are questionable. For several reasons (e.g., different deposition and canopy uptake processes), it cannot be applied for determining total nitrogen deposition to the forest ecosystem (Bredemeier 1988, Spranger 1992). A modification (Beier et al. 1992) and an extension of the model (Draaijers and Erisman 1995) mitigate some of the methodological problems, even though they have not yet been properly evaluated under all circumstances (see Draaijers et al. 1996a,b), but there remains an issue with canopy modelling that, in many cases, a cation surplus exists in the throughfall solutions indicating that major substances have not been measured.

The calibrated watershed method integrates deposition fluxes over a scale compatible to critical load computations for example for lakes and surface waters. However, major fluxes to the groundwater and soil exchange have to be accounted for. It is most useful for conservative elements (e.g., S, Na, Cl) in areas with clearly delineated watersheds. The data are useful to validate deposition estimates derived from modelling.

Concluding remarks. LRT Models will normally be used to calculate patterns of concentration and deposition across Europe. High resolution inferential models may be used to calculate patterns within countries or regions. The role of measurements in the process of mapping is twofold. Low cost devices, such as passive samplers

or bulk samplers, may be used to observe regional patterns of concentrations and wet deposition. If the measurement strategy is good, these measured patterns will be more reliable than those calculated. However for dry deposition the situation is more complex. The deposition rate depends on atmospheric conditions as well as on ecosystem type. Recent developments of low cost dry deposition monitors (Fowler et al. 2001b) will make it possible to determine regional patterns of dry deposition in the near future. But still the application in dense networks is expected to be limited. The limitations of using throughfall measurement networks for estimating regional patterns of total deposition have been described above.

The results of measurements on the other hand are necessary to test, validate and improve model parameterisations. Defendable estimates of the deposition need to be validated by measurements to relevant European ecosystems. It is recommended to establish a network across Europe where detailed measurements of dry and wet deposition will be made. This may be linked to existing monitoring networks such as the EMEP network and the Level II Programme of ICP Forests.

2.3.3 Mapping meteorological parameters

Meteorological parameters are required inputs for most critical levels or critical loads calculations. The data requirements and data provision will vary from country to country. Data are generally available from national weather services. European data can be obtained from European Centre for Medium-Range Weather Forecasts (ECMWF, website: www.ecmwf.int), who provide modelled data based on observations within Europe, and there are other sources for some data such as the US EPA/NCAR global precipitation database.

Precipitation amounts are needed for critical load computations, for wet deposition mapping (see Chapter 2.3.2), and for surface wetness parameterisations (also for materials: "time of wetness"; see Chapter 4).

Fog and cloud occurrence is needed for cloudwater/fog deposition estimates.

Wind speed, temperature and radiation are basic requirements for the inferential modelling of dry deposition. Additionally, *relative humidity, soil water deficit, and atmospheric stability* are often required.

The availability of accurate local meteorological data is often a constraint to detailed local high resolution modelling, and therefore the success of models in improving deposition estimates to specific ecosystems may depend as much on the availability of quality meteorological data as on the quality of the local concentration estimates or measurements.

2.3.4 Mapping ozone (O_3) concentrations and deposition

Ozone concentration data are required to generate maps showing areas where the critical level is exceeded (see Chapter 3.2.4). Data may be available from photochemistry/transport modelling (see (a.) and (b.) below) or from monitoring networks (see (c.) below).

The concentrations of ozone close to terrestrial surfaces (e.g. within 1 m) show a large spatial variability in both rural and urban areas. For urban areas, this variability is mainly caused by chemical consumption of ozone by NO , which is locally emitted. For rural areas away from local sources, this variability is largely caused by spatial and temporal changes in the degree to which individual sites are vertically 'connected' to the main reservoir of ozone in the boundary layer. Like in urban areas O_3 might be consumed by the reaction with NO which can be emitted from bacterial processes in the soil (PORG 1997)

To provide a spatial resolution of the ozone exposure on a horizontal scale which reflects the variations in the orography it is helpful to produce the ozone concentration field at a grid of 1 x 1 km² cell-size at least (see (b.) and (c.) below). As the critical levels are based on the concentration measured in the turbulent layer near the receptor, ozone

levels modelled or measured at higher distances from the ground are not directly related to the observed effects. Therefore a surface-type specific correction should be applied for assessing exceedances of critical levels, but it is hardly possible to quantify the correction from monitoring data to dose-effect data at present (Fuhrer 2002).

The supply of ozone to vegetation is provided by atmospheric turbulence and hence wind speed and the thermal structure of air close to the ground. The deposition of ozone on terrestrial surfaces and vegetation causes a vertical gradient of the ozone concentration, which is largely determined by the sink activity of the soil-vegetation system. Maps of O_3 deposition can be produced from inferential modelling based on parameters obtained from long-term measurements and land-use information (Emberson et al 2000).

(a.) LRT model results

EMEP/MSC-W has available calculations of ozone concentrations in 50 x 50 km² grid-squares with hourly time-resolution and also deposition to specified land cover types, e.g. forests, arable crops, etc. The model calculations are available for a notional height of 45 m above ground and scaling algorithms are available to provide output at lower heights, particularly 3 m and 1 m. *AOT40* for crops and forests is also available, as well as their changes in each grid square per unit of changed country-emissions of VOC and NO_x . The calculations are based on new EMEP/CORINAIR emissions with 11 source sectors and VOC speciation specified for each sector. The model also includes biogenic VOC emissions from forests.

(b.) High resolution modelling

The low spatial resolution of LRT models does not match with the resolution required for the evaluation of ozone exposure of forests ecosystems, and estimates of ozone exposure can be improved by local scale modelling within the 50 x 50 km² EMEP square. The necessary concentration values

at receptor level can be obtained at high resolution from the large scale model average values by correcting them for local emission of nitrogen oxides, orography and deposition. The computation of deposition velocities and deposition fluxes requires land-use maps (see Annex II), as well as meteorological data.

One method of adjusting for local scale effects is to adjust the diurnal cycle in concentrations from the LRT by accounting for the dependence of ozone concentrations on local orography (PORC 1997, Coyle et al. 2002). The elevation of a particular location determines the extent to which it experiences the influence of air from the free troposphere and from the boundary layer. Based on data from the EUROTRAC-TOR and EMEP monitoring programs as well as on results in literature, this dependence can be modelled and combined with small scale orographical data.

High-resolution AOT_{40} maps can also be computed by using other atmospheric transport and photochemistry models, provided that the output data are high-resolution results modelled over a long (for AOT_F : April-September), continuous time period, and that the model results are evaluated with measurements as well as with MSC-W model results.

(c.) Monitoring and interpolating ozone concentrations and fluxes

The monitoring of ozone is necessary to establish or to validate exceedance maps as well as for the verification of the long range transport and chemistry models.

Over large parts of Europe and particularly in South and East Europe there are very few available data. Efforts should be made to obtain data where monitoring stations exist. Elsewhere, the establishment of a network of monitoring stations is strongly recommended. Stations should be linked to the EMEP network.

To provide data from such a network that are representative for an extensive area it is recommended that the monitoring stations be sited at rural locations avoiding local

sources of the oxides of nitrogen such as roads. Anshelm and Gauger (2001) developed a method to classify the suitability of monitoring sites for mapping concentrations.

Some countries have already a sufficiently 'dense' network. If the number of monitoring stations needs to be increased, it is recommended to install them at various altitudes and/or at various distances from the emitters of ozone precursors. Stations at urban locations are not representative for extensive areas, but they may be required for differentiating areas with rural and with urban pollution conditions and for population exposure assessments through mapping exceedances of air quality guidelines based on human health.

The preferred sampling height is 3-5 m and the monitoring station requires an open aspect without the presence of trees or other tall vegetation in the proximity of the sample intake. Appropriate recommendations for sampling and calibration are available from the Chemical Coordinating Centre of EMEP.

More or less simple interpolation procedures exist to obtain an estimate of the exposure of terrestrial surfaces to ozone using topographic and other information. Altitude may be used here as an indicator for the degree to which areas are 'connected' to the ozone reservoir in the boundary layer (see also *b.*)).

One possibility is to interpolate the measured hourly ozone values and then to compute seasonal dose-parameters such as AOT_{40} (see chapter 3.2.4) on the basis of those hourly maps (Loibl and Smidt 1996). But in general it will be easier to calculate the values of the required dose-parameters for each monitoring station first and then to use these values for the spatial application of a regression model. For the interpolation of AOT_{40} values relationships with altitude (height above mean sea level) have been used in the UK (Fowler et al. 1995c) and in the Nordic countries (Löfblad et al. 1996). Relationships with relative height (the height of the site of interest above the valley ground within a certain distance) are applied in Alpine regions (Loibl and Smidt 1996). Such

relationships are reasonably consistent on the regional scale (100 to 500 km) with the exception of coastal and urban areas, but must be established from relatively dense monitoring networks. Dividing the study area into subregions and evaluating region-specific influences on the O_3 concentration or exposure may enhance the quality of the interpolation. Data assimilation, combining observed and LRT modelled concentrations, is another method recently applied to provide improved ozone concentration fields (Flemming 2003).

2.3.5 Mapping sulfur dioxide (SO_2) concentrations and oxidised sulfur (SO_x) deposition

Data on SO_2 gas concentrations, sulfate (SO_4^{2-}) aerosol concentrations and SO_4^{2-} concentrations in rain are required to generate maps showing areas where the critical level is exceeded. Data are available from long-range transport modelling, possibly coupled to small-scale modelling (see (a.) and (b.) below), or from monitoring networks (see (c.) below).

SO_2 , in contrast to ozone or sulfate aerosol, is a primary pollutant. It is emitted by both high (e.g. power plants) and low (e.g. households) sources. Therefore the spatial variability of concentrations tends to be higher than that of ozone and sulfate aerosol but lower than that of ammonia. Close to urban areas, the concentrations of rural sulfur dioxide are elevated and this effect should be modelled explicitly where possible, for example by using urban concentration measurements and areas of urbanisation to model the urban effect (a similar method was used by Stedman et al. (1997) to model NO_x and NO_2 near roads).

For rural areas away from local sources, spatial variability is largely caused by spatial and temporal changes in the degree to which individual sites are vertically 'connected' to the main reservoir in the boundary layer (see preceding subchapter on ozone).

As for ozone, the SO_2 levels measured 3-5 m above ground are not directly related to the

observed effects, since dry deposition causes a systematic vertical concentration gradient towards the surface, while the critical levels are based on the concentration measured close to the receptor. However, surface-type specific corrections are not generally applied and measured/modelled values usually taken uncorrected.

Non-sea-salt inputs of sulfur are needed in the critical loads framework, since critical loads are generally compared with anthropogenic S (and N) (see Chapter 5.3.2). Consequently, the base cation and chloride deposition in the charge balance - from which critical loads are derived with the SMB model - have to be corrected for sea salt contributions as well. Natural marine emissions of reduced sulfur compounds (especially Dimethylsulfate, DMS) are included into the EMEP emission data base (and therefore EMEP model results), whereas sea-salt emissions are not.

Depositions of base cations, sulphur and chloride (given in equivalents) are corrected by assuming that either all sodium or all chloride is derived from sea salts, and that the relations between ions are the same as in sea water (after Lyman and Fleming 1940, cited in Sverdrup 1946):

(2.2)

$$X^*_{dep} = X_{dep} - r_{XY} \cdot Y_{dep}$$

where

X = Ca, Mg, K, Na, Cl or SO_4 ,

Y = Na or Cl ,

r_{XY} = is the ratio of ions X to Y in seawater and the star denotes the sea-salt corrected deposition. Ratios r_{XY} are shown in Table 2.1 with 3-decimal accuracy.

Table 2.1: Ion ratios $r_{XY}=[X]/[Y]$ (in eq/eq) in seawater

Y	X					
	Ca	Mg	K	Na	Cl	SO ₄
Na	0.043	0.228	0.021	1	1.166	0.120
Cl	0.037	0.195	0.018	0.858	1	0.103

Note that for arbitrary ions X , Y and Z the relationships $r_{YX} = 1/r_{XY}$ and $r_{XY}r_{YZ} = r_{XZ}$ hold. If Na (Cl) is chosen to correct for sea salts, $Na^*_{dep}=0$ ($Cl^*_{dep}=0$).

Using such a correction will only yield reliable estimates on non-sea-salt S , Mg , Ca , K , and Cl in areas where sea-salt is the only source of Na in ambient air. This generally will be the case in western and northern Europe. In some parts of southern and south-eastern Europe, however, significant quantities of Na in the atmosphere originate from wind-blown evaporates and applying the sea-salt correction there will result in underestimated non-sea-salt concentrations.

(a.) LRT model results

As for ozone, EMEP/MSC-W has available calculations of sulfur dioxide concentrations and sulfate aerosol concentrations in 50 x 50 km² grid-squares with hourly time-resolution and also deposition to specified land cover types, e.g. forests, arable crops, etc. The model calculations are available for a notional height of 45 m above ground and scaling algorithms are available to provide output at lower heights, particularly 3 m and 1 m. Daily concentrations and deposition of sulfate in rain are also available. Concentrations allocated to emissions in separate countries are available with monthly time-resolution.

(b.) High resolution modelling

Procedures as the ones described for ozone in the preceding subchapter can be applied for SO_2 . However, since SO_2 is a primary

pollutant, the most important factor causing variability is local emission, which has to be accounted for in the high-resolution model. SO_2 deposition velocities depend mostly on stomatal opening (stomatal pathway: to be parametrized using vegetation type/land use, and meteorology data), on surface wetness, and on NH_3 concentrations. When surfaces are wet, and at humidities >90%, surface resistances to deposition become very low and the flux is mostly determined by atmospheric resistances (Erisman et al. 1994a).

For SO_4^{2-} aerosol, dry deposition is highest for forests or other rough surfaces that are far from SO_2 emission sources (Gallagher et al. 1997). Sulfate deposition velocities can be estimated using Slinn's (1982) or a similar simple particle deposition model (e.g., Erisman et al. 1995, Ruijgrok et al. 1996) but there is still significant research effort focussed on improving these estimates and it is reasonable to use site specific models to improve on the LRT sulfate aerosol deposition.

Wet deposition maps can be produced from monitoring data according to the methods described in Chapter 2.3.2, including orographic effects where applicable. The most important factor in improving wet deposition estimation at the local scale is the availability of rainfall maps derived from dense networks of rainfall collectors. If the density of the concentration monitoring network is not sufficient, EMEP/MSC-W modelled concentration data can be combined with local rainfall maps for improved estimates of wet deposition.

c.) Monitoring and interpolating concentrations

Measurement stations for SO_2 should be set up in areas that are not directly affected by local emitters. As for the EMEP network, and contrary to regional, national or EU health-related programmes, the main objective of a measurement network is not necessarily to determine the highest ambient concentrations (leading to high local critical level exceedances) but rather the large-scale concentrations that are due to long-range transport. Individual measurement stations should be representative for a maximum area, thus making interpolation and mapping of concentrations unaffected by local sources possible. Criteria for siting measurement stations are listed in, e.g., EMEP/CCC (1996).

Due to the fact that SO_2 is a primary pollutant, the measurement network density, especially in emitter areas such as Central Europe, has to be high so that the interpolation error (determined, e.g., by variogram analysis when using kriging) is minimal relative to the measured values. The same is true for mountainous areas due to the vertical gradients present. As secondary pollutants with relatively slowly varying concentrations, the measurement network density for SO_4^{2-} aerosol and for SO_4^{2-} in rain can be much lower than for SO_2 . Methods to determine (and data on) representativity of measurements, as well as their precision and accuracy, are listed in Berg and Schaug (1994).

Maps can be produced from measurements by interpolation if all criteria mentioned above (accuracy/precision, representativity) are fulfilled. For some applications a blending height approach is appropriate, where ground-level observations are extrapolated to 50 m height (the blending height) above the ground, using a resistance model. At this height the concentration is less dependent on the surface processes and can be interpolated over larger areas (Erisman and Draaijers 1995). The preferred interpolation procedure is kriging, which also provides an estimated interpolation error.

2.3.6 Mapping nitrogen oxides (NO_x) concentrations and oxidised nitrogen (NO_y) deposition

Data are available from long-range transport modelling, possibly coupled to small-scale modelling (see (a.) and (b.) below), or from monitoring networks (see (c.) below).

NO_x (= $NO+NO_2$), like SO_2 , is emitted by both high (e.g. power plants) and low (e.g. traffic) sources, mostly as NO . The spatial variability of NO_x concentrations tends to be higher than that of ozone and nitrate but lower than that of, e.g., ammonia, due to conversion of NO by reaction with O_3 . In rural areas emission of NO from soils (both agricultural and semi-natural) can likewise contribute to local NO_2 levels. Many national modelling activities are able to provide estimates of surface concentrations of NO_2 at a higher resolution than $50 \times 50 \text{ km}^2$, for example at $5 \times 5 \text{ km}^2$ in the Netherlands and in the UK (the UK Air Quality data base is at www.airquality.co.uk/archive/) and these can incorporate models to adjust concentrations for local emissions, for example by using distance to major roads.

(a.) LRT model results

As for SO_x , EMEP/MSC-W has available concentrations and deposition of NO_x (NO and NO_2), NO_3^- in aerosol and in rainfall, and HNO_3 .

(b.) High resolution modelling

Procedures as the ones described for SO_x can be applied with the following comments. For inferential dry deposition modelling, NO_3^- aerosol and HNO_3 (ideally also $HONO$) concentration maps are needed besides the NO_x concentration maps. Since measurements are too scarce to be interpolated in most countries, they generally will have to be estimated from atmospheric models. The most important factor causing variability in NO_x is local emission which has to be accounted for in the high-resolution model. NO_2 deposition velocities depend almost

exclusively on stomatal opening (stomatal pathway: to be parametrized using vegetation type/land use, and meteorology data) and the importance of surface wetness to SO_2 deposition does not hold for NO_2 . For the aerosol fraction, HNO_3 deposition is determined by atmospheric resistances because the surface resistance is very low (surface roughness and windspeed are most important) and the NO_3^- aerosol deposition velocities are estimated similarly to SO_4^{2-} aerosol.

As was mentioned above, ozone gradients may be affected by fast chemical reactions between O_3 , NO_2 and NO . These reactions will also affect the gradients and hence the uptake of NO_2 . In LRT models this effect is not taken into account. Although no firm evidence is available, it is felt that the uptake by low vegetation is only marginally affected. (Duyzer et al. 1995). On the other hand, the effect on uptake of NO_2 and O_3 by forests could be influenced by chemical reactions taking place in the canopy (Walton et al. 1997).

(c.) Monitoring and interpolating concentrations

Measurement stations for NO_x should be set up in areas that are not directly affected by local emitters (most importantly not near road traffic). Criteria for siting measurement stations are similar to those for SO_x . Due to the fact that NO is a primary pollutant and the reaction to NO_2 is relatively fast, the measurement network density has to be high, as for SO_2 . The other nitrogen compounds are assumed to have slowly varying concentrations and the network density can be reduced accordingly.

2.3.7 Mapping ammonia (NH_3) concentration, reduced nitrogen (NH_x) deposition and total nitrogen deposition

Ammonia is emitted primarily from low level agricultural sources with varying source strengths. Gaseous NH_3 has a short atmospheric residence time (Erisman and Draaijers 1995) and as a result its concentrations in air may show steep horizontal and vertical gradients (Asman et al. 1988). Even in areas not affected by strong local sources, the ambient concentration of ammonia may vary by a factor of three to four on scales less than a few kilometres.

The very localised pattern of ammonia concentration, and also of ammonia dry deposition, has consequences for mapping procedures. Mapping of ammonia concentrations by interpolation from measurements alone is not treated explicitly here, as the required measurement network density would be extremely high and the method is only feasible over small areas. However, the critical level of ammonia is so high that except very near sources (farms) exceedances are not very likely.

A long-range transport model with, for example a 50 x 50 km² spatial resolution, will not resolve these large variations either for ammonia concentrations or for the dry deposition of ammonia which will be the major fraction of total reduced nitrogen deposition close to an ammonia source. So assessments of the exceedances of critical loads will be biased when using LRT models. In the absence of very detailed emission data (on the level of the individual farm), measurements in a dense network are needed to obtain accurate exceedance levels (Asman et al. 1988).

It is also important to note that ammonia may be emitted as well as deposited onto vegetation, and therefore surface-atmosphere exchange modelling must be used to quantify the net exchange over the landscape. The background developments to allow these processes to be simulated use a compensation point approach (Schjorring et al. 1998; Sutton et al. 2000).

(a.) Long-range transport modelling

As for SO_x , EMEP/MSC-W has available concentrations and deposition of NH_3 and NH_4^+ in aerosol and in rainfall. However, the interpretation of the concentration and dry deposition of ammonia estimates for ammonia must be qualified because of the spatial resolution of the model and the effects of local sources. Improvements in the ammonia component of the EMEP/MSC-W LRT model are currently being developed.

(b.) High-resolution modelling

In the LRT model results from EMEP/MSC-W, it is assumed that the concentration distribution of ammonia within a grid cell is homogeneous, whereas generally sub-grid concentration variations will be present. The spatial resolution on which concentrations can be modelled strongly depends on the resolution of the available emission estimates. Where these are available at spatial scales of the order of 1 x 1 km², considerable improvements to the estimates from the EMEP/MSC-W LRT 50 x 50 km² model are possible. Models are available for these more detailed calculations, such as the OPS model for the Netherlands (see below) and the FRAME model for the UK (Singles et al. 1998).

The Operationele Prioritaire Stoffen model (OPS) developed at RIVM is able to calculate dispersion (and deposition) of NH_x on a 5 x 5 km² grid over The Netherlands (Asman and Van Jaarsveld 1992; Erisman et al. 1998b). The model is able to describe both short- and long-distance transport, average concentrations (and depositions) can be computed for time scales from 1 day to more than 10 years, and it can account for both point sources of various heights and area sources of various shapes and heights. The basis for the model on the local scale is formed by the Gaussian plume formulation for a point source. Computations are made for a limited number of meteorological situations (classes) with a representative meteorology for each class derived from actual

observations. The uncertainty in emission values appeared to be the most important factor determining the uncertainty in concentrations. Model results and air concentration measurements in the Netherlands are reasonably well correlated, but substantial differences in the absolute values have yet to be explained quantitatively (Duyzer et al. 2001). Given the concentrations on a 5 x 5 km² scale, deposition of NH_x in the Netherlands was estimated and showed good agreement with results of throughfall (corrected for canopy exchange) and micrometeorological measurements (Erisman et al. 1995).

For aerosol deposition and wet deposition, the procedures as described for SO_x can be applied to NH_4^+ .

(c.) Monitoring and interpolating concentrations

Accurate representative measurement of NH_3 concentrations, especially in high emission density areas, requires many measuring sites. Typically, most of the concentration gradient is present within a few km of the source and local scale monitoring is a valuable tool to understand the processes. With the developments in passive samplers, large-scale monitoring of ammonia concentrations has become possible and there are national ammonia monitoring networks in the Netherlands and in the UK (Sutton et al. 2001a,b). The local site conditions must be noted for NH_3 monitoring so that the data can be correctly interpreted. The main use of the measurement networks for ammonia is to support the models used to predict the local scale variations in concentration, as neither models nor measurements on their own can adequately predict concentrations.

Criteria for siting measurement stations for ammonium are similar to those for SO_x . Ammonium is assumed to have slowly varying concentrations and the network density can be relatively low.

The **deposition of total nitrogen** is needed for many applications in the critical load framework. It is defined as the sum of total deposition of reduced (NH_x) nitrogen [NH_3 dry deposition, NH_4^+ aerosol deposition, NH_4^+ wet deposition, NH_4^+ cloudwater/fog deposition] and oxidised (NO_y) nitrogen [NO_2 dry deposition, HNO_3 dry deposition, NO_3^- aerosol deposition, NO_3^- wet deposition, NO_3^- cloudwater/fog deposition]. The methodological considerations concerning NH_x and NO_y deposition mapping apply accordingly.

2.3.8 Mapping base cation and chloride deposition

The deposition of physiologically active basic cations ($Bc = Ca+Mg+K$; i.e. the sum of calcium, magnesium and potassium) counteracts impacts of acid deposition and can improve the nutrient status of ecosystems with respect to eutrophication by nitrogen inputs. Sodium (Na) fluxes are needed for estimating the sea-salt fraction of sulfur, chloride, and Bc inputs, and as a tracer for canopy and soil budget models. In addition, inputs of Bc as well as Na and chloride (Cl) determine the potential acidity of deposition.

As the aim of the Convention is to minimize acid deposition irrespective of other man-made emissions, base cation inputs not linked to emissions of acidifying compounds (for example from emissions of Sahara dust, large-scale wind erosion of basic topsoil particles, etc.) should in principle not be accounted for within the critical loads framework. The non-anthropogenic, non-sea-salt atmospheric input of base cations is defined as a property of the receptor ecosystem and indirectly enters the critical load equation for acidity (see Chapter 5). However, at present there is no method to differentiate anthropogenic from non-anthropogenic deposition of base cations due to the lack of emission inventories and long-range transport models for this task.

There are so far no emission inventories available and therefore base cation and chloride deposition is not yet estimated using "classical" LRT models. Work is going

on to provide base cation and chloride deposition on a European scale with 50 x 50 km² resolution. As soon as EMEP models based on (anthropogenic) emission inventories are applied to base cations, the different sources of base cations should be identified and only those relevant for control of acid deposition included in critical loads calculations.

The wet deposition of non-sea-salt chloride (Cl^*) can be estimated by correcting site fluxes of Cl for the sea-salt fraction (see Chapter 2.3.5, eq. 2.2), then interpolating the derived Cl^* concentration (see the wet deposition section of Chapter 2.3.2). Similar procedures are applied to map the concentrations of the non-sea-salt base cations Ca^* , Mg^* and K^* to produce non-sea-salt base cation wet deposition.

Base cation particle deposition can be estimated from concentrations in wet deposition and empirical scavenging ratios (Eder and Dennis 1990, Draaijers et al. 1995). Dry deposition velocities can be inferred as for SO_4^{2-} aerosol and the obtained dry deposition estimates added to measured and interpolated wet deposition estimates (e.g., Gauger et al. 2003). A similar approach has been used for the UK (RGAR 1997, CLAG 1997).

Deposition of base cations have been estimated for the Nordic countries based on monitoring data on concentrations of base cations in precipitation and air-borne particles.

2.3.9 Mapping total potential acid deposition

Total Potential Acid Deposition is defined as the sum of total deposition of strong acid anions plus ammonium minus non-sea-salt base cations.

As stated in the preceding subchapter, most chloride inputs are assumed to be of sea-salt origin, and these are removed from the equation by removing all other sea-salt inputs (i.e. of base cations incl. Na and sulfate) using a "sea-salt correction" with Na as a tracer. The implicit assumption is that sea-salt is neutral and containing no carbonates.

Surplus chloride inputs (Cl_{dep}^*) are assumed to be due to anthropogenic HCl emissions.

The sum of critical load (for sulfur) and background (non-anthropogenic) base cation deposition has formerly been defined as critical (sulfur) deposition, as used for the negotiations for the Second Sulfur Protocol (Oslo, 1994). For comparison to $CL(S+N)$, as defined in Chapter 5.3.3 (eq. 5.16), only deposition values of S and N are needed. However, if the amount of total acid input is of interest (e.g., for comparison to $CL(Ac_{pot})$, as defined in Chapter 5.3.2), non-sea-salt base cation and chloride deposition has to be included into the input side of the potential acidity exceedance equation:

(2.3)

$$Ac(pot)_{dep} = SO_{x,dep}^* + NO_{y,dep} + NH_{x,dep} - BC_{dep}^* + Cl_{dep}^*$$

where:

$SO_{x,dep}^*$	= non-sea-salt sulfate deposition
$NO_{y,dep}, NH_{x,dep}$	= total oxidized/reduced nitrogen deposition
BC_{dep}^*, Cl_{dep}^*	= non-sea-salt base cation / chloride deposition

In areas strongly affected by sea spray (high sea-salt Na , Cl , S inputs), the “total potential acid” definition of Eq. 2.3 becomes problematic, since base cations have a beneficial nitrifying effect irrespective of their chemical form (e.g., $CaCl$ vs. $CaCO_3$). At the Grange-over-Sands Workshop 1994 it was concluded that *total Mg+Ca+K* deposition rates should be used for the determination of critical loads for acidity (Sverdrup et al. 1995) (see Chapter 5.3.2).

As stated in Chapter 5.3.2, Eq. 2.3 assumes that deposited NH_x is completely nitrified and exported from the system as NO_3^- , thereby acidifying the system. Thus, with respect to soil acidification it is assumed that 1 mol of SO_x^* is forming 2 moles of H^+ , and 1 mol of

NO_y, NH_x and Cl^* each 1 mol of H^+ .

It is important to be consistent when determining total acid inputs: If results are determined on a site and process level, and if H^+ deposition rates are determined separately, NH_4^+ inputs (max. 2 eq H^+ per mol) have to be distinguished from NH_3 inputs (max. 1 eq H^+ per mol). The same applies to SO_2 (2 eq H^+ per mol) vs. SO_4^{2-} (0 eq H^+ per mol). On a larger scale, this may be neglected: Note that the emission and subsequent deposition of 1 mol and 2 mol NH_3 yields the same potential acid deposition as the deposition of 1 mol of their reaction product $(NH_4)_2SO_4$, namely 4 eq.

2.3.10 Uncertainties of quantification and mapping methods

The errors concomitant with the different methods are strongly dependent on the scale considered and the availability of data. The following analysis is focussed on the mapping of concentrations and depositions from the EMEP/MSC-W LRT model, inferential models and interpolated measurements.

Although it is expected that the revised EMEP/MSC-W 50 x 50 km² Eulerian LRT model will become the standard model from 2003, the results from the model have not been generally available for analysis. However, preliminary indications are that the discrepancies between model output and measurements will be no larger than those from the previous EMEP/MSC-W 150 x 150 km² Lagrangian model and significant improvements are expected with some components. From a critical loads/levels perspective, the change from a 150 x 150 km² scale to a 50 x 50 km² represents a major improvement in mapping the concentrations and deposition. The other notable change in the move from the Lagrangian model to the Eulerian model has been the inclusion of vegetation specific dry deposition fluxes within the EMEP/MSC-W model. This change takes the EMEP/MSC-W model part of the way towards a full local inferential model, as the output pollutant fluxes are now vegetation specific and the issue of grid-average values being inappropriately

applied to specific vegetation types, e.g. forests, should no longer occur. However, the issue of scale is important as the concentrations and the meteorological inputs are still 'average' values for the whole 50 x 50 km² grid square. Where concentrations are expected to be slowly varying, e.g. sulphate aerosol, the 'average' concentration concept should not be an important issue, but the approach is still inadequate for the rapidly varying concentration fields associated with some primary pollutants. There will still be issues to resolve with local meteorology as grid 'average' values, e.g. wind speed, will not be correct for many of the ecosystems, e.g. forests on the higher altitude areas within the grid square. Therefore, the uncertainty in deposition from the Eulerian model should be improved from the Lagrangian model but will not match the levels of uncertainty which could be achieved by a local scale inferential model. A full analysis of uncertainty in the EMEP/MSC-W Eulerian model would be a substantial task.

There are a number of references comparing the EMEP/MSC-W Lagrangian model with available EMEP measurements (e.g. Barrett et al. 1995), and with the results of other models (Iversen 1991) and the previous version of this manual (UBA 1996). When evaluating model-measurement intercomparisons, it is important to recall that (a) there are also uncertainties with the measurements and (b) the model may be estimating something rather different from what is being measured, e.g. the NO_2 concentration at a single site in a 50 x 50 km² grid square is only an estimate from a sample of size one of the 'average' NO_2 concentration in the square, which is the value the EMEP/MSC-W model is attempting to match. An evaluation of the overall uncertainty of the model requires that some further information is available on the effects of the spatial distribution of measurement sites.

Inferential deposition models treat deposition as a one-dimensional (vertical) transfer to homogeneous surfaces with infinite length, assuming a constant flux layer. This means that the flux from the 50 m reference height is assumed to be equal to the flux at

the surface. The reference height must be high enough so that the concentration is not severely affected by dry deposition, but it must be below the surface layer height. Fast chemical reactions as well as the impact of enhanced turbulent exchange induced by local roughness transitions (forest edges, hills, mountains) are not taken into account. Components whose deposition strongly depends on the aerodynamic resistance (e.g. HNO_3 , aerosols and cloud water/fog droplets) will show higher deposition rates than modelled. The impact of transitions on dry deposition rates of components like NO_2 , whose deposition is mainly determined by stomatal conductance, will be relatively small.

However, the main uncertainties in dry deposition of sulfur and nitrogen compounds in the inferential framework are due to (1) uncertainties in surface resistance parametrisations which are not always available for all vegetation species and surface types, and (2) uncertainties in the concentration estimates, which for all the reactive gases show a scale of spatial variation which is too great to quantify from measurement activities. Surface wetness, which is one of the major factors determining dry deposition of soluble gases (NO_2 , NH_3), is up to now parametrized very roughly only. The overall uncertainty in surface resistance varies between 20% and 100%, depending on component and surface type (van Pul et al. 1995).

For the deposition of nitrogen compounds, the main sources of uncertainty were described by Lövblad and Erisman (1992) to be uncertainties in emissions, concentrations and surface resistances to dry deposition, as well as surface wetness and particle deposition for NH_x especially in NW and Central Europe.

Using error propagation methods and assuming that the above mentioned uncertainties represent random errors, the total uncertainty in dry deposition of acidifying compounds for an average 10x20 km² grid is estimated at 50-100%. Systematic errors in

dry deposition may arise from neglecting complex terrain effects in the parametrisation of the deposition velocity, and from other simplifications (see Chapter 2.3.2). As these calculations are scale dependent and are based on a relatively coarse spatial resolution, the uncertainty in reality may be much larger. For NH_3 , for example, much larger uncertainties in even small areas have been shown (Dragosits et al. 2002).

Additional uncertainties arise for estimates of dry deposition for base cations (i) in parametrising the deposition velocity, (ii) in the precipitation concentration maps and (iii) in the scavenging ratios used to derive surface-level airborne particulate concentrations from concentrations in precipitation.

The overall uncertainty in modelled dry deposition velocities integrated over the particle size distribution representative for alkaline particles at the Speulder forest (The Netherlands) was found to equal 60%. For other sites (and for regions) additional uncertainties will arise due to limited availability and accuracy of relevant information on land use and on meteorology. The uncertainty in deposition velocity caused by variations in the size distribution of alkaline particles amounts to 30-50%, assuming a mass median diameter (MMD) of 5 μm and taking a geometric standard deviation of 2-3 to represent the variation (Ruijgrok et al. 1996). The MMD of particles depends on the distance to sources and on relative humidity.

Also scavenging ratios vary with particle diameter, and assuming the same MMD and standard deviation as above, the uncertainty in estimated ambient air concentrations caused by variation in size distribution is estimated at 50-100%. Large uncertainties in air concentrations can be expected very close or far from major sources and/or in areas with strongly deviating precipitation climatology.

Systematic errors arise from (i) using scavenging ratios based on a limited set of simultaneous ambient air and precipitation concentration measurements, (ii) neglecting complex terrain effects in the parametrisation of the deposition velocity, (iii) using annual mean air concentrations and deposition velocities for flux calculation, thereby

neglecting temporal correlations. The total uncertainty in dry deposition of base cations for an average 10x20 km² grid, caused by random errors in deposition velocities and air concentrations, is estimated to be 80-120% (Draaijers et al. 1995).

Errors on wet deposition maps are due to (i) limited accuracy of measurements and (ii) the non-representativity of measurement sites. An in-depth analysis of methods to minimize and to quantify these errors can be found in the proceedings of an EMEP Workshop on these topics (Berg and Schaug 1994) and will not be repeated here. The uncertainty of the wet deposition rate for a 50x50 km² grid square, based on interpolated measurements of precipitation concentration and precipitation amount, is estimated at 50% on average. Larger uncertainties (about 70%) were found by van Leeuwen et al. (1995) in mountainous areas and complex terrain; the same is to be expected if the measurement network is not as dense as in Northwest Europe (Schaug et al. 1993). Using a spatial scale of 5 x 5 km² over the UK, uncertainties were reported as $\pm 35\%$, reflecting the improved information available by using a detailed rainfall map with an appropriate orographic model (Smith and Fowler 2001).

The uncertainty in total deposition is determined by the uncertainty in wet, dry and cloud and fog deposition. The latter is not taken into account by most models and rarely measured. As described above, the uncertainty of dry deposition is generally much larger than that of wet deposition. Total deposition estimates are more uncertain in areas with complex terrain or with strong horizontal concentration gradients. The uncertainty in total deposition (grid square average) of acidifying compounds ($N + S$) and base cations can be estimated to be 70-120% and 90-140%, respectively for grid sizes of the order of 10 x 10 km².

Errors of sulfur deposition rates determined from throughfall measurements vs. inferential models for a forest in the Netherlands were estimated by Draaijers and Erisman (1993). Error estimates for sulfur and other substances are provided by Erisman and Draaijers (1995).

These large uncertainties illustrate the need to validate model results by measurements of airborne concentrations, wet deposition, dry deposition and throughfall, as stated in Chapter 2.3.2.

This, and the scale-specific qualities of the methods, should be kept in mind when reading the substance-specific listing of individual methods in Chapters 2.3.3-2.3.9.

coordinated by comparing results at EMEP or other workshops.

2.4 Use of deposition load and concentration maps

These maps are designed to be used in combination with critical loads and critical levels maps to show where and by how much critical loads and critical levels are exceeded. The use of deposition data with critical loads data very often involves different scales of the different data sources and, in most cases, the critical loads data are provided at a finer resolution than the deposition data resulting in an underestimation of the critical load exceedance. These issues have been discussed above and improved deposition estimates, for example by using national models at a finer spatial resolution, can improve the quality of the critical load exceedances. One important point re-iterated here is that it is essential to note any different scales in the legends to figures and maps.

National maps and model outputs may be compared with data from the EMEP model, since the EMEP data are used for the Integrated Assessment Modelling activities and for the protocol developments. If the national datasets deviate strongly from EMEP model data, EMEP should be notified and scientifically based improvements of the EMEP models should be developed. National datasets may always be used for national purposes, and national model outputs should be calibrated with monitoring results at international (e.g., EMEP), national and subnational levels. This should also ensure that it is possible to compare national maps where they meet at international borders, and these activities at various levels (regional, national, international) should be

Table 2.2: Summary of methods for atmospheric concentration and deposition mapping (see Chapter 2.3), their linkage to emission inventories, and their suitability for mapping and site-level validation (1=good, 2=useful, 3=should not be used) (see text!)

<u>Parameter</u>	<u>Method</u>	<u>Link to emission inventories</u>	<u>Mapping Suitability</u>	<u>Site-Level Validation Suitability</u>	<u>Comments / Requirements</u>	<u>Data sources</u>	<u>Selected References</u>
<u><i>O₃</i> concentration (AOT40 values)</u>	EMEP model results (interpolated) measurements	yes	1/2	3	Suitability for mapping dependent on topography and emission structure	MSC-West	Barrett et al. (1995), Maik et al. (1996)
<u><i>SO₂</i> concentration</u>	EMEP model results (interpolated) measurements	no	1/2/3	1	same as above; dependent on measurement network density	EMEP and national monitoring	CCC(1996), Barrett et al. (1995)
<u><i>NO_x</i> concentration</u>	EMEP model results (interpolated) measurements	yes	1/2	3	Suitability for mapping mostly dependent on emission structure	MSC-West	Barrett et al. (1995)
<u><i>NO_x</i> concentration</u>	EMEP model results (interpolated) measurements	no	1/2/3	1	same as above; dependent on measurement network density	EMEP and national monitoring	CCC(1996), Barrett et al. (1995)
<u><i>NO_x</i> concentration</u>	EMEP model results (interpolated) measurements	yes	1/2	3	Suitability for mapping mostly dependent on emission structure	MSC-West	Barrett et al. (1995)
<u><i>NH₃</i> concentration</u>	EMEP model results (interpolated) measurements	no	1/2/3	1	same as above; dependent on measurement network density	EMEP and national monitoring	CCC(1996), Barrett et al. (1995)
<u><i>NH₃</i> concentration</u>	EMEP model results (interpolated) measurements	yes	2/3	3	EMEP emission inventories not very reliable, large local variations	MSC-West	Barrett et al. (1995)
<u><i>Meteorol. parameters</i></u>	EMEP model results (interpolated) measurements	no	2/3	1	Suitability for mapping mostly dependent on emission structure; high measurement network density required	EMEP and national monitoring	CCC(1996), Barrett et al. (1995)
<u><i>SO_x deposition</i></u>	EMEP model results (interpolated) measurements	n.a.	1/2	1/2	precipitation volume, fog and cloud occurrence, net radiation, temperature, wind speed and direction	national weather services, ECMWF, EPA/NCAR	Potma (1993)
<u><i>SO_x deposition</i></u>	EMEP model results (interpolated) measurements	yes	1/2	3	dependent mostly on quality of emission data, spatial resolution	MSC-West	Barrett et al. (1995)
<u><i>NO_x deposition</i></u>	throughfall measurements	no	3	1	Should not be extrapolated	ICP Forest Level II and national monitoring	ICP Forests (1994), EDC (1993), Lövblad et al. (1993), Draaijers et al. (1996a)
<u><i>NO_x deposition</i></u>	site-level inferential modelling	yes/no	3	1/2	dependent on data quality and adequate parametrization	RIVM, ITE, ...	Lövblad et al. (1993), Erisman et al. (1994)
<u><i>NO_x deposition</i></u>	EMEP model results (interpolated) measurements	yes	1/2	3	dependent mostly on quality of emission data, spatial resolution	MSC-West	Barrett et al. (1995)
<u><i>NO_x deposition</i></u>	throughfall measurements combined with canopy budget modelling	no	3	2	Should not be extrapolated	ICP Forest Level II and national monitoring	ICP Forests (1994), EDC (1993), Lövblad et al. (1993), Draaijers et al. (1996a)
<u><i>NO_x deposition</i></u>	site-level inferential modelling	yes/no	3	1/2	dependent on data quality and adequate parametrization	RIVM, ITE, ...	Lövblad et al. (1993), Erisman et al. (1994)

<u>NH₃ deposition</u>	EMEP model results	yes	2	3	EMEP emission inventories not very reliable, large local variations	MSC-West	Barrett et al. (1995)
	throughfall measurements combined with canopy budget modelling	no	3	2	Should not be extrapolated	ICP Forest Level II and national monitoring	ICP Forests (1994), EDC (1993), Lövblad et al. (1993), Draaijers et al. (1996a)
	site-level inferential modelling	yes/no	3	1/2	dependent on data quality and adequate parametrization	RIVM, ITE, ...	Lövblad et al. (1993) Erisman et al. (1994)
<u>base cation deposition</u>	interpolated wet deposition measurements plus model-derived dry deposition fields	no	2	3	no emission dataset available yet; concentration field (for dry deposition modelling) based on uncertain assumptions	RIVM	Draaijers et al. (1996c)
	throughfall measurements combined with canopy budget modelling	no	3	1	Should not be extrapolated	ICP Forest Level II and national monitoring	ICP Forests (1994), EDC (1993), Lövblad et al. (1993), Draaijers et al. (1996a)
	site-level inferential modelling	no	3	2	dependent on data quality and adequate parametrization	RIVM	Erisman et al. (1995)
<u>total potential acid deposition</u>	EMEP model results	yes	1/2	3	dependent mostly on quality of emission data, spatial resolution	MSC-West	Barrett et al. (1995)
	throughfall measurements combined with canopy budget modelling	no	3	2	Should not be extrapolated	ICP Forest Level II and national monitoring	ICP Forests (1994), EDC (1993), Lövblad et al. (1993), Draaijers et al. (1996a)
	site-level inferential modelling	yes/no	3	2	dependent on data quality and adequate parametrization	RIVM, ITE, ...	Lövblad et al. (1993) Erisman et al. (1994)

References

- Anshelm F, Gauger Th (2001) Mapping of ecosystem specific long-term trends in deposition loads and concentrations of air pollutants in Germany and their comparison with Critical Loads and Critical Levels. Part 2: Mapping Critical Levels exceedances. Final Report of Project 29942210. Inst. for Navigation, Stuttgart University and Umweltbundesamt.
- Asman WAH, Van Jaarsveld HA (1992) A variable-resolution transport model applied for NH_x in Europe. *Atmos. Environ. Part A-General Topics* 26: 445-464.
- Asman WAH, Drukker B, Janssen AJ (1988) Modeled historical concentrations and depositions of ammonia and ammonium in Europe. *Atmos. Environ.* 22: 725-735.
- Aubinet M, Grelle A, Ibrom A, Rannik U, Moncrieff J, Foken T, Kowalski AS, Martin PH, Berbigier P, Bernhofer C, Clement R, Elbers J, Granier A, Grunwald T, Morgenstern K, Pilegaard K, Rebmann C, Snijders W, Valentini R, Vesala T (2000) Estimates of the annual net carbon and water exchange of forests: The EURO-FLUX methodology. *Adv. Ecol. Res.* 30: 113-175.
- Bak J (2001) Uncertainties in large scale assessments of critical loads exceedances. *Water, Air and Soil Pollution Focus*, Vol. 1 Nos.: 1-2, 265-280.
- Barrett K, Seland Ø, Foss A, Mylona S, Sandnes H, Styve H, Tarrasón L (1995) European transboundary acidifying air pollution. EMEP/MS-CW Report 1/95, The Norwegian Meteorological Institute, Oslo, Norway.
- Beier C, Gundersen P, Rasmussen L (1992) A new method for estimation of dry deposition of particles based on throughfall measurements in a forest edge. *Atmos. Environ.* 26A: 1553-1559.
- Berg T, Schaug J (eds.) (1994) Proceedings of the EMEP Workshop on the Accuracy of Measurements with WMO sponsored sessions on Determining the Representativeness of Measured Parameters in a Given Grid Square as Compared to Model Calculations, Passau, Germany, 22-26 Nov. 1993.
- Beswick KM, Hargreaves K, Gallagher MW, Choularton TW, Fowler D (1991) Size resolved measurements of cloud droplet deposition velocity to a forest using an eddy correlation technique. *Roy QJ Meteor. Soc.* 117: 623-645.
- Bredemeier M (1988) forest canopy transformation of atmospheric deposition. *Water Air Soil Poll.* 40: 121138.
- CLAG (1997) Deposition fluxes in the United Kingdom: A compilation of the current deposition maps and mapping methods (1992-1994) used for Critical Loads exceedance assessment in the United Kingdom. Critical Loads Advisory Group Sub-group report on Deposition Fluxes. 45 pp. Penicuik: Institute of Terrestrial Ecology.
- Coyle M, Smith RI, Stedman JR, Weston KJ, Fowler D (2002) Quantifying the spatial distribution of surface ozone concentration in the UK. *Atmos. Environ.* 36: 1013-1024.
- Dore AJ, Choularton TW, Fowler D (1992) An improved wet deposition map of the United Kingdom incorporating the topographic dependence of rainfall concentrations. *Atmos. Environ.* 26A: 1375-1381.
- Draaijers GPJ, Erisman JW (1993) Atmospheric sulfur deposition to forest stands - throughfall estimates compared to estimates from inference. *Atmos. Environ.* 27A: 43-55.
- Draaijers GPJ, Erisman JW (1995) A canopy budget model to assess atmospheric deposition from throughfall measurements. *Water Air Soil Pollut.* 85: 2253-2258.
- Draaijers GPJ, van Leeuwen EP, Potma C, van Pul WAJ, Erisman JW (1995) Mapping base cation deposition in Europe on a 10x20 km grid. *Water Air Soil Pollut.* 85: 2389-2394.

- Draaijers GPJ, Erisman JW, Spranger T, Wyers GP (1996a) The application of throughfall measurements. *Atmos. Environ.* 30: 3349-3361.
- Draaijers GPJ, Erisman JW, van Leeuwen NFM, Römer FG, te Winkel BH, Veltkamp AC, Vermeulen AT, Wyers GP (1996b) The impact of canopy exchange on differences observed between atmospheric deposition and throughfall fluxes. *Atmos. Environ.* 31: 387-397.
- Draaijers GPJ, Bleeker A, van der Veen D, Erisman JW, Möls H, Fonteijn P, Geusenbrock M (2001) Field intercomparison of throughfall, stemflow and precipitation measurements performed within the framework of the Pan European Intensive Monitoring Programme of EU/ICP Forests TNO report R2001/140.
- Dragosits U, Theobald MR, Place CJ, Lord E, Webb J, Hill J, ApSimon HM, Sutton MA (2002) Ammonia emission, deposition and impact assessment at the field scale: a case study of sub-grid spatial variability. *Environ. Pollut.* 117: 147-158.
- Duyzer JH, Deinum G, Baak J (1995) The interpretation of measurements of surface exchange of nitrogen oxides; corrections for chemical reactions. *Philosophical Transactions of the Royal Society of London A* 351: 1-18.
- Duyzer J, Nijenhuis B, Weststrate H (2001) Monitoring and modelling of ammonia concentrations and deposition in agricultural areas of the Netherlands. *Water, Air and Soil Pollution Focus*, Vol 1 Nos. 5-6: 131-144.
- EDC (Environmental Data Centre) (1993) Manual for Integrated Monitoring. Programme Phase 1993-1996. National Board of Waters and the Environment, Helsinki.
- Eder BK, Dennis RL (1990) On the use of scavenging ratios for the inference of surface level concentration. *Water Air Soil Pollut.* 52: 197-215.
- Emberson LD, Ashmore MR, Cambridge HM, Simpson D, Tuovinen JP (2000) Modelling stomatal ozone flux across Europe. *Environ. Pollut.* 109: 403-413.
- EMEP/CCC (1996) EMEP Manual for Sampling and Analysis. EMEP/CCC Report 1/95.
- Erisman JW, Draaijers G (1995) Atmospheric deposition in relation to acidification and eutrophication. *Studies in Environmental Science* 63, Elsevier, Amsterdam.
- Erisman JW, van Pul A, Wyers P (1994a) Parameterization of dry deposition mechanisms for the quantification of atmospheric input to ecosystems. *Atmos. Environ.* 28: 2595-2607.
- Erisman JW, Beier C, Draaijers GPJ, Lindberg S (1994b) Review of deposition monitoring methods. *Tellus* 46B: 79-93.
- Erisman JW, Draaijers G, Duyzer J, Hofschreuder P, van Leeuwen N, Römer F, Ruijgrok W, Wyers P (1995) Particle deposition to forests. In: Heij GJ, Erisman JW (eds.): Proceedings of the conference "Acid rain research: do we have enough answers?", 's-Hertogenbosch, The Netherlands, 10-12 Oct. 1994. *Studies in Environmental Science* 64: 115-126.
- Erisman JW, Mennen MG, Fowler D, Flechard CR, Spindler G, Gr?ner A, Duyzer JH, Ruijgrok W, Wyers GP (1998a) Deposition Monitoring in Europe. *Environ. Monit. Assess.* 53: 279-295.
- Erisman JW, Bleeker A, van Jaarsveld H (1998b) Atmospheric deposition of ammonia to semi-natural vegetation in the Netherlands-methods for mapping and evaluation. *Atmos. Environ.* 32: 481-489.
- Ferm M (2001) Validation of a diffusive sampler for ozone in workplace atmospheres according to EN838. Proceedings from International Conference Measuring Air Pollutants by Diffusive Sampling, Montpellier, France 26-28 September 2001: 298-303.
- Ferm M, Svanberg PA (1998) Cost-efficient techniques for urban and background measurements of SO₂ and NO₂. *Atmos. Environ.* 32: 1377-1381.
- Flechard CR, Fowler D (1998) Atmospheric ammonia at a moorland site. II: Long-term surface/atmosphere micrometeorological

- flux measurements. Roy QJ Meteor. Soc. 124: 733-757.
- Flemming J (2003) Immissionsfelder aus Beobachtung, Modellierung und deren Kombination, PhD thesis, Free University Berlin, FB Geowissenschaften (in German).
- Fowler D, Granat L, Koble R, Lovett G, Moldan F, Simmons C, Slanina SJ, Zapletal M (1993) Wet, cloud water and fog deposition. (Working Group report). In: Models and methods for the quantification of atmospheric input to ecosystems, edited by Lovblad G, Erisman JW, Fowler: 912. Copenhagen: Nordic Council of Ministers.
- Fowler D, Jenkinson DS, Monteith JL, Unsworth MH (eds.) (1995a) The exchange of trace gases between land and atmosphere. Proceedings of a Royal Society discussion meeting. Philos. T. Roy. Soc. A 351 (1696), pp. 205-416.
- Fowler D, Leith ID, Binnie J, Crossley A, Inglis DWF, Choularton TW, Gay M, Longhurst JWS, Conland DE (1995b) Orographic enhancement of wet deposition in the United Kingdom: continuous monitoring. Water Air Soil Pollut. 85: 2107-2112.
- Fowler D, Smith RI, Weston KJ (1995c) Quantifying the spatial distribution of surface ozone exposure at the 1kmx1km scale. In: Fuhrer, Achermann (eds.) (1995): 196-205.
- Fowler D, Pitcairn CER, Erisman JW (eds.) (2001a) Air-Surface Exchange of Gases and Particles (2000). Proceedings of the Sixth International Conference on Air-Surface Exchange of Gases and Particles, Edinburgh 3-7 July, 2000. Water Air and Soil Pollution Focus, Vol. 1 Nos. 5-6: 1-464.
- Fowler D, Coyle M, Flechard C, Hargreaves K, Storeton-West R, Sutton M, Erisman JW (2001b) Advances in micrometeorological methods for the measurement and interpretation of gas and particles nitrogen fluxes. Plant Soil 228: 117-129.
- Fowler D, Sutton MA, Flechard C, Cape JN, Storeton-West R, Coyle M, Smith RI (2001c) The Control of SO₂ dry deposition on to natural surfaces and its effects on regional deposition. Water, Air and Soil Pollution Focus, Vol. 1 Nos. 5-6: 39-48.
- Fuhrer J (2002) Ozone impacts on vegetation. Ozone-Sci. Eng. 24: 69-74.
- Gallagher M, Fontan J, Wyers P, Ruijgrok W, Duyzer J, Hummelsh P, Fowler D (1997) Atmospheric Particles and their Interactions with Natural Surfaces. In: Biosphere-Atmosphere Exchange of Pollutants and Trace Substances (ed. Slanina S.): 45-92. Springer-Verlag.
- Gauger Th, Anshelm F, Schuster H, Erisman JW, Vermeulen AT, Draaijers GPJ, Bleeker A, Nagel HD (2003) Mapping of ecosystem specific long-term trends in deposition loads and concentrations of air pollutants in Germany and their comparison with Critical Loads and Critical Levels. Part 1: Deposition Loads 1990-1999. Final Report of Project 29942210. Inst. for Navigation, Stuttgart University and Umweltbundesamt.
- Grunhage L, Haenel HD (1997) Platin (plant-atmosphere interaction) In: A model of plant-atmosphere interaction for estimating absorbed doses of gaseous air pollutants. Environ. Pollut. 98: 37-50.
- Hicks BB, Baldocchi DD, Meyers TP, Matt DR, Hosker Jr RP (1987) A preliminary multiple resistance routine for deriving dry deposition velocities from measured quantities. Water Air Soil Pollut. 36: 311-330.
- Hicks BB, McMillen R, Turner RS, Holdren Jr GR, Strickland TC (1993) A national critical loads framework for atmospheric deposition effects assessment: III. Deposition characterization. Environ. Manage. 17, No.3: 343-353.
- Iversen T (editor) (1991) Comparison of three models for long term photochemical oxidants in Europe. EMEP/MSC-W Report 3/91. The Norwegian Meteorological Institute, Oslo, Norway.
- Loibl W, Smidt S (1996) Ozone exposure - Areas of potential ozone risk for selected tree species. Environ. Sci. Pollut. R. 3: 213-217.

- Lövblad G (1996) In: Knoflacher M, Schneider J, Soja G (eds.): Exceedance of Critical Loads and Levels - Spatial and Temporal Interpretation of Elements in Landscape Sensitive to Atmospheric Pollutants. Report from a UNECE Workshop held in Vienna, Austria, 22-24 November 1995. Federal Ministry for Environment, Youth and Family, Austria, Conference Papers 15: 236.
- Lövblad G, Erisman JW (1992) Deposition of Nitrogen in Europe. Background document; In Grennfelt P, Thörnelöf E (eds.) (1992) Critical Loads for Nitrogen; report from a workshop held at Lökeberg, Sweden, 6-10 April 1992. Nord 1992: 41.
- Lövblad G, Erisman JW, Fowler D (eds.) (1993) Models and Methods for the Quantification of Atmospheric Input to Ecosystems. Proceedings of an international workshop on the deposition of acidifying substances, Göteborg 4-6 November 1992. Nordiske Seminar- og Arbejdsrapporter 1993: 573, Nordic Council of Ministers.
- Lövblad G, Grennfelt P, Kärenlampi L, Laurila T, Mortensen L, Ojanperä K, Pleijel H, Semb A, Simpson D, Skärby L, Tuovinen JP, Tørseth K (1996) Ozone exposure mapping in the Nordic Countries, Report from a Nordic cooperation project financed by the Nordic Council of Ministers, Report Tema Nord 1996: 528.
- Lyman J, Fleming RH (1940) Composition of sea water. *Journal of Marine Research* 3: 134-146.
- Nemitz E, Milford C, Sutton MA (2001) A two-layer canopy compensation point model for describing bi-directional biosphere-atmosphere exchange of ammonia. *Roy QJ Meteor. Soc.* 127: 815-833.
- PORG (1997) Ozone in the UK. Fourth report of the Photochemical Oxidants Review Group. 234pp. DETR (ITE Edinburgh).
- RGAR (1997) Acid Deposition in the United Kingdom 1992-1994. Fourth Report of the Review Group on Acid Rain. 176 pp. HMSO, London.
- Ruijgrok W, Tieben H, Eisinga P (1996) The dry deposition of particles to a forest canopy: a comparison of model and experimental results. *Atmos. Environ.* 31: 399-415.
- Schaug, J., Iversen, T. and Pedersen, U. (1993): Comparison of measurements and model results for airborne sulfur and nitrogen components with Kriging. *Atmos. Environ.*, 27A, 831-844.
- Schjoerring JK, Husted S, Mattsson M (1998) Physiological parameters controlling plant-atmosphere ammonia exchange. *Atmos. Environ.* 32: 491-498.
- Singles R, Sutton MA, Weston KJ (1998) A multi-layer model to describe the atmospheric transport and deposition of ammonia in Great Britain. *Atmos. Environ.* 32: 393-399.
- Sjöberg K, Lövblad G, Ferm M, Ulrich E, Cecchini S, Dalstein L (2001) Ozone measurements at forest plots using diffusive samplers. Proc. from International Conference Measuring Air Pollutants by Diffusive Sampling, Montpellier, France 26-28 September 2001. p116-123.
- Slanina S ed. (1997) Biosphere-Atmosphere Exchange of Pollutants and Trace Substances. Springer-Verlag.
- Slinn WGN (1982) Predictions for particle deposition to vegetative surfaces. *Atmos. Environ.* 16: 1785-1794.
- Smith RI, Fowler D (2001) Uncertainty in estimation of wet deposition of sulphur. *Water, Air and Soil Pollution Focus*, Vol 1. Nos. 5-6: 341-354.
- Smith RI, Fowler D, Bull KR (1995) Quantifying the scale dependence in estimates of wet and dry deposition and the implication for critical load exceedances. In: Heij GJ, Erisman JW (eds.): Proceedings of the conference "Acid rain research: do we have enough answers?", 's-Hertogenbosch, The Netherlands, 10-12 Oct. 1994. *Studies in Environmental Science* 64: 175-186.
- Smith RI, Fowler D, Sutton MA, Flechard C, Coyle M (2000) Regional estimation of pollutant gas dry deposition in the UK: model description, sensitivity analyses and outputs. *Atmos. Environ.* 34: 3757-3777.

- Spranger T (1992) Erfassung und ökosystemare Bewertung der atmosphärischen Deposition und weiterer oberirdischer Stoffflüsse im Bereich der Bornhöveder Seenkette. Ph.D. thesis, Christian-Albrechts Universität, Kiel, Germany (in German).
- Spranger T, Kunze F, Gauger Th, Nagel HD, Bleeker A, Draaijers GPJ (2001) Critical Loads exceedances in Germany and their dependence on the scale of input data. *Water, Air and Soil Pollution Focus*, Vol. 1 Nos. 1-2: 335-351.
- Stedman JR, Vincent KJ, Campbell GW, Goodwin JW, Downing CEH (1997) New high resolution maps of estimated background ambient Nox and NO₂ concentrations in the UK. *Atmos. Environ.* 31: 3591-3602.
- Sutton MA, Lee DS, Dollard GJ, Fowler D (eds.) (1998): International conference on atmospheric ammonia: emission, deposition and environmental impacts. *Atmos. Environ.* 32: 269-594.
- Sutton MA, Nemitz E, Fowler D, Wyers GP, Otjes RP, Schjoerring JK, Husted S, Nielsen KH, San José, Moreno J, Gallagher MW, Gut A (2000) Fluxes of ammonia over oilseed rape Overview of the EXAMINE experiment. *Agr. Forest Meteorol.* 105: 327-349.
- Sutton MA, Miners B, Tang YS, Milford C, Wyers GP, Duyzer JH, Fowler D (2001a) Comparison of low-cost measurement techniques for long-term monitoring of atmospheric ammonia. *J. Environ. Monitor.* 3: 446-453.
- Sutton MA, Tang YS, Dragosits U, Fournier N, Dore T, Smith RI, Weston KJ, Fowler D (2001b) A spatial analysis of atmospheric ammonia and ammonium in the UK. *The Scientific World*, 1 (S2): 275-286.
- Sverdrup H, De Vries W, Hornung M, Cresser M, Langan S, Reynolds B, Skeffington R, Robertson W (1995) Modification of the simple mass-balance equation for calculation of critical loads of acidity. In: Hornung M, Sutton MA, Wilson RB (eds.) *Mapping and modelling of critical loads for nitrogen: a Workshop Report*, Grange-over-Sands, October 1994. Penicuik: Institute of Terrestrial Ecology: 87-92.
- Sverdrup HU, Johnson MW, Fleming RH (1946) *The Oceans - Their Physics Chemistry and General Biology*. Prentice-Hall, New York, 1087 pp.
- UBA (1996) *Manual on Methodologies and Criteria for Mapping Critical Levels/Loads and geographical areas where they are exceeded*. UBA-Texte 71/96.
- Ulrich B (1983) Interaction of forest canopies with atmospheric constituents: SO₂, alkali and earth alkali cations and chloride. In: Ulrich B, Pankrath J (eds.): *Effects of accumulation of air pollutants in forest ecosystems*: 33-45.
- UNECE ICP Forests (1999) *Manual on methods and criteria for harmonized sampling, assessment, monitoring and analysis of the effects of air pollution on forests. Part VI: Measurement of Deposition and Air Pollution*.
- van Leeuwen EP, Erisman JW, Draaijers GPJ, Potma CJM, van Pul WAJ (1995) *European wet deposition maps based on measurements*. Report No. 722108006, National Institute of Public Health and Environmental Protection, Bilthoven, The Netherlands.
- van Pul WAJ, Potma C, van Leeuwen E, Draaijers G, Erisman JW (1995): *EDACS: European deposition maps of acidifying components on a small scale. Model description and preliminary results*. RIVM Report no. 722401005, Bilthoven, The Netherlands.
- Walton S, Gallagher MW, Duyzer JH (1997) Use of a detailed model to study the exchange of Nox and O₃ above and below a deciduous canopy. *Atmos. Environ.* 31: 2915-2932.

Who do you ask for further advice ?

For questions on please contact:

EMEP long-range transport models:

Erik Berge, The Norwegian Meteorological Institute, P.O. Box 43 - Blindern, N - 0313 Oslo, Norway, Tel. +47 2296 - 3000; Fax. +47 2296 - 3050

High resolution modelling of dry and cloud/fog deposition, combination with maps of interpolated wet deposition:

Jan-Willem Erisman, RIVM-LLO, P.O. Box 1, 3720 BA Bilthoven, The Netherlands, Tel. +31-30-274-2824; Fax. +31-30-2287531
David Fowler, Centre for Ecology and Hydrology, Bush Estate, Penicuik, Midlothian, EH26 0QB, United Kingdom, Tel. +44-131-445-4343; Fax. +44-131-445-3943

Combination of high-resolution models with long-range transport models:

Jan-Willem Erisman, RIVM-LLO, P.O. Box 1, 3720 BA Bilthoven, The Netherlands; Tel. +31-30-274-2824; Fax. +31-30-2287531
Erik Berge, The Norwegian Meteorological Institute, P.O. Box 43 - Blindern, N - 0313 Oslo, Norway, Tel. +47 2296 3000; Fax. +47 2296 3050

Measurement and interpolation methodology (Ambient air concentrations, wet and bulk deposition):

EMEP CCC, NILU, Postbox 100, N-2007 Kjeller, Norway, Tel. +47-6389-8000; Fax. +47-6389-8050

Evaluating total deposition maps with throughfall measurements:

Gun Lövblad, Swedish Environmental Research Institute, Box 47086, 40258 Göteborg, Sweden; Tel. +46-31-725 6240, Fax. +46-31- 725 6290, gun.lovblad@ivl.se
Jan-Willem Erisman, RIVM-LLO, P.O. Box 1, 3720 BA Bilthoven, The Netherlands; Tel +31-30-274-2824; Fax +31-30-2287531

Diffusive samplers for air pollution monitoring:

Martin Fern, Swedish Environmental Research Institute, Box 47086, 40258 Göteborg, Sweden; Tel. +46-31-725 6224, Fax. +46-31-725 6290 martin.fern@ivl.se

General information on mapping exercises can also be obtained by contacting the Coordination Center for Effects, CCE, Netherlands: Jean-Paul Hettelingh, Tel. +31-30-74 30 48; Fax. +31-30-74 29 71

General information on modelling:

Ron Smith, Centre for Ecology and Hydrology, Bush Estate, Penicuik, Midlothian EH26 0QB, Tel. +44 131 445 4343; Fax. +44 131 445 3943

General information on NO_x, NO₃:

Kim Pilegaard, Riso National Laboratory, PO Box 49, DK-4000 Roskilde, Denmark Tel. +45 4677 4677, Fax. +45 4677 4160
Jan Duyzer, TNO-MEP, Postbus 342, 7300 AH, Apeldoorn, The Netherlands, Tel. +31 55 549 3944; Fax. +31 55 549 3252

Mapping Manual 2004

International Cooperative Programme on Effects of Air Pollution on Natural Vegetation and Crops



Photo: The ICP Vegetation Experiments at Cadenazzo, Switzerland (Photo by J Fuhrer).

UNECE CONVENTION ON LONG-RANGE TRANSBOUNDARY AIR POLLUTION

International Cooperative Programme on Effects of Air Pollution on Natural Vegetation and Crops

<http://icpvegetation.ceh.ac.uk>

Chairperson: Dr Harry Harmens, CEH Bangor, UK

The ICP Vegetation is an international programme investigating the impacts of pollutants, primarily ozone, on crops and natural vegetation in Europe and North-America. Accumulation of heavy metals following the deposition of particulates on to vegetation is also being considered.

Chapter 3 was compiled and edited by G. Mills (ICP Vegetation Coordination Centre, UK) using text provided by (in alphabetical order):

M.Ashmore (UK),
V.Bermejo (Spain),
M.Broadmeadow (UK),
H.Danielsson (Sweden),
L.Emberson (UK),
J.Fuhrer (Switzerland),
B.Gimeno (Spain),
M.Holland (UK),
P.E.Karlsson (Sweden),
G.Mills (UK),
G.Pihl Karlsson (Sweden),
H.Pleijel (Sweden) and
D.Simpson (EMEP).

Additional editorial advice was provided by S.Braun (Switzerland), H.Harmens (ICP Vegetation Coordination Centre, UK), M.Johansson (UNECE), U.Lorenz (ICP Modelling and Mapping), M.Posch (CCE), T.Spranger (ICP Modelling and Mapping) and A.Vipond (UK).

3.1 General remarks and objectives

The purpose of this chapter is to provide information on the critical levels for sensitive vegetation and how to calculate critical level exceedance. Methods for mapping pollutant concentrations, deposition and exceedance are provided elsewhere (Chapter 2).

Excessive exposure to atmospheric pollutants has harmful effects for a variety of vegetation. Critical levels are described in different ways for different pollutants, including mean concentrations, cumulative exposures and fluxes through plant stomata. The effects considered significant here vary between receptor and pollutant and include growth changes, yield losses, visible injury and reduced seed production. The receptors are generally divided into five major categories: agricultural crops, horticultural crops, semi-natural vegetation, natural vegetation and forest trees. However, for some pollutants, e.g. ozone, semi-natural vegetation and natural vegetation have been grouped together under the name (semi-) natural vegetation.

Critical levels were defined in the previous version of this manual (UNECE, 1996) as “the atmospheric concentrations of pollutants in the atmosphere above which adverse effects on receptors, such as human beings, plants, ecosystems or materials, may occur according to present knowledge”. For this revised chapter, the critical levels for vegetation are defined as the “concentration, cumulative exposure or cumulative stomatal flux of atmospheric pollutants above which direct adverse effects on sensitive vegetation may occur according to present knowledge”. Critical level exceedance maps show the difference between the critical level and the mapped, monitored or modelled air pollutant concentration, cumulative exposure or cumulative flux.

The critical level values have been set, reviewed and revised for O_3 , SO_2 , NO_2 and NH_3 at a series of UNECE Workshops: Bad Harzburg (1988); Bad Harzburg (1989);

Egham (1992; Ashmore and Wilson, 1993); Bern (1993; Fuhrer and Achermann, 1994); Kuopio (1996; Kärenlampi and Skärby, 1996), Gerzensee (1999; Fuhrer and Achermann, 1999) and Gothenburg (2002; Karlsson, Selldén and Pleijel, 2003).

For SO_2 , NO_x and NH_3 , recommendations are made for concentration-based critical levels. For ozone, separate cumulative concentration-based (previously described as level I) and cumulative stomatal flux-based (previously described as level II) critical levels are described which use different scientific bases of risk assessment, as explained in Section 3.3. Since the previous version of this manual was published (UNECE, 1996), much progress has been made with the critical levels for ozone and this chapter provides an in-depth description of the critical levels, their scientific bases and how to calculate exceedance. As part of this progress, it was agreed that the level I and level II terminology is no longer appropriate to describe critical levels for ozone and these terms are not used in this chapter.

3.2 Critical levels for SO_2 , NO_x , NH_4 and O_3

3.2.1 SO_2

The critical levels for SO_2 that were established in Egham in 1992 (Ashmore and Wilson, 1993) are still valid (Table 3.1). There are critical levels for four categories of receptors – for sensitive groups of lichens, for forest ecosystems, (semi-) natural vegetation and agricultural crops. These critical levels have been adopted by WHO (2000).

Exceedance of the critical level for (semi-) natural vegetation, forests, and, when appropriate, agricultural crops occurs when either the annual mean concentration or the winter half-year mean concentration is greater than the critical level; this is because of the greater impact of SO_2 under winter conditions.

Table 3.1: Critical levels for SO_2 ($\mu\text{g m}^{-3}$) by vegetation category

Vegetation Types	Critical Level SO_2 ($\mu\text{g m}^{-3}$)	Time Period
Cyanobacterial lichens	10	Annual mean
Forest ecosystems*	20	Annual mean and half-year (October-March) mean
(Semi-) natural vegetation	20	Annual mean and half-year (October-March) mean
Agricultural crops	30	Annual mean and half-year (October-March) mean

*The forest ecosystem includes the response of the understorey vegetation.

3.2.2 NO_x

The critical levels for NO_x are based on the sum of the NO and NO_2 concentrations because there is insufficient knowledge to establish separate critical levels for the two

pollutants, although some evidence indicates that at low concentrations typical of ambient conditions, NO is more phytotoxic than NO_2 . Since the type of response varies from a fertilizer effect to toxicity depending on concentration, all effects were considered to be adverse. Growth stimulations were of greatest concern for (semi-) natural vegetation because of the likelihood of changes in interspecific competition.

Separate critical levels were not set for classes of vegetation because of the lack of available information. However, the following ranking of sensitivity was established:

(semi-) natural vegetation > forests > crops

Critical levels for NO_x were first established in 1992 at the Egham workshop. The background papers on NO_x and NH_3 presented at the Egham workshop (Ashmore & Wilson, 1993) were further developed as the basis of the Air Quality Guidelines for Europe,

published by WHO in 2000. This further analysis incorporated a formal statistical model to identify concentrations to protect 95% of species at a 95% confidence level. In this re-analysis, growth stimulation was also considered as a potentially adverse

ecological effect. Furthermore, a critical level based on 24h mean concentrations was considered to be more effective than one based on 4h mean concentrations as included in the previous version of the Mapping Manual (UNECE, 1996). Since the WHO guidelines were largely based on analysis extending the background information presented at the Egham workshop, the critical levels in Table 3.2, which are identical to those of WHO (2000), should now be used. For application for mapping critical levels and their exceedance, it is strongly recommended that only the annual mean values are used, as mapped and modelled values of this parameter have much greater reliability, and the long-term effects of NO_x are thought to be more significant than the short-term effects.

Table 3.2: Critical levels for NO_x (NO and NO_2 added), expressed as NO_2 ($\mu g m^{-3}$)

Vegetation type	Critical level NO_x (expressed as $NO_2 \mu g m^{-3}$)	Time period
All	30	Annual mean
All	75	24-hour mean

Some biochemical changes may occur at concentrations lower than the critical levels, but there is presently insufficient evidence to interpret such effects in terms of critical levels.

3.2.3 NH_3

The fertilisation effect of NH_3 can in the longer term lead to a variety of adverse effects, including growth stimulation and increased susceptibility to abiotic (drought, frost) and biotic stresses. In the short-term there are also direct effects. As for NO_x , for application for mapping critical levels and their exceedance, it is strongly recommended that only the annual mean values of NH_3 are used, as mapped and modelled values of

this parameter have much greater reliability, and the long-term effects of NH_3 are thought to be more significant than the short-term effects.

The critical levels in Table 3.3 refer to all vegetation types, including the most sensitive. The aim of the critical levels defined is to protect the functioning of plants and plant communities. The following distinction in receptor sensitivity is proposed:

(semi-) natural vegetation > forests > crops

As for NO_x , the Air Quality Guidelines for Europe for NH_3 (WHO, 2000) were based on background papers developing information presented at the Egham workshop. Therefore, the critical levels for NH_3 are now those proposed by WHO (2000), in which the previous values for averaging times of 1 hour and 1 month have been deleted.

Table 3.3: Critical levels for NH_3 ($\mu g m^{-3}$)

Vegetation type	Critical level NH_3 ($\mu g m^{-3}$)	Time period
All	8	Annual mean
All	270	24-hour mean

3.2.4 O_3

Three cumulative exposure approaches are used to define critical levels for ozone: stomatal fluxes, ozone concentrations and vapour-pressure deficit-modified ozone concentrations. Each approach uses the ozone concentration at the top of the canopy and incorporates the concept that the effects of ozone are cumulative and values are summed over a defined time period. In each case, a specific threshold is used and only ozone concentrations, vapour-pressure deficit-modified ozone concentrations or instantaneous stomatal fluxes above that threshold are summed. When the sum of the values above the threshold exceeds the

critical value defined in the relevant table for each approach and vegetation type, then the critical level for that approach and vegetation type has been exceeded.

The previous version of this manual (UNECE, 1996) included concentration-based critical levels that used *AOTX* (ozone concentrations accumulated over a threshold of X ppb) as the ozone parameter. However, several important limitations and uncertainties have been recognised for using *AOTX*. In particular, the real impacts of ozone depend on the amount of ozone reaching the sites of damage within the leaf, whereas *AOTX*-based critical levels only consider the ozone concentration at the top of the canopy. The Gerzensee Workshop in 1999, recognised the importance of developing an alternative critical level approach based on the flux of ozone from the exterior of the leaf through the stomatal pores to the sites of damage (stomatal flux). This approach required the development of mathematical models to estimate stomatal flux, primarily from knowledge of stomatal responses to environmental factors. It was agreed at the Gothenburg Workshop in November 2002 that ozone flux-effect models were sufficiently robust for the derivation of flux-based critical levels, and such critical levels should be included in this revised Manual for wheat, potato and provisionally for beech.

To accommodate these different approaches, the terminology and symbols used in describing critical levels of ozone have been revised and are described in Table 3.4 and the critical levels are provided in Table 3.5. For guidance on the selection of critical levels and which methods to use, a flow chart is provided in Figure 3.1. The scientific bases of these critical levels are provided in Section 3.3 and methods for calculating exceedance are in Sections 3.4 and 3.5. The three approaches can be summarised as follows:

Stomatal flux-based critical levels (CL_{ef}) for ozone take into account the varying influences of temperature, water vapour pressure deficit (*VPD*), light (irradiance), soil water potential

(*SWP*), ozone concentration and plant development (phenology) on the stomatal flux of ozone. They therefore provide an estimate of the critical amount of ozone entering through the stomata and reaching the sites of action inside the plant. This is an important new development in the derivation of critical levels because, for example, for a given ozone concentration, the stomatal flux in warm, humid conditions with moist soil can be much greater than that in hot, dry conditions with dry soil because the stomatal pores will be more widely open. Concentration-based critical levels do not differentiate between such climatic conditions and would not indicate the increased risk of damage in warm, humid conditions. The hourly mean stomatal flux of ozone based on the projected leaf area (*PLA*), F_{st} (in $nmol\ m^{-2}\ PLA\ s^{-1}$), is accumulated over a stomatal flux threshold of $Y\ nmol\ m^{-2}\ s^{-1}$. The accumulated stomatal flux of ozone above a flux threshold of Y ($AF_{st}Y$), is calculated for the appropriate time-window as the sum over time of the differences between hourly mean values of F_{st} and $Y\ nmol\ m^{-2}\ PLA\ s^{-1}$ for the periods when F_{st} exceeds Y . The stomatal flux-based critical level of ozone, $CL_{ef}\ nmol\ m^{-2}\ PLA$, is then the cumulative stomatal flux of ozone, $AF_{st}Y$, above which direct adverse effects may occur according to present knowledge. Values of CL_{ef} have been identified for some crops (wheat and potato) and provisionally for sensitive forest trees (represented by birch and beech). This approach cannot yet be applied to (semi-) natural vegetation.

Concentration-based critical levels (CL_c) for ozone use the concentration at the top of the canopy accumulated over a threshold concentration for the appropriate time-window and

thus do not take account of the stomatal influence on the amount of ozone entering the plant. This value is expressed in units of $ppm\ h$ ($\mu mol\ mol^{-1}\ h$). The term $AOTX$ (concentration accumulated over a threshold ozone concentration of X ppb) has been adopted for this index; in this manual "X" is either 30 or 40 ppb for $AOT30$ and $AOT40$ respectively. Values of CLe_c are defined for agricultural and horticultural crops, forests and (semi-) natural vegetation.

VPD-modified concentration-based critical levels take into account the modifying influence of VPD on the stomatal flux of ozone by multiplying the hourly mean ozone concentration at the top of the canopy by an f_{VPD} factor to get the VPD -modified ozone concentration ($[O_3]_{VPD}$). The $[O_3]_{VPD}$ is accumulated over a threshold concentration during daylight hours over the appropriate time-window. This value is expressed in units of $ppm\ h$ ($\mu mol\ mol^{-1}\ h$). The term $AOT30_{VPD}$ (VPD -modified concentration accumulated over a threshold ozone concentration of 30 ppb) has been adopted for this index; this index is only used to define the short-term critical level for the development of visible injury on crops.

this approach. Further validation and development of the methodology may be possible under the framework of ICP Forests. A brief description of the MPOC approach is provided in Chapter 3, Annex 1.

It should be noted that consideration was given at the Gothenburg Workshop (November 2002) to a fourth approach, the Maximum Permissible Ozone Concentration (MPOC) (Krause *et al.*, 2003). The MPOC approach could possibly be adopted as an additional concentration-based index for mapping potential risk in national evaluations, but should not be used for mapping purposes at the European scale. This approach was considered as potentially useful in the context of forest trees, but not for (semi-) natural vegetation and crops. Economic losses attributable to ozone pollution could not be estimated on the basis of

3 Mapping Critical Levels for Vegetation

Table 3.4: Terminology for critical levels of ozone

Term	Abbreviation	Units	Explanation
Terms for concentration-based critical levels			
Concentration accumulated over a threshold ozone concentration of X ppb	AOTX	ppm h	The sum of the differences between the hourly mean ozone concentration (in ppb) and X ppb when the concentration exceeds X ppb during daylight hours, accumulated over a stated time period. Units of ppb and ppm are parts per billion (nmol mol^{-1}) and parts per million ($\mu\text{mol mol}^{-1}$) respectively, calculated on a volume/volume basis.
Concentration-based critical level of ozone	CLe_c	ppm h	AOTX over a stated time period, above which direct adverse effects on sensitive vegetation may occur according to present knowledge.
Concentration accumulated over a threshold ozone concentration of X ppb modified by vapour pressure deficit (VPD)	AOTX_{VPD}	ppm h	The sum of the differences between the hourly mean ozone concentration (in ppb) modified by a vapour pressure deficit factor ($[\text{O}_3]_{\text{VPD}}$), and X ppb when the concentration exceeds X ppb during daylight hours, accumulated over a stated time period.
Terms for flux-based critical levels			
Projected leaf area	PLA	m^2	The projected leaf area is the total area of the sides of the leaves that are projected towards the sun. PLA is in contrast to the total leaf area, which considers both sides of the leaves. For flat leaves the total leaf area is simply $2 \times \text{PLA}$.
Stomatal flux of ozone	F_{st}	$\text{nmol m}^{-2} \text{PLA s}^{-1}$	Instantaneous flux of ozone through the stomatal pores per unit projected leaf area (PLA). F_{st} can be defined for any part of the plant, or the whole leaf area of the plant, but for this manual, F_{st} refers specifically to the sunlit leaves at the top of the canopy. F_{st} is normally calculated from hourly mean values and is regarded here as the hourly mean flux of ozone through the stomata.
Stomatal flux of ozone above a flux threshold of $Y \text{ nmol m}^{-2} \text{PLA s}^{-1}$	$F_{\text{st}} Y$	$\text{nmol m}^{-2} \text{PLA s}^{-1}$	Instantaneous flux of ozone above a flux threshold of $Y \text{ nmol m}^{-2} \text{s}^{-1}$, through the stomatal pores per unit projected leaf area. $F_{\text{st}} Y$ can be defined for any part of the plant, or the whole leaf area of the plant, but for this manual $F_{\text{st}} Y$ refers specifically to the sunlit leaves at the top of the canopy. $F_{\text{st}} Y$ is normally calculated from hourly mean values and is regarded here as the hourly mean flux of ozone through the stomata.
Accumulated stomatal flux of ozone above a flux threshold of $Y \text{ nmol m}^{-2} \text{PLA s}^{-1}$	$\text{AF}_{\text{st}} Y$	$\text{mmol m}^{-2} \text{PLA}$	Accumulated flux above a flux threshold of $Y \text{ nmol m}^{-2} \text{s}^{-1}$, accumulated over a stated time period during daylight hours. Similar in concept to AOTX.
Flux-based critical level of ozone	CLe_f	$\text{mmol m}^{-2} \text{PLA}$	Accumulated flux above a flux threshold of $Y \text{ nmol m}^{-2} \text{s}^{-1}$ ($\text{AF}_{\text{st}} Y$), over a stated time period during daylight hours, above which direct adverse effects may occur on sensitive vegetation according to present knowledge.

Table 3.5: Critical levels for ozone. The methods for calculating each critical level are described in Sections 3.4 and 3.5.

Approach		Crops	(Semi-) natural vegetation	Forest trees
Stomatal flux-based critical level	CL _{ef}	<i>Wheat</i> : An AF _{st} 6 of 1 mmol m ⁻² PLA <i>Potato</i> : An AF _{st} 6 of 5 mmol m ⁻² PLA	Not available	<i>Birch and beech</i> : Provisionally AF _{st} 1.6 of 4 mmol m ⁻² PLA
	Time period	<i>Wheat</i> : Either 970°C days, starting 270°C days before mid-anthesis (flowering) or 55 days starting 15 days before mid-anthesis <i>Potato</i> : Either 1130°C days starting at plant emergence or 70 days starting at plant emergence		One growing season
	Effect	Yield reduction		Growth reduction
Concentration-based critical level	CL _{ec}	<i>Agricultural crops</i> : An AOT40 of 3 ppm h <i>Horticultural crops</i> : An AOT40 of 6 ppm h	An AOT40 of 3 ppm h	An AOT40 of 5 ppm h
	Time period	<i>Agricultural crops</i> : 3 months <i>Horticultural crops</i> : 3.5 months	3 months (or growing season, if shorter)	Growing season
	Effect	Yield reduction for both agricultural and horticultural crops	Growth reduction in perennial species and growth reduction and/or seed production in annual species	Growth reduction
VPD-modified concentration-based critical level	CL _{ec}	An AOT30 _{VPD} of 0.16 ppm h	Not available	Not available
	Time period	Preceding 8 days		
	Effect	Visible injury to leaves		

Note: The recommendations of the Gothenburg Workshop (2002), the 16th Task Force Meeting of the ICP Vegetation and the 17th Task Force Meeting of the ICP Modelling and Mapping were:

For agricultural crops: use stomatal flux-based critical levels based on AF_{st}6 if the necessary inputs are available for a quantitative assessment of impacts on wheat and potato, and the AOT40-based critical level to assess the risk of yield reduction if only ozone concentration is available and a risk assessment for all crops is needed. The AOT30_{VPD} critical level should be used to assess the risk of visible ozone injury and

cannot be used to indicate the risk of yield reduction.

For horticultural crops: use the AOT40-based critical level to assess the risk of effects on yield. The AOT30_{VPD} critical level should be used to assess the risk of visible ozone injury and cannot be used to indicate the risk of yield reduction.

For (semi-) natural vegetation: use the AOT40-based critical level.

For forest trees: use the AOT40-based critical level to assess the risk of growth reduction. The provisional stomatal flux-based critical level is provided for guidance only.

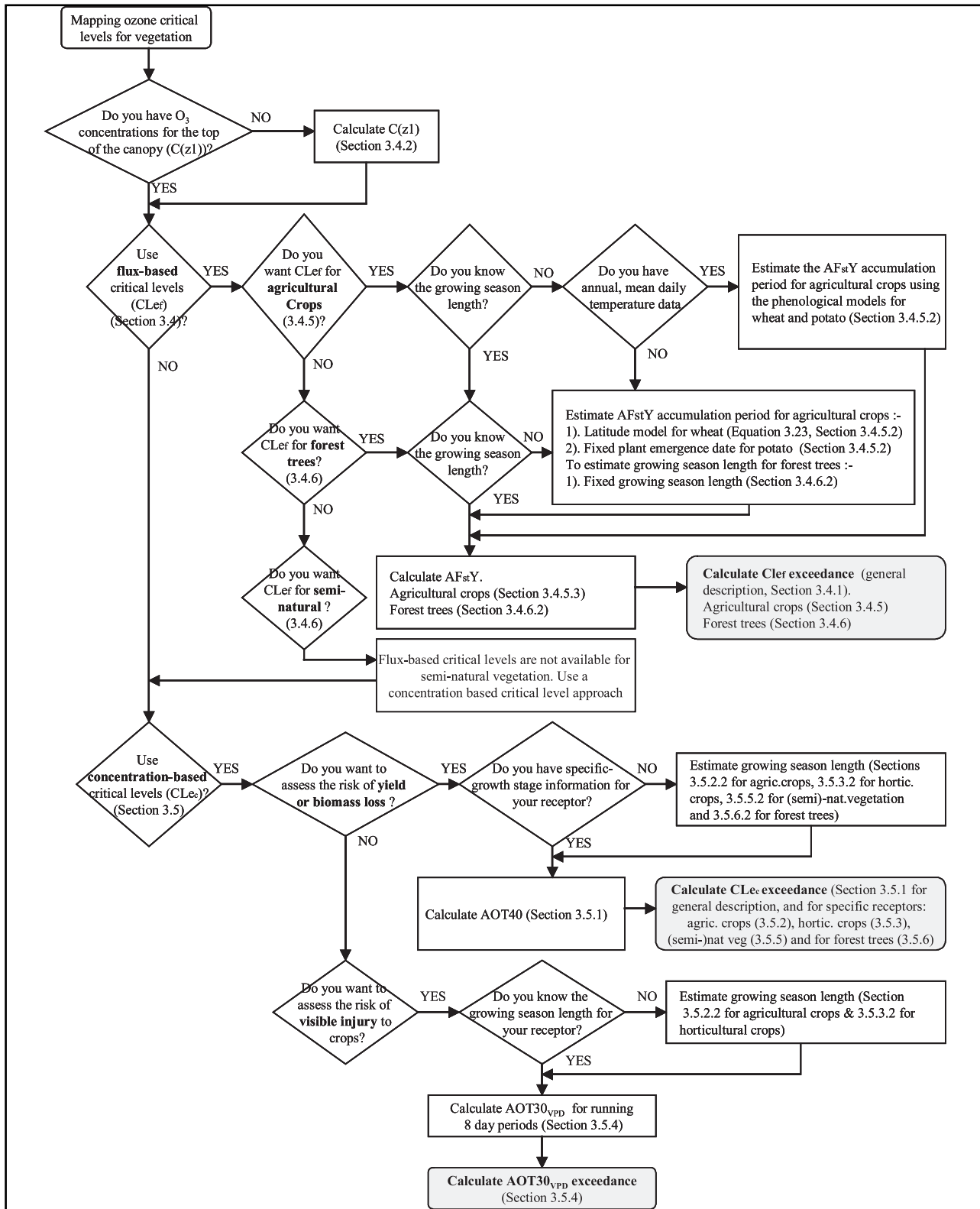


Figure 3.1: A schematic diagram illustrating the steps involved in calculating exceedance of the flux-based and concentration-based critical levels of ozone for agricultural and horticultural crops, (semi-) natural vegetation and forest trees.

3.3 Scientific bases of the critical levels for ozone

3.3.1 Crops

3.3.1.1 Crop sensitivity to ozone

Table 3.6 provides an indication of the relative sensitivity to ozone of a wide range of agricultural and horticultural crops. This table was derived from a comprehensive review of over 700 published papers on crop responses to ozone leading to the derivation of response-functions for 19 crops (Mills *et al.*, 2003). Data were included only where ozone conditions were recorded as 7h, 8h or 24h means or *AOT40*, and exposure to ozone occurred for a whole growing season using field-based exposure systems. The yield data presented in the published papers ranged from “% of control treatment” to “t ha⁻¹” and were all converted to the yield relative to that in the charcoal-filtered air treatment. Where the data were published as 7h or 8h means, data points were omitted from the analysis if the O_3 concentration exceeded 100 ppb (considered to be outside the normal range for Europe). Data were converted to *AOT40* using a function derived from the ICP Vegetation ambient ozone database (Mills *et al.*, 2003). Dose-response functions were derived for each crop using linear regression.

The crops were ranked in sensitivity to ozone by determining the *AOT40* associated with a 5% reduction in yield. Wheat, pulses, cotton and soybean were the most sensitive of the agricultural crops, with several horticultural crops such as tomato and lettuce

being of comparable sensitivity. Crops such as potato and sugar beet that have green foliage throughout the summer months were classified as moderately sensitive to ozone. In contrast, important cereal crops such as maize and barley can be considered to be moderately resistant and insensitive to ozone respectively.

3.3.1.2 Stomatal flux-based critical levels for yield reduction in wheat and potato

At the workshop in Gothenburg, November 2002, it was concluded that for the time being, it is only possible to derive flux-based ozone critical levels for the crops of wheat and potato. Ozone fluxes through the stomata of leaves found at the top of the canopy are calculated using a multiplicative algorithm based on the methodology described by Emberson *et al.* (2000b). The stomatal flux algorithm used within the EMEP ozone deposition module is described in Section 3.4.4.

The index $AF_{st}Y$ is used to quantify the flux of ozone through the stomata of the uppermost leaf level that is directly exposed to solar radiation and thus no calculation of light exclusion, caused by the filtering of light through the leaves of the canopy, is required. The sunlit leaf level has the largest gas exchange in terms of net photosynthesis (i.e. contributes most strongly to yield) and ozone flux, both because it receives most solar radiation and because it is least senescent. Thus, the ozone flux is expressed as the cumulative stomatal flux per unit sunlit leaf area in order to reflect the influence of ozone on the fraction of the leaf area which is most important for yield.

Table 3.6: The range of sensitivity of agricultural and horticultural crops to ozone (see Mills *et al.*, 2003 for response functions and definition of sensitivities)

Sensitive	Moderately sensitive	Moderately resistant	Insensitive
Cotton, Lettuce, Pulses, Soybean, Salad Onion, Tomato, Turnip, Watermelon, Wheat	Potato, Rapeseed, Sugarbeet, Tobacco	Broccoli, Grape, Maize, Rice	Barley, Fruit (plum & strawberry)

In deriving relationships between the relative yield and the stomatal flux of ozone in wheat and potato, it has been observed that the best correlations between effect and accumulated stomatal flux are obtained when using a stomatal flux threshold (Y) (Danielsson *et al.*, 2003; Pleijel *et al.*, 2002). The strongest relationships between yield effects and $AF_{st}Y$ were obtained using $Y = 6 \text{ mmol m}^{-2} \text{ s}^{-1}$ for both wheat and potato. In effect, this means that ozone exposure started to contribute to $AF_{st}Y$ at an ozone concentration at the top of the crop canopy of approximately 22 ppb for wheat and at approximately 14 ppb for potato if the stomatal conductance was at its maximum. In the case of lower conductance, which prevails in most situations, a higher ozone concentration than 22 ppb and 14 ppb is required to contribute to $AF_{st}6$ for wheat and potato, respectively. The threshold of 6 provides the highest r^2 value for the relationship between yield reduction and $AF_{st}Y$ for all of the thresholds tested for both crops. For example, for wheat the r^2 values were 0.51, 0.74, 0.83 and 0.77 for $Y = 0, 3, 6$ and 9 respectively, whilst for potato, the r^2 values were 0.6, 0.72, 0.76 and 0.75 for $Y = 0, 3, 6$ and 9 respectively.

Based on the combination of data from a number of open-top chamber experiments with field-grown crops performed in several European countries, relationships between relative yield (RY) and stomatal ozone flux (F_{st}) have been derived using the principles introduced by Fuhrer (1994) to calculate relative yield. A relative yield of 1 represents the absence of ozone effects. In the case of wheat, thirteen experiments with field-grown wheat exposed to different ozone levels in open-top chambers from four different countries (Belgium, Finland, Italy and Sweden), representing five cultivars (Minaret, Dragon, Drabant, Satu and Duilio) were used, and for potato seven experiments from four different countries (Belgium, Denmark, Finland, and Sweden) were included, representing one commonly grown cultivar (Bintje) (Pleijel *et al.*, 2003).

In order to derive response relationships which are consistent with the ozone deposi-

tion module of the EMEP model (Emberson *et al.*, 2000b), the parameterisations of the conductance model presented in Pleijel *et al.* (2002, 2003) and Danielsson *et al.* (2003) were revised to achieve a full compatibility with the EMEP model calibration. The resulting algorithms and their parameterisation are presented in Sections 3.4.4 and 3.4.5. This revision resulted in stronger correlations between relative yield and $AF_{st}Y$ for both wheat (a change in r^2 from 0.77 to 0.83) and potato (a change in r^2 from 0.64 to 0.76), compared to the relationships presented in Pleijel *et al.* (2003).

The response relationship for wheat:

(3.1)

$$RY_{\text{wheat}} = 1.00 - (0.048 * AF_{st}6)$$

is presented in Figure 3.2.

The response relationship for potato:

(3.2)

$$RY_{\text{potato}} = 1.01 - (0.013 * AF_{st}6)$$

is presented in Figure 3.3.

In line with earlier concepts used for crop critical levels, 5% yield reduction was used as the loss criterion for the identification of stomatal flux-based critical levels (UNECE, 1996). For wheat the suggested stomatal flux-based critical level for 5% yield loss of an $AF_{st}6$ of 1 mmol m^{-2} was statistically significant according to the confidence limits of the yield response regressions, which is an important criterion when using a yield loss level such as 5% (Pleijel, 1996). For potato, the value was rounded upwards from $4.6 \text{ mmol O}_3 \text{ m}^{-2}$ (representing 5% yield loss) to $5 \text{ mmol O}_3 \text{ m}^{-2}$.

As such, the flux-based critical level, CL_{ef} of ozone for wheat is an $AF_{st}6$ of 1 mmol O_3 per unit projected flag leaf area, accumulated during an effective temperature sum period

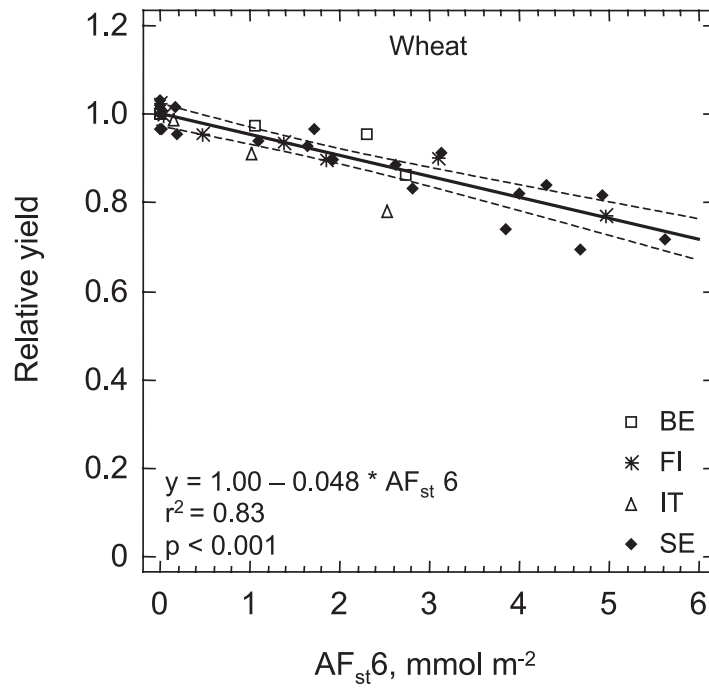


Figure 3.2: The relationship between the relative yield of wheat and AF_{st6} for the wheat flag leaf based on five wheat cultivars from four European countries using effective temperature sum to describe phenology.

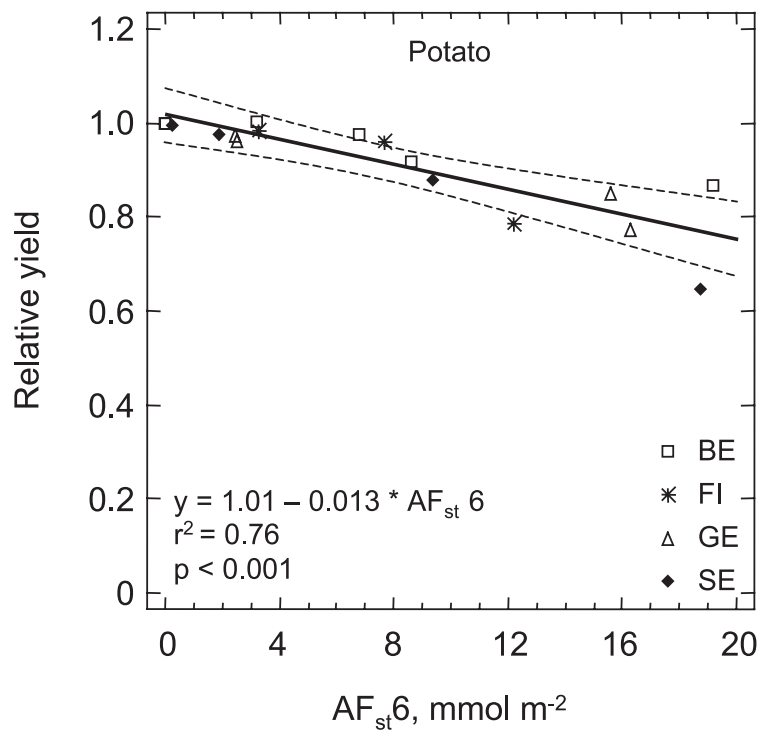


Figure 3.3: The relationship between the relative yield of potato and the AF_{st6} for sunlit leaves based on data from four European countries and using effective temperature sum to describe phenology.

starting 270°C days before anthesis (flowering) and ending 700°C days after anthesis. The total period is 970°C days (base temperature 0°C). On average, the 970°C days corresponded to 54 days in the experiments used to calibrate the function.

The flux-based critical level, $CL_{e\beta}$ of ozone for potato is an AF_{st6} of 5 mmol O_3 per m² projected, sunlit leaf area accumulated over 1130°C days starting at plant emergence (base temperature 0°C). On average, the 1130°C days corresponded to 66 days in the experiments used to calibrate the function; this value has been rounded up to 70 days for Table 3.5.

3.3.1.3 AOTX-based critical levels for crop yield reduction

Agricultural crops

The concentration-based critical level for agricultural crops has been derived from a linear relationship between AOT_{40} and relative yield for wheat, developed from the results of open-top chamber experiments

conducted in Europe and the USA (Figure 3.4). Newly published data (Gelang *et al.* 2000) has been added to that derived by Fuhrer *et al.* (1997) and quoted in the previous version of the Mapping Manual (UNECE, 1996). Thus, the critical level for wheat is based on a comprehensive dataset including 9 cultivars. The AOT_{40} corresponding to a 5% reduction in yield is 3.3 ppm h (95% Confidence Interval range 2.3-4.4 ppm h). This value has been rounded down to 3 ppm h for the critical level. The critical level for agricultural crops is only applicable when nutrient supply and soil moisture are not limiting, the latter because of sufficient precipitation or irrigation (Fuhrer, 1995).

The time period over which the AOT_{40} is calculated should be three months and the timing should reflect the period of active growth of wheat and be centred around the start of anthesis (see Section 3.5.2.2 for guidance).

An optional additional AOT_{30} -based critical level of ozone has also been derived for agricultural crops, based on a re-working of the wheat response-function data used by

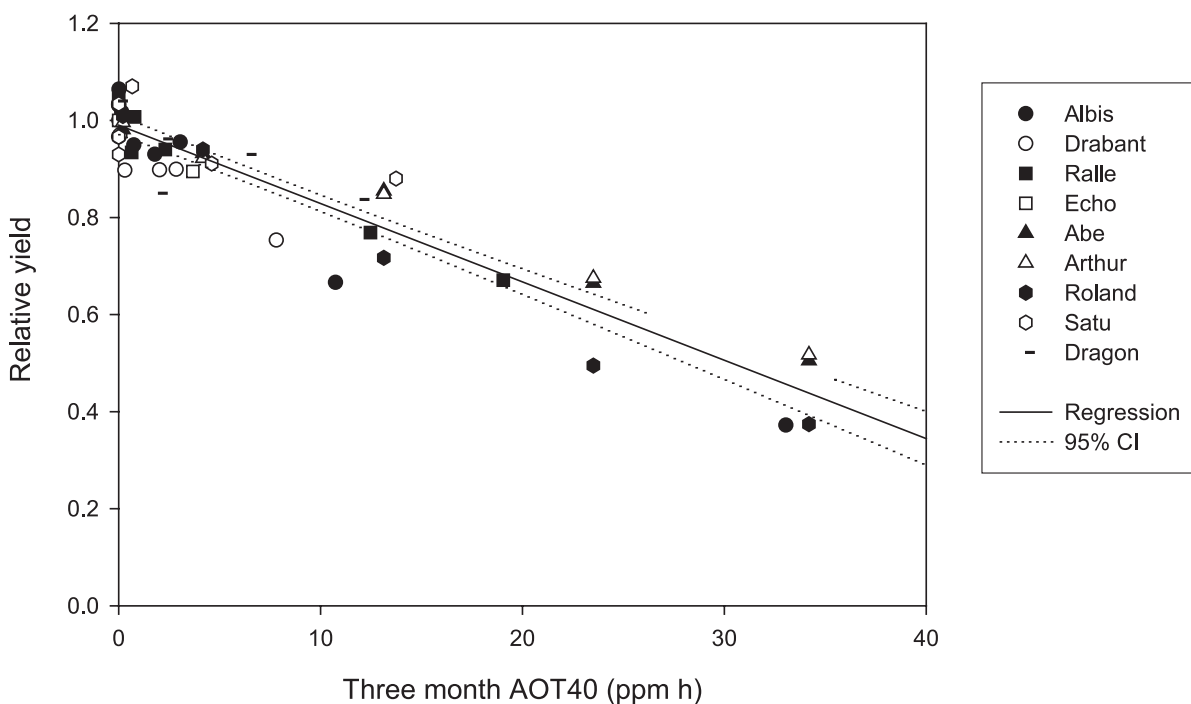


Figure 3.4: Wheat yield-response function used to derive the concentration-based critical levels for agricultural crops ($r^2 = 0.89$) (Fuhrer *et al.*, 1997, Gelang *et al.*, 2000).

Fuhrer *et al.*, 1997 using *AOT30* as the dose parameter ($r^2 = 0.90$, data not presented). The value for this critical level is an *AOT30* of 4 ppm h applied to the same time-windows as described for *AOT40*. Following discussions at the Gothenburg Workshop, the 16th Task Force Meeting of the ICP Vegetation and the 19th Task Force Meeting of the ICP Modelling and Mapping, it was concluded that *AOT40* should continue to be used for the concentration-based critical level for agricultural crops, but that *AOT30* could be used in integrated assessment modelling on the European scale if this considerably reduces uncertainty in the overall integrated assessment model.

It is not recommended that exceedance of the concentration-based critical level for agricultural crops is converted into economic loss; it should only be used as an indication of ecological risk (Fuhrer, 1995).

Horticultural Crops

A concentration-based critical level has been derived for horticultural crops that are growing with adequate nutrient and water supply. An *AOT40* of 6.02 ppm h is equivalent to a 5% reduction in fruit yield for tomato, and has been derived from a dose-response function (Figure 3.5) developed from a comprehensive dataset including 14 cultivars ($r^2 = 0.48$, $p < 0.001$). This value has been rounded down to 6 ppm h for the critical level. Although statistical analysis has indicated that water melon may be more sensitive to ozone than tomato, the dataset for water melon is not sufficiently robust for use in the derivation of a critical level because the data is only for one cultivar (Mills *et al.*, 2003). Tomato is considered suitable for the derivation of the critical level since it is classified as an ozone-sensitive crop (Table 3.6). The data used in the derivation of the critical level for horticultural crops is from experiments conducted in the USA (California and North Carolina), Germany and Spain. The time period for accumulation of *AOT40* is 3.5 months, starting from the emergence of the crop (see Section 3.5.3.2 for guidance).

It is not recommended that the exceedance of the concentration-based critical level for horticultural crops is converted into economic loss; it should only be used as an indication of ecological risk during the most sensitive environmental conditions (Fuhrer, 1995).

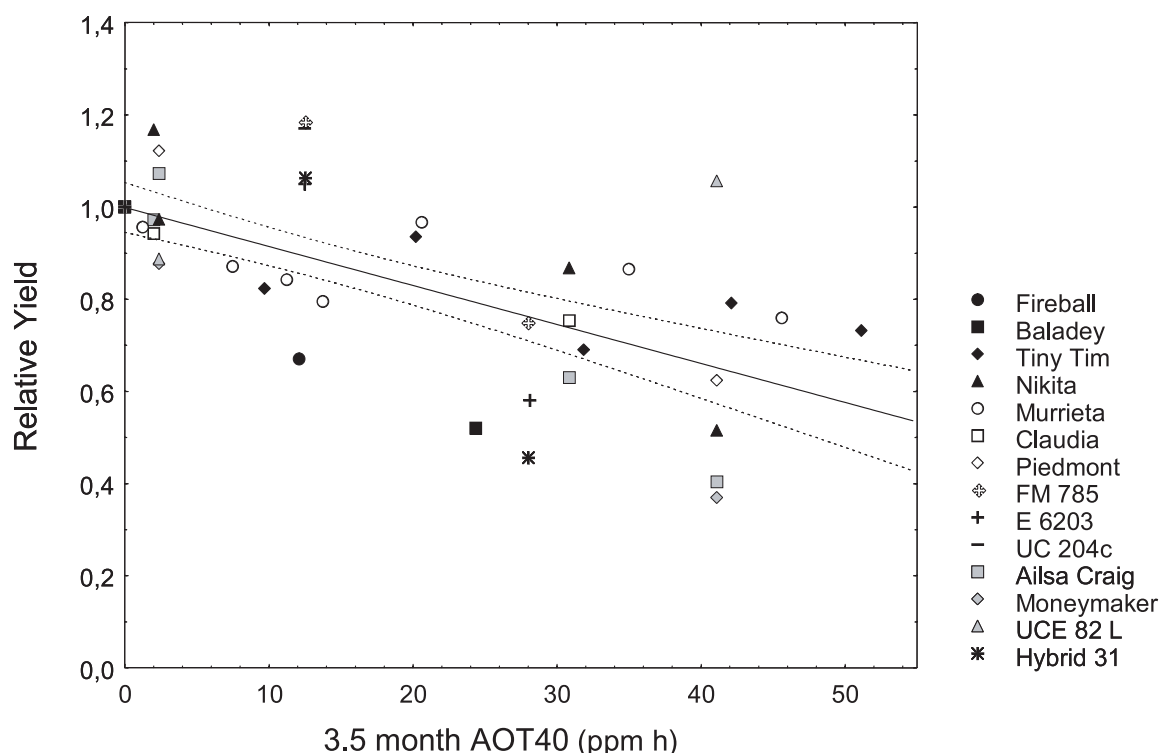


Figure 3.5: Tomato yield-response function used to derive the concentration-based critical levels for horticultural crops ($r^2 = 0.48$, $p < 0.001$) (dotted line = 95% confidence limits). (Hassan et al., 1999; McLean & Schneider, 1976; Reinert et al., 1997; Temple et al., 1985; Temple, 1990; Bermejo, 2002; Calvo, 2003).

3.3.1.4 *VPD-modified AOT30 – based critical level for visible injury on crops*

Note: This critical level was revised following new analysis conducted after the 17th Task Force meeting of the ICP Vegetation (Kalamata, February 2004); participants were asked by email if they objected to the changes made and no objections were raised.

Acute visible ozone injury, resulting from short-term ozone exposure, represents the most direct evidence of the harmfulness of elevated ozone concentrations. The aim of this short-term critical level is to reflect the risk for this type of injury. For some horticultural crops, such as spinach, lettuce, salad onion and chicory sold for their foliage, visible ozone injury can cause significant financial loss to farmers. In addition, visible ozone injury can be easily demonstrated and thus used to highlight the problem of phytotoxic ozone to a broad audience (Klumpp et al., 2002).

The short-term critical level is based on results from experiments performed with

subterranean clover (*Trifolium subterraneum*) which was used as the key bioindicator plant for a number of years within the ICP Vegetation (Benton et al., 1995). Data from three participating countries (Sweden, Belgium and Austria) were used to derive a common relationship between ozone exposure and the risk for visible injury (Pihl Karlsson et al., 2004). Since *Trifolium subterraneum* is well-documented as a very ozone sensitive plant in terms of having visible symptoms after ozone exposure, the critical level for visible injury on crops is expected to protect other ozone sensitive plants from visible injury.

It has been shown that *AOT30* is the best *AOTX* exposure index to describe the risk for visible ozone injury in subterranean clover under low *VPD*, i.e. relatively humid conditions (Pihl Karlsson et al., 2003). However, it has also been demonstrated that in drier climates *VPD* is a very important modifier of ozone uptake through its limiting effect on stomatal conductance and thus of the risk that a certain ozone concentration would contribute to visible injury (Ribas & Peñuelas, 2003). A *VPD* modified *AOT30*

($AOT30_{VPD}$) approach adequately describes the relationship between ozone exposure and risk for visible injury in subterranean clover when grown in well-watered conditions (as in the ICP Vegetation experiments).

The critical level for visible injury is exceeded when the $AOT30_{VPD}$ during daylight hours over eight days exceeds 0.16 ppm h. This represents a significant risk of having visible ozone injury on at least 10% ($\pm 3.5\%$ according to the 99% confidence limits of the regression shown in Figure 3.6) of the leaves on sensitive plants, such as subterranean clover. The 10% level for visible ozone injury was chosen based on the conclusion from the studies by Pihl Karlsson *et al.* (2003).

The $AOT30_{VPD}$ index accumulated during daylight hours, using an exposure period of eight days explained 60% of the variation of the observed extent of visible injury (% injured leaves) accumulated during daylight hours ($p < 0.001$ for the slope and intercept). The relationship between visible injury and $AOT30_{VPD}$ during eight days

before observation of visible injury is shown in Figure 3.6.

It is not recommended that the exceedance of the concentration-based critical level for visible injury on agricultural and horticultural crops is converted into economic loss; it should only be used as an indication of risk of injury during the most sensitive environmental conditions.

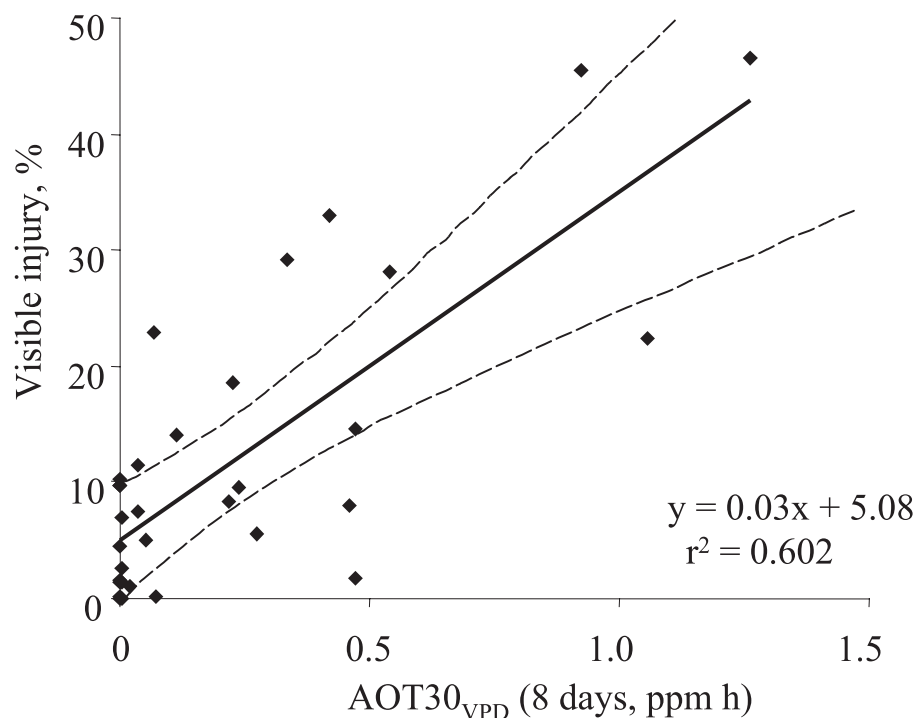


Figure 3.6: The extent of visible injury (percentage ozone injured leaves) versus $AOT30_{VPD}$. The accumulation period was eight days before observation of visible injury. The accumulation was made during daylight hours. Confidence limits for $p = 0.99$ are also presented (Pihl Karlsson *et al.*, 2004).

3.3.2 (Semi-) natural vegetation

The critical level for (semi-) natural vegetation is concentration based; flux-based methods are not sufficiently advanced for this vegetation type for inclusion in this manual.

The criteria for adverse effects on (semi-) natural vegetation are an effect on growth for perennial species, and effects on growth and seed production for annual species. The critical level is based on statistically significant effects or growth reductions of greater than 10% on sensitive taxa of grassland and field margin communities and is applicable to all sensitive semi-natural vegetation and natural vegetation, described here collectively as (semi-) natural vegetation (forest trees and woodlands are not included here as (semi-) natural vegetation). The value of 3 ppm h is sufficient to protect the most sensitive annual and short-lived perennial species when grown in a competitive environment.

In contrast to crops and tree species, only

limited experimental data are available for a small proportion of the vast range of species found across Europe. This means that analysis of exposure-response data for individual species to derive a critical level value is more difficult. Instead, the recommended critical level is based on data from a limited number of sensitive species. The value of 3 ppm h was originally proposed at the Kuopio workshop (Kärenlampi & Skärby, 1996) and confirmed at the Gerzensee workshop (Fuhrer & Achermann, 1999). At the time of the Kuopio workshop, no exposure-response studies were available for derivation of the critical level for (semi-) natural vegetation, based on a 10% response. Instead, data from field-based experiments with control and ozone treatments were used to identify studies showing significant effects at relatively low ozone exposures. Table 3.7 summarises the key field chamber and field fumigation experiments which supported the original proposal of this critical level for (semi-) natural vegetation.

Table 3.7: Summary of key experiments supporting the critical level of 3ppm h, as proposed at the Kuopio workshop (Ashmore & Davison, 1996)

Species or community	Most sensitive species	Ozone (AOT40, ppm h)	Response	Reference
Individual plants	<i>Solanum nigrum</i> <i>Malva sylvestris</i>	4.2 3.9	-23%; shoot mass -54%; seed mass	Bergmann <i>et al.</i> , 1996
Mesocosms of four species	<i>Trifolium repens</i>	5.0	-13%; shoot mass	Ashmore & Ainsworth, 1995
Mesocosms of seven species	<i>Festuca ovina</i> <i>Leontodon hispidus</i>	7.0 7.0	-32%; shoot mass -22%; shoot mass	Ashmore <i>et al.</i> , 1996
Ryegrass-clover sward	<i>Trifolium repens</i>	5.0	-20%; shoot mass	Nussbaum <i>et al.</i> , 1995

A number of studies have clearly demonstrated that the effects of ozone in species mixtures may be greater than those on species grown alone or only subject to intraspecific competition. Therefore, the critical level needs to take into account the possibility of effects of interspecific competition in reducing the threshold for significant effects; indeed three of the four experiments listed in Table 3.7 include such competitive effects. The most comprehensive study of ozone effects on species mixtures involving species which are representative of different communities across Europe, is the EU-FP5 BIOSTRESS (BIOdiversity in Herbaceous Semi-Natural Ecosystems Under STRESS by Global Change Components) programme. Results to date from the BIOSTRESS programme, including experiments with species from the Mediterranean dehesa community, indicate that exposures to ozone exceeding an *AOT40* of around 3 ppm h may cause significant negative effects on annual and

perennial plant species (see Fuhrer *et al.*, 2003). The BIOSTRESS mesocosm experiments with two-species mixtures indicated that exposures during only 4-6 weeks early in the growing season may cause shifts in species balance. The effect of this early stress may last for the rest of the growing season. This new evidence meant that the proposal of a six month growth period for perennial species adopted at the Gerzensee Workshop was no longer supported at the Gothenburg Workshop, and that the time-window for both annuals and perennials is now set to three months.

The key experiments from the BIOSTRESS programme which support the proposed critical level are summarised in Table 3.8. Taken together, these studies support a critical level in the range 2.5-4.5 ppm h, with a mean value of 3.3 ppm h.

Table 3.8: Summary of experiments from the BIOSTRESS programme which support the recommended critical levels (reviewed by Fuhrer *et al.*, 2003)

Responsive species	Competitor species	Variable showing significant response	Corresponding AOT40	Reference
<i>Trifolium pratense</i>	<i>Poa pratensis</i>	Biomass (-10%)	4.4 ppm h*	Gillespie & Barnes, unpublished data
<i>Veronica chamaedrys</i>	<i>Poa pratensis</i>	Species biomass ratio	3.6 ppm h	Bender <i>et al.</i> (2002)
<i>Trifolium cherleri</i> , <i>T. striatum</i>	<i>Briza maxima</i>	Flower production	2.2-2.7 ppm h	Gimeno <i>et al.</i> (2003a); Gimeno <i>et al.</i> (2004).
<i>Trifolium cherleri</i>	<i>Briza maxima</i>	Seed output	2.4 ppm h	Gimeno <i>et al.</i> (2004)

*estimated from exposure-response functions

The value of the critical level is further supported by more recent published data, for instance, for wetland species by Power and Ashmore (2002) and Franzaring *et al.* (2000). The latter authors observed a significant reduction in the shoot:root ratio in *Cirsium dissectum* at 3.3 ppm h after 28 days of exposure. In individual plants from wild strawberry populations growing at high latitudes, Manninen *et al.* (2003) observed a significant biomass decline of >10% at 5 ppm h from June-August.

Guidance on the time-window for calculating *AOT40*, for mapping (semi-) natural communities at risk of ozone and determining the ozone concentration at the canopy height is provided in Section 3.5.5.

3.3.3 Forest trees

3.3.3.1 Provisional flux-based critical levels

At the UNECE workshop in Gothenburg in November 2002 (Karlsson *et al.*, 2003a) it was concluded that the effective ozone dose, based on the flux of ozone into the leaves through the stomatal pores, represents the most appropriate approach for setting future ozone critical levels for forest trees. However, uncertainties in the development and application of flux-based approaches to setting critical levels for forest trees are at present too large to justify their application as a standard risk assessment method at a European scale. Although $AF_{st}Y$ is much more physiologically relevant than *AOTX*, more time and data are needed before $AF_{st}Y$ -response relationships for trees could be considered sufficiently robust for establishing a stomatal flux-based critical level of ozone for forest trees; calculation of exceedance of a provisional flux-based critical level for beech and birch is described in Section 3.4.6. Although model parameterisation and flux-response relationships are available for other species (Karlsson *et al.*, 2003b), parameterisation of the multiplicative model is given only for beech and birch, and it is intended that these species are used as indicators of risk to sensitive recep-

tors. The choice of beech and birch also ensures continuity with the concentration-based critical level described below.

As for crop species, ozone flux is estimated on a projected leaf area basis for sunlit upper canopy leaves. Ozone flux should be accumulated for an exposure window as defined in Section 3.4.6, either using the default values given, locally derived information or phenological models. Ozone concentrations used for the calculation of stomatal ozone flux are those at the top of the canopy, as discussed in Section 3.4.6.1. As is the case for both wheat and potato, a flux threshold, Y , should be applied. For beech and birch, a value of $1.6 \text{ nmol m}^{-2} \text{ PLA s}^{-1}$ is proposed for Y , based on the statistical analysis of flux-response relationships for a variety of sensitive deciduous tree species (Karlsson *et al.*, 2003b, 2004). This same analysis concluded that for $Y=1.6 \text{ nmol m}^{-2} \text{ s}^{-1}$, a growing season cumulative stomatal flux ($AF_{st}1.6$) of 4 mmol m^{-2} was statistically significant (99% confidence) and represented a 5% reduction in biomass under experimental conditions. This indicative value represents the provisional flux-based critical level, above which there is a risk of a negative impact of ozone on growth for the most sensitive tree species. The dataset on which this analysis is based, is identical to that from which the *AOT40*-based critical level was derived, and represents a combination of data for both birch and beech.

It should be emphasised that this provisional critical level should be viewed as a first step in the derivation of new critical levels which could be used to make quantitative assessments of the ozone impacts on mature forest trees since the value currently selected is based on a number of assumptions (these are discussed in more detail in Karlsson *et al.*, 2003b, 2004). In the future it is envisaged that additional analysis and reworking of existing experimental data and improvement of stomatal conductance models for forest trees should provide better estimates of both cumulative stomatal flux and associated flux thresholds and critical levels to provide more robust estimates of damage for forest trees.

3.3.3.2 *AOTX*-based critical levels for forest trees

The *AOTX* approach is retained as the recommended method for calculating critical levels for forest trees until the stomatal flux approach becomes sufficiently refined. However, the methodology and critical levels have been substantially revised since the previous version of this Manual was published (UNECE, 1996).

The experimental database that was presented at the UNECE Workshop in Gothenburg 2002 has been re-analysed and expanded to include additional correlations with *AOT20*, *AOT30*, and *AOT50* (Karlsson *et al.*, 2003b). Furthermore, the tree species included in the analysis have been separated into four species categories (Table 3.9) based on the sensitivity of growth responses to ozone. It should be emphasised that this categorisation is based on growth as a measure of effect, and that the relative sensitivity of a given species may differ when an alternative measure such as visible injury is used. As a result of this differentiation of species, linear regressions between exposure and response have the highest r^2 values and there are no significant intercepts (Table 3.10). The disadvantage was that there are insufficient data available for the moderately sensitive coniferous category for adequate statistical analysis. This may change in the future, if more datasets become available.

Using the sensitivity categories described above, *AOT40* gave the highest r^2 values of the *AOTX* indices tested (Figure 3.6). However, the difference between the r^2 values for *AOT40* and *AOT30* was small (0.62 and 0.61 respectively for the combined birch and beech dataset, Table 3.10).

Table 3.9: Sensitivity classes for the tree species based on effects of ozone on growth

Ozone-sensitive species		Moderately ozone-sensitive species	
Deciduous	Coniferous	Deciduous	Coniferous
<i>Fagus sylvatica</i>	<i>Picea abies</i>	<i>Quercus petrea</i> ,	<i>Pinus halepensis</i>
<i>Betula pendula</i>	<i>Pinus sylvestris</i>	<i>Quercus robur</i>	

Table 3.10: Statistical data for regression analysis of the relationship between *AOTX* ozone exposure indices (in ppm h) and percentage reduction of total and above-ground biomass for different tree species categories

Ozone index/ plant category	Linear regression			
	r ²	p for the slope	p for the intercept	slope
<i>AOT20</i>				
Birch, beech	0.52	<0.01	0.70	- 0.357
Oak	0.57	<0.01	0.73	- 0.142
Norway spruce, Scots pine	0.73	<0.01	0.31	- 0.086
<i>AOT30</i>				
Birch, beech	0.61	<0.01	0.63	- 0.494
Oak	0.61	<0.01	0.79	- 0.170
Norway spruce, Scots pine	0.76	<0.01	0.61	- 0.110
<i>AOT40</i>				
Birch, beech	0.62	<0.01	0.31	- 0.732
Oak	0.65	<0.01	0.73	- 0.216
Norway spruce, Scots pine	0.79	<0.01	0.86	- 0.154
<i>AOT50</i>				
Birch, beech	0.53	<0.01	0.05	- 1.033
Oak	0.62	<0.01	0.82	- 0.248
Norway spruce, Scots pine	0.76	<0.01	0.16	- 0.188

Based on the analysis described above, the concentration-based critical level of ozone for forest trees, CL_{e_c} , has been reduced from an *AOT40* value of 10 ppm h (Kärenlampi & Skärby, 1996) to 5 ppm h (range 1-9 ppm h, determined by the 99% confidence intervals), accumulated over one growing season (Figure 3.7). This value of 5 ppm h is associated with a 5% growth reduction per growing season for the deciduous sensitive tree species category (beech and birch, Figure 3.7). The 5% growth reduction was clearly significant as judged by the 99% confidence intervals in Figure 3.7. This

increase in the robustness of the dataset and the critical level represents a substantial improvement compared to the 10% growth reduction associated with the previous ozone critical level of an *AOT40* of 10 ppm h (Kärenlampi & Skärby, 1996). Furthermore, it represents a continued use of sensitive, deciduous tree species to represent the most sensitive species under most sensitive conditions. As previously, it should be strongly emphasized that these values should not be used to quantify ozone impacts for forest trees under field conditions.

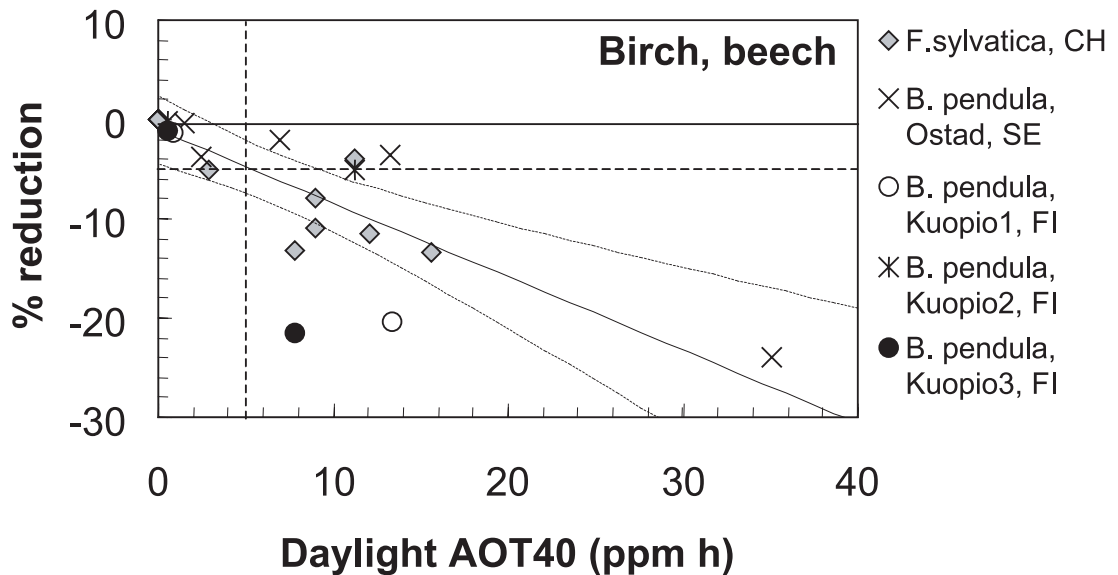


Figure 3.7: The relationship between percentage reduction in biomass and AOT_{40} , on an annual basis, for the deciduous, sensitive tree species category, represented by beech and birch. The relationship was analysed by linear regression with 99% confidence intervals. Explanations for the figure legends can be found in Karlsson et al. (2003b).

Additional evidence to support the new ozone critical levels for forest trees comes from the observation of visible injury in young trees in ambient air at Lattecaldo, in southern Switzerland. It was concluded that a reduction of the ozone critical level to 5 ppm h AOT_{40} was needed in order to protect the most sensitive species from visible injury (Van der Hayden et al., 2001, Novak et al., 2003). Furthermore, Baumgarten et al. (2000) detected visible injury on the leaves of mature beech trees in Bavaria well below 10 ppm h AOT_{40} .

An optional additional AOT_{30} -based critical level of ozone has also been derived for forest trees based on the response function for birch and beech. The value for this critical level is an AOT_{30} of 9 ppm h applied to the same time-windows as described for AOT_{40} . Following discussions at the Gothenburg Workshop, the 16th Task Force Meeting of the ICP Vegetation and the 19th Task Force Meeting of the ICP Modelling and Mapping, it was concluded that AOT_{40} should be used for the concentration-based critical level for forest trees, but that AOT_{30} could be used in integrated assessment modelling on the European scale if this considerably reduces uncertainty in the overall integrated assessment model.

3.4 Calculating exceedance of stomatal flux-based critical levels for ozone

3.4.1 Stages in calculating $AF_{st}Y$ and CLe_f exceedance

To calculate the relevant $AF_{st}Y$ to sunlit leaves and exceedance of the stomatal flux-based critical level, the following steps have to be taken:

1. Hourly ozone concentrations at the top of the canopy are determined (see Section 3.4.2 for conversion of concentrations considering ozone concentration gradients above the canopy).
2. The time period to consider is determined as described in Section 3.4.3. The hourly stomatal conductance (g_{sto}) values for the relevant periods, for sunlit leaves of the receptor plant are identified using the algorithm presented in Eq. 3.12.
3. Every hourly stomatal conductance thus identified is multiplied by the corresponding hourly ozone concentra-

tion at the top of the canopy, resulting in hourly stomatal fluxes of ozone, F_{st} expressed in $nmol\ m^{-2}\ PLA\ s^{-1}$ (Eq. 3.9).

4. The value Y is subtracted from each hourly F_{st} value, and then multiplied by 3600 to obtain hourly $F_{st}Y$ values in $nmol\ O_3\ m^{-2}\ PLA\ h^{-1}$.
5. The sum of all hourly $F_{st}Y$ values is calculated for the specified accumulated period. The resulting value is $AF_{st}Y$ in units $nmol\ m^{-2}\ PLA$.
6. If the $AF_{st}Y$ value is larger than the flux-based critical level for ozone CLe_f , there is exceedance of the critical level.

3.4.2 Ozone concentrations at the canopy height

Note: Sources of ozone concentration estimates and their spatial interpolation are considered in Chapter 2 of this manual.

All ozone indices described in this chapter are based on ozone concentrations at the top of the canopy. For crops and other low vegetation, canopy-top concentrations may be significantly lower than those at conventional measurement heights of 2-5 m above the ground, and hence use of measured data directly or after spatial interpolation may lead to significant over-estimates of ozone concentrations and hence of the degree of exceedance of CLe_c and CLe_f . In contrast, for forests, measured data may underestimate ozone concentration at the top of the canopy. The difference between measurement height and canopy height is a function of several factors, including wind speed and other meteorological factors, canopy height and the total flux of ozone, F_{tot} .

Conversion of ozone concentration at measurement height to that at canopy-top height (z_1) can be best achieved with an appropriate deposition model. It should be noted, however, that the flux-gradient relationships these models depend on are not strictly valid within the roughness sub-layer (ground level

to 2-3 times canopy height), so even such detailed calculations can provide only approximate answers. The model chosen will depend upon the amount of meteorological data that is available. Two simple methods are included here which can be used to achieve the necessary conversion if (a) no meteorological data are available, or (b) some basic measurements are available.

Method (a): Tabulated gradient

If no meteorological data are available at all, then a simple tabulation of O_3 gradients can be used. The relationship between O_3 concentrations at a number of different heights has been estimated with the EMEP deposition module (Emberson *et al.*, 2000a), using meteorology from about 30 sites across Europe. Data were produced for an arbitrary crop surface and for short grasslands. For the crop surface, the assumptions made here are that we have a 1 m high crop with $g_{max} = 450\ mmol\ O_3\ m^{-2}\ PLA\ s^{-1}$. The total leaf surface area index (LAI) is set to $5\ m^2\ PLA / m^2$, and the green LAI is set at $3\ m^2\ PLA / m^2$, assumed to give a canopy-scale phenology factor (f_{phen}) of 0.6. The soil moisture factor (f_{SWP}) is set to 1.0. Constant values of these parameters are used throughout the year in order to avoid problems with trying to estimate growth-stage in different areas of Europe. The concentration gradients thus derived are most appropriate to a fully developed crop but will serve as a reasonable approximation for the whole growing season. Other stomatal conductance modifiers are allowed to vary according to the wheat-functions. For short grasslands, canopy height was set to 0.1 m, g_{max} to $270\ mmol\ O_3\ m^{-2}\ PLA\ s^{-1}$ and f_{SWP} set to 1.0. All other factors are as given for grasslands in Emberson *et al.* (2000b). For the micrometeorology, the displacement height (d) and roughness length (z_0) are set to 0.7 and 0.1 of canopy height (z_1), respectively. Thus, the upper-boundary of the quasi-laminar layer ($d+z_0$), is simply $0.8z_1$, where z_1 is canopy height.

Table 3.11 shows the average relationship between O_3 concentrations at selected heights, derived from runs of the EMEP module over May-July, and selecting the noontime factors as representative of daytime multipliers. O_3 concentrations are normalised by setting the 20 m value to 1.0. To use Table 3.11, measurements made above crops or grasslands may simply be extrapolated downwards to the canopy top for the respective vegetation. For example, with 30 ppb measured at 3 m height (above ground level) in a crop field, the concentration at 1 m would be $30.0 * (0.88/0.95) = 27.8$ ppb. For short grasslands we would obtain

$30.0 * (0.74/0.96) = 23.1$ ppb at canopy height, 0.1 m. Experiments have shown that the vertical gradients found above for crops also apply well to tall (0.5 m) grasslands. Some judgement may then be required to choose values appropriate to different vegetation types.

Table 3.11: Representative O_3 gradients above artificial (1 m) crop, and short grasslands (0.1 m). O_3 concentrations are normalised by setting the 20 m value to 1.0. These gradients are derived from noontime factors and are intended for daytime use only.

Height (m)	O_3 concentration gradient	
	Crops (where $z_1=1$ m, $g_{\max}=450$ mmol O_3 m^{-2} PLA s^{-1})	Short Grasslands (where $z_1=0.1$ m, $g_{\max}=270$ mmol O_3 m^{-2} PLA s^{-1})
20	1.0	1.0
10	0.99	0.99
5	0.97	0.97
4	0.96	0.97
3	0.95	0.96
2	0.93	0.95
1	0.88	0.92
0.5	0.81*	0.89
0.2	-	0.83
0.1	-	0.74

*0.5 m is below the displacement height of crops, but may be used for taller grasslands, see text.

For forests, ozone concentrations must often be derived from measurements made over grassy areas or other land-cover types. In principal, the O_3 concentration measured over land-use X (e.g. short grasslands) could be used to estimate the O_3 concentration at a reference height, and then the gradient profile appropriate for desired land use Y could be applied. However, in order to keep this simple methodology manageable, and in view of the uncertainties inherent in making use of any profile near the canopy itself, it is suggested that concentrations are estimated by extrapolating the profiles given in Table 3.11 upwards to the canopy height for forests. As an example, if we measure 30 ppb at 3 m above short grassland, the concentration at 20 m is estimated to be $30.0 \cdot (1.0/0.96) = 31.3$ ppb.

It should be noted that the profiles shown in Table 3.11 are representative only, and that site-specific calculations would provide somewhat different numbers. However, without local meteorology and the use of a deposition model, the suggested procedure should give an acceptable level of accuracy for most purposes.

Method (b): Use of neutral stability profiles

If we have wind speed, u ($m\ s^{-1}$) at reference height z_R , and an estimate of z_0 , then we find concentration values appropriate to a height z_I (e.g. 1 m) by making use of the constant-flux assumption and definition of aerodynamic resistance:

(3.3)

$$\begin{aligned} \text{Total flux} &= V_g(z_R) \cdot C(z_R) \\ &= (C(z_R) - C(z_I)) / R_a(z_R, z_I) \end{aligned}$$

Where $V_g(z_R)$ is the deposition velocity ($m\ s^{-1}$) at height z_R , and $R_a(z_R, z_I)$ is the aerodynamic resistance between the two heights ($s\ m^{-1}$). Re-arranging the second two terms, we get:

(3.4)

$$C(z_I) = C(z_R) \cdot [1 - (R_a(z_R, z_I) \cdot V_g(z_R))]$$

In neutral stability, friction velocity (u^*) and R_a are easily obtained:

(3.5)

$$u^* = \frac{u(z)k}{\ln\left(\frac{z-d}{z_0}\right)}$$

(3.6)

$$R_a(z_R, z_I) = \frac{1}{ku^*} \ln\left(\frac{z_R - d}{z_I - d}\right)$$

where the von Kármán konstant, $k = 0.4$

The deposition velocity requires further information:

(3.7)

$$V_g(z_R) = 1 / (R_a(z_R, z_0) + R_b + R_c)$$

Note: R_a is here the aerodynamic resistance from z_R to z_0 (the level where R_a becomes zero), not to z_I (which is any height fairly near the ground, for example the height of the top of the canopy). For ozone, $R_b = 6.85/u^*$. The canopy resistance, R_c , is a function of temperature, radiation, relative humidity and soil water. If local meteorology allows an assessment of these, the formulation of R_c may be directly estimated using a canopy-scale stomatal flux algorithm (see Emberson *et al.*, 2000b).

3.4.3 Accumulation period

It is important that the cumulative period over which the $AF_{st}Y$ value is calculated is consistent with the period when the relevant crop or forest species is actively growing and most sensitive to the absorbed ozone dose. Thus, receptor specific time periods

are defined in the appropriate sections below. For flux-based critical levels this is achieved by identifying, within the growing season, the start (A_{start}) and end (A_{end}) of the accumulation period by receptor type. The following sources of information can be considered for determining the accumulation period:-

- a) *Information from local or national agricultural or forest experts*
- b) *Phenological models.* These predict the start and end of the growing season, typically defined as a function of climatic factors such as cumulative temperature and water availability.

3.4.4 The stomatal flux algorithm

The estimation of stomatal flux of ozone (F_{st}) is based on the assumption that the concentration of ozone at the top of the canopy represents a reasonable estimate of the concentration at the upper surface of the laminar layer near the flag leaf (in the case of wheat) and the sunlit upper canopy leaves (in the case of potato and trees). If $c(z_1)$ is the concentration of ozone at canopy top (height z_1 , unit: m), in $nmol\ m^{-3}$, then F_{st} ($nmol\ m^{-2}\ PLA\ s^{-1}$), is given by:

$$(3.8) \quad F_{st} = c(z_1) * \frac{1}{r_b + r_c} * \frac{g_{sto}}{g_{sto} + g_{ext}}$$

The $1/(r_b+r_c)$ term represents the deposition rate to the leaf through resistances r_b (quasi-laminar resistance) and r_c (leaf surface resistance). The fraction of this ozone taken up by the stomata is given by $g_{sto}/(g_{sto}+g_{ext})$, where g_{sto} is the stomatal conductance, and g_{ext} is the external leaf, or cuticular, resistance. As the leaf surface resistance, r_c , is given by $r_c = 1/(g_{sto}+g_{ext})$, we can also write Eq. 3.8 as:

$$(3.9) \quad F_{st} = c(z_1) * g_{sto} * \frac{r_c}{r_b + r_c}$$

A value for g_{ext} has been chosen to keep consistency with the EMEP deposition modules "big-leaf" external resistance, $R_{ext} = 2500/SAI$, where SAI is the surface area index (green + senescent LAI). Assuming that SAI can be simply scaled:

$$(3.10) \quad g_{ext} = 1/2500 \quad (m\ s^{-1})$$

In order to be used correctly in Eq. 3.8 and 3.9, g_{sto} from Eq. 3.12 has to be converted from units $mmol\ m^{-2}\ s^{-1}$ to units $m\ s^{-1}$. At normal temperatures and air pressure, the conversion is made by dividing the conductance value expressed in $mmol\ m^{-2}\ s^{-1}$ by 41000 to give conductance in $m\ s^{-1}$.

Consistency of the quasi-laminar boundary layer is harder to achieve, so the use of a leaf-level r_b term (McNaughton & van der Hink, 1995) is suggested, making use of the cross-wind leaf dimension L (unit: m) and the wind speed at height z_1 , $u(z_1)$:

$$(3.11) \quad r_b = 1.3 * 150 * \sqrt{\frac{L}{u(z_1)}} \quad (s\ m^{-1})$$

Where the factor 1.3 accounts for the differences in diffusivity between heat and ozone. Potential values of L for wheat, potato and beech/birch are 0.02 m, 0.04 m and 0.05 m respectively.

The core of the leaf ozone flux model is the stomatal conductance (g_{sto}) multiplicative algorithm which has been developed over the past few years as described in Emberson *et al.* (2000b) and incorporated within the EMEP ozone deposition module (Emberson *et al.* 2000a). The multiplicative algorithm has the following formulation:

(3.12)

$$g_{sto} = g_{max} * [\min(f_{phen}, f_{O_3})] * f_{light} * \max\{f_{min}, (f_{temp} * f_{VPD} * f_{SWP})\}$$

Where g_{sto} is the actual stomatal conductance ($mmol\ O_3\ m^{-2}\ PLA\ s^{-1}$) and g_{max} is the species-specific maximum stomatal conductance ($mmol\ O_3\ m^{-2}\ PLA\ s^{-1}$). The parameters f_{phen} , f_{O_3} , f_{light} , f_{temp} , f_{VPD} and f_{SWP} are all expressed in relative terms (i.e. they take values between 0 and 1) as a proportion of g_{max} .

These parameters allow for the modifying influence of phenology and ozone, and four environmental variables (light (irradiance), temperature, atmospheric vapour pressure deficit (VPD) and soil water potential (SWP)) on stomatal conductance to be estimated. Figure 3.8 shows the derivation of these functions and sources of data for parameterisation are provided in Table 3.12 and 3.13 (at the end of the chapter). The part of Eq. 3.12 related to f_{phen} and f_{O_3} is a most limiting factor approach. Either senescence due to normal ageing is limiting or the premature senescence induced by ozone is limiting. Early in the growing season and at low ozone exposure f_{phen} is always limiting and f_{O_3} then does not come into operation. The original parameterisations given in Emberson *et al.* (2000b) have been revised recently based on data collected from the literature and from ozone exposure experiments conducted in Sweden for wheat (Danielsson *et al.*, 2003) and from a number of sites across Europe for potato (Pleijel *et al.*, 2003).

To account for the effect by transpiration on leaf water potential, which may lead to a limitation of stomatal conductance in the afternoon hours, an additional ΣVPD algorithm is included (Eq. 3.18). This may result in a stronger limitation of stomatal conductance than that suggested by Eq. 3.12 which represents the original formulation given in Emberson *et al.* (2000b). Receptor specific parameterisations are provided for wheat and potato in Table 3.15 (see Section 3.4.5.3)

and provisionally for birch/beech in Table 3.16 (see Section 3.4.6.2).

The range of g_{max} values for different wheat and potato cultivars grown in Europe, and additional data for potato cultivars grown in the USA. The horizontal line represents the chosen g_{max} values (450 $mmol\ m^{-2}\ s^{-1}$ for wheat, (average of observations: 455 $mmol\ m^{-2}\ s^{-1}$); 750 $mmol\ m^{-2}\ s^{-1}$ for potato (average of observations 738 $mmol\ m^{-2}\ s^{-1}$)). g_{max} values are expressed on a projected leaf area basis.

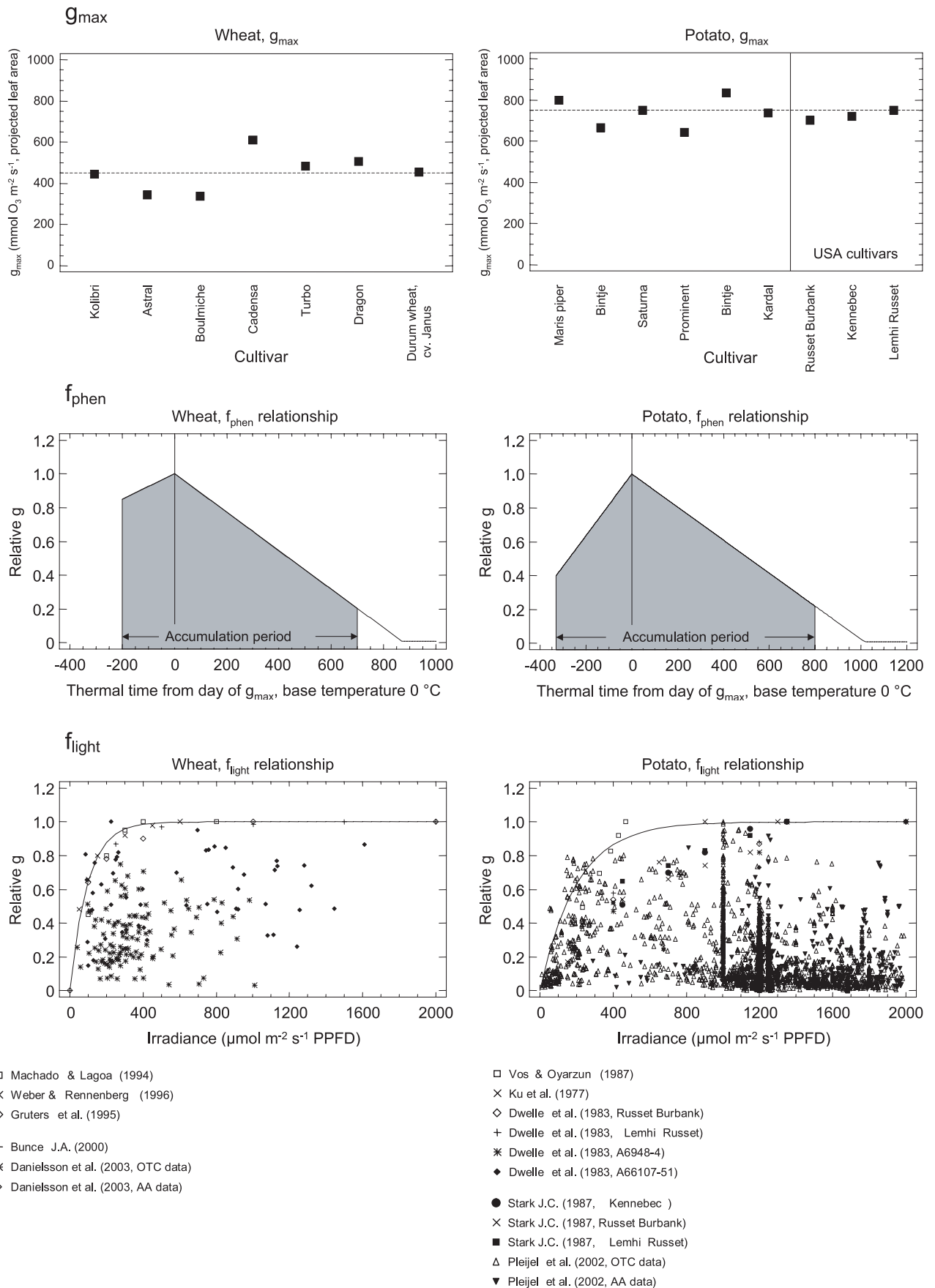


Figure 3.8: Parameterisation of wheat and potato stomatal conductance models

3 Mapping Critical Levels for Vegetation

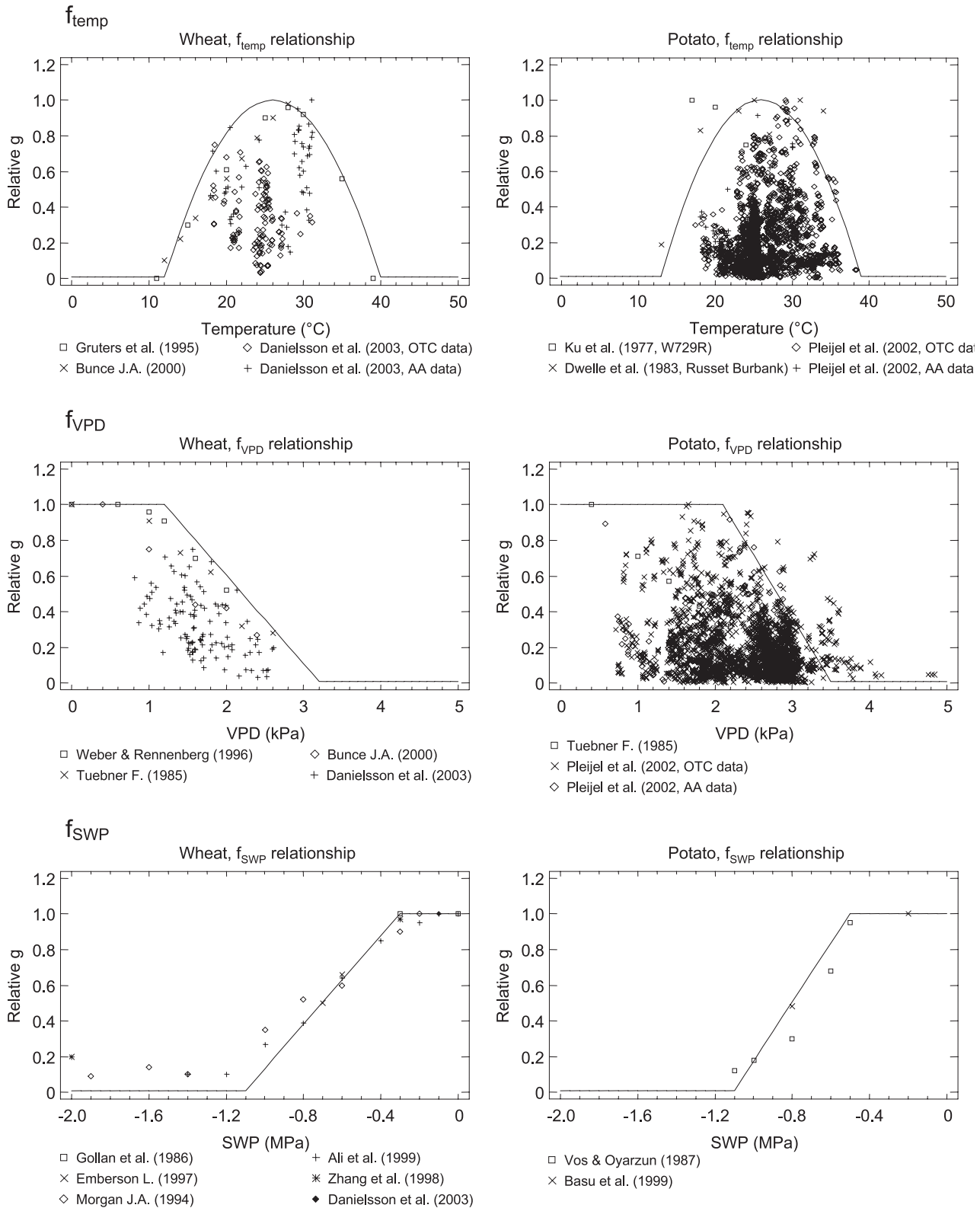


Figure 3.8 (cont):

g_{max} and f_{min}

Receptor-specific values are provided for g_{max} and f_{min} based on analysis of published data (see Sections 3.4.5 and 3.4.6 for details).

f_{phen}

The phenology function can be based on either a fixed number of days or effective temperature sum accumulation and has the same shape for both approaches. However, use of the effective temperature sum is generally accepted to describe plant development more accurately than using a fixed time period since it allows for the influence of temperature on growth. f_{phen} is calculated according to Eq.s 3.13a, b and c (when using a fixed number of days) and 3.14a, b and c (when using effective temperature sum accumulation). Each pair of equations gives f_{phen} in relation to the accumulation period for AF_{stY} where A_{start} and A_{end} are the start and end of the accumulation period respectively.

Method (a): based on a fixed time interval

(3.13a)

when $A_{start} \leq yd < (A_{start} + f_{phen_c})$

$$f_{phen} = (1 - f_{phen_a}) * ((yd - A_{start}) / f_{phen_c}) + f_{phen_a}$$

(3.13b)

when $(A_{start} + f_{phen_c}) \leq yd \leq (A_{end} - f_{phen_d})$

$$f_{phen} = 1$$

(3.13c)

when $(A_{end} - f_{phen_d}) < yd \leq A_{end}$

$$f_{phen} = (1 - f_{phen_b}) * ((A_{end} - yd) / f_{phen_d}) + f_{phen_b}$$

where yd is the year day; A_{start} and A_{end} are the year days for the start and end of the ozone accumulation period respectively.

Method (b): based on thermal time accumulation

(3.14a)

when $A_{start} \leq tt < (A_{start} + f_{phen_e})$

$$f_{phen} = 1 - \left(\frac{1 - f_{phen_a}}{f_{phen_e}} \right) ((A_{start} + f_{phen_e}) - tt)$$

(3.14b)

when $(A_{start} + f_{phen_e}) \leq tt \leq (A_{end} - f_{phen_f})$

$$f_{phen} = 1$$

(3.14c)

when $(A_{end} - f_{phen_d}) < tt \leq A_{end}$

$$f_{phen} = 1 - \left(\frac{1 - f_{phen_b}}{f_{phen_f}} \right) (tt - (A_{end} - f_{phen_f}))$$

where tt is the effective temperature sum in °C days using a base temperature of 0°C and A_{start} and A_{end} are the effective temperature sums (above a base temperature of 0 °C) at the start and end of the ozone accumulation period respectively. As such A_{start} will be equal to 0°C days

f_{light}

The function used to describe f_{light} is given in Eq. 3.15

(3.15)

$$f_{light} = 1 - \text{EXP}((-light_a) * PFD)$$

where PFD represents the photosynthetic photon flux density in units of $\mu\text{mol m}^{-2} \text{s}^{-1}$.

f_{temp}

The function used to describe f_{temp} is given in Eq. 3.16.

(3.16a)

when $T_{min} < T < T_{max}$

$$f_{temp} = \max \{ f_{min}, [(T - T_{min}) / (T_{opt} - T_{min})] * [(T_{max} - T) / (T_{max} - T_{opt})]^{bt} \}$$

(3.16b)

when $T_{min} > T > T_{max}$

$$f_{temp} = f_{min}$$

where T is the air temperature in °C, T_{min} and T_{max} are the minimum and maximum temperatures at which stomatal closure occurs to f_{min} , T_{opt} is the optimum temperature and bt is defined as follows:

(3.17)

$$bt = (T_{max} - T_{opt}) / (T_{opt} - T_{min})$$

f_{VPD} and ΣVPD routine

The VPD of the air surrounding the leaves is used in two different ways. First, there is a more or less instantaneous effect of high VPD levels on stomata resulting in stomatal closure which reduces the high rate of transpiration water vapor flux rates out of the leaf under such conditions. Under dry and hot conditions such limitation of VPD may occur early during the day after the sunrise. This instantaneous response of the stomata to VPD is described by the f_{VPD} function.

The data used to establish the f_{VPD} relationship for both wheat and potato are shown in Figure 3.8. The functions used to describe f_{VPD} are given in Eq. 3.18.

(3.18)

$$f_{VPD} = \min \{ 1, \max \{ f_{min}, ((1 - f_{min}) * (VPD_{min} - VPD) / (VPD_{min} - VPD_{max})) + f_{min} \} \}$$

Secondly, there is another effect on stomata by water relations which can be modelled using VPD . During the afternoon, the air temperature typically decreases, which is normally, but not always, followed (if the absolute humidity of the air remains constant or increases) by declining VPD . According to the f_{VPD} function this would allow the stomata to re-open if there had been a limitation by f_{VPD} earlier during the day. Most commonly this does not happen. This is related to the fact that during the day the plant loses water through transpiration at a faster rate than it is replaced by root uptake. This results in a reduction of the plant water potential during the course of the day and prevents stomata re-opening in the afternoon. The plant water potential then recovers during the following night when the rate of transpiration is low. A simple way to model the extent of water loss by the plant is to use the sum of hourly VPD values during the daylight hours (as suggested by Uddling *et al.*, 2003). If there is a large sum it is likely to be related to a larger amount of transpiration, and if the accumulated amount of transpiration during the course of the day (as represented by a VPD sum) exceeds a certain value, then stomatal re-opening in the afternoon does not occur. This is represented by the VPD_{sum} function (ΣVPD) which is calculated in the following manner:

(3.19)

$$\text{If } \Sigma VPD \geq \Sigma VPD_{crit}, \text{ then } g_{sto_hour_n+1} \leq g_{sto_hour_n}$$

Where $g_{sto_hour_n}$ and $g_{sto_hour_n+1}$ are the g_{sto} values for hour n and hour $n+1$ respectively calculated according to Eq. 3.12.

ΣVPD (kPa) should be calculated for each daylight hour until the dawn of the next day. Thus, if ΣVPD is larger than or equal to ΣVPD_{crit} , the g_{sto} value calculated using Eq. 3.12 is valid if it is smaller or equal to the g_{sto} value of the preceding hour. If g_{sto} according to Eq. 3.12 is larger than g_{sto} of the preceding hour, given that ΣVPD is larger than or equal to ΣVPD_{crit} , it is replaced by the g_{sto} of the preceding hour in the

estimation of stomatal conductance.

The ΣVPD routine acts as a more mechanistically oriented replacement of the time of day function used in the Pleijel *et al.* (2002) and Danielsson *et al.* (2003) parameterisations. The instantaneous effect of VPD represented by f_{VPD} is allowed to be in operation as a function to further reduce the stomatal conductance also after the ΣVPD routine has started to limit stomatal conductance.

f_{SWP}

The function used to describe f_{SWP} is given in Eq. 3.20.

(3.20)

$$f_{SWP} = \min \{ 1, \max \{ f_{\min}, ((1-f_{\min}) * (SWP_{\min} - SWP) / (SWP_{\min} - SWP_{\max})) + f_{\min} \} \}$$

f_{O_3}

The flux-effect models developed by Pleijel *et al.* (2002) and Danielsson *et al.* (2003) include a function to allow for the influence of ozone concentrations on stomatal conductance (f_{O_3}) on wheat and potato via the onset of early senescence. As such this function is used in association with the f_{phen} function to estimate g_{sto} . The f_{O_3} function typically operates over a one-month period and only comes into operation if it has a stronger senescence-promoting effect than normal senescence. The functions are given in Eq.s 3.21 and 3.22.

The ozone function for spring wheat (based on Danielsson *et al.* (2003) but recalculated for PLA):

(3.21)

$$f_{O_3} = \frac{1}{(1+(AF_{st} O/11.5)^{10})}$$

where $AF_{st}O$ is accumulated from A_{start}

The ozone function for potato (based on Pleijel *et al.* (2002)):

(3.22)

$$f_{O_3} = \frac{1}{(1+(AOT0/40)^5)}$$

where $AOT0$ is accumulated from A_{start}

3.4.5 Calculation of $AF_{st}Y$ and exceedance of CLe_f for agricultural crops

Wheat	CLe_f	An $AF_{st}6$ of $1 \text{ mmol m}^{-2} \text{ PLA}$
	Time period	Either 970°C days, starting 200°C days before mid-anthesis or 55 days starting 15 days before mid-anthesis
	Effect	Yield reduction
Potato	CLe_f	An $AF_{st}6$ of $5 \text{ mmol m}^{-2} \text{ PLA}$
	Time period	Either 1130°C days, starting at plant emergence or 70 days starting at plant emergence
	Effect	Yield reduction

3.4.5.1 Ozone concentration at the top of the wheat and potato canopy

The ozone concentration at the top of the canopy can be calculated using the methods described in Section 3.4.2. For wheat and potato the default height of the top of the canopy is 1.0 m.

3.4.5.2 Estimating the time period for ozone flux accumulation for wheat and potato

Section 3.4.3 described two methods to estimate the influence of phenology on stomatal conductance (i.e. f_{phen}) based on a fixed time interval and based on thermal time accumulation. This section describes, for each of these methods, the procedures to estimate the $AF_{st}Y$ accumulation period for both wheat and potato. The start and end of the accumulation period are identified by A_{start} and A_{end} respectively. Application of the fixed time interval method requires that A_{start} and A_{end} be defined in terms of day of the year whilst application of the thermal time method requires that A_{start} and A_{end} be defined in terms of $^\circ\text{C}$ days above a base temperature of 0°C ; in this case A_{start} will always equal 0°C days though it is necessary to determine the year day for A_{start} .

The four methods that are suggested for estimating the timing of the $AF_{st}Y$ accumu-

lation period listed in order of desirability are: i) the use of observational data describing actual growth stages; ii) the use of local agricultural statistics/information describing the timings of growth stages by region or country iii) the use of phenological growth models in conjunction with daily meteorological data and iv) the use of fixed time periods (which may be moderated by climatic region or latitude).

Wheat

It is necessary to identify the timing of mid-anthesis (defined as growth stage 65 according to Zadoks *et al.*, 1974) for both *spring* and *winter wheat*. In the absence of observational or statistical information describing growth stages, mid-anthesis can be defined using phenological models if daily mean temperature data for the entire year are available.

For *spring wheat*, mid-anthesis can be estimated using a temperature sum value of 1075°C days calculated from plant emergence. In the absence of local information plant emergence can be estimated from typical sowing dates given for *spring wheat* by climatic region in Table 3.14. These can be used to estimate the timing of emergence by assuming that the temperature sum (above a base temperature of 0°C) required for emergence would be 70°C days (assuming an average sowing depth of 3 cm) (Hodges & Ritchie, 1991).

Table 3.12: Derivation of wheat (*Triticum aestivum*) g_{max} parameterisation. PLA = projected leaf area

Reference	g_{max} ($mmol O_3$ $m^{-2} s^{-1}$) PLA	g_{max} derivation	Country	Wheat type and cultivar	Time of day	Time of year	g_{st0} measuring apparatus	Gas / leaf area	Growing conditions	Leaf
Ali <i>et al.</i> (1999)	610 (± 73)	From graph showing leaf conductance plotted against time in days. Maximum approximately $1 mol H_2O m^{-2} s^{-1}$; ± 0.12 . $\pm SE$ of 4 to 6 replicates.	Denmark	Spring wheat, Cadensa	(Assumed mid-day)	August	IRGA LI-6200	H_2O / \times (Assume PLA as use LAI)	Field Lysimeter	Flag
Araus <i>et al.</i> (1989)	444	Value in Table. Cultivar and sowing time (average of 3) g_{st0} used. Means of 5 to 7 replicates. g_{st0} $mmol CO_2 m^{-2} s^{-1}$. Adaxial: 313, abaxial: 149.	Spain	Spring wheat, Kolibri	9 to 13 hrs	14 March to 21 May	LI 1600 steady state porometer	CO_2 / PLA	Field	Flag
Araus <i>et al.</i> (1989)	345	Value in Table. Means and SE \pm of 5 to 7 replicates. g_{st0} $mmol CO_2$ $m^{-2} s^{-1}$. Adaxial: 267 ± 29 , abaxial: 92 ± 16 .	Spain	Spring wheat, Astral	9 to 13 hrs	14 March to 21 May	LI 1600 steady state porometer	CO_2 / PLA	Field	Flag
Araus <i>et al.</i> (1989)	336	Value in Table. Means and SE \pm of 5 to 7 replicates. g_{st0} $mmol CO_2$ $m^{-2} s^{-1}$. Adaxial: 251 ± 15 , abaxial: 99 ± 22 .	Spain	Spring wheat, Boulmiche	9 to 13 hrs	14 March to 21 May	LI 1600 steady state porometer	CO_2 / PLA	Field	Flag
Grueters <i>et al.</i> (1995)	485	Value in text. Maximum measured conductance ($0.97 cm s^{-1}$ H_2O total leaf area after Jones (1983)).	Germany	Spring wheat, Turbo	11 to 12 hrs	17 June to 7 August	LI 1600 steady state porometer	$H_2O / total$ leaf area	Field	Flag
Kömer <i>et al.</i> (1979)	455	Value given in table. $0.91 cm s^{-1}$ for H_2O on a total leaf surface area basis.	Austria	Durum wheat, Janus	-	-	Ventilated diffusion porometer	$H_2O / total$ leaf area	Field	Flag
Danielsson <i>et al.</i> (2003)	507	Value in text. "The maximum conductance value, $414 mmol$ $H_2O m^{-2} s^{-1}$, was taken as g_{max} for the Östad multiplicative model. The conductance values represent the flag leaf and are given per total leaf area".	Sweden	Spring wheat, Dragon	13 hrs	13 Aug, 1996 (AA)	Li-Cor 6200	$H_2O / total$ leaf area	Field OTC and AA	Flag
Mean	455	Range: 336 to 610								
Median	455									

Table 3.13: Derivation of potato (*Solanum tuberosum*) g_{\max} parameterisation. PLA = projected leaf area

Reference	g_{\max} (mmol O_3 $\text{m}^{-2} \text{s}^{-1}$) PLA	g_{\max} derivation	Country	Potato cultivar	Time of day	Time of year	$g_{\text{st}0}$ measuring apparatus	Gas / leaf area	Growing conditions	Leaf
Jeffries (1994)	800	Value given in Figure. Maximum value of 16 mm s^{-1} . Error bar represents SE of the difference between two means ($n=48$).	Scotland	Maris piper	8 to 16 hrs	June	Diffusion porometer	Assumed H_2O / assumed PLA	Field	Fully expanded in upper canopy
Vos & Groenwald (1989)	665	Value given in Figure. Maximum value of 13.3 mm s^{-1} . Replicates approx. 20, the co-efficient of variation typically ranged from 15 to 25%.	Netherlands	Binije	-	June/July	Li-Cor 1600 steady state diffusion porometer	H_2O / PLA	Field	Youngest fully grown leaf
Vos & Groenwald (1989)	750	Value given in Figure. Maximum value of 15 mm s^{-1} . Replicates approx. 20, the co-efficient of variation typically ranged from 15 to 25%.	Netherlands	Saturna	-	June	Li-Cor 1600 steady state diffusion porometer	H_2O / PLA	Field	Youngest fully grown leaf
Marshall & Vos (1991)	643	Value given in Figure. g_{\max} of $527 \text{ mmol H}_2\text{O m}^{-2} \text{ s}^{-1}$ at intermediate N supply. Each point represents the mean of at least three leaves (usually four).	Netherlands	Prominent	-	July	LCA2 portable infra-red gas analyser	H_2O / assumed PLA	Field	Most recently expanded measurable leaf
Pleijel <i>et al.</i> (2002)	836	Value given in Table. g_{\max} of $1371 \text{ mmol m}^{-2} \text{ s}^{-1}$ for H_2O per projected leaf area.	Germany	Binije	12	June	Li-Cor 6200	H_2O / PLA	Field	Fully expanded in upper canopy
Danielsson (2003)	737	Value given in text. g_{\max} of $604 \text{ mmol H}_2\text{O m}^{-2} \text{ s}^{-1}$ per total leaf area.	Sweden	Kardal	11	July	Li-Cor 6200	H_2O / Total leaf area	Field	Fully expanded in upper canopy
Mean Median	738 743	Range: 643 to 836								

For *winter wheat*, growth can be assumed to restart after the winter when temperature exceeds 0°C. Traditionally, the starting date for the accumulation of the effective temperature sum to mid-anthesis for winter wheat is the first date after 1 January when the temperature exceeds 0°C, or 1 January if the temperature exceeds 0°C on that date. Using this start point, mid-anthesis can be estimated using a temperature sum of 1075°C days after 1 January (it should be noted that these calculations ignore any effects of photoperiod).

In the absence of appropriate temperature data, the timing of mid-anthesis for both *spring* and *winter wheat* could be approximated as a function of latitude (degrees *N*) using Eq. 3.23. However, it should be recognised that this method is less preferable to the use of the effective temperature sum models described above since latitude is not directly related to temperature and this method will not distinguish between *spring* and *winter wheat* growth patterns.

(3.23)

$$\text{Mid-anthesis} = 2.57 * \text{latitude} + 40$$

Eq. 3.23 is based on data collected by the ICP Vegetation (Mills *et al.*, 1998) from ten sites across Europe (ranging in latitude from Finland to Slovenia) describing the date of anthesis of commercial winter wheat. Applying Eq. 3.23 across the European wheat growing region would give mid-anthesis dates ranging from the end of April to mid-August at latitudes of 35 to 65°N respectively. These anthesis dates fall appropriately within recognised spring wheat growing seasons as described by Peterson (1965) and also from data for winter wheat supplied for Spain by Gimeno *et al.* (2003b).

Table 3.14: Observed sowing dates for spring wheat in Europe¹

Region	Range	Default
<u>Northern Europe</u>		
Finland	1-30 May	30 May
Norway	1-20 May	20 May
Sweden	1-20 Apr	20 April
Denmark	1 Mar-20 Apr	20 March
<u>Continental Central Europe</u>		
Poland	1-20 Apr	10 April
Czech Republic	10-30 Apr	20 April
Slovakia	10-30 Apr	20 April
Romania	-	
Hungary	-	
Germany	10 Mar-10 Apr	1 April
<u>Atlantic Central Europe</u>		
UK	20 Feb-20 Mar	10 March
The Netherlands	1-30 Mar	15 March
France	1 Mar-10 Apr	20 March
<u>Mediterranean Europe</u>		
Bulgaria	-	
Portugal	20 Jan-10 Mar	10 February
Spain	1-28 Feb	10 February
Italy (soft and durum wheat)	-	(not grown)

¹According to Broekhuizen (1969)

Potato

For potato, it is necessary to identify plant emergence, which normally takes place one week to ten days after sowing. Although the sowing date varies to a considerable extent across Europe, information from the EU-funded research programme CHIP, which investigated the effects of ozone and other stresses on potato, found that plant emergence was obtained on average on day of year 146, with a variation from day 135 at southern and most western European sites to day 162 in Finland. As such, in the absence of local information describing sowing dates it is suggested that year day 146 be used as a default to define A_{start} for potato plant emergence. No phenological models are suggested for use to define A_{start} for this species.

3.4.5.3 Parameterisation of stomatal flux models for wheat and potato

The original parameterisations given in Emberson *et al.* (2000b) have been revised based on data collected from more recently published literature and from ozone exposure experiments conducted in Sweden for wheat (Danielsson *et al.*, 2003) and from a number of sites across Europe for potato (Pleijel *et al.*, 2003). Those recommended for use in calculating AF_{st}^Y using the stomatal flux algorithm described in Section 3.4.4 are shown in Table 3.15.

Table 3.15: Summary of the parameterisation for the stomatal flux algorithms for wheat flag leaves and potato upper-canopy sunlit leaves.

Parameter	Units	Wheat (<i>Triticum aestivum</i>)	Potato (<i>Solanum tuberosum</i>)
g_{max}	mmol O ₃ m ⁻² PLA s ⁻¹	450	750
f_{min}	(fraction)	0.01	0.01
$f_{phen a}$	(fraction)	0.8	0.4
$f_{phen b}$	(fraction)	0.2	0.2
$f_{phen c}$	days	15	20
$f_{phen d}$	days	40	50
$f_{phen e}$	°C days	270	330
$f_{phen f}$	°C days	700	800
light _a	(constant)	0.0105	0.005
T _{min}	°C	12	13
T _{opt}	°C	26	28
T _{max}	°C	40	39
VPD _{max}	kPa	1.2	2.1
VPD _{min}	kPa	3.2	3.5
ΣVPD _{crit}	kPa	8	10
SWP _{max}	MPa	-0.3	-0.5
SWP _{min}	MPa	-1.1	-1.1

The g_{max} values for wheat and potato have been derived from published data conforming to a strict set of criteria so as to be deemed acceptable for use in establishing this key parameter of the flux algorithm. Only data obtained from g_{sto} measurements made on cultivars grown either under field conditions or using field-grown plants in open top chambers in Europe were considered. Measurements had to be made during those times of the day and year when g_{max} would be expected to occur and full details had to be given of the gas for which conductance measurements were made (e.g. H_2O , CO_2 , O_3) and the leaf surface area basis on which the measurements were given (e.g. total or projected). All g_{sto} measurements were made on the flag leaf for wheat and for sunlit leaves of the upper canopy for potato using recognized g_{sto} measurement apparatus. Tables 3.12 and 3.13 give details of the published data used for g_{max} derivation on adherence to these rigorous criteria. Figure 3.8 shows the mean, median and range of g_{max} values for each of the six and four different cultivars that provide the approximated g_{max} values of 450 and 750 $mmol O_3 m^{-2} PLA s^{-1}$ for wheat and potato, respectively.

It should be noted that the wheat g_{max} value has been parameterised from data collected for spring wheat cultivars. Comparisons with data for winter wheat presented by Bunce (2000) would suggest that the g_{max} for spring and winter wheat are likely to be similar. Bunce (2000) gives a g_{max} value of 464 $mmol O_3 m^{-2} s^{-1}$ on a projected leaf area basis for winter wheat. These measurements were conducted in the USA but nevertheless are useful in indicating a similarity in the g_{max} of both wheat types. Similarly, for potato additional g_{max} values from three USA grown cultivars are included in Figure 3.8 for comparison (Stark, 1987) further substantiating the g_{max} value established for this crop type.

f_{min}

The data presented in Pleijel et al. (2003) and Danielsson et al. (2003) clearly show that for

both species, f_{min} under field conditions frequently reaches values as low as 1% of g_{max} . Hence an f_{min} of 1% of g_{max} is used to parameterise the model for both species.

f_{phen}

The data used to establish the f_{phen} relationships for both wheat and potato are given in Figure 3.2 as °C days from g_{max} (where g_{max} is assumed to occur at mid-anthesis for wheat and at the emergence of the first generation of fully developed leaves in potato). Methods are also provided in Section 3.4.4 to estimate f_{phen} according to fixed time periods using the parameterisation given in Table 3.15. These data not shown in Figure 3.8.

f_{light}

The data used to establish the f_{light} relationship for both wheat and potato are shown in Figure 3.8.

f_{temp}

The data used to establish the f_{temp} relationship for both wheat and potato are shown in Figure 3.8.

f_{VPD} and ΣVPD_{crit}

The data used to establish the f_{VPD} relationship for both wheat and potato are shown in Figure 3.8.

Values of ΣVPD_{crit} for wheat and potato are given in Table 3.15.

f_{SWP}

The data used to establish the f_{SWP} relationship for both wheat and potato are given in Figure 3.8. It should be noted that the f_{SWP} relationship for potato is derived from data that describe the response of potato g_{sto} to leaf water potential rather than soil water potential. Vos and Oyarzun (1987) state that their results represent long-term effects of drought, caused by limiting supply of water

rather than by high evaporative demand, and hence can be assumed to apply to situations where pre-dawn leaf water potential is less than 0.1 to 0.2 MPa. As such, it may be necessary to revise this f_{SWP} relationship so that potato g_{sto} responds more sensitively to increased soil water stress.

f_{O_3}

The functions described for wheat and potato in Section 3.4.4 should be used.

Once parameterisation of the model is complete for the species being studied, $AF_{st}Y$ and CLe_f exceedance can be calculated following the stages described in Section 3.4.1.

3.4.6 Calculation of $AF_{st}Y$ and exceedance of CLe_f for forest trees

Beech and birch	CLe_f	Provisionally an $AF_{st}1.6$ of $4 \text{ mmol m}^{-2} \text{ PLA}$
	Time period	One growing season
	Effect	Growth reduction

Note: The recommended method for forest trees is *AOTX*-based critical levels; a provisional $AF_{st}Y$ method is provided for guidance only.

As proposed at the Gothenburg workshop (Karlsson *et al.*, 2003a), a default methodology for a flux-based risk assessment for forest trees is presented, as an alternative to concentration-based *AOT40* exposure assessments. Concentration-based assessment methods do not take climatic limitation (soil moisture deficit, water vapour pressure deficit) of exposure into account and *AOTX*-based approaches may, for example, overestimate environmental risk in southern Europe where summer moisture deficits are commonplace. However, at the time of writing this manual, it was considered that the uncertainties associated with using a flux-based assessment for forest trees for all of Europe were too large for the method to be fully recommended for use (these are dis-

cussed in detail in Karlsson *et al.*, 2003b, 2004). It should also be emphasised that the methodology presented here should not be used for economic assessments of damage or yield loss, but should be used solely for mapping areas at potential risk from ozone and as an alternative to the recommended *AOT40* approach.

3.4.6.1 Ozone concentration at the top of the forest canopy

The ozone concentration at the top of the canopy can be calculated using the methods described in Section 3.4.2. For beech and birch, the default height is 20 m.

3.4.6.2 Parameterisation of the stomatal flux model for beech and birch

The calculation of stomatal conductance (g_{sto}) for sunlit leaves in the upper canopy uses the same multiplicative model as described in Eq. 3.12 for wheat and potato and described in Section 3.4.4, with the exceptions that there is no f_{O_3} function and the ΣVPD routine is not applied to estimate f_{VPD} (see later). The parameterisation of this model is similar to that described in Emberson *et al.* (2000a), but has been improved as information has become available from recently published literature (as described in Karlsson *et al.*, 2003b, 2004). The most significant change has been to the f_{temp} parameterisation that now allows g_{sto} to occur at temperatures down to -5°C (previously the T_{min} value had been 13°C). The model parameterisation described here was used for the derivation of the forest tree flux-based critical level $AF_{st}1.6$ of $4 \text{ mmol m}^{-2} \text{ PLA}$ as described in Karlsson *et al.* (2003b, 2004).

The accumulation period for $AF_{st}Y$ for forest trees currently lasts for the entire growing season since no information is available to define a particular phenologically sensitive period. As such, A_{start} and A_{end} will be equal to the start (onset of bud-burst) and the end (end of leaf senescence period) of the growing season respectively. The default value for

A_{start} is year day 90 and for A_{end} is year day 270. Currently, no data are available to define f_{phen} according to effective temperature sum models so only the fixed time interval f_{phen} methods described in Section 3.4.3 are applied. Where local parameterisations of the model are used, it is recommended that parallel assessments are also made and reported using the default values given in Table 3.16, thus maintaining compatibility between individual national assessments.

Insufficient information is available to define f_{O_3} for forest trees and thus it is recommended that f_{O_3} is set to 1.0 in Eq. 3.12.

The ΣVPD routine described for wheat and potato that accounts for lack of re-opening of stomata in the afternoon, cannot be applied to forest trees with confidence as insufficient data exists to complete the parameterisation. It is thus recommended that this routine is omitted from the f_{VPD} procedure described in Section 3.4.4.

$AF_{st}Y$ and CL_{ef} exceedance should be calculated following the stages described in Section 3.4.1.

Table 3.16: Default parameters for beech for use in estimating ozone flux for forest tree species.

Parameter	Value
g_{max}	134 mmol O ₃ m ⁻² projected leaf area s ⁻¹
f_{min}	0.13 (fraction)
$f_{phen\ a}$	0.3 (fraction)
$f_{phen\ b}$	0.3 (fraction)
$f_{phen\ c}$	50 (days)
$f_{phen\ d}$	50 (days)
$f_{phen\ e}$	no parameterisation available, use fixed time period method
$f_{phen\ f}$	no parameterisation available, use fixed time period method
light a	0.006
T_{min}	-5°C
T_{opt}	22°C
T_{max}	35°C
VPD_{max}	0.93 kPa
VPD_{min}	3.4 kPa
ΣVPD_{crit}	No parameterisation available, omit ΣVPD routine
SWP_{max}	-0.05 MPa
SWP_{min}	-1.5 MPa

Note: values have been modified since original publication of Emberson *et al.* (2000a).

3.5 Calculating exceedance of concentration-based critical levels for ozone

3.5.1 Stages in calculating AOTX and CLe_c exceedance

The calculation of *AOTX* for comparison with the CLe_c value for a given vegetation type or plant species is based on hourly mean values of ozone at the top of the canopy (see Section 3.4.2 for estimating the canopy height ozone concentration from the measurement height ozone concentration). For all daylight hours the difference between the hourly mean concentration and X ppb is calculated; then the sum of all hourly values with a positive value (i.e. with hourly mean ozone concentrations above X ppb) is calculated for the growth period of the receptor. This calculation is illustrated in Figure 3.9.

It is recommended that *AOTX* values for comparison with CLe_c should be calculated as the mean value over the most recent five

years for which appropriate quality assured data are available. For local and national risk assessment, it may also be valuable to choose the year with the highest *AOT40* from the five years.

In summary, the following stages are required for calculation of *AOTX* and exceedance of CLe_c :

1. Identify the relevant growth periods for the receptor for accumulation of the exposure index.
2. Obtain high quality ozone data for this growth period for the five most recent years.
3. Adjust the ozone data from measurement height to canopy height using an appropriate model or the algorithm in this manual.
4. Calculate the *AOTX* index for each of the five years.
5. Obtain the mean of the five values of *AOTX* and compare with CLe_c for the receptor.

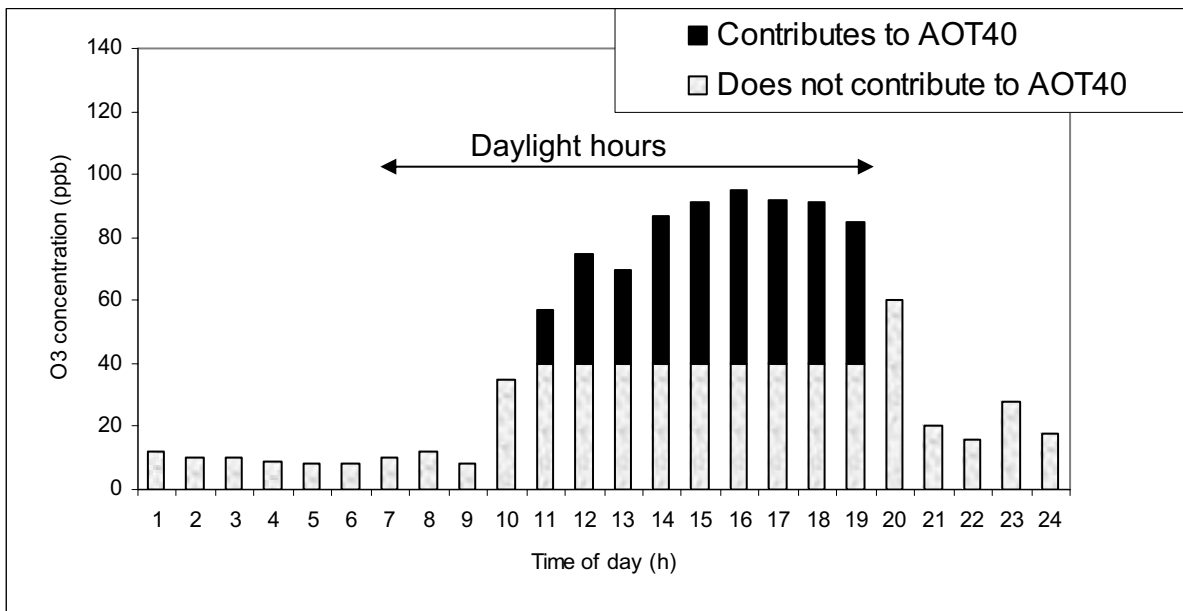


Figure 3.9: Calculation of ozone accumulated over a threshold of 40 ppb (*AOT40*) in ppb h for Balingen (6 May, 1992). The *AOT40* for this day is 383 ppb h, calculated as 17 (exceedance of 40 ppb for 11th hour) + 35 (12th hour) + 30 (13th hour) + 47 (14th hour) + 51 (15th hour) + 55 (16th hour) + 52 (17th hour) + 51 (18th hour) + 45 (19th hour). Exceedance of 40 ppb in the 20th hour is not included because it occurred after daylight had ended.

3.5.2 Calculation of AOTX and CLe_c exceedance for agricultural crops

Agricultural crops	CLe_c	An AOT40 of 3 ppm h
	Time period	3 months
	Effect	Yield reduction

These critical levels are only applicable when nutrient supply and soil moisture are not limiting, the latter because of sufficient precipitation or irrigation.

3.5.2.1 Ozone concentrations at the canopy height for agricultural crops

In all AOTX calculations, the ozone concentration at the canopy height is used and calculated as described in Section 3.4.2. The default canopy height is 1 m for agricultural crops.

3.5.2.2 Accumulation period for agricultural crops

The timing of the three month accumulation period for agricultural crops should reflect the period of active growth of wheat and be centred on the timing of anthesis. A survey of the development of winter wheat conducted at 13 sites in Europe by ICP Vegetation participants in 1997 and 1998, revealed that anthesis can occur as early as 2 May in Spain and as late as 3 July in Finland (Mills *et al.*, 1998). Thus, a risk assessment for ozone impacts on crops would benefit from the use of a moving time interval to reflect the later growing seasons in northern Europe. For guidance, default time periods have been provided for five geographical regions as indicated in Table 3.17.

Once the time period has been established, AOT40 and CLe_c exceedance can be calculated following the stages described in Section 3.5.1.

Table 3.17: Regional classification of countries for default time periods for calculation of AOTX for agricultural crops

Region	Three month time period	Possible default countries
Eastern Mediterranean	1 March to 31 May	Albania, Bosnia and Herzegovina, Bulgaria, Croatia, Cyprus, Greece, FYR Macedonia, Malta, Slovenia, Turkey, Yugoslavia
Western Mediterranean	1 April to 30 June	Italy, Portugal, Spain
Continental Central Europe	15 April to 15 July	Armenia, Austria, Azerbaijan, Belarus, Czech Republic, France ¹ , Georgia, Germany, Hungary, Kazakhstan, Krygyzstan, Liechtenstein, Moldova, Poland, Romania, Russian Federation, Slovakia, Switzerland, Ukraine
Atlantic Central Europe	1 May to 31 July	Belgium, Ireland, Luxembourg, Netherlands, United Kingdom
Northern Europe	1 June to 31 August	Denmark, Estonia, Faero Islands, Finland, Iceland, Latvia, Lithuania, Norway, Sweden

¹as an average between Western Mediterranean and Atlantic Central Europe

3.5.3 Calculation of AOTX and CLe_c exceedance for horticultural crops

Horticultural crops	CLe_c	An AOT40 of 6 ppm h
	Time period	3.5 months
	Effect	Yield reduction

These critical levels are only applicable when nutrient supply and soil moisture are not limiting, the latter because of sufficient precipitation or irrigation.

3.5.3.1 Ozone concentrations at the canopy height for horticultural crops

In all AOTX calculations, the ozone concentration at the canopy height is used and calculated as described in Section 3.4.2. The default canopy height is 1 m for horticultural crops.

3.5.3.2 Accumulation period for horticultural crops

Since horticultural crops are repeatedly sown over several months in many Mediterranean regions, it is recommended that locally-appropriate 3.5 month periods are selected between March and August for eastern Mediterranean areas, and March and October for western Mediterranean areas, although other time periods could be used depending on local crops and horticultural practices. Whereas it is most appropriate to recommend usage of this critical level for Mediterranean regions, it may also be appropriate to apply the critical level to other parts of Europe since several of the cultivars used to derive the critical level are grown in other regions of Europe (Figure 3.5). For such countries, appropriate 3.5 month periods should be selected within the period April to September.

Once the time period has been established, AOT40 and CLe_c exceedance can be calculated following the stages described in Section 3.5.1.

3.5.4 Calculation of $AOTX_{VPD}$ and exceedance of the short-term critical level for ozone injury

Agricultural and horticultural crops	CLe_c	A VPD-modified AOT30 of 0.16 ppm h
	Time period	Previous 8 days
	Effect	Visible injury to leaves

This critical level represents the risk of development of visible injury on sensitive agricultural and horticultural crop species. If VPD values are not available, the AOT30 value can be taken as an indication of potential risk for visible injury without modifying the ozone concentrations. However, over large areas of Europe, VPD typically exerts a considerable restriction to stomatal conductance during the growing season in situations with elevated ozone concentrations.

The $AOTX_{VPD}$ index is calculated by using hourly values of the ozone concentration, expressed in ppb at the height of the top of the canopy (see Section 3.4.2). A default height of 1 m is applicable to agricultural and horticultural crops. Each hourly ozone concentration $[O_3]$ is multiplied by an hourly f_{VPD} factor, reflecting the influence of VPD on stomatal conductance, to get hourly, modified ozone concentrations $[O_3]_{VPD}$:

(3.24)

$$[O_3]_{VPD} = f_{vpd} * [O_3]$$

where:

$$f_{VPD} = 1 \text{ if } VPD < 1.1 \text{ kPa}$$

$$f_{VPD} = - 1.1 * VPD + 2.2 \text{ if } 1.1 \text{ kPa} \leq VPD \leq 1.9 \text{ kPa}$$

$$f_{VPD} = 0.02 \text{ if } VPD > 1.9 \text{ kPa}$$

The calculation of VPD is described in text books (e.g. Jones, 1992).

In the case of the short-term critical level for ozone injury X, in $AOTX_{VPD}$, is 30 ppb. The $AOT30_{VPD}$ is obtained by first subtracting

30 ppb from each hourly $[O_3]_{VPD} > 30$ ppb, and then making a sum of the resulting values. Thus, $[O_3]_{VPD}$ values ≤ 30 ppb do not contribute to $AOTX30_{VPD}$. $AOT30_{VPD}$ is calculated over eight day periods to identify the potential risk of ozone injury on sensitive crops and expressed in units of ppm h. Thus, if the eight day $AOT30_{VPD}$ exceeds the CLe_c for ozone injury, then injury is likely. It is important that the period over which the $AOT30_{VPD}$ value is calculated is consistent with the period when the relevant receptor is actively growing and absorbing ozone. The $AOT30_{VPD}$ value is calculated using running eight day periods throughout the season.

3.5.5 Calculation of AOTX and CLe_c exceedance for (semi-) natural vegetation

(Semi-) natural vegetation	Parameter	An AOT40 of 3 ppm h
	Time period	3 months (or growing season, if shorter)
	Effect	Growth reduction in perennial species and growth reduction and/or seed production reduction in annual species

The concentration-based critical level shown above should be applied to all (semi-) natural vegetation.

3.5.5.1 Ozone concentrations at canopy height

The $AOT40$ value should be calculated as the concentration at canopy height, using the information provided in Section 3.4.2. The transfer functions to make this calculation, based on deposition models, depend on a number of factors which may vary systematically between EUNIS categories (described in Section 3.5.5.3). These include canopy height and leaf area index (both natural variation and effects of management) and environmental variables such as vapour pressure deficit and soil moisture deficit. If such infor-

mation is not available, it is recommended that the conversion factors described in Section 3.4.2 for short grasslands are used as a default.

3.5.5.2 Time window for calculating AOT40 for (semi-) natural vegetation

Ideally, a variable time-window should be used in the mapping procedure to account for different growth periods of annuals and perennials in different regions of Europe. The $AOT40$ is calculated over the first three months of the growing season. The start of the growing season can be identified using:

1. appropriate phenological models;
2. information from local or national experts; and
3. the default table below (Table 3.18).

For a small number of species, the growing season may be less than three months in duration. In such cases, values of $AOT40$ should be calculated over the growing season, identified using appropriate local information.

Once the time period has been established, $AOT40$ and CLe_c exceedance can be calculated following the stages described in Section 3.5.1.

Table 3.18: Default timing for the start and end of ozone exposure windows for (semi-) natural vegetation.

Note: regional classifications of countries are suggested in Table 3.17.

Region	Start	End
Eastern Mediterranean*	1 March	31 May
Western Mediterranean*	1 March	31 May
Continental central Europe	1 April	30 June
Atlantic central Europe	1 April	30 June
Northern Europe	1 May	31 July

*Note: For mountainous areas where altitude is >1500 m use 1 April to 30 June.

3.5.5.3 Mapping (semi-) natural vegetation communities at risk from exceedance of the critical level

For more detailed mapping based on communities which are more likely to be sensitive to ozone, the classification of the European Nature Information System, EUNIS (refer to <http://mrw.wallonie.be/dgrne/sibw/Eunis/>) may be used for the preliminary identification of those grassland types across Europe for which the critical level is supported by experimental data. The EUNIS classes for which evidence exists to support the critical level are:

- E1: Dry grasslands
- E2: Mesic grasslands
- E3: Seasonally-wet and wet grasslands
- E7.3: Dehesa

In addition, from reports of substantial visible injury in the field, a further EUNIS category can be identified as probably sensitive:

- E5: Woodland fringes and clearings and tall forb habitats

Within these categories, particular sub-divisions may be identified as sensitive from their species composition, for example the presence of high proportions of legumes. However, no specific mapping recommendations for EUNIS sub-divisions can be proposed at this stage.

3.5.6 Calculation of AOTX and CLe_c exceedance for forest trees

Forest trees	CLe_c	An AOT40 of 5 ppmh
	Time period	Growing season
	Effect	Growth reduction

3.5.6.1 Ozone concentrations at canopy height.

It is important that the calculation of AOT_{40} is based on ozone concentrations at the top of the canopy as described in Section 3.4.2. The default canopy height for forest trees is 20 m.

3.5.6.2 Time-window for calculating ozone exposure for forest trees

For the purposes of this manual, the default exposure window for the accumulation of AOT_{40} is suggested to be 1 April to 30 September for all deciduous and evergreen species in all regions throughout Europe. This time period does not take altitudinal variation into account and should be viewed as indicative only. It should be stressed that it should only be used where local information is not available. When developing local exposure windows, the following definitions should be used:

- Onset of growing season in deciduous species: the time at which flushing has initiated throughout the entire depth of crown.
- Cessation of growing season in deciduous species: the time at which the first indication of autumn colour change is apparent.
- Onset of growing season in evergreen species: when the night temperatures are above -4°C for 5 days: if they do not fall below -4°C , the exposure window is continuous.
- Cessation of growing season in evergreen species: when the night temperatures are below -4°C for 5 days: if they do not fall below -4°C , the exposure window is continuous.

Once the time period has been established, AOT_{40} and CLe_c exceedance can be calculated following the stages described in Section 3.5.1.

ANNEX1: MPOC approach to risk assessment for forest trees

Note: This method should not be used for mapping at the European scale or for economic impact assessment.

A second approach is provisionally available for application in national-level evaluations, using an alternative concentration-based indicator of potential risk. The Maximum Permissible Ozone Concentration approach (*MPOC*: see Grünhage et al., 2001; Krause et al., 2003 for detailed descriptions of the methodology) is a largely qualitative indicator, relating a range of significant response effects (including growth and physiology) to the concentration of ozone above the canopy over a variety of timeframes. This method should not be used for mapping at the European scale. Using the data for longer term effects identified with the *MPOC* approach, it is possible to indicate that the upper and lower range for effects reported in the literature are seasonal (April to September) 24h mean ozone concentrations in the range 25-74 ppb. As is the case with the *AOT40* approach to mapping areas in which sensitive receptors are at risk from ozone pollution, the *MPOC* approach does not account for environmental limitations (soil moisture deficit, leaf-air vapour pressure deficit) to physiologically effective ozone exposure. The methodology is based on a review of 22 peer-review publications and 50 individual datasets, including a range of different exposure facilities. Although the datasets on which the concept are based cover a range of species and locations across Europe, species common in southern Europe and the Mediterranean region are under-represented. The methodology has also only been validated for sites in Germany, while datasets published after 1999 have not been included in the analysis to date. It is thus suggested that the approach could possibly be adopted as an additional concentration-based index for mapping potential risk in national evaluations, but that economic losses attributable

to ozone pollution could not be estimated on the basis of this approach. Further validation and development of the methodology may be possible under the framework of ICP Forests.

ANNEX 2: Guidance for assessing impacts of ozone on vegetation using the models described in this chapter

The critical levels and methods described for ozone in this chapter were prepared by leading European experts from available knowledge on impacts of ozone on vegetation, and thus represent the current "state of knowledge". As described in the chapter, all indicators for ozone impacts are based on the accumulation of ozone (either as concentration or stomatal flux) above a predetermined threshold over a specified time period. The scientific support for the critical levels of ozone is described in Section 3.3 and the different methods are suitable for various purposes. For ease of use, this annex compiles the suggestions included in the chapter for their application for integrated modelling and where appropriate, for an economic impact assessment. In general, the flux-based approach is deemed suitable for estimating both risk of damage and magnitude of damage, whereas the concentration-based approach is only considered suitable for indicating the risk of damage.

A schematic illustrating the steps involved in calculating exceedance and including references to relevant sections is included in the chapter as Figure 3.1, Section 3.2.4.

Yield loss in agricultural crops: The stomatal flux-effect models for wheat and potato use $AF_{st,6}$ as the ozone parameter (Section 3.4.5), and provide the best available method for estimating impacts of ozone on crops. The impacts can be quantified in various ways, inter alia, by assessing the risk of damage measured as area of flux-based critical level exceedance, or by estimating yield loss using stomatal flux-based functions (Eq. 3.1 and 3.2) which could also be used for economic loss evaluation. The risk of damage can also be determined for agricultural crops using *AOT40*-based critical levels (Section 3.5.2) using a three month time interval for the five climatic zones of Europe (Table 3.17,

Section 3.5.2.2) and a canopy height of 1m (Section 3.5.2.1). An *AOT30*-based critical level has been defined in Section 3.3.1.3 for agricultural crops that could also be used in integrated modelling to determine the risk of damage. However, the *AOT40* and *AOT30* methods do not take into account the influence of climatic conditions on ozone flux and therefore have greater uncertainty associated with them. The methods presented here would enable the quantification of direct effects on yield loss and related economic value for two agricultural crops (wheat and potato). However, it is recognised that an in depth economic assessment of impacts on crops would include direct (e.g. yield, injury) as well as indirect effects (e.g. on pests and diseases) and the associated uncertainty for a range of crops including wheat and potato.

Yield loss in horticultural crops: The only option currently available is to determine the risk of damage as exceedance of the *AOT40*-based critical level for horticultural crops (Section 3.5.3). A canopy height of 1 m should be used (Section 3.5.3.1) as well as a time interval of 3.5 months for the climatic zones suggested (Section 3.5.3.2).

Visible injury on agricultural and horticultural crops: Use the *VPD*-modified *AOT30* (*AOT30VPD*) critical level to assess the frequency of risk of ozone injury over running 8 day periods (Section 3.5.4) using a canopy height of 1 m. If hourly *VPD* data is not available, the *AOT30*-based critical level could be used as an alternative, but with less certainty.

(Semi-) natural vegetation: The only option available at this stage is to determine the risk of damage (growth reduction or reduced seed production) as exceedance of the *AOT40*-based critical level for semi-natural vegetation (Section 3.5.5) using a time interval of three months for five climatic zones as indicated in Table 3.18 and a canopy height of 0.5 m.

Forest trees: The risk of damage (growth reduction) to forest trees can be determined as exceedance of the *AOT40*-based critical level for forest trees (Section 3.5.6) for the growing season (April to September) and a canopy height of 20 m. An *AOT30*-based critical level has been defined in Section 3.3.3 for forest trees that could also be used in integrated modelling to determine the risk of damage. A provisional flux-based critical level for forest trees has been presented in Section 3.4.6, however, it should be not be applied to integrated modelling at this stage. The methods described in this chapter for forest trees should only be used to define risk of damage as the area of exceedance of the critical level; the methods should not be used to quantify the magnitude of effects on growth.

References

- Ali M, Jensen CR, Mogensen VO, Andersen MN, Hensen IE (1999) Root signalling and osmotic adjustment during intermittent soil drying sustain grain yield of field grown wheat. *Field Crops Research* 62: 35-52.
- Araus JL, Tapia L, Alegre L (1989) The effect of changing sowing date on leaf structure and gas exchange characteristics of wheat flag leaves grown under Mediterranean climate conditions. *Journal of Experimental Botany* 40 (215): 639-646.
- Ashmore MR, Ainsworth N (1995) The effect of ozone and cutting on the species composition of artificial grassland communities. *Functional Ecology* 9: 708-712.
- Ashmore MR, Davison AW (1996) Towards a critical level of ozone for natural vegetation. In: Kärenlampi L, Skärby L (eds) (1996). *Op. cit.*: 58-71.
- Ashmore MR, Power SA, Cousins DA, Ainsworth N (1996) Effects of ozone on native grass and forb species: a comparison of responses of individual plants and artificial communities. In: Kärenlampi L, Skärby L (eds) (1996). *Op. cit.*: 193-197.
- Ashmore MR, Wilson RB (eds) (1993) *Critical levels of Air Pollutants for Europe. Background Papers prepared for the ECE Workshop on critical levels, Egham, UK: 23-26 March 1992.*
- Basu PS, Sharma A, Garg ID, Sukumaran NP (1999) Tuber sink modifies photosynthetic response in potato under water stress. *Environmental and Experimental Botany* 42: 25-39.
- Baumgarten M, Werner H, Häberle KH, Emberson L, Fabian P, Matyssek R (2000) Seasonal ozone exposure of mature beech trees (*Fagus sylvatica*) at high altitude in the Bavarian forest (Germany) in comparison with young beech grown in the field and in phytotrons. *Environmental Pollution* 109: 431-442.
- Bender J, Bergmann E, Dohrmann A, Tebbe CC, Weigel HJ (2002) Impact of ozone on plant competition and structural diversity of rhizosphere microbial communities in grassland mesocosms. *Phyton* 42: 7-12.
- Benton J, Fuhrer J, Sanchez-Gimeno B, Skärby L, Sanders GE (1995) Results from the UN/ECE ICP-Crops indicate the extent of exceedance of the critical levels of ozone in Europe. *Water, Air and Soil Pollution* 85: 1473-1478.
- Bergmann E, Bender J, Weigel HJ (1996) Ozone and natural vegetation: Native species sensitivity to different ozone exposure regimes. In: Fuhrer J, Achermann B (eds) (1999): *Op. cit.*: 205-209.
- Bermejo V (2002) *Efectos del ozono sobre la producción y la calidad de frutos de Lycopersicon esculentum. Modulación por factores ambientales. Facultad de Ciencias, Departamento de Biología, Universidad Autónoma de Madrid. PhD Thesis.*
- Broekhuizen S (1969) *Atlas of the cereal-growing areas in Europe. Pudoc, Center for Agricultural Publishing and Documentation, Wageningen, The Netherlands.*
- Bunce JA (2000) Responses of stomatal conductance to light, humidity and temperature in winter wheat and barley grown at three concentrations of carbon dioxide in the field. *Global Change Biology* 6: 371-382.
- Calvo E (2003) *Efectos del ozono sobre algunas hortalizas de interés en la cuenca mediterránea occidental. Universitat de Valencia. PhD Thesis.*
- Danielsson H (2003) *Exposure, uptake and effects of ozone. Department of Environmental Science, Göteborg University, Sweden. PhD Thesis.*
- Danielsson H, Pihl Karlsson G, Karlsson PE, Pleijel H (2003) Ozone uptake modelling and flux-response relationships – an assessment of ozone-induced yield loss in spring wheat. *Atmospheric Environment* 37: 475-485.
- Dwelle RB, Hurley PJ, Pavek JJ (1983) Photosynthesis and stomatal conductance of potato clones (*Solanum tuberosum* L.). *Plant Physiology* 72: 172-176.
- Emberson LD (1997) *Defining and mapping relative potential sensitivity of European vegetation to ozone. Imperial College, University of London. PhD Thesis.*

- Emberson LD, Ashmore MR, Cambridge HM, Simpson D, Tuovinen JP (2000a) Modelling stomatal ozone flux across Europe. *Environmental Pollution* 109: 403-413.
- Emberson L, Simpson D, Tuovinen JP, Ashmore MR, Cambridge HM (2000b) Towards a model of ozone deposition and stomatal uptake over Europe. EMEP MSC-W Note 6/2000.
- Franzaring J, Tonneijck AEG, Kooijman AWN, Dueck TA (2000) Growth responses to ozone in plant species from wetlands. *Environmental and Experimental Botany* 44: 39-48.
- Fuhrer J, Ashmore MR, Mills G, Hayes F, Davison AW (2003) Critical levels for semi-natural vegetation. In: Karlsson PE, Selldén G, Pleijel H (eds) (2003a): Op. cit.
- Fuhrer J (1995) Integration of the ozone critical level approach in modelling activities. Background paper to the EMEP Workshop on the Control of Photochemical Oxidants over Europe, 24-27 October 1995 in St. Gallen, Switzerland. Federal Office of Environment, Forest and Landscape, Berne.
- Fuhrer J (1994) The critical level for ozone to protect agricultural crops – An assessment of data from European open-top chamber experiments. In: Fuhrer J, Achermann B (eds) (1994): Op. cit.: 42-57.
- Fuhrer J, Achermann B (eds) (1999) Critical Levels for Ozone – Level II. Swiss Agency for the Environment, Forests and Landscape, Berne. Environmental Documentation No. 115.
- Fuhrer J, Achermann B (eds) (1994) Critical Levels for Ozone. UNECE Workshop Report, Schriftenreihe der FAC Berne-Liebefeld.
- Fuhrer J, Skärby L, Ashmore MR (1997) Critical levels for ozone effects on vegetation in Europe. *Environmental Pollution* 97(1-2): 91-106.
- Gelang J, Pleijel H, Sild E, Danielsson H, Younis S, Sellden G (2000) Rate and duration of grain filling in relation to flag leaf senescence and grain yield in spring wheat (*Triticum aestivum*) exposed to different concentrations of ozone. *Physiologia Plantarum* 110: 366-375.
- Gimeno BS, Bermejo V, Sanz J, De La Torre D, Gil JM (2003a) Ambient ozone levels induce adverse effects on the flower production of three clover species from Iberian Rangelands. In: Karlsson PE, Selldén G, Pleijel H (eds) (2003a): Op. cit.
- Gimeno BS, De la Torre D, Gonzalez A, Lopez A, Serra J (2003b) Determination of weighting factors related with soil water availability to assess ozone impact on Mediterranean wheat crops (*T. aestivum* L.). In: Karlsson PE, Selldén G, Pleijel H (eds) (2003a): Op. cit.
- Gimeno BS, Bermejo V, Sanz J, De la Torre D, Gil JM (2004) Assessment of the effects of ozone exposure and plant competition on the reproductive ability of three therophytic clover species from Iberian pastures. *Atmospheric Environment* (in press).
- Gollan T, Passioura JB, Munns R (1986) Soil water status effects the stomatal conductance of fully turgid wheat and sunflower leaves. *Australian Journal of Plant Physiology* 13: 459-464.
- Grünhage L, Krause GHM, Köllner B, Bender J, Weigel HJ, Jäger HJ, Guderian R (2001) A new flux-orientated concept to derive Critical Levels for ozone to protect vegetation. *Environmental Pollution* 111: 355-362.
- Gruters U, Fangmeier A, Jager HJ (1995) Modelling stomatal responses of spring wheat (*Triticum aestivum* L. cv. Turbo) to ozone at different levels of water supply. *Environmental Pollution* 87: 141-149.
- Hassan IA, Bender J, Weigel HJ (1999) Effects of ozone and drought stress on growth, yield and physiology of tomatoes (*Lycopersicon esculentum* Mill. Cv. Baladey). *Gartenbauwissenschaft* 64: 152-157.
- Hodges T, Ritchie J (1991) The CERES-Wheat phenology model. In: Hodges T (ed.), *Predicting crops phenology*, CRC Press, Boca Raton, FL: 131-141.
- Jeffries RA (1994) Drought and chlorophyll fluorescence in field-grown potato (*Solanum tuberosum*). *Physiologia Plantarum* 90: 93-97.
- Jones HG (1992) *Plants and microclimate: A quantitative approach to environmental plant physiology* (2nd edition). Cambridge University Press, Cambridge.

- Kärenlampi L, Skärby L (eds) (1996) Critical levels for ozone in Europe: testing and finalising the concepts. UNECE Workshop Report, University of Kuopio, Department of Ecology and Environmental Science.
- Karlsson PE, Selldén G, Pleijel H (eds) (2003a) Establishing Ozone Critical Levels II. UNECE Workshop Report, IVL report B 1523, IVL Swedish Environmental Research Institute, Gothenburg, Sweden. <http://www.ivl.se>
- Karlsson PE, Uddling J, Braun S, Broadmeadow M, Elvira S, Gimeno BS, Le Thiec D, Oksanen E, Vandermeiren K, Wilkinson M, Emberson L (2003b) New Critical Levels for Ozone Impact on Trees Based on AOT40 and Leaf Cumulated Uptake of Ozone. In: Karlsson PE, Selldén G, Pleijel H (eds) (2003a): Op. cit.
- Karlsson PE, Uddling J, Braun S, Broadmeadow M, Elvira S, Gimeno BS, Le Thiec D, Oksanen E, Vandermeiren K, Wilkinson M, Emberson L (2004) New critical levels for ozone effects on young trees based on AOT40 and simulated cumulative leaf uptake of ozone. *Atmospheric Environment* (in press).
- Klumpp A, Ansel A, Klumpp G, Belluzzo N, Calatayud V, Chaplin N, Garrec JP, Gutsche HJ, Hayes M, Hentze HW, Kambezidis H, Laurent O, Peñuelas J, Rasmussen S, Ribas A, Ro-Poulsen H, Rossi S, Sanz MJ, Shang H, Sifakis N, Vergne P (2002) EuroBionet: A pan-European biominotoring network for urban air quality assessment. *Environmental Science and Pollution Research* 9: 199-203.
- Korner C, Scheel JA, Bauer H (1979) Maximum leaf diffusive conductance in vascular plants. *Photosynthetica* 13(1): 45-82.
- Krause GHM, Kollner B, Grünhage L (2003) Effects of ozone on European forest tree species – a concept of local risk evaluation within ICP-Forests. In: Karlsson PE, Selldén G, Pleijel H (eds) (2003a): Op. cit.
- Ku SB, Edwards GE, Tanner CB (1977) Effects of light, carbon dioxide and temperature on photosynthesis, oxygen inhibition of photosynthesis, and transpiration in *Solanum tuberosum*. *Plant Physiology* 59: 868-872.
- Machado EC, Lagôa AMMA (1994) Trocas gasosas e condutancia estomatosa em tres especies de gramíneas. *Bragantia Campinas* 53(2): 141-149.
- Manninen S, Siivonen N, Timonen U, Huttunen S (2003) Differences in ozone response between two Finnish wild strawberry populations. *Environmental and Experimental Botany* 49: 29-39.
- Marshall B, Vos J (1991) The relationship between the nitrogen concentration and photosynthetic capacity of potato (*Solanum tuberosum* L.) leaves. *Annals of Botany* 68: 33-39.
- McLean DC, Schneider RE (1976) Photochemical Oxidants in Yonkers, New York: Effects on Yield of Bean and Tomato. *Journal of Environmental Quality* 5: 75-78.
- McNaughton KG, Van der Hurk BJJM (1995) 'Lagrangian' revision of the resistors in the two-layer model for calculating the energy budget of a plant canopy. *Boundary Layer Meteorology* 74: 261-288.
- Mills GE, Ball GR (1998) Annual Progress Report for the ICP-Crops (September 1997-August 1998). ICP-Crops Coordination Centre, CEH Bangor, UK.
- Mills G, Holland M, Buse A, Cinderby S, Hayes F, Emberson L, Cambridge H, Ashmore M, Terry A (2003) Introducing response modifying factors into a risk assessment for ozone effects on crops in Europe. In: Karlsson PE, Selldén G, Pleijel H (eds) (2003a): Op. cit.
- Morgan JA (1984) Interaction of water supply and N in wheat. *Plant Physiology* 76: 112-117.
- Novak K, Skelly JM, Schaub M, Kräuchi N, Hug C, Landolt W, Bleuler P (2003) Ozone air pollution and foliar injury development on native plants of Switzerland. *Environmental Pollution* (in press).
- Nussbaum S, Geissmann M, Fuhrer J (1995) Ozone exposure-response relationships for mixtures of perennial ryegrass and white clover depend on ozone exposure patterns. *Atmospheric Environment* 29(9), 989-995.
- Oshima RJ, Taylor OC, Braegelmann PK, Baldwin DW (1975) Effect of ozone on the yield and plant biomass of a commercial variety of tomato. *Journal of*

- Environmental Quality 4: 463-464.
- Peterson RF (1965) *Wheat: Botany, cultivation, and utilization*. Leonard Hill Books, London.
- Pihl Karlsson G, Karlsson PE, Danielsson H, Pleijel H (2003) Clover as a tool for bioindication of phytotoxic ozone – 5 years of experience from Southern Sweden – consequences for the short-term Critical Level. *Science of the Total Environment* 301: 1-3, 205-213.
- Pihl Karlsson G, Soja G, Vandermeiren K, Karlsson PE, Pleijel H (2004) Test of the short-term Critical Levels for acute ozone injury on plants – improvements by ozone uptake modelling and the use of an effect threshold. *Atmospheric Environment*, in press.
- Pleijel H (1996) Statistical aspects of Critical Levels for ozone. In: Kärenlampi L, Skärby L (eds) (1996): Op. cit.
- Pleijel H, Danielsson H, Ojanperä K, De Temmerman L, Högy P, Karlsson PE (2003) Relationships between ozone exposure and yield loss in European wheat and potato – A comparison of concentration based and flux based exposure indices. In: Karlsson PE, Selldén G, Pleijel H (eds) (2003a): Op. cit.
- Pleijel H, Danielsson H, Vandermeiren K, Blum C, Colls J, Ojanperä K (2002) Stomatal conductance and ozone exposure in relation to potato tuber yield – results from the European CHIP programme. *European Journal of Agronomy* 17: 303-317.
- Power SA, Ashmore MR (2002) Responses of fen and fen meadow communities to ozone. *New Phytologist* 156: 399-408.
- Reinert RA, Eason G, Barton J (1997) Growth and fruiting of tomato as influenced by elevated carbon dioxide and ozone. *New Phytologist* 137: 411-420.
- Ribas A, Peñuelas J (2003) Biomonitoring of tropospheric ozone phytotoxicity in rural Catalonia. *Atmospheric Environment* 37: 63-71.
- Skärby L, Karlsson PE (1996) Critical levels for ozone to protect forest trees - best available knowledge from the Nordic countries and the rest of Europe. In: Kärenlampi L, Skärby L (eds) (1996): Op. cit.
- Stark JC (1987) Stomatal behaviour of potatoes under non-limiting soil water conditions. *American Potato Journal* 64: 301-309.
- Temple PJ (1990) Growth and yield responses of processing tomato (*Lycopersicon esculentum*) cultivars to ozone. *Environmental and Experimental Botany* 30: 283-291.
- Temple PJ, Surano KA, Muttters RG, Bingham GE, Shinn JH (1985) Air Pollution causes moderate damage to tomatoes. *California Agriculture*: 21-23.
- Tuebner F (1985) *Messung der Photosynthese und Transpiration an Weizen, Kartoffel und Sonnenblume*. Diplomarbeit University Bayreuth, West Germany.
- Uddling J, Pleijel H, Karlsson PE (2004) Modelling leaf diffusive conductance in juvenile silver birch, *Betula pendula*. *Agricultural and Forest Meteorology* (in press).
- UNECE (1988) Final Draft Report of the Critical Levels Workshop, Bad Harzburg, Germany, 14-18 March 1988. Available at Federal Environmental Agency Berlin, c/o Dr. Heinz Gregor, Germany.
- UNECE (1995) Effects of Nitrogen and Ozone. Report of the International Cooperative Programmes and the Mapping Program of the Working Group on Effects. EB.AIR/WG.1/R.110.
- UNECE (1996) Manual on methodologies and criteria for mapping critical levels/loads and geographical areas where they are exceeded. Texte 71/96, Umweltbundesamt, Berlin, Germany.
- Van der Heyden D, Skelly J, Innes J, Hug C, Zhang J, Landolt W, Bleuler P (2001) Ozone exposure thresholds and foliar injury on forest plants in Switzerland. *Environmental Pollution* 11: 321-331.
- Vos J, Groenwald J (1989) Characteristics of photosynthesis and conductance of potato canopies and the effects of cultivar and transient drought. *Field Crops Research* 20: 237-250.
- Vos J, Oyarzun PJ (1987) Photosynthesis and stomatal conductance of potato leaves - effects of leaf age, irradiance, and leaf water potential. *Photosynthesis Research* 11: 253-264.

Weber P, Rennenberg H (1996) Dependency of Nitrogen dioxide (NO₂) fluxes to wheat (*Triticum aestivum* L.) leaves from NO₂ concentration, light intensity, temperature and relative humidity determined from controlled dynamic chamber experiments. *Atmospheric Environment* 30(17): 3001-3009.

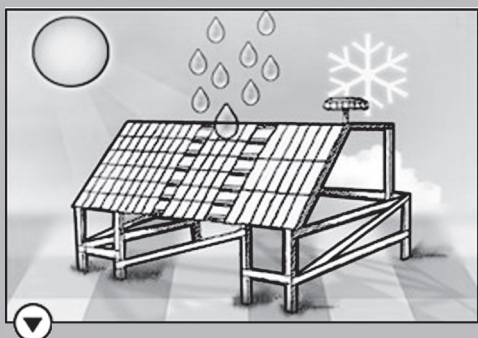
WHO (2000) Air Quality Guidelines for Europe. WHO Regional Publications, No. 91, World Health Organisation, Copenhagen. Available at <http://www.who.dk/>

Zadoks JC, Chang TT, Konzak CF (1974) A decimal code for the growth stages of cereals. *Weed Research* 14: 415-421.

Zhang J, Xiangzhen S, Li B, Su B, Li J, Zhou D (1998) An improved water-use efficiency for winter wheat grown under reduced irrigation. *Field Crops Research* 59: 91-98.

Mapping Manual 2004

International Co-operative Programme on Effects on Materials, including Historic and Cultural Monuments



UNECE CONVENTION ON LONG-RANGE TRANSBOUNDARY AIR POLLUTION

ICP Materials is one of several effect oriented International Co-operative Programmes (ICPs) within the United Nations Economic Commission for Europe (UN ECE) and its Environment and Human Settlements Division. Early in the discussions on the Convention on Long-range Transboundary Air Pollution (CLRTAP) it was recognised that a good understanding of the harmful effects of air pollution was a prerequisite for reaching agreement on effective pollution control. To develop the necessary international co-operation in the research on and the monitoring of pollutant effects, the Working Group on Effects (WGE) was established under the Convention. For further information about the ICP, see the home page www.corr-institute.se/ICP-Materials

Chapter4 was compiled and edited by V.Kucera (ICP Materials Coordination Centre, Sweden)

4.1 Introduction - objectives, definitions and general remarks

Atmospheric pollution is an important factor in material deterioration including degradation of systems used for material protection. Due to pollution, the lifetime of technological products is shortened. Buildings, other structures, as well as objects of cultural heritage exposed to the atmosphere deteriorate more rapidly. The resulting physico-chemical and economic damage can be significant - not to mention the loss of unique parts of our cultural heritage and hazards due to endangered reliability of complicated technological devices.

Also, as the result of weathering due to especially acidifying pollutants, a significant part of the metals used in constructions and products are emitted to the biosphere with a potential hazard to the environment.

This part of the manual was revised in connection with the UNECE Workshop on Mapping Air Pollution Effects on Materials, Including Stock at Risk, held in Stockholm, Sweden on 14-16 June 2000 (UNECE 2000). The present revision has been performed by the UNECE ICP on Materials with support from ICP Modelling and Mapping, based on results obtained at evaluation of deterioration of materials after 8-year field exposure (Tidblad, Kucera, Mikhailov 1998) his chapter considers the corrosive effects of gaseous SO_2 , NO_x , ozone and acid rainfall in combination with climatic parameters. It aims to define procedures for mapping "acceptable values" of pollutants for buildings and materials including cultural and historical monuments in an analogous way to the methods defined elsewhere for critical levels and loads for natural ecosystems.

Because atmospheric deterioration of materials is a cumulative, irreversible process, which proceeds even in the absence of pollutants, "critical" values are not as easily defined as for some natural ecosystems. Some rate of deterioration must be defined which may be considered "acceptable"

based on technical and economic considerations. This approach provides the basis for mapping "acceptable areas" for corrosion and deriving areas where the acceptable pollution level/load is exceeded, in an analogous way to the maps produced for natural ecosystems.

Acceptable load/level. The "acceptable level or load" of pollutants for buildings and materials is the concentration or load which does not lead to an unacceptable increase in the rate of corrosion or deterioration.

Acceptable rate of corrosion or deterioration (K_a) may be defined as the corrosion, which is considered "acceptable" based on technical and economic considerations. In reality this may not be considered practical. Therefore, it is recommended that the acceptable corrosion rate should be expressed in terms of average corrosion rates in areas with "background" pollution. Within the UNECE ICP on Materials it was decided to recommend the **background corrosion or deterioration rate (K_b)** as the lower 10 percentile of the observed corrosion rates in the materials exposure programme which started in 1987 and ended in 1995. Acceptable corrosion rates are then defined as a multiple (n) of the background corrosion rate

(4.1)

$$K_a = n \cdot K_b$$

It is possible to relate such rates of corrosion to the "lifetimes" or economic values of materials.

Dose-response function. The relationship between the corrosion or deterioration rate and the levels or loads of pollutants in combination with climatic parameters.

Using the above definitions it is possible to calculate the acceptable pollution level from the acceptable corrosion rate and a dose-response function which relates corrosion rate to pollutant and climate exposure.

4.2 Mapping “acceptable corrosion rates” and “acceptable levels/loads” for pollutants

4.2.1 Introduction

Deterioration rates can be calculated using dose-response functions. The functions recommended have been derived from the field research programme undertaken as part of the UNECE ICP Materials Exposure Programme. However, if other functions of the same or of other form are considered more suitable, then they can be used as an alternative. The range of values over which the dose-response function is considered valid must be considered. At this time, scientific evidence from field exposure is limited, in contrary to laboratory experiments. Even if NO_x is not included in the dose-response functions included in this manual it may be included for some materials in the future.

The following equations are based on 8-year results from the exposure within UNECE ICP

on Materials. They reflect the increased level of the physico-chemical understanding of the corrosion mechanisms including the synergistic effects of SO_2 and O_3 in the case of copper. The calculation of an acceptable level for sulfur dioxide and ozone for materials where the synergistic effect with SO_2 is included in the dose-response function is described in 4.2.3.

The impact of wet deposition of acidic species on sensitive materials is in this revision of the Mapping Manual considered as an effect of the total load of H^+ deposition. The calculation and mapping of the acceptable load for materials where the H^+ load is included in the dose-response function is described in 4.2.3.

4.2.2 Dose-response functions

The equations for the following materials are at present available for mapping purposes. The equations are valid for unsheltered exposure of materials (Tidblad, Kucera, Mikhailov 1998, see also the ICP website: www.corrinstitute.se/ICPMaterials).

Structural metals

Weathering steel (C<0.12%, Mn 0.3-0.8%, Si 0.25-0.7%, P 0.07-0.15%,

S<0.04%, Cr 0.5-1.2%, Ni 0.3-0.6%, Cu 0.3-0.55%, Al<0.01%)

$$ML = 34[SO_2]^{0.33} \exp\{0.020Rh\} 34[SO_2]^{0.13} \exp\{0.020Rh + f(T)\} t^{0.33} \quad 0.68 \quad 148 \quad (4.2)$$

$f(T) = 0.059(T-10)$ when $T \leq 10^\circ C$, otherwise $-0.036(T-10)$

Zinc

$$ML = 1.4[SO_2]^{0.22} \exp\{0.018Rh + f(T)\} t^{0.85} + 0.029Rain[H^+]t \quad 0.84 \quad 98 \quad (4.3)$$

$f(T) = 0.062(T-10)$ when $T \leq 10^\circ C$, otherwise $-0.021(T-10)$

Aluminium

$$ML = 0.0021[SO_2]^{0.23} Rh \cdot \exp\{f(T)\} t^{1.2} + 0.000023Rain[Cl^-]t \quad 0.74 \quad 106 \quad (4.4)$$

$f(T) = 0.031(T-10)$ when $T \leq 10^\circ C$, otherwise $-0.061(T-10)$

Copper

$$ML = 0.0027[SO_2]^{0.32} [O_3]^{0.79} Rh \cdot \exp\{f(T)\} t^{0.78} + 0.050Rain[H^+]t^{0.89} \quad 0.73 \quad 95 \quad (4.5)$$

$f(T) = 0.083(T-10)$ when $T \leq 10^\circ C$, otherwise $-0.032(T-10)$

Bronze (Cu Sn6Pb7Zn5, ISO/R 1338 (Cu 81%, Sn 5.8%, Pb 6.7%, Zn 4.5%, Ni 1.6% + trace elements))

$$ML = 0.026[SO_2]^{0.44} Rh \cdot \exp\{f(T)\} t^{0.86} + 0.029 Rain [H^+] t^{0.76} + 0.00043 Rain [Cl] t^{0.76} \quad 0.81 \quad 144 \quad (4.6)$$

$f(T) = 0.060(T-11)$ when $T \leq 11^\circ C$, otherwise $-0.067(T-11)$

Stone materials

Limestone

$$R = 2.7[SO_2]^{0.48} \exp\{-0.018T\} t^{0.96} + 0.019 Rain [H^+] t^{0.96} \quad 0.88 \quad 100 \quad (4.7)$$

Sandstone (White Mansfield dolomitic sandstone)

$$R = 2.0[SO_2]^{0.52} \exp\{f(T)\} t^{0.91} + 0.028 Rain [H^+] t^{0.91} \quad 0.86 \quad 101 \quad (4.8)$$

$f(T) = 0$ when $T \leq 10^\circ C$, otherwise $-0.013(T-10)$

Paint coatings

Coil coated galv. steel with alkyd melamine

$$L = [5 / (0.084[SO_2] + 0.015Rh + f(T) + 0.00082 Rain)]^{1/0.43} \quad 0.73 \quad 138 \quad (4.9)$$

$f(T) = 0.040(T-10)$ when $T \leq 10^\circ C$, otherwise $-0.064(T-10)$

Steel panels with alkyd

$$L = [5 / (0.033[SO_2] + 0.013Rh + f(T) + 0.0013 Rain)]^{1/0.41} \quad 0.68 \quad 139 \quad (4.10)$$

$f(T) = 0.015(T-11)$ when $T \leq 11^\circ C$, otherwise $-0.15(T-11)$

where

<p>ML = mass loss, $g m^{-2}$</p> <p>R = surface recession, μm</p> <p>t = exposure time, years</p> <p>L = maintenance interval (life time), years</p> <p>Rh = relative humidity, % - annual average</p> <p>T = temperature, $^\circ C$ - annual average</p> <p>$[SO_2]$ = concentration, $\mu g m^{-3}$ - annual average</p>	<p>$[O_3]$ = concentration, $\mu g m^{-3}$ - annual average</p> <p>$Rain$ = amount of precipitation, $m year^{-1}$ - annual average</p> <p>$[H^+]$ = concentration, $mg l^{-1}$ - annual average</p> <p>$[Cl^-]$ = concentration, $mg l^{-1}$ - annual average</p>
--	--

The equations are valid for regions without strong influence of sea salts with a chloride content in precipitation $< 5 \text{ mg l}^{-1}$ approx.

The functions for paint coatings are expressed as lifetime equations. These lifetimes can be mapped but the functions can not be used for calculating acceptable levels/loads using the concept of acceptable corrosion rates.

For all these materials, however, also equations for exposure in sheltered positions are available. Also equations are available for glass materials representative of medieval stained glass windows, for paint

coatings and for the electric contact materials nickel and tin (Tidblad, Kucera, Mikhailov 1998).

The preferably recommended value of the background corrosion rate for individual materials is given in Table 4.1. In order to simplify the procedure of obtaining acceptable levels/loads as described in section 4.2.3 the rates in Table 4.1 are expressed for a 1-year exposure period. An analysis of the dose-response functions shows that using longer exposure periods than 1 year leads in principle to very similar acceptable levels/loads.

Table 4.1: Background corrosion rates K_b , expressed for a 1-year exposure period (1997-98), for different materials based on results from the UNECE ICP Materials exposure programme after 1, 2, 4 and 8 years of exposure.

Material	1-year background corrosion rate, K_b
Weathering steel	72 g m ⁻²
Zinc	3.3 g m ⁻²
Aluminium	0.09 g m ⁻²
Copper	3.0 g m ⁻²
Bronze	2.1 g m ⁻²
Limestone	3.2 μm
Sandstone	2.8 μm

4.2.3 Calculation and mapping of acceptable levels/loads and their exceedances

Mapping will produce a map which depicts the mapping units that exceed the acceptable deterioration rate (K_a) for simple samples of material used in particular locations expressed in a number of defined classes. It makes no correction for the form in which the material is used (e.g. the type of component). At present it is recommended that n values 1.5, 2.0 and 2.5 are used (see eq. 4.1). It should, however, be emphasised that lower n values can be used for, e.g.

areas with valuable objects of cultural heritage.

The data requirements are annual mean SO_2 and O_3 concentrations in $\mu\text{g m}^{-3}$, the temperature in $^{\circ}\text{C}$, the relative humidity in %, the total rainfall in mm year^{-1} , and the concentration of H^+ and Cl^- in mg/l for each mapping unit (e.g. the EMEP grid size 50 x 50 km or smaller, preferably as a fraction of the EMEP size). In addition, the value for the background corrosion rate is required. The values are then used to calculate the corrosion rate and the corrosion rate as a ratio of

the background corrosion rate. All mapping units that exceed the acceptable corrosion rate ($n \cdot K_b$) are then identified.

In each mapping unit that exceeds the acceptable corrosion rate, the same data sets and dose-response functions are then used to calculate the

- SO_2 concentration
- O_3 concentration (for copper)
- H^+ load

that keeps this rate at an acceptable level.

(4.11)

$$[SO_2]_{accCu} = [(3.0 \cdot n - 0.050 \text{Rain}[H^+]) / (0.0027[O_3]^{0.79} \text{Rh} \cdot \exp\{f(T)\})]^{1/0.32}$$

(4.12)

$$[O_2]_{accCu}[O_3]_{accCu} = [(3.0 \cdot n - 0.050 \text{Rain}[H^+]) / (0.0027[SO_2]^{0.32} \text{Rh} \cdot \exp\{f(T)\})]^{1/0.79}$$

(4.13)

$$(\text{Rain}[H^+])_{accCu} = (3.0 \cdot n - 0.0027[SO_2]^{0.32}[O_3]^{0.79} \text{Rh} \cdot \exp\{f(T)\}) / 0.050$$

where

$[SO_2]_{accCu}$ = acceptable concentration for corrosion of copper at given values of other parameters, $\mu g m^{-3}$

$[O_3]_{accCu}$ = acceptable concentration for corrosion of copper at given values of other parameters, $\mu g m^{-3}$

$\text{Rain}[H^+]_{accCu}$ = acceptable value of H^+ load for corrosion of copper at given values of other parameters (product of amount of precipitation, $mm year^{-1}$, and concentration of H^+ , $mg l^{-1}$)

n = acceptable corrosion/deterioration rate (see eq. 4.1)
background corrosion/deterioration rate

and the other symbols as in point 4.2.2.

The equations have the following form, illustrated on the example of copper. For the other materials the equations for SO_2 concentration and H^+ load are created from the dose-response relations in an analogous way, except that O_3 is not included in the functions. The basis for the calculations should be one year of exposure ($t=1$) since K_b is expressed for this period.

The values of the climatic and pollution data for each grid square can usually be obtained from national or international meteorological centres, international organisations e.g. (WHO), international research programmes (e.g. EMEP) or national organisations or authorities responsible for environmental protection.

When data on ozone concentrations are not available, but concentrations of NO_2 are known, a crude approximation of ozone values can be obtained using one of the following empirical equations, which are based on data from the UNECE ICP Materials Programme:

$$(4.14) \quad [O_3] = 57 \cdot \exp\{-0.012[NO_2]\} \quad r^2 = 0.70 \quad n = 103$$

$$(4.15) \quad [O_3] = (38 + 0.013Sun) \cdot \exp\{(-0.022 - 0.000005Sun)[NO_2]\} \quad r^2 = 0.78 \quad n = 132$$

where

$[O_3]$ = average annual concentration, $\mu g m^{-3}$

$[NO_2]$ = average annual concentration, $\mu g m^{-3}$

Sun = sunshine duration, $h year^{-1}$

Eq. 4.14 is based on values from the five first years of exposure (1987-1992) while eq. 4.15 is based on values from all eight one-year exposure periods (1987-1995). Eq. 4.15 is preferred but 4.14 may be used if data on sunshine duration is not available. It should be stressed that the equations are empirical and obtained in the absence of a theory from which a relation between ozone and nitrogen dioxide concentrations could be derived. More importantly, the equations are based on a set of NO_x and ozone concentration data that include inner-city data. The latter are characterised by very high NO_x and low O_3 , which is a situation not found in rural/remote areas that are of most interest for the other parts of the mapping pro-

gramme and in the general framework of the Convention on Long-range Transboundary Air Pollution. If only those values typical for rural/remote areas were used, a different relationship between O_3 and NO_x would emerge. Note that, according to eq. 4.14, a long-term average ozone concentration larger than $57 \mu g m^{-3}$ would not be possible; however, this is a relatively low value in rural/remote areas.

4.2.4 Calculations and mapping of costs resulting from corrosion

The ultimate goal of the mapping activities in the field of materials is the calculation of cost of damage caused by air pollutants to materials. While it is not recommended to assess the absolute cost, it is possible to estimate the difference in cost between two alternative scenarios using the equation

$$(4.16) \quad \Delta C = C \cdot S \cdot (L_{s1}^{-1} - L_{s2}^{-1})$$

where ΔC is the cost difference, C is the cost per surface area of material, for maintenance/replacement, S is the surface area of material, $L_p L_{s1}$ is the maintenance interval (life time) in polluted areas and L_c for scenario 1 and L_{s2} is the maintenance interval for scenario 2. If eq. 4.16 is to be used for estimating the cost of corrosion due to pollutants in the present situation it is in clean areas. recommended to use the present pollution situation as scenario 1 and the background corrosion as scenario 2. When calculating the lifetime from the background scenario it is recommended to use the time dependence from the dry deposition term given in eqs. 4.2 - 4.8, for example $t^{0.85}$ for zinc. For the paint coatings it is not recommended to use eqs. 4.9 - 4.10 for cost calculations since the evaluation are based on damage from an intentionally made scratch, which may be regarded as a form of accelerated testing.

Instead the practical functions described in Kucera et al. (1993) are recommended.

A UNECE Workshop on economic evaluation of air pollution abatement and damage to buildings including cultural heritage took place in Stockholm on 23-25 January 1996 (UNECE 1997). The proceedings of the workshop summarised the state of the art, and is given in the reference list together with a selection of other important publications (Kucera et al. 1993, ECOTEC 1986, Tolstoy et al. 1989, Cowell, Apsimon 1996). In the ECOTEC study of 1986, building identikits for Birmingham (UK), Dortmund and Koeln (Germany) were compiled (ECOTEC 1986). For Stockholm (Sweden), Sarpsborg (Norway), and Prague (Czech Republic) statistically based inventories of outdoor material surfaces were compiled by Kucera et al. (1993). These studies include percentage values of the most common construction materials and their distribution, which in absence of stock at risk data may provisionally be used as default values.

Mapping of cost of damage will be similar to mapping of acceptable levels/loads but will include data on the stock of material in each mapping unit and the economic costs associated with deterioration of these materials (e.g. replacement or repair costs). The classes to be used are based on multiples of the Background Deterioration Rate. The change in the rate of deterioration can be used to estimate the cost associated with the deterioration. This can be used to estimate the costs resulting from the deterioration and to undertake a cost benefit analysis of pollutant emission reduction scenarios in the mapping area.

In addition to the data required for mapping acceptable levels/loads estimates of the total area of the respective building material in each mapping unit and the cost for replacement and/or maintenance of the material is required.

4.2.5 Sources of uncertainty

The main sources of uncertainty will result from

- use of yearly mean values of pollution parameters which do not take into

account the effect of fluctuations of pollutant levels,

- use of dose-response functions, which may be further developed i.a. after the evaluation of results of the ongoing "multi-pollutant" exposure in ICP Materials,
- assessment of environmental data and their extrapolation to each mapping square taking into account the importance of the difference in local environment in populated and rural areas,
- translation of dose-response functions obtained by exposure of test specimens to damage functions taking into account the exposure situation on a construction and rational maintenance practice.
- assessment of the stock of materials at risk,
- characterisation of reduced service lifetime, and
- quantification of costs associated with reduced service lifetime.

4.3 Direct effects of ozone

The effect of ozone on corrosion of materials is complex and there are today serious gaps of knowledge. Both ozone and NO_2 have a direct effect on corrosion and degradation of especially some organic materials. In recent years the synergistic effect of SO_2 in combination with O_3 and NO_2 has been shown to lead to severely increased corrosion on several inorganic materials in laboratory exposures. In field exposures so far only the synergistic effect of SO_2 and O_3 has been shown in the UNECE exposure programme.

Recent studies of historical ozone measurements indicate that background tropospheric ozone concentrations over Europe have approximately doubled since the end of the 19th century. This change is due to increased emissions of precursor compounds from human activities in form of NO_x and VOC (volatile organic compounds). In urban areas the ozone concentrations are suppressed due to local emissions of NO_x primarily from motor vehicle exhausts. Motor vehicle emission controls will serve to

reduce local emissions of NO_x and as a consequence ozone concentrations in urban areas will increase. Over the last decade the background ozone concentrations have increased by up to a few percent per year over northern and central Europe and are at present approximately 30 ppb. For sensitive organic materials exposed to outdoor atmospheres an acceptable level for ozone is proposed to be 20 ppb as an annual mean. It may provisionally represent a acceptable above which unacceptable shortening of the material lifetime will result. It should, however, be emphasised that for protection of sensitive organic materials in e.g. museums, galleries and archives much lower levels for ozone are recommended.

4.4 Data and mapping procedure

Any user who are considering to produce maps on effect of materials based on procedures specified in this chapter should also consult the general chapters of this manual, Chapter 1 Introduction and, especially, Chapter 2 Guidance on Mapping Concentration Levels and Deposition Loads. In chapter 2 the general methods of mapping, their underlying assumptions and data requirements are given for many of the parameters needed for mapping effects on materials. Regarding the wet deposition parameters it should be noted that the term $Rain[Cl^-]$ given in this chapter is identical to the chloride wet deposition parameter described in chapter 2. Deposition of protons ($Rain[H^+]$) is not mentioned explicitly in chapter 2 but it should be noted that the recommendation that maps of annual wet deposition should not be drawn by interpolating measured wet deposition but instead by combining maps of interpolated solute concentrations and precipitation amounts separately is valid also for H^+ .

For materials damage the following types of maps are recommended. For recommended n values see 4.2.3.

Assisting maps

These maps illustrates the geographical distribution of some of the most important environmental parameters and their combinations used in the dose-response functions:

- $[SO_2]$
- $[O_3]$
- T
- Rh
- $Rain$
- pH
- Cl^-
- $Rain[H^+]$

Material damage maps (for each selected material)

Maps for present value of corrosion effects (based on dose-response functions):

- Exceedance of acceptable corrosion rate quantifying the degree of exceedance in classes $K_d/(n \cdot K_b)$, preferably for $n = 1.5, 2.0$ and 2.5 .
- Contribution of wet deposition to the total corrosion effect or ratio between corrosion effect of wet and dry deposition

Maps for different scenarios:

- Comparison between present corrosion rate with the rate at different levels of $[SO_2]$, $[O_3]$ and $[H^+]$

Acceptable pollution levels/loads maps (for each selected material)

- Acceptable SO_2 levels for present level of $[O_3]$ and $[H^+]$
- Acceptable O_3 levels for copper for present level of $[SO_2]$ and $[H^+]$
- Acceptable H^+ loads for present level of $[SO_2]$ and $[O_3]$

Maps for different scenarios:

- Acceptable SO_2 , O_3 (for copper) levels or H^+ loads for different levels/loads of the two other pollutant parameters.

4.4.1 Data and scale of mapping

It is recommended that countries make use of best available data and generate information at appropriate national scales. These data when incorporated into European maps will be mapped for EMEP grid areas (50 km currently). It is thus advisable to use a grid network which coincide with the EMEP network or if smaller (which is preferable) is a fraction of the EMEP size.

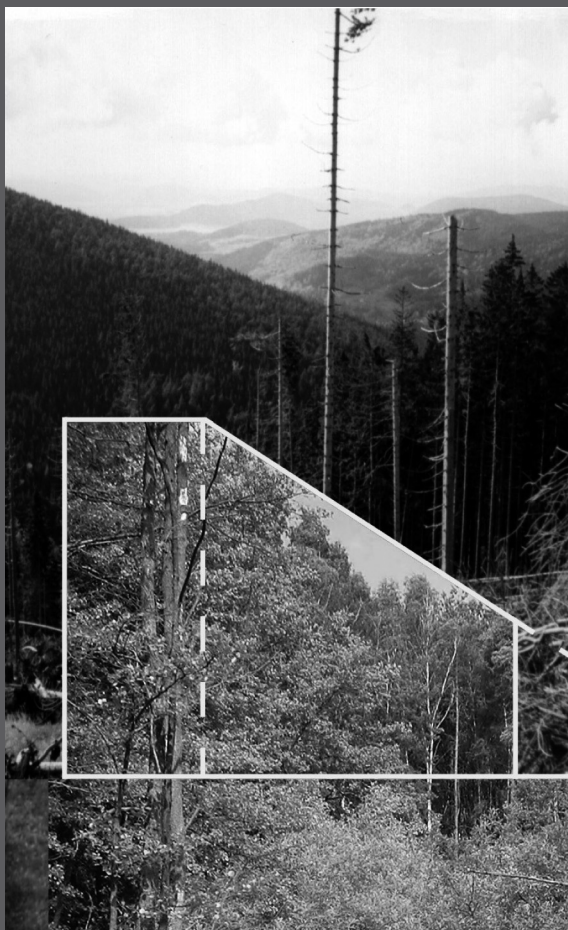
4.4.2 Urban and rural areas

It is recognised that urban areas differ from rural especially in levels of pollutants. Also relevant climatic data as temperature and relative humidity may show variations between urban and rural areas. Having in mind that corrosion of materials is affected both by long-range transported pollutants and by more local emissions it is advisable to produce maps with considerably smaller grids especially for mapping of effects in urban areas.

References

- Cowell, Apsimon H (1996) Estimating the cost of damage to buildings by acidifying atmospheric pollution in Europe, *Atmos. Env.*, Vol. 30, pp. 2959-2968.
- ECOTEC (1986) Identification and Assessment of Materials Damage to Buildings and Historic Monuments by Air Pollution. Report to the UK Department of the Environment. ECOTEC Consulting Ltd., Birmingham.
- Kucera V, Henriksen J, Knotkova D, Sjöström C (1993) Model for Calculations of Corrosion Costs Caused by Air Pollution and its Applications in three Cities, Proc. 10th European Corros. Congr., Barcelona.
- Tidblad J, Kucera V, Mikhailov AA (1998) UNECE International Co-operative Programme on Effects on Materials Including Historic and Cultural Monuments. Report No 30. Statistical analysis of 8-year materials exposure and acceptable deterioration and pollution levels. Swedish Corrosion Institute, Stockholm, Sweden.
- Tolstoy N, Andersson G, Sjöström C, Kucera V (1989) External building materials – quantities and degradation. Statens institut för byggnadsforskning, Gävle. ISBN 91-540-9315-5.
- UNECE (1997) Economic Evaluation of Air Pollution Damage to Materials. Proceedings of the UNECE Workshop on Economic Evaluation of Air Pollution Abatement and Damage to Buildings including Cultural Heritage, Eds V. Kucera, D. Pearce and Y.-W. Brodin, Report 4761, Swedish Environmental Protection Agency, Stockholm, Sweden, 1997.
- UNECE (2000) Mapping Air Pollution Effects on Materials, including Stock at Risk, EB.AIR/WG.1/2000/15, Workshop Report prepared by the Chairman of the Task Force on the International Cooperative Programme on Effects of Air Pollution on Materials, Including Historic and Cultural Monuments and by the Chairman of the Task Force on the International Co-operative Programme on Modelling and Mapping.

Mapping Manual 2004



Sections 5.1–5.4 are an update and extension of the relevant parts in the 1996 Mapping Manual. T. Spranger (Germany) has prepared the introductory section 5.1 and J. Hall (United Kingdom) section 5.2 on empirical critical loads. M. Posch has compiled sections 5.3 and 5.4 on terrestrial and aquatic critical load models for nitrogen and sulphur. B. Reynolds (United Kingdom), S. Augustin (Germany) and G.J. Reinds (The Netherlands) provided valuable comments. The careful reading and the many suggestions by J. Aherne (Canada) are greatly appreciated.

The new section 5.5 on critical loads for heavy metals has been prepared by G. Schuetze (Germany) in close cooperation with W. de Vries (The Netherlands), E. Tipping and St. Lofts (UK), M. Meili (Sweden) and B.J. Groenenberg (The Netherlands). Comments by other colleagues of the Expert Panel on Critical Loads of Heavy Metals are acknowledged.

5.1 Introduction

The general definition of a critical load is “a quantitative estimate of an exposure to one or more pollutants below which significant harmful effects on specified sensitive elements of the environment do not occur according to present knowledge”.

This definition applies to different receptors (e.g., terrestrial ecosystems, groundwater, aquatic ecosystems, and/or human health). ‘Sensitive elements’ can be part or whole of an ecosystem or of ecosystem development processes, such as their structure and function. Critical loads have been defined for several pollutants and effects resulting from their deposition.

Critical loads of sulphur and nitrogen acidity for an ecosystem have been specifically defined at the Skokloster Workshop as (Nilsson and Grennfelt 1988):

“the highest deposition of acidifying compounds that will not cause chemical changes leading to long-term harmful effects on ecosystem structure and function.”

Both sulphur and nitrogen compounds contribute to the total deposition of acidity. The acidity input has to be considered in this balance regardless whether it is due to *S* or *N* depositions. Thus, the ratio between sulphur and nitrogen may vary without change in the acidity load (see section 5.3.2 for details).

In addition to acidification, inputs of nitrogen may influence the eutrophication and nutrient balances of ecosystems. The critical load for nitrogen nutrition effects is defined as:

“the highest deposition of nitrogen as NH_x and/or NO_y ¹ below which harmful effects in ecosystem structure and function do not occur according to present knowledge.”

Critical loads for heavy metals are defined accordingly.

The basic idea of the critical load concept is to balance the depositions which an eco-

system is exposed to with the capacity of this ecosystem to buffer the input (e.g. the acidity input buffered by the weathering rate), or to remove it from the system (e.g. nitrogen by harvest) without harmful effects within or outside the system.

In the context of a multi-pollutant multi-effects approach it is desirable to consider all effects simultaneously as far as possible. For eutrophication and acidification, this has been done using so-called critical load functions. These are described in detail in section 5.3.

Critical loads can be determined either by steady-state methods or by dynamic models with varying degree of complexity. Since critical loads are steady-state quantities, the use of dynamic models for the sole purpose of deriving critical loads is somewhat inadequate. However, if dynamic models are used to simulate the transition to a steady state for the comparison with critical loads, care has to be taken that the steady-state version of the dynamic model is compatible with the critical load model. Dynamic models are dealt with in a separate chapter (Chapter 6).

¹ $NH_x = NH_3 + NH_4^+$; $NO_y = NO + NO_2 + NO_2^- + NO_3^-$

5.2 Empirical Critical Loads

5.2.1 Empirical critical loads of nutrient nitrogen

5.2.1.1 Introduction

The emissions of ammonia (NH_x) and nitrogen oxides (NO_y) have strongly increased in Europe in the second half of the 20th century. Because of short- and long-range transport of these nitrogenous compounds, atmospheric nitrogen (N) deposition has clearly increased in many natural and semi-natural ecosystems. The availability of nutrients is one of the most important abiotic factors, which determine the plant species composition in ecosystems. Nitrogen is the limiting nutrient for plant growth in many natural and semi-natural ecosystems, especially of oligotrophic and mesotrophic habitats. Most of the plant species from such conditions are adapted to nutrient-poor conditions, and can only survive or compete successfully on soils with low nitrogen availability. In addition, the N cycle in ecosystems is complex and strongly regulated by biological and microbiological processes, and thus many changes may occur in plant growth, inter-specific relationships and soil-based processes as a result of increased deposition of air-borne N pollutants.

The series of events which occurs when N inputs increase in an area with originally low background deposition rates is highly complex. Many ecological processes interact and operate at different temporal and spatial scales. As a consequence, high variations in sensitivity to atmospheric nitrogen deposition have been observed between different natural and semi-natural ecosystems. Despite this diverse sequence of events, the following main effect “categories” can be recognised:

(a) Direct toxicity of nitrogen gases and aerosols to individual species (see N critical levels);

(b) Accumulation of nitrogen compounds, resulting in increased N availability and changes of species composition;

(c) Long-term negative effect of ammonium and ammonia;

(d) Soil-mediated effects of acidification;

(e) Increased susceptibility to secondary stress and disturbance factors such as drought, frost, pathogens or herbivores.

Recent experimental evidence, and practical field experience in ecosystem restoration, suggests that, once the process of altered species composition and increased N mineralisation occurred, spontaneous recovery of the vegetation may happen only over very long time scales, or with very active management intervention to decrease nitrogen status and cycling. This emphasises the need for caution in setting critical loads at which these major changes in vegetation composition and nitrogen cycling do not occur.

5.2.1.2 Data

Within the Convention on Long-range Transboundary Air Pollution (LRTAP), empirical procedures have been developed to set critical loads for atmospheric N deposition. Empirical critical loads of N for natural and semi-natural terrestrial ecosystems and wetland ecosystems were firstly presented in a background document for the 1992 workshop on critical loads held under the UNECE LRTAP Convention at Lökeberg (Sweden) (Bobbink et al. 1992). After detailed discussion before and during the meeting, the proposed values were set at that meeting (Grennfelt and Thörnelöf 1992). Additional information from the period 1992–1995 was evaluated and summarised in an updated background paper (Bobbink et al. 1996) and published as Annex III in the previous version of the Mapping Manual (UBA 1996). The updated N critical loads were discussed and accepted at an expert meeting held in December 1995 in Geneva (Switzerland). They were also used in the Air Quality Guidelines for Europe (2nd edition) of the

World Health Organisation (WHO 2000). It became clear that considerable new insights into, and data on, the impacts of N deposition on natural and semi-natural ecosystems have become available since the compilation of the last values in the mid-1990s. Therefore, new information from the period 1996–2002 on the impacts of increased nitrogen deposition on the structure and function of natural and semi-natural ecosystems was evaluated and evaluated in a fully adapted background paper (Bobbink et al. 2003). The updated N critical loads were discussed and approved by full consensus at the November 2002 expert meeting held under the LRTAP Convention in Berne (Switzerland, Achermann and Bobbink 2003) and are given in Table 5.1.

Approach:

Based on observed changes in the structure and function of ecosystems, reported in a range of publications, empirical N critical loads were evaluated for specific receptor groups of natural and semi-natural ecosystems in both 1992 and 1996. In the 2002 updating procedure a similar 'empirical approach' was used as for the earlier background documents. For this purpose, European publications on the effects of N in natural and semi-natural ecosystems from the period 1996 to mid 2002 were collected as completely as possible. Peer-reviewed publications, book chapters, nationally published papers and 'grey' reports of institutes or organisations, if available by request, were incorporated. Results from field addition experiments and mesocosm studies, from correlative or retrospective field studies, and, in few cases, dynamic ecosystem modelling was relevant in this respect.

Ranges and reliability:

As in the 1992 and 1996, the empirical N critical loads were established within a range for each ecosystem class, because of: (i) real intra-ecosystem variation between different regions where an ecosystem has been investigated; (ii) the intervals between experimental additions of nitrogen; and (iii) uncertainties in presented total atmospheric deposition values, although the latter have

been checked by local specialists on atmospheric N deposition. Some additional information has been given on how to interpret this range in specific situations for an ecosystem. For every group of ecosystems, the empirical N critical loads are given with an indication of exceedance and of their reliability.

The reliability of the presented N critical load figures is indicated as before (Bobbink et al. 1996):

- reliable ##: when a number of published papers of various studies show comparable results;
- quite reliable #: when the results of some studies are comparable;
- expert judgement (#): when no empirical data are available for this type of ecosystem. The N critical load is then based upon expert judgement and knowledge of ecosystems, which are likely to be more or less comparable with this ecosystem.

5.2.1.3 Ecosystem classification

To facilitate and harmonise the mapping procedure, the receptor groups of natural and semi-natural ecosystems were classified and ordered according to the EUNIS habitat classification for Europe (Davies and Moss 2002, <http://eunis.eea.eu.int/index.jsp>). For an introduction of EUNIS classification with respect to empirical N critical loads (see Hall et al. 2003). In general, the ecosystems used in the 2002 updating procedure, were classified down to level 2 or 3 of the EUNIS hierarchy. The following habitats groups (with EUNIS level 1 code between brackets) were treated:

- Woodland and forests habitats (**G**)
- Heathland, scrub and tundra habitats (**F**)
- Grassland and tall forb habitats (**E**)
- Mire, bog and fen habitats (**D**)
- Inland surface water habitats (**C**)
- Coastal habitats (**B**)
- Marine habitats (**A**)

5 Mapping Critical Loads

Table 5.1: Empirical critical loads for nitrogen deposition ($kgN/ha/yr$) to natural and semi-natural groups of ecosystems classified according EUNIS (except for forests). Reliability: ### reliable, # quite reliable and (#) expert judgement.

Ecosystem type	EUNIS-code	Critical load ($kg\ N/ha/yr$)	Reliability	Indication of exceedance
Forest habitats (G)				
Soil processes				
Deciduous & coniferous	-	10-15	#	Increased N mineralisation, nitrification
Coniferous forests	-	10-15	##	Increased nitrate leaching
Deciduous forests	-	10-15	(#)	Increased nitrate leaching
Trees				
Deciduous & coniferous	-	15-20	#	Changed N/macro nutrients ratios, decreased P, K, Mg and increased N concentrations in foliar tissue
Temperate forests	-	15-20	(#)	Increased susceptibility to pathogens and pests, change in fungistatic phenolics
Mycorrhiza				
Temperate and boreal forests	-	10-20	(#)	Reduced sporocarp production, changed/reduced below-ground species composition
Ground vegetation				
Temperate and boreal forests	-	10-15	#	Changed species composition, increase of nitrophilous species, increased susceptibility to parasites
Lichens and algae				
Temperate and boreal forests	-	10-15	(#)	Increase of algae, decrease of lichens
Overall				
Temperate forests	-	10-20	#	Changes in soil processes, ground vegetation mycorrhiza and increased risk of nutrient imbalances and susceptibility to parasites
Boreal forests	-	10-20	#	Changes in soil processes, ground vegetation mycorrhiza and increased risk of nutrient imbalances and susceptibility to parasites
Heathland, scrub and tundra habitats (F)				
Tundra	F1	5-10 ^a	#	Changes in biomass, physiological effects, changes in species composition in moss layer, and decrease in lichens
Arctic, alpine and subalpine scrub habitats	F2	5-15 ^a	(#)	Decline in lichens mosses, and evergreen shrubs
Northern wet heath	F4.11			
'U' <i>Calluna</i> -dominated wet heath (upland moorland)	F4.11	10-20 ^a	(#)	Decreased heather dominance, decline in lichens and mosses
'L' <i>Erica tetralix</i> dominated wet heath	F4.11	10-25 ^{a,b}	(#)	Transition heather to grass
Dry heaths	F4.2	10-20 ^{a,b}	##	Transition heather to grass; decline in lichens
Grasslands and tall forb habitats (E)				
Sub-atlantic semi-dry calcareous grassland	E1.26	15-25	##	Increase tall grasses, decline in diversity; increased mineralisation and N leaching
Non-mediterranean dry acid and neutral closed grassland	E1.7	10-20	#	Increase in graminoids, decline typical species
Inland dune pioneer grasslands	E1.94	10-20	(#)	Decrease in lichens, increase biomass
Inland dune siliceous grasslands	E1.95	10-20	(#)	Decrease in lichens, increase biomass, increased succession

Low and medium altitude hay meadows	E2.2	20-30	(#)	Increase in tall grasses, decrease in diversity
Mountain hay meadows	E2.3	10-20	(#)	Increase in nitrophilous graminoids; changes in diversity
Moist and wet oligotrophic grasslands	E3.5			
<i>Molinia caerulea</i> meadows	E3.51	15-25	(#)	Increase in tall graminoids; decreased diversity; decrease of bryophytes
Heath (<i>Juncus</i>) meadows and humid (<i>Nardus stricta</i>) swards	E3.52	10-20	#	Increase in tall graminoids; decreased diversity; decrease of bryophytes
Alpine and subalpine grasslands	E4.3 and E4.4	10-15	(#)	Increase in nitrophilic graminoids; biodiversity change
Moss and lichen dominated mountain summits	E4.2	5-10	#	Effects upon bryophytes or lichens
Mire, bog and fen habitats (D)				
Raised and blanket bogs	D1	5-10 ^{a,c}	##	Change in species composition, N saturation of <i>Sphagnum</i>
Poor fens	D2.2 ^d	10-20	#	Increase sedges and vascular plants; negative effects on peat mosses
Rich fens	D4.1 ^e	15-25	(#)	Increase tall graminoids, decrease diversity, decrease of characteristic mosses
Mountain rich fens	D4.2	15-25	(#)	Increase vascular plants, decrease bryophytes
Inland surface water habitats (C)				
Permanent oligotrophic waters				
Softwater lakes	C1.1	5-10	##	Isoetid species negatively affected
Dune slack pools	C1.16	10-20	(#)	Increased biomass and rate of succession
Coastal habitat (B)				
Shifting coastal dunes	B1.3	10-20	(#)	Biomass increase, increase N leaching
Coastal stable dune grasslands	B1.4	10-20	#	Increase tall grasses, decrease prostrate plants, increased N leaching
Coastal dune heaths	B1.5	10-20	(#)	Increase plant production; increase N leaching, accelerated succession
Moist to wet dune slacks	B1.8	10-25	(#)	Increased biomass tall graminoids
Marine habitats (A)				
Pioneer and low-mid salt marshes	A2.64 and A2.65	30-40	(#)	Increase late-successional species, increase productivity

- a) use towards high end of range at P limitation, and towards lower end if P is not limiting;
- b) use towards high end of range when sod cutting has been practised, use towards lower end of range with low intensity management;
- c) use towards high end of range with high precipitation and towards low end of range with low precipitation;
- d) for *D2.1* (quaking fens and transition mires): use lower end of range (#) and for *D2.3* (valley mires): use higher end of range (#);
- e) for high latitude or N-limited systems: use lower end of range.

In general, a good agreement was found between the previously used classification of ecosystem groups (Bobbink et al. 1996) and the EUNIS habitat classification now adopted. A main limitation for the use of many subcategories of the EUNIS classification was, unfortunately, a lack of research and data on N impacts for those habitats. Finally, it was at this moment not possible to use the EUNIS classification with respect to the setting of empirical N critical loads for forest ecosystems below level 1. It was only possible to set values of three broad EUNIS classes ($G1$, $G3$ & $G4$) for forest, with, however, some separation for grouping of forest types, such as coniferous versus deciduous and boreal versus temperate. Even within $G1$, $G3$ and $G4$ there are several types, e.g. wet-swamp forest and Mediterranean forests for which no data were available and thus left out. As before, studies based on pure plantation stands were (if possible) not accepted in the forest section, because the N critical loads of these intensively used systems are obtained via the steady-state mass balance method (see section 5.3). An overview of the old and new classification is presented in Table 5.3 to assist the shift to the EUNIS classification.

5.2.1.4 Use of empirical critical loads

Most of the Earth's biodiversity is present in semi-natural and natural ecosystems. It is thus crucial to control the atmospheric N loads, in order to prevent negative effects on these semi-natural and natural systems. The empirical N critical loads updated in 2002 (Table 5.1) should be used to revise critical load databases. High-resolution maps of the sensitive ecosystems of high conservation value are needed per country to map N critical loads for these systems. It is advised to use both the mass balance and empirically derived N critical loads for forest ecosystems and other ecosystems for which data needed for the application of steady state models is available. If the two approaches yield different values, the one with the lowest values should be used until the background for this difference has been clarified. Furthermore, it is suggested to the different countries, where insufficient national data

for specific national ecosystems are available, to use the lower, middle or upper part of the ranges of the N critical loads for (semi-)natural ecosystem groups according to the general relationships between abiotic factors and critical loads for N as given in Table 5.2.

Countries are advised to identify those receptor ecosystems of high sensitivity within the mentioned EUNIS classification relating to their individual interest. Effort should be directed to produce fine resolution maps of sensitive ecosystems of high conservation value. At this moment the empirical N critical loads have been set in values of total atmospheric N ($kgN/ha/yr$). More information is needed on the relative effects of oxidised and reduced N deposition. It was emphasised during the last two UNECE expert meetings that there is increasing evidence of NH_x having greater evidence than NO_y .

Particularly, bryophytes and lichens in a number of ecosystems, and several, mostly weakly buffered, ecosystems of EUNIS class F, E, C and B are (probably) more sensitive to deposition of reduced N . It is, however, at present not possible to set critical loads for both forms of N , separately.

5.2.1.5 Recommendations

Serious gaps in knowledge exist on the effects of enhanced N deposition (NO_y and NH_x) on semi-natural and natural ecosystems, although considerably progress has been made in several habitat groups from 1996 to 2002. The following gaps in knowledge have been recognised as most important:

- research/data collection is required to establish a critical load for the following ecosystems: steppe grasslands, all Mediterranean vegetation types, wet-swamp forests, many mire & fens, several coastal habitats and high altitude systems;
- more research is needed in all distinguished EUNIS items with expert judgement or few research;
- impacts of N enrichment in (sensitive) freshwater and shallow marine ecosystems

- tems needs further research and are sometimes overlooked;
- additional effort is needed to allocated observed *N* effects to the appropriate EUNIS forest subtypes (division 2 & 3);
 - the EUNIS classification needs clarification/adjustment with respect to some grasslands groups, Nordic bogs and mires and surface water habitats;
 - the possible differential effects of the deposited nitrogen species (NO_y or NH_x) are insufficiently known to make a differentiation between these *N* species for critical load establishment;

Table 5.2: Suggested action for using lower, middle or upper part of the set critical loads of terrestrial ecosystems (excluding wetlands), if national data are insufficient.

Temperature/ Frost period	Soil wetness	Base cation availability	P limitation	Management intensity	Action
Cold/long	Dry	Low	N-limited	Low	Move to lower part
Intermediate	Normal	Intermediate	Unknown	Usual	Use middle part
Hot/none	Wet	High	P-limited	High	Move to higher part

Table 5.3: Cross-comparison between the ecosystem classification used in the 2002 empirical *N* critical load setting (according to the EUNIS system) and the classification previously used (Bobbink et al. 1996) (with n.d. = not distinguished).

Ecosystem classification 2002	EUNIS	Ecosystem classification 1996
Heathland, scrub and tundra habitats	F	Heathlands
Tundra	F1	n.d.
Arctic, alpine and subalpine scrub	F2	Arctic and Alpine heaths
Northern wet heaths		
• 'U' <i>Calluna</i> dominated wet heath	F4.11	Upland <i>Calluna</i> heath
• 'L' <i>Erica tetralix</i> dominated wet heath	F4.11	Lowland wet heathlands
Dry Heaths	F4.2	Lowland dry heathlands
Grasslands and tall forb habitats	E	Species-rich grassland
Sub-atlantic semi-dry calcareous grasslands	E1.26	Calcareous grasslands
Non-mediterranean dry acid and neutral closed grasslands	E1.7	Species-rich heaths and neutral acidic grasslands (partly)
Inland dune pioneer grasslands	E1.94	n.d.
Inland dune siliceous grasslands	E1.95	n.d.
Low and medium altitude hay meadows	E2.2	Neutral-acid grasslands (partly)
Mountain hay meadows	E2.3	Montane-subalpine grasslands
Moist and wet oligotrophic grasslands	E3.5	Neutral-acid grasslands (partly)
• <i>Molinia caerulea</i> meadows	E3.51	Mesotrophic fens (partly)
• Heath (<i>Juncus</i>) meadows and humid (<i>Nardus stricta</i>) swards	E3.52	n.d.
Alpine and subalpine grasslands	E4.3 and E4.4	Montane-subalpine grasslands (partly)
Moss and lichen dominated mountain summits	E4.2	n.d.
Mire, bog and fen habitats	D	Wetlands
Raised and blanket bogs	D1	Ombrotrophic bogs
Poor fens	D2.2	n.d.
Rich fens	D4.1	Mesotrophic fens
Montane rich fens	D4.2	n.d.
Inland surface water habitats	C	Wetlands
Permanent oligotrophic waters	C1.1	n.d.
• Softwater lakes	C1.1	Shallow softwater bodies
• Dune slack pools	C1.16	n.d.
Coastal habitats	B	n.d.
Shifting coastal dunes	B1.3	n.d.
Coastal stable dune grasslands	B1.4	Neutral-acid grasslands (partly)
Coastal dune heaths	B1.5	n.d.
Moist to wet dune slacks	B1.8	n.d.
Marine habitats	A	n.d.
Pioneer and low-mid salt marshes	A2.64 and A2.65	n.d.

5 Mapping Critical Loads

- in order to refine current critical loads, long-term (> 3–5 years) *N* addition experiments with a high resolution of treatments between 5 and 50 kgN/ha/yr at low background regions or in mesocosms are useful. This would increase the certainty of deriving critical loads when the lowest treatment level considerably exceeds the critical load;

In conclusion, it is crucial to understand the long-term effects of increased *N* deposition on ecosystem processes in a representative range of ecosystems. It is thus very important to quantify the effects of nitrogen loads by manipulation of *N* inputs in long-term ecosystem studies in unaffected and affected areas. These data are essential to validate the set critical loads and to develop robust dynamic ecosystem models and/or multiple correlative species models, which are reliable enough to calculate critical loads for nitrogen deposition in (semi-) natural ecosystems and to predict (natural) recovery rates for *N*-affected systems.

5.2.2 Empirical Critical loads of acidity

Empirical approaches assign an acidity critical load to soils on the basis of soil mineralogy and/or chemistry. For example, at the Critical Loads Workshop at Skokloster (Nilsson and Grennfelt 1988) soil forming materials were divided into five classes on the basis of the dominant weatherable minerals. A critical load range, rather than a single value, was assigned to each of these classes according to the amount of acidity that could be neutralised by the base cations produced by mineral weathering (Table 5.4). Other methods of estimating base cation weathering are discussed in Chapter 5.3.2.

In addition, a number of modifying factors were identified that would enable the critical load value to be adjusted within the ranges (Table 5.5, after Nilsson and Grennfelt 1988). For example, some factors could make the soil more sensitive to acidification, requiring the critical load to be set at the lower end of the range; while other factors could make the soil less sensitive, setting the critical load at the upper end of the range.

The classification of soil materials developed at Skokloster (Table 5.4) used a relatively

Table 5.4: Mineralogical classification of soil materials and soil critical loads.

Minerals controlling weathering	Critical load range (eq/ha/yr)
Quartz, K-feldspar	<200
Muscovite, Plagioclase, Biotite (<5%)	200–500
Biotite, Amphibole (<5%)	500–1000
Pyroxene, Epidote, Olivine (<5%)	1000–2000
Carbonates	>2000

Table 5.5: Modifying factors causing an increase or decrease in critical loads.

Modifying factor	Effect on critical load:	
	<i>Decrease</i>	<i>Increase</i>
Precipitation	High	Low
Vegetation	Coniferous forest	Deciduous forest
Elevation, slope	High	Low
Soil texture	Coarse-sandy	Fine
Soil drainage	Free	Impeded
Soil sulphate adsorption capacity	Low	High
Base cation deposition	Low	High

small range of primary silicate minerals and carbonates. A larger range of minerals has been classified by Sverdrup and Warfvinge (1988) and Sverdrup et al. (1990). The following mineral classes have been identified:

Very fast weathering minerals (carbonates) include minerals that have the potential to dissolve very rapidly, in a geological perspective. The group includes calcite, dolomite, magnesite and brucite.

Fast weathering minerals include the silicate minerals with the fastest weathering rate. The group comprises minerals such as anorthite and nepheline, olivine, garnet, jadeite, diopside. A soil with a major content of these minerals would be resistant to soil acidification.

Intermediate weathering minerals include enstatite, hypersthene, augite, hornblende, glaucophane, chlorite, biotite, epidote, zoisite.

Slow weathering minerals include albite, oligoclase, labradorite, illite. Soils with a majority of such minerals will be sensitive to soil acidification.

Very slow weathering minerals include K-feldspar, muscovite, mica, montmorillonite, vermiculite. Soils with a majority of these minerals will be sensitive to soil acidification.

Inert minerals are those that dissolve so slowly or provide so little neutralising substance that they may be considered as inert for soil acidification purposes. This includes minerals such as quartz, rutile, anatase, kaolinite, gibbsite.

For each of the above mineral classes, weathering rates for soils with different mineral contents have been proposed (Table 5.6, Sverdrup et al. 1990).

The information provided in Tables 5.4 to 5.6 above provide the basis on which empirical acidity critical loads can be assigned to soils. If mineralogical data are available for the units of a soil map, critical loads can be assigned to each unit and a critical loads map produced.

An example of the development of a critical load map at the national scale using empirical approaches is given by Hornung et al. (1995). In the UK this approach has been used to define acidity critical loads for non-forest ecosystems, by setting a critical load that will protect the soil upon which the habitat depends (Hall et al. 1998, 2003). The critical load is effectively the base cation weathering rate, with the leaching of acid neutralising capacity (ANC) set to zero (see section 5.3.2), and can be used in the calculations of the maximum critical loads of sulphur and nitrogen (see section 5.3.3).

Table 5.6: Weathering rates (in $eq/(ha\cdot m)/yr$) for four selected mineral classes of soil material based on a soil depth of one meter – to convert to critical load values multiply by soil thickness in meters.

Mineral class	Average soil mineral class content			
	100%	30%	3%	0.3%
Very fast weathering	25000	15000	10000	3000
Fast weathering	15000	10000	3000	300
Intermediate weathering	10000	3000	300	30
Slow weathering	600	200	20	-
Very slow weathering	300	100	10	-
Inert	100	100	-	-

5.3 Modelling Critical Loads for Terrestrial Ecosystems

The purpose of a model-based approach to calculating critical loads is to link, via mathematical equations, a chemical criterion (critical limit) with the maximum deposition(s) 'below which significant harmful effects on specified sensitive elements of the environment do not occur', i.e. for which the criterion is not violated. In most cases the 'sensitive element of the environment' will be of a biological nature (e.g., the vitality of a tree, the species composition of a heather ecosystem) and thus the criterion should be a biological one. However, there is a dearth of simple yet reliable models that adequately describe the whole chain from deposition to biological impact. Therefore, chemical criteria are used instead, and simple chemical models are used to derive critical loads. This simplifies the modelling process somewhat, but shifts the burden to find, or derive, appropriate (soil) chemical criteria (and critical limits) with proven (empirical) relationships to biological effects. The choice of the critical limit is an important step in deriving a critical load, and much of the uncertainty in critical load calculations stems from the uncertainty in the link between (soil) chemistry and biological impact.

In the following we consider only steady-state models, and concentrate on the so-called Simple Mass Balance (SMB) model as the standard model for calculating critical loads for terrestrial ecosystems under the LRTAP Convention (Sverdrup et al. 1990, Sverdrup and De Vries 1994). The SMB model is a single-layer model, i.e., the soil is treated as a single homogeneous compartment. Furthermore, it is assumed that the soil depth is (at least) the depth of the rooting zone, which allows us to neglect the nutrient cycle and to deal with net growth uptake only. Additional simplifying assumptions include:

- all evapotranspiration occurs on the top of the soil profile
- percolation is constant through the soil profile and occurs only vertically

- physico-chemical constants are assumed uniform throughout the whole soil profile
- internal fluxes (such as the weathering rates, nitrogen immobilisation etc.) are independent of soil chemical conditions (such as pH)

Since the SMB model describes steady-state conditions, it requires long-term averages for input fluxes. Short-term variations – e.g., episodic, seasonal, inter-annual, due to harvest and as a result of short-term natural perturbations – are not considered, but are assumed to be included in the calculation of the long-term mean. In this context 'long-term' is defined as about 100 years, i.e. at least one rotation period for forests. Ecosystem interactions and processes like competition, pests, herbivore influences etc. are not considered in the SMB model. Although the SMB model is formulated for undisturbed (semi-natural) ecosystems, the effects of extensive management, such as grazing and the burning of moor, could be included.

Besides the single-layer SMB model, there exist multi-layer steady-state models for calculating critical loads. Examples are the MACAL model (De Vries 1988) and the widely-used PROFILE model (Warfvinge and Sverdrup 1992), which has at its core a model for calculating weathering rates from total mineral analyses. These models will not be discussed here, and the interested reader is referred to the literature.

In the following sections we will derive the SMB model for critical loads of nutrient nitrogen (eutrophication) and critical loads of acidifying sulphur and nitrogen.

5.3.1 Critical loads of nutrient nitrogen (eutrophication)

5.3.1.1 Model derivation

The starting point for calculating critical loads of nutrient N with the SMB model is the mass balance of total nitrogen (N) for the soil compartment under consideration (inputs = sinks + outputs):

(5.1)

$$N_{dep} + N_{fix} = N_{ad} + N_i + N_u + N_{de} + N_{eros} + N_{fire} + N_{vol} + N_{le}$$

where:

- N_{dep} = total N deposition
- N_{fix} = N 'input' by biological fixation
- N_{ad} = N adsorption
- N_i = long-term net immobilisation of N in soil organic matter
- N_u = net removal of N in harvested vegetation and animals
- N_{de} = flux of N to the atmosphere due to denitrification
- N_{eros} = N losses through erosion
- N_{fire} = N losses in smoke due to (wild or controlled) fires
- N_{vol} = N losses to the atmosphere via NH_3 volatilisation
- N_{le} = leaching of N below the root zone

The units used are $eq/ha/yr$ (or $mol_c/ha/yr$ in proper *SI* nomenclature).

The following assumptions lead to a simplification of eq. 5.1:

- Nitrogen adsorption, e.g., the adsorption of NH_4 by clay minerals, can temporarily lead to an accumulation of N in the soil, however it is stored/released only when the deposition *changes*, and can thus be neglected in steady state considerations.
- Nitrogen fixation is negligible in most (forest) ecosystems, except for N -fixing species.
- The loss of N due to fire, erosion and volatilisation is small for most ecosystems in Europe, and therefore neglected

in the following discussion. Alternatively, one could replace N_i by $N_i + N_{eros} + N_{fire} + N_{vol} - N_{fix}$ in the subsequent equations.

- The leaching of ammonium (NH_4) can be neglected in all forest ecosystems due to (preferential) uptake and complete nitrification within the root zone (i.e. $NH_{4,le} = 0$, $N_{le} = NO_{3,le}$).

Under these simplifying assumptions eq. 5.1 becomes:

(5.2)

$$N_{dep} = N_i + N_u + N_{de} + N_{le}$$

From this equation a critical load is obtained by defining an acceptable limit to the leaching of N , $N_{le(acc)}$, the choice of this limit depending on the 'sensitive element of the environment' to be protected. If an acceptable leaching is inserted into eq. 5.2, the deposition of N becomes the critical load of nutrient nitrogen, $CL_{nut}(N)$:

(5.3)

$$CL_{nut}(N) = N_i + N_u + N_{de} + N_{le(acc)}$$

In deriving the critical load of nutrient N as eq. 5.3, it is assumed that the sources and sinks do not depend on the deposition of N . This is unlikely to be the case and thus all quantities should be taken 'at critical load'. However, to compute, e.g., 'denitrification at critical load' one needs to know the critical load, the very quantity one wants to compute. The only clean way to avoid this circular reasoning is to establish a functional relationship between deposition and the sink of N , insert this function into eq. 5.2 and solve for the deposition (to obtain the critical load). This has been done for denitrification: In the simplest case denitrification is linearly related to the net input of N (De Vries et al. 1993, 1994):

(5.4)

$$N_{de} = \begin{cases} f_{de} \cdot (N_{dep} - N_i - N_u) & \text{if } N_{dep} > N_i + N_u \\ 0 & \text{else} \end{cases}$$

where f_{de} ($0 \leq f_{de} < 1$) is the so-called denitrification fraction, a site-specific quantity. This formulation implicitly assumes that immobilisation and uptake are faster processes than denitrification. Inserting this expression for N_{de} into eq. 5.2 and solving for the deposition leads to the following expression for the critical load of nutrient N :

$$(5.5) \quad CL_{nut}(N) = N_i + N_u + \frac{N_{le(acc)}}{1 - f_{de}}$$

An alternative, non-linear, equation for the deposition-dependence of denitrification has been proposed by Sverdrup and Ineson (1993) based on the Michaelis-Menten reaction mechanism and includes a dependence on soil moisture, pH and temperature. Also in this case $CL_{nut}(N)$ can be calculated explicitly, and for details the reader is referred to Posch et al. (1993).

More generally, it would be desirable to have deposition-dependent equations (models) for all N fluxes in the critical load equation. However, these either do not exist or are so involved that no (simple) explicit expression for $CL_{nut}(N)$ can be found. Although this does not matter in principle, it would reduce the appeal and widespread use of the critical load concept. Therefore, when calculating critical loads from eq. 5.3 or eq. 5.5, the N fluxes should be estimated as long-term averages derived from conditions not influenced by elevated anthropogenic N inputs.

5.3.1.2 The acceptable leaching of nitrogen

The value set for the acceptable N leaching depends on the 'harmful effects' that should be avoided. In general, it is not the N leaching flux itself that is 'harmful', but the concentration of N in the leaching flux. The acceptable N leaching (in $eq/ha/yr$) is calculated as:

$$(5.6) \quad N_{le(acc)} = Q \cdot [N]_{acc}$$

where $[N]_{acc}$ is the acceptable N concentration (eq/m^3) and Q is the precipitation surplus (in $m^3/ha/yr$). Some values for acceptable N concentrations are shown in Table 5.7.

Although literature data indicate that nutrient imbalances may occur when N leaching increases above natural background values (Van Dam 1990), no direct relationship between N leaching and vegetation changes has been substantiated. In general, the low leaching values from the above table lead to critical loads that are lower than empirical data on vegetation changes (e.g. Bobbink et al. 1998). It is the increase in N availability through enhanced N cycling that triggers changes (Berendse et al. 1987).

An acceptable N leaching could also be derived with the objective to avoid N pollution of groundwater using, e.g., the EC target or limit value (25 and 50 mgN/L , resp.) as acceptable (but high!) concentration.

Table 5.7: Acceptable N leachate concentrations to avoid nutrient imbalances or vegetation changes (quoted from Posch et al. 1993).

Impact	$[N]_{acc}$ ($mgN/L = gN/m^3$)	$[N]_{acc}$ (eq/m^3)
Nutrient imbalance, conifers	0.2	0.0143
Nutrient imbalance, deciduous trees	0.2–0.4	0.0143–0.0276
Change lichens → cranberry	0.2–0.4	0.0143–0.0276
Change lingon → blueberry	0.4–0.6	0.0276–0.0429
Change blueberry → grass	1–2	0.0714–0.1429
Change grass → herbs	3–5	0.2143–0.3571

5.3.1.3 Sources and derivation of input data

The obvious sources of input data for calculating critical loads are measurements at the site under consideration. However, in many cases these will not be available. A discussion on N sources and sinks can be found in Hornung et al. (1995) and UNECE (1995). Some data sources and default values and procedures to derive them are summarised below.

Nitrogen immobilisation:

N_i refers to the long-term net immobilisation (accumulation) of N in the root zone, i.e., the continuous build-up of stable C-N-compounds in (forest) soils. In other words, this immobilisation of N should not lead to significant changes in the prevailing C/N ratio. This has to be distinguished from the high amounts of N accumulated in the soils over many years (decades) due to the increased deposition of N , leading to a decrease in the C/N ratio in the topsoil.

Using data from Swedish forest soil plots, Rosén et al. (1992) estimated the annual N immobilisation since the last glaciation at 0.2–0.5 kgN/ha/yr (14.286–35714 eq/ha/yr). Considering that the immobilisation of N is probably higher in warmer climates, values of up to 1 kgN/ha/yr (71.428 eq/ha/yr) could be used for N_i , without causing unsustainable accumulation of N in the soil. It should be pointed out, however, that even higher values (closer to present-day immobilisation rates) have been used in critical load calculations. Although studies on the capacity of forests to absorb nitrogen have been carried out (see, e.g., Sogn et al. 1999), there is no consensus yet on long-term sustainable immobilisation rates.

Nitrogen uptake:

The uptake flux N_u equals the long-term average removal of N from the ecosystem. For unmanaged ecosystems (e.g., national parks) the long-term (steady-state) net uptake is basically zero whereas for managed forests it is the long-term net growth uptake. The harvesting practice is of

crucial importance, i.e., whether stems only, stems plus (parts of) branches or stems plus branches plus leaves/needles (whole-tree harvesting) are removed. The uptake of N is then calculated as:

(5.7)

$$N_u = \frac{\text{N removed in harvested biomass (eq/ha)}}{\text{interval between harvests (rotation period)(yr)}}$$

The amount of N in the harvested biomass (stems and branches) can be calculated as following:

(5.8)

$$N_u = k_{gr} \cdot \rho_{st} \cdot (ctN_{st} + f_{br,st} \cdot ctN_{br})$$

where k_{gr} is the average annual growth rate ($m^3/ha/yr$), ρ_{st} is the density of stem wood (kg/m^3), ctN is the N content in stems (subscript st) and branches (subscript br) (eq/kg) and $f_{br,st}$ is the branch-to-stem ratio (kg/kg). The contribution of branches should be neglected in case of stem removal.

Values for the density of stem wood of most trees are in the range of 400–500 kg/m^3 for conifers and 550–700 kg/m^3 for deciduous trees. The branch-to-stem ratio is about 0.15 kg/kg for conifers and 0.20 kg/kg for deciduous trees (Kimmins et al. 1985, De Vries et al. 1990). According to Swedish data (Rosén 1990; see also Reinds et al. 2001) the contents of N in stems are 1 g/kg for conifers and 1.5 g/kg in deciduous trees, whereas in branches of all tree species the N content is 4 g/kg in the south and 2 g/kg in the north. In a recent report Jacobsen et al. (2002) have summarised the results of a large number of studies on that subject, and Table 5.8 shows the average element contents in 4 major tree species, both for stems and branches. For N , the values have to be multiplied by $1/14=0.07143$ to obtain the N contents in eq/kg .

Growth rates used should be long-term average values, typical for the site. It has to be noted that recent growth rates are higher due to increased N input. Therefore it is

recommended to use older investigations (yield tables), preferably from before 1960–70. An example of how to use national inventory information to compute forest growth (and critical loads) in Germany can be found in Nagel and Gregor (1999).

Net uptake of N in non-forest natural and semi-natural ecosystems is insignificant, unless they are used for extensive grazing. For example, in the United Kingdom net removal of N in sheep (mutton/wool) due to extensive grazing is between 0.5 and 2.0 $kgN/ha/yr$, depending on site fertility and grazing density.

Denitrification:

Dutch and Ineson (1990) reviewed data on rates of denitrification. Typical values of N_{de} for boreal and temperate ecosystems are in the range of 0.1–3.0 $kgN/ha/yr$ (=7.14–214.3 $eq/ha/yr$), where the higher values apply to wet(ter) soils; rates for well drained soils are generally below 0.5 $kgN/ha/yr$.

With respect to deposition-dependent denitrification, values for the denitrification fraction f_{de} have been given by De Vries et al. (1993) based on data from Breeuwsma et al. (1991) and Steenvorden (1984): $f_{de}=0.8$ for

peat soils, 0.7 for clay soils, 0.5 for sandy soils with gleyic features and $f_{de}=0-0.1$ for sandy soils without gleyic features. Reinds et al. (2001) related the denitrification fraction to the drainage status of the soil according to Table 5.9:

Precipitation surplus:

The precipitation surplus Q is the amount of water percolating from the root zone. It is conveniently calculated as the difference between precipitation and actual evapotranspiration and it should be the long-term climatic mean annual value. In many cases evapotranspiration will have to be calculated by a model using basic meteorological input data (precipitation, temperature, radiation etc.). For the basics of modelling evapotranspiration see Monteith and Unsworth (1990) and for an extensive collection of models see Burman and Pochop (1994). Historical time series of meteorological data can be found, e.g., on the website of the Climate Change Research Unit of the University of East Anglia (<http://www.cru.uea.ac.uk/cru/data/hrg.htm>).

Table 5.8: Mean (and standard deviation) of the element contents in stems and branches (both incl. bark) of four tree species (Jacobsen et al. 2002; the number of data points ranges from 6 to 32).

Tree species	Contents (g/kg) in stems (incl. bark)				Contents (g/kg) in branches (incl. bark)			
	N	Ca ^{a)}	Mg	K	N	Ca	Mg	K
Oak <i>quercus spp</i>	2.10 (0.46)	2.47 (1.42)	0.18 (0.07)	1.05 (0.51)	6.19 (1.02)	4.41 (0.65)	0.44 (0.14)	2.00 (0.47)
Beech <i>fagus sylv.</i>	1.54 (0.25)	1.80 (1.12)	0.26 (0.09)	1.04 (0.13)	4.27 (1.36)	4.02 (1.91)	0.36 (0.13)	1.50 (0.44)
Spruce <i>picea abies</i>	1.22 (0.49)	1.41 (0.40)	0.18 (0.06)	0.77 (0.43)	5.24 (1.66)	3.33 (1.06)	0.53 (0.27)	2.39 (1.35)
Pine <i>pinus sylv.</i>	1.09 (0.30)	1.08 (0.30)	0.24 (0.09)	0.65 (0.28)	3.61 (1.28)	2.07 (0.65)	0.43 (0.11)	1.67 (0.68)

^{a)}Note that for Ca data points from calcareous sites are included in the statistics.

Table 5.9: Denitrification fraction f_{de} as a function of the soil drainage (Reinds et al. 2001).

Drainage status	Excessive	Good	Moderate	Imperfect	Poor	Very poor
f_{de}	0	0.1	0.2	0.4	0.7	0.8

5.3.2 Critical loads of acidity

5.3.2.1 Model derivation: the Simple Mass Balance (SMB) model

The starting point for deriving critical loads of acidifying *S* and *N* for soils is the charge balance of the ions in the soil leaching flux (De Vries 1991):

$$(5.9) \quad H_{le} + Al_{le} + BC_{le} + NH_{4,le} = SO_{4,le} + NO_{3,le} + Cl_{le} + HCO_{3,le} + RCOO_{le}$$

where the subscript *le* stands for leaching, *Al* stands for the sum of all positively charged aluminium species, *BC* is the sum of base cations ($BC = Ca + Mg + K + Na$) and *RCOO* is the sum of organic anions. A leaching term is given by $X_{le} = Q[X]$, where $[X]$ is the soil solution concentration of ion *X* and *Q* is the precipitation surplus. All fluxes are expressed in equivalents (moles of charge) per unit area and time (*eq/ha/yr*). The concentrations of *OH* and *CO₃* are assumed zero, which is a reasonable assumption even for calcareous soils. The leaching of Acid Neutralising Capacity (*ANC*) is defined as:

$$(5.10) \quad ANC_{le} = HCO_{3,le} + RCOO_{le} - H_{le} - Al_{le}$$

Combination with eq. 5.9 yields:

$$(5.11) \quad BC_{le} + NH_{4,le} - SO_{4,le} - NO_{3,le} - Cl_{le} = ANC_{le}$$

This shows the alternative definition of *ANC* as 'sum of (base) cations minus strong acid anions'. For more detailed discussions on the processes and concepts of (soil) chemistry encountered in the context of acidification see, e.g., the books by Reuss and Johnson (1986) or Ulrich and Sumner (1991).

Chloride is assumed to be a tracer, i.e., there are no sources or sinks of *Cl* within the soil compartment, and chloride leaching is therefore equal to the *Cl* deposition (subscript *dep*):

$$(5.12) \quad Cl_{le} = Cl_{dep}$$

In a steady-state situation the leaching of base cations has to be balanced by the net input of base cations. Consequently the following equation holds:

$$(5.13) \quad BC_{le} = BC_{dep} + BC_w - BC_u$$

where the subscripts *w* and *u* stand for weathering and net growth uptake, i.e. the net uptake by vegetation that is needed for long-term average growth; $Bc = Ca + Mg + K$, reflecting the fact that *Na* is not taken up by vegetation. Base cation input by litterfall and *Bc* removal by maintenance uptake (needed to re-supply base cations in leaves) is not considered here, assuming that both fluxes are equal (in a steady-state situation). Also the finite pool of base cations at the exchange sites (cation exchange capacity, CEC) is not considered. Although cation exchange might buffer incoming acidity for decades, its influence is only a temporary phenomenon, which cannot be taken into account when considering long-term steady-state conditions.

The leaching of sulphate and nitrate can be linked to the deposition of these compounds by means of mass balances for *S* and *N*. For *S* this reads (De Vries 1991):

$$(5.14) \quad S_{le} = S_{dep} - S_{ad} - S_i - S_u - S_{re} - S_{pr}$$

where the subscripts *ad*, *i*, *re* and *pr* refer to adsorption, immobilisation, reduction and precipitation, respectively. An overview of sulphur cycling in forests by Johnson (1984) suggests that uptake, immobilisation and reduction of *S* have generally insignificant. Adsorption (and in some cases precipitation with Al complexes) can temporarily lead to a strong accumulation of sulphate (Johnson et al. 1979, 1982). However, sulphate is only stored or released at the adsorption complex when the input (deposition) changes, since the adsorbed *S* is assumed in

equilibrium with the soil solution S . Only dynamic models can describe the time pattern of ad- and desorption of sulphate, but under steady-state conditions S ad- and desorption and precipitation/mobilisation are not considered. Since sulphur is completely oxidised in the soil profile, $SO_{4,le}$ equals S_{le} , and consequently:

$$(5.15) \quad SO_{4,le} = S_{dep}$$

For nitrogen, the mass balance in soil is (see Section 5.3.1):

$$(5.16) \quad N_{le} = N_{dep} + N_{fix} - N_{ad} - N_i - N_u - N_{de} - N_{eros} - N_{fire} - N_{vol}$$

where the subscripts *fix* refers to fixation of N , *de* to denitrification, and *eros*, *fire* and *vol* to the loss of N due to erosion, forest fires and volatilisation, respectively. N_i is the long-term immobilisation of N in the root zone, and N_u the net growth uptake (see above). Furthermore, the leaching of NH_4 can be neglected in almost all forest ecosystems due to (preferential) uptake and complete nitrification within the root zone, i.e. $NH_{4,le}=0$. Under these various assumptions eq. 5.16 simplifies to:

$$(5.17) \quad N_{le} = NO_{3,le} = N_{dep} - N_i - N_u - N_{de}$$

Inserting eqs. 5.12, 5.13, 5.15 and 5.17 into eq. 5.11 leads to the following simplified charge balance for the soil compartment:

$$(5.18) \quad S_{dep} + N_{dep} = BC_{dep} - Cl_{dep} + BC_w - BC_u + N_i + N_u + N_{de} - ANC_{le}$$

Strictly speaking, we should replace $NO_{3,le}$ in the charge balance not by the right-hand side of eq. 5.17, but by $\max\{N_{dep} - N_i - N_u - N_{de}, 0\}$, since leaching cannot

become negative; and the same holds true for base cations. However, this would lead to unwieldy critical load expressions; therefore we go ahead with eq. 5.18, keeping this constraint in mind.

Since the aim of the LRTAP Convention is to reduce *anthropogenic* emissions of S and N , sea-salt derived sulphate should not be considered in the balance. To retain charge balance, this is achieved by applying a sea-salt correction to sulphate, chloride and base cations, using either Cl or Na as a tracer, whichever can be (safer) assumed to originate from sea-salts only. Denoting sea-salt corrected depositions with an asterisk, one has either $Cl_{dep}^*=0$ or $Na_{dep}^*=0$ (and $BC_{dep}^*=BC_{dep}^*$), respectively. For procedures to compute sea-salt corrected depositions, see Chapter 2.

For given values for the sources and sinks of S , N and Bc , eq. 5.18 allows the calculation of the leaching of ANC , and thus assessment of the acidification status of the soil. Conversely, critical loads of S , $CL(S)$, and N , $CL(N)$, can be computed by defining a critical ANC leaching, $ANC_{le,crit}$:

$$(5.19) \quad CL(S) + CL(N) = BC_{dep}^* - Cl_{dep}^* + BC_w - BC_u + N_i + N_u + N_{de} - ANC_{le,crit}$$

A so-called critical load of potential acidity has earlier been defined (see Sverdrup et al. 1990) as:

$$(5.20) \quad CL(Ac_{pot}) = BC_w - BC_u + N_i + N_u + N_{de} - ANC_{le,crit}$$

with $Ac_{pot} = S_{dep} + N_{dep} - BC_{dep}^* + Cl_{dep}^*$. The term 'potential' is used since NH_3 is treated as (potential) acid due to the assumed complete nitrification. $CL(Ac_{pot})$ has been defined to have no deposition terms in its definition, since Bc and Cl deposition are not really an ecosystem property and can (and often do) change over time. However, since these depositions are partly of non-anthro-

pogenic origin (e.g., Saharan dust) and since they are not subject to emission reduction negotiations, they are kept in the critical load definition for convenience.

A further distinction has been made earlier (see, e.g., Sverdrup and De Vries 1994) between ‘land use acidity’ $Bc_u - N_f - N_u - N_{de}$ and ‘soil acidity’ which is used to define a so-called critical load of (actual) acidity as:

(5.21)

$$CL(A) = BC_w - ANC_{le,crit}$$

The reason for making this distinction was to exclude all variables that may change in the long term such as uptake of Bc and N , which are influenced by forest management, and N immobilisation and denitrification, which may change due to changes in the hydrological regime. There are two problems with this reasoning: (a) the remaining terms in eq. 5.21 are also liable to change (e.g. ANC leaching depends on precipitation surplus, see

below), and (b) uptake and other N processes are a defining part of the ecosystem (vegetation) itself. In other words, $CL(A)$ may be a critical load of soil acidity, but it is rarely the soil as such that is the ‘sensitive element’ to be protected, but the vegetation growing on that soil! Nevertheless, quantities such as $CL(A)$ are computed and reported, and they can have a role as useful short-hand notation for the variables involved.

Note that eq. 5.19 does not give a unique critical load for S or N . However, nitrogen sinks cannot compensate incoming sulphur acidity, and therefore the maximum critical load for sulphur is given by:

(5.22)

$$\begin{aligned} CL_{max}(S) &= BC_{dep}^* - Cl_{dep}^* + BC_w - Bc_u - ANC_{le,crit} \\ &= BC_{dep}^* - Cl_{dep}^* - Bc_u + CL(A) \end{aligned}$$

as long as N deposition is lower than all the N sinks, termed the minimum critical load of N , i.e. as long as

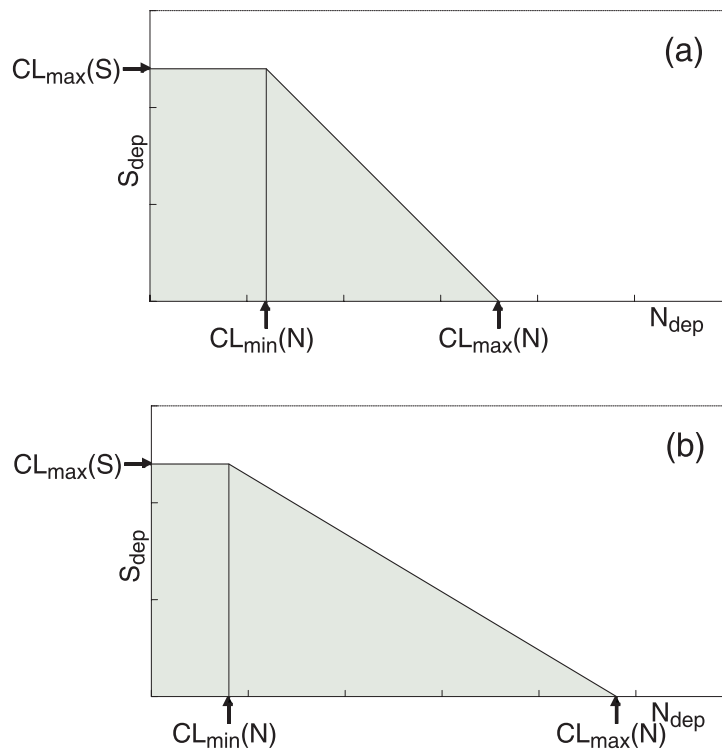


Figure 5.1: Critical load function (CLF) of sulphur and acidifying nitrogen, defined by the three quantities $CL_{max}(S)$, $CL_{min}(N)$ and $CL_{max}(N)$. (a) with constant denitrification N_{de} , and thus a 45° slope of the CLF; (b) with deposition-dependent denitrification, resulting in a smaller $CL_{min}(N)$ and a flatter slope, depending on f_{de} . The grey area below the CLF denotes deposition pairs resulting in an ANC leaching greater than $ANC_{le,crit}$ (non-exceedance of critical loads; see Chapter 7).

(5.23)

$$N_{dep} \leq CL_{min}(N) = N_i + N_u + N_{de}$$

Finally, the maximum critical load of nitrogen (in the case of zero S deposition) is given by:

(5.24)

$$CL_{max}(N) = CL_{min}(N) + CL_{max}(S)$$

The three quantities $CL_{max}(S)$, $CL_{min}(N)$ and $CL_{max}(N)$ define the **critical load function** (CLF; depicted in Figure 5.1a). Every deposition pair (N_{dep}, S_{dep}) lying on the CLF are critical loads of acidifying S and N .

Deriving critical loads as above assumes that the sources and sinks of N do not depend on the N deposition. This is unlikely to be true; and as in Section 5.3.1 we consider also the case of denitrification being linearly related to the net input of N . Substituting eq. 5.4 for N_{de} into the equations above results in the following expressions for $CL_{min}(N)$ and $CL_{max}(N)$:

(5.25)

$$CL_{min}(N) = N_i + N_u$$

and

(5.26)

$$CL_{max}(N) = CL_{min}(N) + \frac{CL_{max}(S)}{1 - f_{de}}$$

where f_{de} ($0 \leq f_{de} < 1$) is the denitrification fraction; $CL_{max}(S)$ remains the same (eq. 5.22). An example of a critical load function with $f_{de} > 0$ is shown in Figure 5.1b.

5.3.2.2 Chemical criteria and the critical leaching of Acid Neutralising Capacity

The leaching of Acid Neutralising Capacity (ANC) is defined in eq. 5.10. In the simplest case bicarbonate (HCO_3) and organic anions ($RCOO$) are neglected since in general they do not contribute significantly at low pH values. In this case the ANC leaching is given by:

(5.27)

$$ANC_{le} = -H_{le} - Al_{le} = -Q \cdot ([H] + [Al])$$

where Q is the precipitation surplus in $m^3/ha/yr$ (see Section 5.3.1.3 for data).

It is within the calculation of ANC_{le} that the critical chemical criterion for effects on the receptor is set. Selecting the most appropriate method of calculating ANC_{le} is important, since the different methods may result in very different critical loads. If, for the same ecosystem, critical loads are calculated using different criteria, the final critical load is the minimum of all those calculated. The main decision in setting the criterion will depend on whether the receptor considered is more sensitive to unfavourable pH conditions or to the toxic effects of aluminium. ANC_{le} can then be calculated by either setting a hydrogen ion criterion (i.e., a critical soil solution pH) and calculating the critical aluminium concentration, or vice versa.

The relationship between $[H]$ and $[Al]$ is described by an (apparent) gibbsite equilibrium:

(5.28)

$$[Al] = K_{gibb} \cdot [H]^3$$

where K_{gibb} is the gibbsite equilibrium constant (see below). Eq. 5.28 is used to calculate the (critical) Al concentration from a given proton concentration, or vice versa.

Different critical chemical criteria are listed below together with the equations for calcu-

lating $ANC_{le,crit}$. In this context the reader could also consult the minutes of an Expert Workshop on 'Chemical Criteria and Critical Limits' (UNECE 2001, Hall et al. 2001).

Aluminium criteria:

Aluminium criteria are generally considered most appropriate for mineral soils with a low organic matter content. Three commonly used criteria are listed below.

(a) Critical aluminium concentration:

Critical limits for Al have been suggested for forest soils, e.g., $[Al]_{crit} = 0.2 \text{ eq/m}^3$. These are especially useful for drinking water (ground water) protection, e.g., the EC drinking water standard for $[Al]$ of maximally 0.2 mg/L (about 0.02 eq/m³). $ANC_{le,crit}$ can then be calculated as:

$$(5.29) \quad ANC_{le,crit} = -Q \cdot \left(\left([Al]_{crit} / K_{gibb} \right)^{1/3} + [Al]_{crit} \right)$$

(b) Critical base cation to aluminium ratio:

Most widely used for soils is the connection between soil chemical status and plant response (damage to fine root) via a critical molar ratio of the concentrations of base cations ($Bc = Ca + Mg + K$) and Al in soil solution, denoted as $(Bc/Al)_{crit}$. Values for a large variety of plant species can be found in Sverdrup and Warfvinge (1993). The most commonly used value is $(Bc/Al)_{crit} = 1$, the value for coniferous forests.

The critical Al leaching is calculated from the leaching of Bc (compare eq. 5.13):

$$(5.30) \quad Al_{le,crit} = 1.5 \cdot \frac{Bc_{le}}{(Bc/Al)_{crit}}$$

The factor 1.5 arises from the conversion of mols to equivalents (assuming K as divalent). Using eqs. 5.27 and 5.28, this yields for the critical ANC leaching:

$$(5.31) \quad ANC_{le,crit} = -Q^{2/3} \cdot \left(1.5 \cdot \frac{Bc_{dep} + Bc_w - Bc_u}{K_{gibb} \cdot (Bc/Al)_{crit}} \right)^{1/3} - 1.5 \cdot \frac{Bc_{dep} + Bc_w - Bc_u}{(Bc/Al)_{crit}}$$

Note that the expression $Bc_{le} = Bc_{dep} + Bc_w - Bc_u$ has to be non-negative. In fact, it has been suggested that it should be above a minimum leaching or, more precisely, there is a minimum concentration of base cations in the leachate, below which they cannot be taken up by vegetation, i.e., Bc_{le} is set equal to $\max\{0, Bc_{dep} + Bc_w - Bc_u - Q \cdot [Bc]_{min}\}$, with $[Bc]_{min}$ in the order of 0.01 eq/m³.

Alternatively, if considered more appropriate, a critical molar ratio of calcium to aluminium in soil solution can be used, by replacing all the Bc-terms in eq. 5.31 with Ca-terms.

(c) Critical aluminium mobilisation rate:

Critical ANC leaching can also be calculated using a criterion to prevent the depletion of secondary Al phases and complexes which may cause structural changes in soils and a further pH decline. Aluminium depletion occurs when the acid deposition leads to an Al leaching in excess of the Al produced by the weathering of primary minerals. Thus the critical leaching of Al is given by:

$$(5.32) \quad Al_{le,crit} = Al_w$$

where Al_w is the weathering of Al from primary minerals (eq/ha/yr). The weathering of Al can be related to the Bc weathering via:

$$(5.33) \quad Al_w = p \cdot BC_w$$

where p is the stoichiometric ratio of Al to Bc weathering in primary minerals (eq/eq), with a default value of $p=2$ for typical mineralogy of Northern European soils (range: 1.5–3.0). The critical leaching of ANC becomes then:

(5.34)

$$ANC_{le,crit} = -Q^{2/3} \cdot \left(\frac{p \cdot BC_w}{K_{gibb}} \right)^{1/3} - p \cdot BC_w$$

Hydrogen ion criteria:

A proton criterion is generally recommended for soils with a high organic matter content. Two such criteria are listed below.

(a) Critical pH:

A critical pH limit is set at a pH below which the receptor is adversely affected. Critical limits have been suggested for forest soils, for example, $pH_{crit}=4.0$ (corresponding to $[H]_{crit}=0.1 \text{ eq/m}^3$). $ANC_{le,crit}$ can then be calculated as:

(5.35)

$$ANC_{le,crit} = -Q \cdot \left([H]_{crit} + K_{gibb} \cdot [H]_{crit}^3 \right)$$

(b) Critical base cation to proton ratio:

For organic soils which do not contain Al-(hydr)oxides (such as peat lands), it is suggested to use a critical molar base cation to proton ratio $(Bc/H)_{crit}$. The critical ANC leaching is then given by (no Al leaching!):

(5.36)

$$ANC_{le,crit} = 0.5 \cdot \frac{Bc_{dep} + Bc_w - Bc_u}{(Bc/H)_{crit}}$$

where the factor 0.5 comes from converting mols to equivalents. For organic soils the weathering in eq. 5.36 will probably be negligible ($Bc_w=0$). Values suggested for $(Bc/H)_{crit}$ are expressed as multiples of $(Bc/Al)_{crit}$, these multiples ranging from 0.3 for deciduous trees and ground vegetation to 1 for spruce and pine (Sverdrup and Warfvinge 1993).

Critical base saturation

Base saturation, i.e., the fraction of base cations at the cation exchange complex, is an indicator of the acidity status of a soil, and one may want to keep this pool above a certain level to avoid nutrient deficiencies. Thus a critical (acceptable, minimum) base saturation could be chosen as a criterion for calculating critical loads of acidity (see Hall et al. 2001, UNECE 2001).

To relate base saturation to ANC requires the description of the exchange of cations between the exchange complex and the soil solution. Two descriptions are the most commonly used in dynamic soil models: the Gapon and the Gaines-Thomas exchange model. For a comparison between different exchange models and the implications for the relationship between base saturation and soil solution concentrations see Reuss (1983).

As an example, we consider the description of the exchange between H , Al and $Bc=Ca+Mg+K$ as implemented in the Very Simple Dynamic (VSD) as well as the SAFE model (see Posch et al. 2003a or Chapter 6 on dynamic modelling). For both models the critical concentration $[H]_{crit}$ can be found as a solution of an equation of the type:

(5.37)

$$A \cdot [H]_{crit}^p + B \cdot [H]_{crit} = 1 - E_{Bc,crit}$$

where the coefficients A , B and the exponent p are given in Table 5.10.

Table 5.10: Coefficients in eq. 5.37 for the Gapon and Gaines-Thomas exchange model.

Exchange model	A	p	B
Gapon	$K_{Alox}^{1/3} \cdot k_{AlBc} \cdot E_{Bc,crit} / \sqrt{[Bc]}$	$a/3$	$k_{HBc} \cdot E_{Bc,crit} / \sqrt{[Bc]}$
Gaines-Thomas	$K_{Alox} \cdot \sqrt{K_{AlBc} \cdot (E_{Bc,crit} / [Bc])^3}$	a	$\sqrt{K_{HBc} \cdot E_{Bc,crit} / [Bc]}$

Note: The generalised relationship $[Al]=K_{Alox} [H]^a$ has been used (see below).

In general, eq. 5.37 is non-linear and will have to be solved numerically. Only for the Gapon model and the gibbsite equilibrium ($a=3, K_{AlOx}=K_{gibb}$) it becomes a linear equation with the solution:

(5.38)

$$[H]_{crit} = K_{Gap} \cdot \sqrt{[Bc]} \cdot \left(\frac{1}{E_{Bc,crit}} - 1 \right)$$

with

$$K_{Gap} = \frac{1}{k_{HBc} + k_{AlBc} \cdot K_{gibb}^{1/3}}$$

where k_{HBc} and k_{AlBc} are the two (site-specific) selectivity coefficients describing cation exchange and $[Bc]=Bc_{le}/Q$ as above. $[Al]_{crit}$ is then computed from the gibbsite equilibrium (eq. 5.28) and from that the critical ANC leaching can be obtained via eq. 5.29. Values of selectivity coefficients for a range of (Dutch) soil types and combinations of exchangeable ions are given by De Vries and Posch (2003).

In Figure 5.2 the critical ANC leaching is shown for a range of constants K_{Gap} . This range encompasses a wide range of values for the exchange constants. The figure shows that ANC leaching is very sensitive to low values of the critical base saturation.

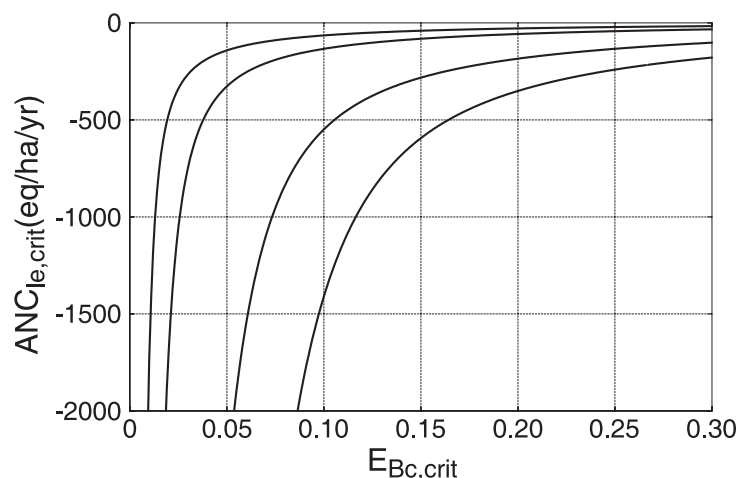


Figure 5.2: Critical ANC leaching (as defined by eq. 5.27, for $Q=1$ m/yr) as a function of the critical base saturation, $E_{Bc,crit}$ for $[Bc]=0.02\text{eq/m}^3$, $K_{gibb}=10^8$ and $K_{Gap}=0.005$ (leftmost curve), 0.01, 0.03 and 0.05 (rightmost curve). (To obtain $ANC_{le,crit}$ for arbitrary Q , multiply the values on the vertical axis by Q in m/yr; see also Figure 5.4 below.)

Base saturation is also used as criterion in the New England Governors/Eastern Canadian Premiers ‘Acid Rain Action Plan’ for calculating sustainable S and N depositions to upland forests with the SMB model (NEG/ECP 2001).

5.3.2.3 Sources and derivation of input data

The obvious sources of input data for calculating acidity critical loads are measurements at the site under consideration. However, in many cases these will not be available. For data on the different N quantities see Section 5.3.1. Some data sources and default values for the other variables, and procedures to derive them, are summarised below.

Gibbsite equilibrium constant (K_{gibb}):

The equilibrium constant relating the Al concentration to pH (eq. 5.28) depends on the soil. Table 5.11 presents ranges of K_{gibb} (and $pK_{gibb}=-\log_{10}(K_{gibb}$ in $(\text{mol/L})^{-2}$) as a function of the soil organic matter content. A widely used default value is $K_{gibb}=10^8 (\text{mol/L})^{-2}=300 \text{ m}^6/\text{eq}^2$.

If sufficient empirical data are available to derive the relationship between $[H]$ and $[Al]$, these should be used in preference to the gibbsite equilibrium (see Sec. 5.3.2.4).

Base cation and chloride deposition:

The base cation and chloride depositions entering the critical load calculations should be the deposition after all feasible abatement measures have been taken (ideally the non-anthropogenic deposition), and they should be sea-salt corrected. Observations on a European scale are available from the EMEP Chemical Co-ordinating Centre (www.emep.int) or from national sources. See Chapter 2 for more details.

Base cation weathering:

Weathering here refers to the release of base cations from minerals in the soil matrix due to chemical dissolution, and the neutralisation and production of alkalinity connected to this process. This has to be distinguished from the denudation of base cations from ion exchange complexes (cation exchange) and the degradation of soil organic matter. Many methods for determining weathering rates have been suggested, and here we list those with the highest potential for regional applications (in order of increasing complexity).

(a) The Skokloster assignment:

This is a (semi-)empirical method devised at the Critical Loads Workshop at Skokloster (Sweden) (Table 1, p.40 in Nilsson and Grennfelt 1988). Details can be found in the section on empirical acidity critical loads (Section 5.2.2).

(b) The soil type – texture approximation:

Since mineralogy controls weathering rates, weathering rate classes were assigned to European (forest) soils by De Vries et al. (1993), based on texture class and parent material class. Texture classes are defined in Table 5.12 as a function of their clay and sand content:

Using the FAO soil classification (FAO 1981), the parent material class has been defined for each soil type in Table 5.13 (updated from De Vries et al. 1993).

From texture and parent material class the weathering rate class is obtained from Table 5.14 (modified from De Vries et al. 1993).

Table 5.11: Ranges for K_{gibb} as a function of soil organic matter content.

Soil type; layer	Organic matter (%)	K_{gibb} (m^6/eq^2)	$-pK_{gibb}$
Mineral soils; C-layer	<5	950–9500	8.5–9.5
Soils with low organic matter; B/C layers	5–15	300–3000	8–9
Soils with some organic material; A/E layers	15–30	100	7.6
Peaty and organic soils; organic layers	>70	9.5	6.5

Table 5.12: Soil texture classes as a function of their clay and sand content (Eurosoil 1999).

Texture class	Name	Definition
1	coarse	clay < 18 % and sand \geq 65 %
2	medium	clay < 35% and sand > 15 %, but clay \geq 18 % if sand \geq 65 %
3	medium fine	clay < 35% and sand < 15 %
4	fine	35 % \leq clay < 60 %
5	very fine	clay \geq 60 %

Table 5.13: Parent material classes for common FAO soil types (Posch et al. 2003b).

Parent material	FAO soil type
Acidic	Ah, Ao, Ap, B, Ba, Bd, Be, Bf, Bh, Bm, Bx, D, Dd, De, Dg, Gx, I, Id, Ie, Jd, P, Pf, Pg, Ph, Pl, Po, Pp, Q, Qa, Qc, Qh, Ql, Rd, Rx, U, Ud, Wd
Intermediate	A, Af, Ag, Bv, C, Cg, Ch, Cl, G, Gd, Ge, Gf, Gh, Gi, Gl, Gm, Gs, Gt, H, Hg, Hh, Hl, J, Je, Jm, Jt, L, La, Ld, Lf, Lg, Lh, Lo, Lp, Mo, R, Re, V, Vg, Vp, W, We
Basic	F, T, Th, Tm, To, Tv
Organic	O, Od, Oe, Ox

Acidic: Sand(stone), gravel, granite, quartzine, gneiss (schist, shale, greywacke, glacial till)

Intermediate: Gronodiorite, loess, fluvial and marine sediments (schist, shale, greywacke, glacial till)

Basic: Gabbro, basalt, dolomite, volcanic deposits.

Table 5.14: Weathering rate classes as a function of texture and parent material classes (Posch et al. 2003b).

Parent material	Texture class				
	1	2	3	4	5
Acidic	1	3	3	6	6
Intermediate	2	4	4	6	6
Basic	2	5	5	6	6
Organic	class 6 for Oe and class 1 for other organic soils				

The actual weathering rate (in *eq/ha/yr*) for a non-calcareous soil of depth *z* (in m) is then computed as:

(5.39)

$$BC_w = z \cdot 500 \cdot (WRc - 0.5) \cdot \exp\left(\frac{A}{281} - \frac{A}{273 + T}\right)$$

where *WRc* is the weathering rate class (Table 5.14), *T* (°C) is the average annual (soil) temperature and *A*=3600 K (Sverdrup 1990). For calcareous soil, for which critical loads are not really of interest, one could set, e.g., *WRc*=20 in eq. 5.39.

The above procedure provides weathering rates for *BC*=*Ca*+*Mg*+*K*+*Na*. However, for computing the critical *ANC* leaching according to eq. 5.31, the weathering rate for *Bc*=*Ca*+*Mg*+*K* is needed. *Bc_w* can be approximated by multiplying *Bc_w* with a factor between 0.70 for poor sandy soils and 0.85 for rich (sandy) soils. Van der Salm et al. (1998) (for texture classes 2–5, see Table 5.12) and De Vries (1994) (for texture class 1) provide regression equations for weathering rates of *Ca*, *Mg*, *K* and *Na* as a function of the

sand (and silt) content of the soil, which can be used to split *Bc_w* into individual weathering rates.

(c) *The total base cation content correlation:* Using the ‘zirconium method’, Olsson et al. (1993) derived from 11 Swedish sites a correlation between the historical average weathering rates of base cations and the total content of the respective element in the undisturbed bottom soil, with an additional temperature correction. For *Ca*, *Mg* and *K* the equations are (Olsson et al. 1993, converted to *eq/ha/yr*):

(5.40)

$$Ca_w = 0.13 \cdot (Ca)_{tot} \cdot ETS - 55.5$$

$$Mg_w = 0.23 \cdot (Mg)_{tot} \cdot ETS - 24.1$$

$$K_w = 0.05 \cdot (K)_{tot} \cdot ETS - 79.8$$

where *(X)_{tot}* is the total content of element *X* (in dry weight %) in the coarse fraction (<2mm) of the undisturbed C-horizon soil and *ETS* is the annual sum of daily temperatures above a threshold of +5°C. Care has to be taken when applying these formulae, since they are based on Nordic geological history, they do not predict the weatherable

soil depth, which was found to vary between 20 and 200 cm in the field data, and they don't cover many soil types (mostly podzols).

Using the part of the Swedish data (7-8 sites depending on the element, covering a weatherable depth of 20–100 cm), this method was adapted in Finland for estimating weathering rates on a national scale (Johansson and Tarvainen 1997, Joki-Heiskala et al. 2003).

(d) The calculation of weathering rates with the PROFILE model:

Weathering rates can be computed with the multi-layer steady-state model PROFILE (Warfvinge and Sverdrup 1992 and 1995). Basic input data are the mineralogy of the site or a total element analysis, from which the mineralogy is derived by a normative procedure. Generic weathering rates of each mineral are modified by the concentration of protons, base cations, aluminium and organic anions as well as the partial pressure of CO_2 and temperature. The total weathering rate is proportional to soil depth and the wetted surface area of all minerals present. For the theoretical foundations of the weathering rate model see Sverdrup (1990). For further information on the PROFILE model see www2.chemeng.lth.se.

(e) Other methods:

Weathering rates can also be estimated from budget studies of small catchments (see, e.g., Paces 1983). Be aware, however, that budget studies can easily overestimate weathering rates where there is significant cation release due to weathering of the bedrock. Other methods are listed and described in Sverdrup et al. (1990).

Base cation uptake:

The uptake flux of base cations, Bc_u , entering the critical load calculations is the long-term average removal of base cations from the ecosystem. The uptake fluxes should be calculated for the individual base cations (Ca , Mg and K) separately. The considerations and calculations are exactly the same as for the uptake of N (see Section 5.3.1). Average contents of Ca , Mg and K in

stems and branches can be found in Table 5.8 (see also Jacobsen et al. 2002). Values have to be multiplied by 2/40.08, 2/24.31 and 1/39.10 for Ca , Mg and K , respectively, to obtain contents in eq/kg.

The (long-term) net uptake of base cations is limited by their availability through deposition and weathering (neglecting the depletion of exchangeable base cations). Furthermore, base cations will not be taken up below a certain concentration in soil solution, or due to other limiting factors, such as a temperature. Thus the values entering critical load calculations should be constrained by:

(5.41)

$$Y_u \leq Y_{dep} + Y_w - Q \cdot [Y]_{min}$$

for $Y = Ca, Mg, K$

This is preferable to constraining the sum $Bc_u = Ca_u + Mg_u + K_u$ (see eq. 5.31). Suggested values are 5 meq/m³ for $[Ca]_{min}$ and $[Mg]_{min}$, and zero for $[K]_{min}$ (Warfvinge and Sverdrup 1992). It should also be taken into account that vegetation takes up nutrients in fairly constant (vegetation-specific) ratios. Thus, when adjusting the uptake value for one element, the values for the other elements (including N) should be adjusted proportionally.

5.3.2.4 Possible extensions to the SMB model

In the following three suggestions are made for generalising the SMB model, with the idea of improving the critical load calculations but also with the aim to enhance the compatibility with dynamic models. All three suggestions are 'backwards-compatible', i.e. by setting key parameters to zero the original SMB model is obtained. For an earlier discussion of these extensions see also Posch (2000).

(a) Generalisation of the Al-H relationship:

In the SMB model the relationship between Al concentration and pH is described as

gibbsite equilibrium (see eq. 5.21). However, *Al* concentrations, especially in the topsoil, can be influenced by the complexation of *Al* with organic matter (Cronan et al. 1986, Mulder and Stein 1994). Therefore, the gibbsite equilibrium in the SMB model could be generalised by:

(5.42)

$$[Al] = K_{Alox} \cdot [H]^a$$

with equilibrium constant K_{Alox} and exponent a . Obviously, the gibbsite equilibrium is a special case of eq. 5.42 (setting $a=3$ and $K_{Alox}=K_{gibb}$). The exponent a and K_{Alox} depend on the soil type and especially on the soil horizon. As an example, in Table 5.15 values for K_{Alox} and a are presented for different soil groups and soil depths derived from several hundred Dutch forest soil solution samples (see Van der Salm and De Vries 2001).

The data in Table 5.15 show that a standard gibbsite equilibrium constant and $a=3$ is reasonable for (Dutch) sandy soils. Very different values, however, are obtained for peat soils and, to a lesser extent, also for loess and clay soils (especially for shallow parts of the soil, where the organic matter content is highest). Data from intensive forest monitoring plots show that there is a strong correlation between a and $\log_{10}K_{Alox}$ (De Vries et al. 2003, p.118), which emphasises that these two parameters cannot be chosen independently.

Figure 5.3 shows the relationship between $[H]$ and $[Al]$ as well as its logarithmic form for different values of K_{Alox} and a . Defining $pX = -\log_{10}[X]$, with $[X]$ given in mol/L, one has $pH = 3 - \log_{10}([H])$, if $[H]$ is expressed in eq/m³; and for $[Al]$ in eq/m³ the relationship is $pAl = 3 - \log_{10}([Al]/3)$.

Note that, when using eq. 5.42 instead of eq. 5.28, the formulae for $ANC_{le,crit}$ have to be adapted as well (mostly replacing the exponent 3 by a and $1/3$ by $1/a$).

(b) Including bicarbonate leaching:

The charge balance (eq. 5.9) and the definition of ANC leaching in eq. 5.10 also includes the leaching of bicarbonate anions ($HCO_{3,le} = Q \cdot [HCO_3]$). The concentration of bicarbonates is a function of the pH:

(5.43)

$$[HCO_3] = \frac{K_1 \cdot K_H \cdot p_{CO_2}}{[H]}$$

where K_1 is the first dissociation constant, K_H is Henry's constant and p_{CO_2} is the partial pressure of CO_2 in the soil solution (in atm). The two constants are weakly temperature-dependent, and the value for their product at 8°C is $K_1 \cdot K_H = 10^{-1.7} = 0.02 \text{ eq}^2/\text{m}^6/\text{atm}$. For systems open to the atmosphere, p_{CO_2} is about 370 ppm or $3.7 \cdot 10^{-4}$ atm (in the year 2000). However, in soils p_{CO_2} is generally higher (ranging from 10^{-2} to 10^{-1} atm, Bolt and Bruggenwert 1976), due to respiration

Table 5.15: Estimated values of K_{Alox} and the exponent a based on regression between pAl and pH in the soil solution of Dutch forests (N = number of samples).

Soil type	Depth (cm)	$\log_{10} K_{Alox}^a)$	a	N
All	humus layer	-1.03	1.17	275
Sandy soils	0–10	3.54	2.26	274
	10–30	5.59	2.68	377
	30–100	7.88	3.13	271
Loess soils	0–10	-0.38	1.04	45
	10–30	3.14	1.83	46
	30–100	4.97	2.21	40
Clay	all depths	4.68	2.15	152
Peat	all depths	1.41	1.85	163

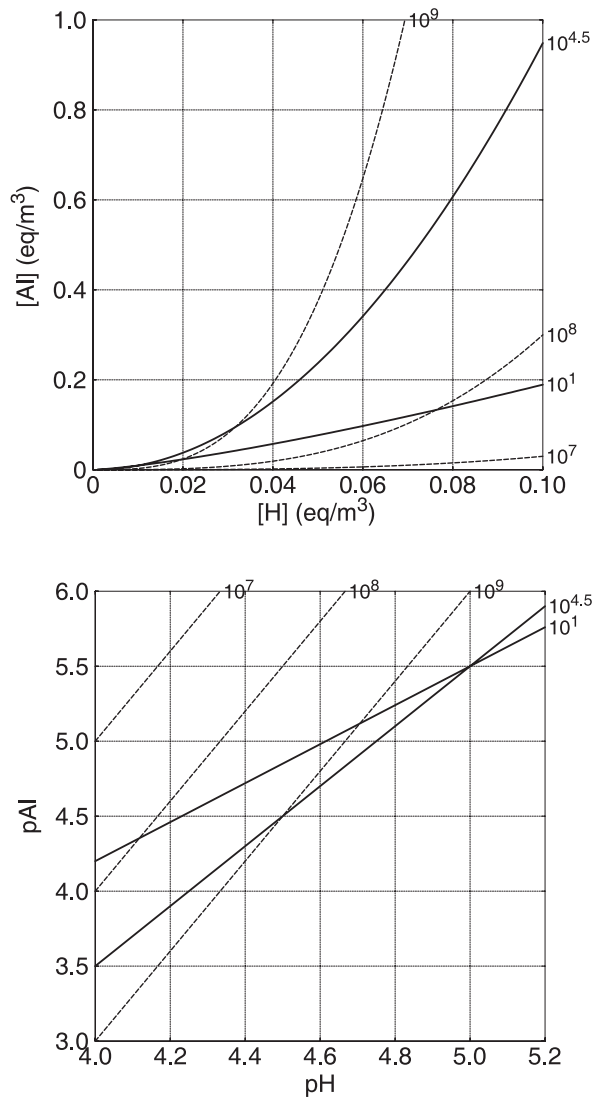


Figure 5.3: Relationships between H and Al concentration in eq/m^3 (left) and in their logarithmic forms (right) for $K_{Al_{ox}} = 10^1$, $a=2$ and $K_{Al_{ox}} = 10^{4.5}$, $a=1.3$ (solid lines) as well as three gibbsite equilibria ($a=3$) with $K_{gibb} = 10^7$, 10^8 and 10^9 (dashed lines). Note: $[H] = 0.1 \text{ eq/m}^3$ corresponds to $pH = 4$.

and oxidation of below-ground organic matter. Respiratory production of CO_2 is highly temperature dependant (e.g. Witkamp 1966); based on soil temperature and mean growing season soil p_{CO_2} , Gunn and Trudgill (1982) derived the following relationship:

$$(5.44) \quad \log_{10} p_{CO_2} = -2.38 + 0.031 \cdot T$$

where T is the (soil) temperature ($^{\circ}C$). Brook et al. (1983) present a similar regression equation based on data for 19 regions of the world. In the absence of data or such relationships, the following default ranges

have been suggested (Bouten et al., 1987): 5–10 times atmospheric pressure in the organic layer, 5–15 times atmospheric pressure in the E-layer, 15–20 times atmospheric pressure in the B-layer and 15–30 times atmospheric pressure in the upper C-layer.

For $p_{CO_2} = 0.0055 \text{ atm}$ (about 15 times the partial CO_2 pressure in air) and $Q = 0.3 \text{ m/yr}$, eq. 5.43 yields a bicarbonate leaching of almost 100 eq/ha/yr at $pH = 5.5$, not always a negligible quantity. Therefore, it would make sense to include the bicarbonate leaching into the SMB model. Not only would this make critical loads more compatible with

steady-state solutions of dynamic models, but it is also the only way to allow the ANC leaching to obtain positive values! Eq. 5.27 would then read:

$$(5.45) \quad \begin{aligned} ANC_{le} &= -H_{le} - Al_{le} + HCO_{3,le} \\ &= Q \cdot ([HCO_3] - [H] - [Al]) \end{aligned}$$

All chemical criteria could be used, since bicarbonate leaching could always be calculated from H_{le} via eq. 5.43. We illustrate the influence of bicarbonates on the ANC leaching by re-drawing Figure 5.2, but now using eq. 5.45 to calculate the ANC leaching. Comparing Figure 5.4 with Figure 5.2 illustrates that, depending on the parameters of the site, bicarbonate leaching can make a significant contribution to the overall ANC leaching.

(c) Including the dissociation of organic acids:

The charge balance (eq. 5.9) and the definition of ANC leaching in eq. 5.10 also include the leaching of organic anions ($RCOO_{le}$). This has been neglected in the SMB model for (at least) two reasons: (i) to keep the SMB model simple, and/or (ii) assuming that the

negatively charged organic anion concentration balances the positively charged organic Al-complexes. However, this does not hold for a wide range of pH values, and at sites with high concentrations of organic matter the contribution of organic anions to ANC leaching can be considerable.

Since it is difficult to characterise (let alone model) the heterogeneous mixture of naturally occurring organic solutes, so-called 'analogue models' are used. The simplest assumes that only monovalent organic anions are produced by the dissociation of dissolved organic carbon:

(5.46)

$$[RCOO^-] = \frac{m \cdot DOC \cdot K_1}{K_1 + [H]}$$

where DOC is the concentration of dissolved organic carbon (in $molC/m^3$), m is the concentration of functional groups (the 'charge density', in $mol/molC$) and K_1 the dissociation constant. Both DOC and m are site-specific quantities. While DOC estimates are often available, data for m are less easy to obtain. For example, Santore et al. (1995) report val-

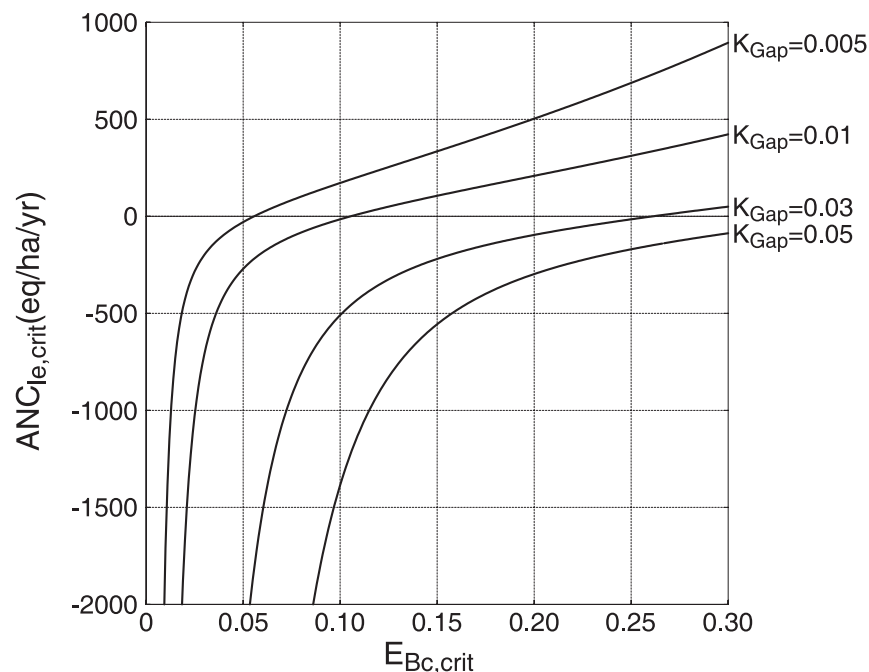


Figure 5.4: Critical ANC leaching (for $Q=1$ m/yr) including bicarbonate leaching as a function of the critical base saturation, $E_{Bc,crit}$, using the same parameters as in Figure 5.2.

ues of m between 0.014 for topsoil samples and 0.044 mol/molC for a B-horizon in the Hubbard Brook experimental forest in New Hampshire.

Since a single value of K_1 does not always model the dissociation of organic acids satisfactorily, Oliver et al. (1983) have derived an empirical relationship between K_1 and pH:

$$(5.47) \quad pK_1 = -\log_{10} K_1 = a + b \cdot pH - c \cdot (pH)^2$$

with $a=0.96$, $b=0.90$ and $c=0.039$ (and $m=0.120$ mol/molC). Note that eq. 5.47 gives K_1 in mol/L. In Figure 5.5 the fraction of $m \cdot DOC$ dissociated as a function of pH is shown for the Oliver model and a mono-protic acid with a 'widely-used' value of $pK_1=4.5$.

Figure 5.5 shows that, depending on the amount of DOC , the contribution of organic anions to the ANC leaching, even at fairly low pH , can be considerable.

Other models for the dissociation of organic acids have been suggested and are in use in dynamic models, such as di- and tri-protic analogue models (see, e.g., Driscoll et al. 1994), or more detailed models of the speciation of humic substances, such as the

WHAM model (Tipping 1994). Any model could be used for the calculation of critical loads as long as the dissociation depends only on $[H]$, so that a critical leaching of organic anions can be derived from $[H]_{crit}$ (or $[Al]_{crit}$).

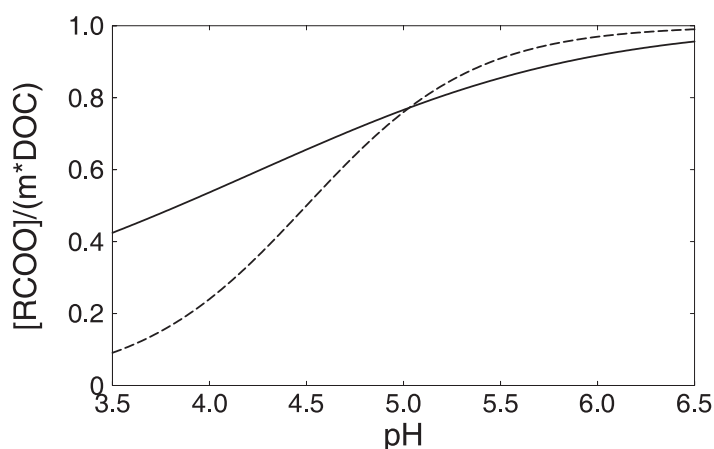


Figure 5.5: Fraction of organic acids ($m \cdot DOC$) dissociated as a function of pH for the Oliver model (solid line) and the mono-protic model (eq.5.46) with $pK_1=4.5$ (dashed line).

5.4 Critical Loads for Aquatic Ecosystems

The purpose of critical loads for aquatic ecosystems is to estimate the maximum deposition(s) below which 'significant harmful effects' on biological species do not occur. Similar to terrestrial ecosystems, the links between water chemistry and biological impacts cannot be modelled adequately at present (see also Wright and Lie 2002) as such, water quality criteria are generally used to derive critical loads for aquatic ecosystems.

In this Section we deal only with the modelling of critical loads of acidity for aquatic ecosystems. The models are restricted to freshwater systems, since models for marine ecosystems do not seem to exist. Empirical critical loads of nitrogen for fresh waters, as well as coastal and marine habitats, can be found in Section 5.2.

The following description is largely based on the review by Henriksen and Posch (2001), but amended with new or additional information where available. Three models for calculating critical loads of acidifying *N* and *S* deposition are described. Models of critical loads for surface waters also include their terrestrial catchment to a greater or lesser extent. Therefore, it is advised to consult Section 5.3 for some of the terminology and variables used in the context of critical loads for soils.

5.4.1 The Steady-State Water Chemistry (SSWC) model

5.4.1.1 Model derivation

The critical load of a lake or stream can be derived from present day water chemistry using the SSWC model, if weighted annual mean values, or estimates thereof, are available. It assumes that all sulphate (SO_4^{2-} in runoff originates from sea salt spray and anthropogenic deposition (no adsorption or retention). The model uses Acid Neutralising Capacity (*ANC*) as the variable linking water

chemistry to sensitive indicator organisms in freshwaters.

In the SSWC model (Sverdrup et al. 1990, Henriksen et al. 1992, Henriksen and Posch 2001) a critical load of acidity, $CL(A)$, is calculated from the principle that the acid load should not exceed the non-marine, non-anthropogenic base cation input and sources and sinks in the catchment minus a buffer to protect selected biota from being damaged, i.e.:

(5.48)

$$CL(A) = BC_{dep}^* + BC_w - Bc_u - ANC_{limit}$$

where BC_{dep}^* ($BC = Ca + Mg + K + Na$) is the sea-salt corrected (with *Cl* as a tracer; see Chapter 2) non-anthropogenic deposition of base cations, BC_w is the average weathering flux, Bc_u ($Bc = Ca + Mg + K$) is the net long-term average uptake of base cations in the biomass (i.e., the annual average removal of base cations due to harvesting), and ANC_{limit} the lowest *ANC*-flux that does not damage the selected biota. Since the average flux of base cations weathered in a catchment and reaching the lake is difficult to measure or to compute from available information, a critical load equation that uses water quality data alone has been derived.

In pre-acidification times the non-marine flux of base cations from the lake, BC_0^* , is given by (all parameters are expressed as annual fluxes, e.g. in $eq/m^2/yr$):

(5.49)

$$BC_0^* = BC_{dep}^* + BC_w - Bc_u$$

Thus we have for the critical load from eq. 5.48:

(5.50)

$$CL(A) = BC_0^* - ANC_{limit} \\ = Q \cdot ([BC^*]_0 - [ANC]_{limit})$$

where the second identity expresses the critical load in terms of the catchment runoff Q (in m/yr) and concentrations ($[X] = X/Q$).

To estimate the pre-acidification flux of base cations we start with the present flux of base cations, BC_t^* , given by:

(5.51)

$$BC_t^* = BC_{dep}^* + BC_w - BC_u + BC_{exc}$$

where BC_{exc} is the release of base cations due to ion-exchange processes. Assuming that deposition, weathering rate and net uptake have not changed over time, we obtain BC_{exc} by subtracting eq. 5.49 from eq. 5.51:

(5.52)

$$BC_{exc} = BC_t^* - BC_0^*$$

This present-day excess production of base cations in the catchment is related to the long-term changes in inputs of non-marine acid anions by the so-called F -factor (see below):

(5.53)

$$BC_{exc} = F \cdot (\Delta SO_4^* + \Delta NO_3)$$

For the pre-acidification base cation flux we thus get from eq. 5.52 ($\Delta X = X_t - X_0$):

(5.54)

$$BC_0^* = BC_t^* - F \cdot (SO_{4,t}^* - SO_{4,0}^* + NO_{3,t} - NO_{3,0})$$

The pre-acidification nitrate concentration, $NO_{3,0}$, is generally assumed zero.

5.4.1.2 The F -factor

According to eqs. 5.52 and 5.53, and using concentrations instead of fluxes, the F -factor is defined as the ratio of change in non-marine base cation concentrations due to changes in strong acid anion concentrations (Henriksen 1984, Brakke et al. 1990):

(5.55)

$$F = \frac{[BC^*]_t - [BC^*]_0}{[SO_4^*]_t - [SO_4^*]_0 + [NO_3]_t - [NO_3]_0}$$

where the subscripts t and 0 refer to present and pre-acidification concentrations, respectively. If $F=1$, all incoming protons are neutralised in the catchment (only soil acidification), at $F=0$ none of the incoming protons are neutralised in the catchment (only water acidification). The F -factor was estimated empirically to be in the range 0.2–0.4, based on the analysis of historical data from Norway, Sweden, U.S.A. and Canada (Henriksen 1984). Brakke et al. (1990) later suggested that the F -factor should be a function of the base cation concentration:

(5.56)

$$F = \sin\left(\frac{\pi}{2} [BC^*]_t / [S]\right)$$

where $[S]$ is the base cation concentration at which $F=1$; and for $[BC^*]_t > [S]$ F is set to 1. For Norway $[S]$ has been set to 400 meq/m³ (ca. 8 mgCa/L) (Brakke et al. 1990).

In eq. 5.56 the present base cation concentration is used for practical reasons. To render the F -factor independent from the present base cation concentration (and to simplify the functional form), Posch et al. (1993) suggested the following relationship between F and the pre-acidification base cation concentration $[BC^*]_0$:

(5.57)

$$F = 1 - \exp\left(-[BC^*]_0 / [B]\right)$$

where $[B]$ is a scaling concentration estimated to be 131 meq/m³ from paleolimnological data from Finland (Posch et al. 1993). Inserting this expression into eq. 5.55 gives a non-linear equation for $[BC^*]_0$ which has to be solved by an iterative procedure. The two expressions for the F -factor give similar results when used to calculate critical loads for surface waters in Norway (see Henriksen and Posch 2001).

The use of the F -factor, defined as a function of the base cation concentration (Henriksen 1984) was originally derived from Norwegian lake data. In Norway the range of runoff is wide (0.3–5 m/yr), with an average of about

1 m/yr. In other Nordic countries, such as Sweden and Finland, runoff is low compared to most of Norway. The weathering rate of a catchment is largely dependent on the bedrock and overburden. Thus, catchments with similar bedrock and overburden characteristics should have similar weathering rates. If one catchment has a high runoff, e.g., 2 m/yr, and another one has a low runoff, e.g., 0.3 m/yr, their base cation fluxes will be similar, but their concentrations will differ considerably. Thus, in the F -factor (eq. 5.56) the BC -flux should be used instead of the concentration (Henriksen and Posch 2001):

$$(5.58) \quad F = \sin\left(\frac{\pi}{2} Q \cdot [BC^*]_t / S\right)$$

where S is the base cation flux at which $F=1$. For Norway, S has been estimated at 400 meq/m²/yr. Again, if $Q \cdot [BC^*]_t > S$, F is set to 1. Similarly, fluxes could be introduced for the formulation in eq. 5.57.

5.4.1.3 The non-anthropogenic sulphate concentration

The pre-acidification sulphate concentration in lakes, $[SO_4^*]_0$, is assumed to consist of a constant atmospheric contribution and a geologic contribution proportional to the concentration of base cations (Brakke et al. 1989):

$$(5.59) \quad [SO_4^*]_0 = a + b \cdot [BC^*]_t$$

The coefficients in this equation, estimated

for different areas and by different authors, are summarised in Table 5.16.

Details on the procedures and data sources for estimating these coefficients can be found in the references given. In Henriksen and Posch (2001) it is shown that the exceeded area for Norwegian lakes (in 1994) is influenced very little by the choice of coefficients for calculating non-anthropogenic sulphate. Similar results have been reported for Irish lakes (Aherne and Curtis 2003).

Larssen and Høgåsen (2003) suggested that the atmospheric contribution in eq. 5.59 be derived from background S deposition, as estimated by atmospheric transport models:

$$(5.60) \quad [SO_4^*]_0 = S_{dep,0} / Q + b \cdot [BC^*]_t$$

For southern Norway, $S_{dep,0}$ is about 50 mgS/m²/yr from the EMEP long-range transport model, i.e., about 3 meq/m²/yr. With Q varying between 0.5 and 1 m/yr this results in an atmospheric contribution to $[SO_4^*]_0$ of about 3–6 meq/m³.

The SSWC model has been developed for and is particularly applicable to dilute oligotrophic waters located on granitic and gneissic bedrock with thin overburden, such as large parts of Fennoscandia, Scotland, Canada and Ireland. In such areas, surface waters are generally more sensitive to acid inputs than soils. The model assumes that all sulphate in runoff originates from deposition alone, except for a small geologic contribution. In areas where the geological conditions lead to more alkaline waters, the SSWC model has to be modified, since significant

Table 5.16: Constants to estimate the non-anthropogenic sulphate concentration with eq. 5.59, derived from empirical data (N is the number of samples and r is the correlation coefficient).

a (meq/m ³)	b	N	r	Reference
15	0.16	143	0.38	Lakes, Norway (Brakke et al 1989)
8	0.17	289	0.78	Lakes, Norway (Henriksen and Posch 2001)
5	0.05	n.g.	n.g.	Groundwater, Sweden (Wilander 1994)
14	0.10	61	0.29	Lakes, Finland (Posch et al. 1993)
19	0.08	251	0.66	Lakes, N. Norway+Finland+Sweden (Posch et al. 1997)
9.5	0.08	60	0.66	Lakes, Ireland (Aherne et al. 2002)

amounts of sulphate from geological sources can be present in the runoff water. A modification for this kind of conditions has been developed for Slovakia (Závodský et al. 1995).

5.4.1.4 The *ANC*-limit

Lien et al. (1996) analysed the status of fish and invertebrate populations in the context of surface water acidification and loss of *ANC* in Norwegian lakes and streams. The data for fish came from populations in 1095 lakes, mostly from the regional lake survey carried out in 1986 (Henriksen et al. 1988, 1989). The critical level of *ANC* varied among fish species, with Atlantic salmon being the most sensitive, followed by brown trout. They concluded that Atlantic salmon appeared to be a good indicator of acidification of rivers, and trout seemed to be a useful indicator for acidification of lakes. Based on an evaluation of fish and invertebrate populations, a critical lower limit of $[ANC]=20 \text{ meq/m}^3$ was suggested as the tolerance level for Norwegian surface waters (Lien et al. 1996; see Figure 5.6). This limit has been widely used (Kola, northern Russia: Moiseenko 1994; southern central Alps: Boggero et al. 1998; China: Duan et al. 2000); however, it has been set to zero in the United Kingdom (CLAG 1995) and to 40 meq/m^3 in south-central Ontario, Canada (Henriksen et al. 2002).

Lydersen et al. (2004) argued that the *ANC*-limit should be corrected with the amount of

organic acids present in the lake. And they showed that the fit between observed fish status and *ANC* can be (slightly) improved, if an 'organic acid adjusted' *ANC*, $[ANC]_{\text{aaa}}$, is used (instead of the 'standard' *ANC*). They define this quantity as:

(5.61)

$$[ANC]_{\text{aaa}} = [ANC] - \frac{1}{3} \cdot m \cdot \text{TOC}$$

where $m \cdot \text{TOC}$ is the total organic carbon expressed in meq/m^3 (m being the charge density). Such a correction leads to a lower *ANC*-limit, i.e., higher critical loads.

Figure 5.6 indicates that in the *ANC* range 0–50 meq/m^3 there is a decreasing probability from about 50 to 0% of damage to fish populations. The lakes studied receive very low to very high (for Norway) levels of deposition, thus including a wide range of affected lakes. This implies that for a given *ANC*-value lakes of varying sensitivity exist, receiving varying amounts of deposition. This could reflect that fish have responded to the same *ANC* differently in different lakes, indicating that a catchment-dependent *ANC*-limit would be more appropriate than a fixed value for all lakes. In other words, every lake has its own characteristic *ANC*-limit (in the range shown in Figure 5.6). Less sensitive lakes, i.e., lakes with higher critical loads, should have a higher *ANC*-limit, since less sensitive ecosystems will have a higher biological variety/diversity and thus require a higher *ANC*-limit to keep that diversity intact.

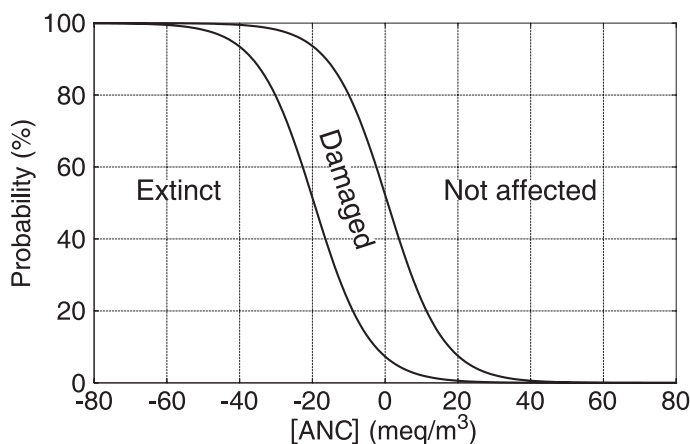


Figure 5.6: Relationship between the *ANC* concentration in lake water and the probability for damage and extinction of fish (brown trout) populations in lakes, derived from Norwegian data (after Lien et al. 1996).

The simplest functional relationship with this feature is a linear relationship between $[ANC]_{limit}$ and the critical load CL :

$$(5.62) \quad [ANC]_{limit} = k \cdot CL$$

This gives the following implicit equation for the critical load (see eq. 5.50):

$$(5.63) \quad CL = Q \cdot ([BC^*]_0 - k \cdot CL)$$

which yields after re-arranging for CL :

$$(5.64) \quad CL = Q \cdot [BC^*]_0 / (1 + k \cdot Q)$$

and thus from eq. 5.62:

$$(5.65) \quad [ANC]_{limit} = k \cdot Q \cdot [BC^*]_0 / (1 + k \cdot Q)$$

This is a special case of a more general expression derived earlier using somewhat different arguments (Henriksen et al. 1995). As for the constant $[ANC]_{limit}$ used earlier, the proportionality constant k should be derived from data. If we assume that for $CL=0$, the $[ANC]_{limit}=0$; if we further assume that for a critical load of 200 meq/m²/yr the ANC-limit should not exceed 50 meq/m³, as has been assumed in Sweden, we arrive at a k -value of 50/200 = 0.25 yr/m. In addition, for CL -values above 200 meq/m²/yr we set the $[ANC]_{limit}$ to the constant value of 50 meq/m³. The value of k is derived from experience in the Nordic countries and, as such, reflects the geology, deposition history and biological diversity (fish species) of that region. For different regions other k -values may be more appropriate.

5.4.2 The empirical diatom model

The empirical diatom model is an alternative approach to the SSWC model and is devel-

oped from paleolimnological data (Battarbee et al. 1995). Diatom assemblages in cores from acidified lakes usually show that prior to acidification the diatom flora, and therefore water chemistry, changed little over time. The point of acidification is indicated by a shift towards a more acidophilous diatom flora. Diatoms are amongst the most sensitive indicators of acidification in freshwater ecosystems, hence it can be argued that the point of change in the diatom record indicates the time at which the critical load for the site was exceeded.

The acidification status (as defined by diatom analyses) of 41 sites in the United Kingdom (UK) was compared to site sensitivity (defined by lake-water calcium concentrations) and current deposition loading. The optimal separation of acidified and non-acidified sites is given by a $[Ca]:S_{dep}$ ratio of 94:1 (Battarbee et al. 1995), acidified sites having a ratio less than 94:1. This critical ratio, determined by logistic regression, can be used to define critical sulphur loads for any site, including streams. Critical load values are calculated from pre-acidification calcium concentrations using the F -factor (Brakke et al. 1990). For example, the critical sulphur load for a lake with a $[Ca]_0$ -value of 40 meq/m³ is approximately 0.43 keq/ha/yr.

The diatom model has been adapted to provide critical loads, and critical load exceedances, for total acidity (sulphur and nitrogen). Exceedance values for total acidity require a measure of the fraction of deposited nitrogen leached to the surface waters. This is calculated from the differences between the ratios of sulphate/nitrate in the water and in the deposition at the site. In this way the fraction of the nitrogen deposition contributing to acidification, f_N , is added to the value of sulphur deposition to provide a total 'effective' acid deposition:

$$(5.66) \quad f_N = \frac{S_{dep}^*}{N_{dep}} \left/ \frac{[SO_4^*]}{[NO_3^*]} \right.$$

This model assumes equilibrium between sulphur deposition and sulphate in water, and only applies to sites with no additional catchment nitrogen inputs. The diatom model has been re-calibrated for total acidity loads by substituting total effective acid deposition for sulphur deposition. The resulting critical ratio is 89:1, slightly lower than when considering sulphur alone. The basic equation for the critical load of total acidity in the empirical diatom model is therefore as follows:

$$(5.67) \quad CL(A) = \frac{[Ca^*]_0}{89}$$

where $CL(A)$ is in keq/ha/yr and $[Ca^*]_0$ in meq/m³. The pre-acidification Ca -concentration is calculated as:

$$(5.68) \quad [Ca^*]_0 = [Ca^*]_t - F_{Ca} \cdot ([SO_4^*]_t - [SO_4^*]_0 + [NO_3]_t - [NO_3]_0)$$

with

$$(5.69) \quad F_{Ca} = \sin\left(\frac{\pi}{2} \frac{[Ca^*]_t}{[S_{Ca}]}\right)$$

and $[S_{Ca}]$ is the Ca -concentration at which $F_{Ca}=1$. It can vary between 200 and 400 meq/m³, depending on location. In the UK critical loads mapping exercise a value of $[S_{Ca}]=400$ meq/m³ has been used, and in waters with $[Ca^*]_t > [S_{Ca}]$, F_{Ca} was set to 1. The pre-acidification nitrate concentration, $[NO_3]_0$, is assumed zero. The pre-acidification sea-salt corrected sulphate concentration, $[SO_4^*]_0$, is estimated according to eq. 5.59 (Brakke et al.1989).

The diatom model has been calibrated using sites and data from the UK. However, a major advantage of the approach is that predictions for any lake can be validated by analysing diatoms in a sediment core. In this way the applicability of the model to sites outside the UK can be tested.

5.4.3 The First-order Acidity Balance (FAB) model

The First-order Acidity Balance (FAB) model for calculating critical loads of sulphur (S) and nitrogen (N) for a lake takes into account sources and sinks within the lake and its terrestrial catchment. The original version of the FAB model has been developed and applied to Finland, Norway and Sweden in Henriksen et al. (1993) and further described in Posch et al. (1997). A modified version was first reported in Hindar et al. (2000) and is described in Henriksen and Posch (2001). The FAB model is designed to be equivalent to the Simple Mass Balance model for a catchment, and it largely follows its derivation (see Section 5.3), the main difference being that the leaching of ANC is modelled according to the SSWC model (see section 5.4.1).

5.4.3.1 Model derivation

The lake and its catchment are assumed small enough to be properly characterised by average soil and lake water properties. With A we denote the total catchment area (lake + terrestrial catchment), A_l is the lake area, A_f the forested area and A_g the area covered with grass/heath land. We have $A_l + A_f + A_g \leq A$, and a non-zero difference represents a land area on which no transformations of the deposited ions take place ('bare rock').

Starting point for the derivation of the FAB model is the charge balance ('acidity balance') in the lake water running off the catchment:

$$(5.70) \quad S_{runoff} + N_{runoff} = BC_{runoff}^* - ANC_{runoff}$$

where BC^* stands for the sum of (non-marine) base cations and ANC is the acid neutralising capacity. In the above equation we assume that the quantities are total amounts per time (e.g. eq/yr). In order to derive critical loads we have to link the ions in the lake water to their depositions, taking into account their sources and sinks

in the terrestrial catchment and in the lake.

For $X = S, N$ and BC the mass balance in the lake is given by:

$$(5.71) \quad X_{runoff} = X_{in} - X_{ret}, \quad X = S, N, BC$$

where X_{in} is the total amount of ion X entering the lake and X_{ret} the amount of X retained in the lake. The in-lake retention of S and N is assumed to be proportional to the input of the respective ion into the lake:

$$(5.72) \quad X_{ret} = \rho_X \cdot X_{in}, \quad X = S, N$$

where $0 \leq \rho_X \leq 1$ is a dimensionless retention factor. Thus the mass balances for the lake become:

$$(5.73) \quad X_{runoff} = (1 - \rho_X) \cdot X_{in}, \quad X = S, N$$

The total amount of sulphur entering the lake is given by:

$$(5.74) \quad S_{in} = A \cdot S_{dep}$$

where S_{dep} is the total deposition of S per unit area. Immobilisation, reduction and uptake of sulphate in the terrestrial catchment are assumed negligible, and sulphate ad/desorption is not considered since we model steady-state processes only. eq. 5.74 states that all sulphur deposited onto the catchment enters the lake, and no sources or sinks are considered in the terrestrial catchment.

In the case of nitrogen we assume that immobilisation and denitrification occur both in forest and grass/heath land soils, whereas net uptake occurs in forests only (equalling the annual average amount of N removed by harvesting); the deposition onto the remaining area (lake + 'bare rocks') enters the lake unchanged. Thus the amount of N entering

the lake is:

$$(5.75) \quad \begin{aligned} N_{in} &= (A - A_f - A_g) \cdot N_{dep} \\ &+ A_f \cdot (N_{dep} - N_i - N_u - N_{de})_+ \\ &+ A_g \cdot (N_{dep} - N_i - N_{de})_+ \end{aligned}$$

where N_{dep} is the total N deposition, N_i is the long-term net immobilisation of N (which may include other long-term steady-state sources and sinks; see Chapter 5.3), N_{de} is N lost by denitrification, and N_u the net growth uptake of N , all per unit area. The symbol $(x)_+$ or x_+ is a short-hand notation for $\max\{x, 0\}$, i.e., $x_+ = x$ for $x > 0$ and $x_+ = 0$ for $x \leq 0$. The effects of nutrient cycling are ignored and the leaching of ammonium is considered negligible, implying its complete uptake and/or nitrification in the terrestrial catchment.

While immobilisation and net growth uptake are assumed independent of the N deposition, denitrification is modelled as fraction of the available N :

$$(5.76) \quad N_{de} = \begin{cases} f_{de} \cdot (N_{dep} - N_i - N_u)_+ & \text{on } A_f \\ f_{de} \cdot (N_{dep} - N_i)_+ & \text{on } A_g \end{cases}$$

where $0 \leq f_{de} < 1$ is the (soil-dependent) denitrification fraction. The above equation is based on the assumption that denitrification is a slower process than immobilisation and growth uptake. Inserting eq. 5.76 into eq. 5.75 one obtains:

$$(5.77) \quad \begin{aligned} N_{in} &= (A - A_f - A_g) \cdot N_{dep} \\ &+ A_f \cdot (1 - f_{de}) \cdot (N_{dep} - N_i - N_u)_+ \\ &+ A_g \cdot (1 - f_{de}) \cdot (N_{dep} - N_i)_+ \end{aligned}$$

If sufficient data for quantifying the sources and sinks of base cations in the catchment, such as deposition, weathering and uptake,

are available, the runoff of base cations (BC^*_{runoff}) could be described in the same way as S and N . This would be in analogy to the derivation of the SMB model for (forest) soils. Alternatively, water quality data can be used to quantify the runoff of base cations and ANC , as is done in the SSWC model (see section 5.4.1).

To arrive at an equation for critical loads, a link has to be established between a chemical variable and effects on aquatic biota. The most commonly used criterion is the so-called ANC -limit (see above), i.e. a minimum concentration of ANC derived to avoid 'harmful effects' on fish: $ANC_{runoff,crit} = A \cdot Q \cdot [ANC]_{limit}$

Defining $L_{crit} = (BC^*_{runoff} - ANC_{runoff,crit})/A$, inserting eq. 5.74 and 5.77 into eq. 5.73 and eq. 5.70 and dividing by A yields the following equation to be fulfilled by critical depositions (loads) of S and N :

$$(5.78) \quad (1 - \rho_S) \cdot S_{dep} + (1 - \rho_N) \cdot \{(1 - f - g) \cdot N_{dep}\}$$

where we have defined:

$$(5.79) \quad f = A_f / A, \quad g = A_g / A \\ \Rightarrow 1 - f - g \geq r \quad \text{with} \quad r = A_l / A$$

Eq. 5.78 defines a function in the (N_{dep}, S_{dep}) -plane, the so-called critical load function (see Figure 5.7), and in the following we will look at this function in more detail. The general form of the critical load function is:

$$(5.80) \quad a_S \cdot S_{dep} + a_N \cdot N_{dep} = L_N + L_{crit}$$

with

$$(5.81) \quad a_S = 1 - \rho_S, \quad a_N = (1 - \rho_N) \cdot b_N, \\ L_N = (1 - \rho_N) \cdot M_N$$

The quantity M_N and the dimensionless coefficient b_N depend on N_{dep} :

(a) $N_{dep} \leq N_i$: In this case $(N_{dep} - N_i)_+ = 0$ and $(N_{dep} - N_i - N_u)_+ = 0$, which means that all N falling onto forests and grassland is immobilised and only the N deposition falling directly onto the lake and 'bare rocks' contributes to the leaching of N :

$$(5.82) \quad b_N = b_1 = 1 - f - g, \quad M_N = M_1 = 0$$

(b) $N_i < N_{dep} \leq N_i + N_u$: In this case $(N_{dep} - N_i)_+ = N_{dep} - N_i$, but $(N_{dep} - N_i - N_u)_+ = 0$, meaning that all N deposition falling onto forests is immobilised or taken up, but N falling onto the other areas is (partially) leached:

$$(5.83) \quad b_N = b_2 = 1 - f - g \cdot f_{de}, \\ M_N = M_2 = (1 - f_{de}) \cdot g \cdot N_i$$

(c) $N_{dep} > N_i + N_u$: Some N deposition is leached from all areas:

$$(5.84) \quad b_N = b_3 = 1 - (f + g) \cdot f_{de}, \\ M_N = M_3 = (1 - f_{de}) \cdot [(f + g) \cdot N_i + f \cdot N_u]$$

The maximum critical load of sulphur is obtained by setting $N_{dep} = 0$ in eq. 5.78:

$$(5.85) \quad CL_{max}(S) = L_{crit} / a_S$$

Setting $S_{dep} = 0$ and considering the three different cases for N_{dep} , gives the following expression for the maximum critical load for nitrogen:

$$(5.86) \quad CL_{max}(N) = \min \left\{ (L_{crit} / (1 - \rho_N) + M_i) / b_i, \right. \\ \left. i = 1, 2, 3 \right\}$$

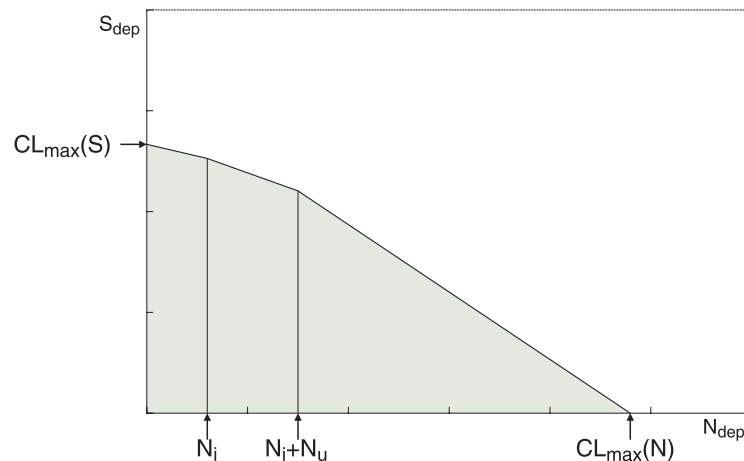


Figure 5.7: Piece-wise linear critical load function of S and acidifying N for a lake as defined by catchment properties. Note the difference with the critical load function for soils (see Figure 5.1). The grey area below the CL function denotes deposition pairs resulting in an ANC leaching greater than $Q[ANC]_{limit}$ (non-exceedance of critical loads; see Chapter 7).

5.4.3.2 Systems of lakes

The above derivation of the FAB model is for (small) headwater lakes only. Critical loads are generally calculated for such lakes, since lakes with (many) upstream lakes tend to have larger catchments, and several (implicit) assumptions of the FAB model, e.g. uniform depositions, will be violated. Nevertheless, in some areas systems of lakes can be found on a small scale, and therefore a model for such systems is desirable.

When computing the critical load of acidity with the SSWC model (which uses annual average lake water chemistry) for a lake receiving runoff from upstream lakes, one implicitly computes *the critical load for that lake including all its upstream lakes*, since water samples taken from (the outlet of) the lowest lake is a mixture of the water of that lake and all its upstream lakes. Consequently, when applying the FAB model to such a lake, one has to be aware that one also computes the critical load for the whole system of lakes and thus must take into account the catchment and lake characteristics of all lakes in the system. To do this in a more explicit way, two methods for computing the critical load of a system of lakes have been developed (Hindar et al. 2000). Both require the same input data, but they differ in the complexity of the calculations

involved. The formulae will not be derived here, and the interested reader is referred to the literature (see also Hindar et al. 2001), where also the differences between the methods are demonstrated, using data from lake systems in the Killarney Provincial Park in Ontario, Canada. An application to lakes in the Muskoka river catchment (Ontario, Canada) can be found in Aherne et al. (2004).

5.4.4 Input data

In addition to the data required for the SSWC and diatom model (runoff and concentrations of major ions in the lake runoff water), the FAB model needs also information on (a) the area of lake, catchment and different land cover classes, (b) terrestrial nitrogen sinks, and (c) parameters for in-lake retention of N and S .

Runoff:

The runoff Q is the amount of water leaving the catchment at the lake outlet, expressed in m/yr. It is derived from measurements or can be calculated as the difference between precipitation and actual evapotranspiration, averaged over the catchment area. A long-term climatic mean annual value should be taken. Sources for data and models for evapotranspiration can be found in Section 5.3.

Ion concentrations:

In addition to runoff, the concentrations of major ions in the runoff water, i.e. sulphate, nitrate and base cations, are needed to calculate SSWC critical loads, and these come from the analysis of representative water samples.

The critical load for a site should be calculated with yearly flow-weighted average chemistry and yearly average runoff. Since such values are not available for a large number of lakes, critical loads are mostly calculated on the basis of a single sample considered representative of yearly flow-weighted averages. A sample collected shortly after the fall circulation of a lake is generally assumed to fulfil this purpose. To check this claim, Henriksen and Posch (2001) compared critical load values calculated from yearly flow-weighted average concentrations with critical loads calculated from a single fall value for sites for which long-term data series are available. Results for seven Norwegian catchments show that the single fall value is fairly representative for the annual average chemistry. Similarly, results from eight Canadian catchments show that a single spring sample is fairly representative of the annual average chemistry (Henriksen and Dillon 2001).

Lake and catchment characteristics:

The area parameters A , A_l , A_f and A_g , which are needed in the FAB model, can generally be derived from (digital or paper) maps.

Terrestrial N sinks:

The uptake of N can be computed from the annual average amount of N in the harvested biomass. If there is no removal of trees from the catchment, $N_u=0$.

N_i is the long-term annual immobilisation (accumulation) rate of N in the catchment soil. Note that at present immobilisation may be substantially higher due to elevated N deposition.

The denitrification fraction f_{de} depends on the soil type and its moisture status. In earlier FAB applications it has been estimated from the fraction of peat-lands, f_{peat} in the catchment by $f_{de}=0.1+0.7 \cdot f_{peat}$

(Posch et al. 1997).

For more details on these parameters see Section 5.3.

In-lake retention of N and S :

Concerning in-lake processes, the retention factor for nitrogen r_N (see eq. 5.72) is modelled by a kinetic equation (Kelly et al. 1987):

(5.87)

$$\rho_N = \frac{s_N}{s_N + z/\tau} = \frac{s_N}{s_N + Q/r}$$

where z is the mean lake depth, t is the lake's residence time, r is the lake:catchment ratio ($=A_l/A$) and s_N is the net mass transfer coefficient. There is a lack of observational data for the mass transfer coefficients, especially from European catchments, but Dillon and Molot (1990) give a range of 2–8 m/yr for s_N . Values for Canadian and Norwegian catchments are given in Kaste and Dillon (2003).

An equation analogous eq. 5.87 for r_S with a mass transfer coefficient s_S is used to model the in-lake retention of sulphur. Baker and Brezonik (1988) give a range of 0.2–0.8 m/yr for s_S .

5.5 Critical Loads of cadmium, lead and mercury

5.5.1 General methodological aspects of mapping critical loads of heavy metals

5.5.1.1 Calculation of different types of critical loads

The method to calculate critical loads of heavy metals is based on the balance of all relevant metal fluxes in and out of a considered ecosystem in a steady state situation. In order to keep the approach compatible with the simple mass balance approach used for nitrogen and acidity, the internal metal cycling within an ecosystem is ignored, such that calculations can be kept as simple as possible. In consequence the critical load of a metal can be calculated from the sum of tolerable outputs from the considered system in terms of net metal uptake and metal leaching.

The assumption of steady state signifies that the concentration in the system does not change in time because the amount of heavy metal entering the system is equal to the amount that leaves the system. The validity of this assumption depends on the magnitude of the time scales of the various input and output processes. If e.g. a metal sorbs very strongly to the soil, it may take a long time (up to hundreds of years), before a steady state is reached. This has to be kept in mind when comparing a present load with the critical load (De Vries and Bakker 1998). Critical loads of cadmium (*Cd*), lead (*Pb*) and mercury (*Hg*) can be calculated in dependence on the receptors and the metal of concern. Critical limits of these heavy metals addressing either ecotoxicological ecosystem effects or human health effects are derived with specific approaches. Critical loads on the basis of such limits should be calculated separately for aquatic and terrestrial ecosystems. In consequence four types of critical loads can be derived for each metal, an overview is provided in Table 5.17, which is however not a complete review of

possible effects of these metals.

Indicators of effects on ecosystems listed in Table 5.17 are mainly ecotoxicological effects. Secondary poisoning through the food chain has also been studied (De Vries et al. 2003). These effects give partly more stringent critical limits, however their modelling includes more uncertainties and is therefore not considered in this manual.

Critical loads for terrestrial ecosystems addressing human health effects can be calculated, either in view of not violating food quality criteria in crops or in view of ground water protection (keeping quality criteria for drinking water of WHO 2004). An appropriate indicator for critical load calculations addressing human health effects via food intake is the *Cd* content in wheat. Keeping a conservative food quality criterion for wheat, as described in Section 5.5.2.1, protects at the same time against effects on human health via other food and fodder crops (including also the quality of animal products, since the pathway of *Cd* to wheat leads to the lowest critical *Cd* content in soils according to De Vries et al. (2003). Such critical load calculations are in principle also possible for lead, and for other food and fodder crops, if the soil-plant transfer can be described with sufficient accuracy and can be done in addition on a voluntary basis.

Among terrestrial ecosystems, critical loads of *Cd* and *Pb* are to be calculated from the viewpoint of ecotoxicology for areas covered by non-agricultural land (forests, semi-natural vegetation) or agricultural land (arable land and grassland). Organic forest (top)soils are considered as the only critical receptor with respect to atmospheric *Hg* pollution, based on knowledge on effects on microbial processes and invertebrates (Meili et al. 2003a). The critical exposure of terrestrial ecosystems to atmospheric *Hg* pollution can be calculated in much the same way as for *Pb* and *Cd* by a simple mass balance, as discussed in Section 5.5.3.2.

Table 5.17: Four types of critical loads of *Pb*, *Cd*, *Hg*, related receptors and indicators

Receptor ecosystem	Critical loads related to	Metals of concern	Land cover types to be considered	Indicator addressed by the critical limit
1) Terrestrial ^{*)}	a) Human health effects	<i>Cd</i> , <i>Pb</i> , <i>Hg</i> <i>Cd</i> , <i>Pb</i> , <i>Hg</i> <i>Cd</i> , <i>Pb</i> , <i>Hg</i>	Arable land <i>Grassland</i> Arable land, grassland, non-agricultural land	Metal content in food/ <i>fodder</i> crops <i>Metal content in gras, animal products (cow, sheep)</i> Total metal concentration in soil water below the rooting zone (aiming at ground water protection)
	b) Ecosystem functioning	<i>Pb</i> , <i>Cd</i> , <i>Hg</i>	Non-agricultural land, arable land, grassland, Forests only	Free metal ion concentration in soil solution in view of effects on soil micro-organisms, plants and invertebrates Total metal concentration in humus layer in view of effects on soil micro-organisms and invertebrates
2) Aquatic	a) Human health effects	<i>Hg</i>	Freshwaters	Metal concentration in fish
	b) Ecosystem functioning	<i>Pb</i> , <i>Cd</i> , <i>Hg</i>	Freshwaters	Total metal concentration in freshwaters in view of effects on algae, crustacea, worms, fish, top predators

^{*)} In italics: these calculations can be done in addition on a voluntary basis. To perform such calculations, more information on the derivation of critical limits based on critical metal contents in food/fodder crops and in animal products is given in Annex 2 and 3, respectively, of the background document (De Vries et al. 2004b).

For aquatic ecosystems the critical limits of *Pb* and *Cd* are related to ecotoxicological effects, while human health effects by this pathway are less relevant and therefore not considered here. Critical limits of *Hg* refer to both human health effects (*Hg* concentration in fish and other animals that serve as a food source to humans) and ecotoxicological effects, since microbiota and higher wildlife itself may also be affected.

Although it might be useful to calculate and map each of the different types of critical loads and the critical *Hg* level in precipitation separately for comparison purposes, the aim is ultimately to provide maps for at most four critical loads per metal (or *Hg* level, respectively) related to:

- Ecotoxicological effects for all terrestrial ecosystems.

- Human health effects for all terrestrial ecosystems.
- Ecotoxicological effects for all aquatic ecosystems.
- Human health effects for all aquatic ecosystems.

If different indicators within each category (map) have been considered (e.g. *Cd* in wheat and *Cd* in soil drainage water in view of ground water protection for human health), the final map should indicate the minimum critical *Cd* load for both effects to human health. The reason for providing different critical loads for different types of ecosystems is because the critical load for terrestrial ecosystems does not automatically protect aquatic ecosystems, receiving much or most of their metal load by drainage from the surrounding soils, and vice versa.

A critical load indicates only the sensitivity of an ecosystem against the anthropogenic input of the metal of interest. It implies a potential risk at sites where the critical load is exceeded. In agricultural ecosystems, the exceedance of critical loads of heavy metals is not only determined by atmospheric inputs (being generally the only source in non-agricultural ecosystems), but by total inputs, including fertilizer and animal manure inputs.

5.5.1.2 Limitations in sites that allow critical load calculations

Critical load calculations can not be carried out for sites with:

- Negative water balances, since there is no leaching but a seepage influx of water, leading to accumulation of salts and very high *pH*; such regions do, however, hardly occur in Europe.
- Soils with reducing conditions (e.g. wetlands), because the transfer functions do not apply for such soils. In the topsoil, to which the critical load calculations apply, such situations do, however, hardly occur apart from water logged soils where the simplified critical load calculation can not be applied anyhow because of a deviating hydrology.

Weathering inputs of metals are neglected due to i) low relevance of such inputs and ii) high uncertainties of respective calculation methods. It is, however, recommended to use estimates of weathering rate to identify sites with a high geogenic metal input, where natural weathering may already exceed the critical load. This should be considered, when critical limits and loads exceedances are to be interpreted. For methods to calculate weathering rates, see De Vries and Bakker (1998) and Hettelingh et al. (2002). More information on how sites with high geogenic contents of metals can be identified are described in Farret et al. (2003). The most important information is summarised in Annex 6 of the background document (De Vries et al. 2004b).

5.5.1.3 Definitions and symbols/abbreviations used in critical load calculations

General definitions of critical loads, critical levels and exceedances, and others can be found in the related chapters of the Modelling and Mapping Manual. The following definitions refer specifically to the application in the context of critical loads of heavy metals.

Definitions

The receptor is a living element of the environment that is subject to an adverse effect. It can be a species of interest including human beings, or several species considered representative of a larger group (e.g. plants, soil invertebrates, fish, algae, etc), or the whole ecosystem (typically the subject of interest in the critical load approach).

The critical limit is a concentration threshold within the ecosystem, based on adverse effects, i.e. it is a short expression of "effect-based critical limit". Below this critical limit significant harmful effects on human health or specified sensitive elements of the environment do not occur, according to present knowledge. To avoid confusion, limits that are not based on effects should not be called "critical limits".

The critical load is the highest total metal input rate (deposition, fertilisers, other anthropogenic sources) below which harmful effects on human health as well as on ecosystem structure and function will not occur at the site of interest in a long-term perspective, according to present knowledge. The critical load is derived from the critical limit through a biogeochemical flux model, assuming steady-state for the fluxes as well as chemical equilibrium (which is a theoretical situation in an undetermined future, consistent with concepts of sustainability). For this purpose the critical limit has to be transformed to a critical total concentration of the metal in the output fluxes by water (leaching from the soil or outflow from an aquatic ecosystem).

5 Mapping Critical Loads

An overview of used symbols and abbreviations is given below (Table 5.18).

Some general abbreviations:

M	= a flux of a metal M	f	= a fraction
$[M]$	= a content (in soil, plants, other biota) or a concentration (in a liquid) of a metal M	c	= a factor for conversion of units, not explained in the table
$[M]_{\dots(crit)}$	= a critical content (in soil, plants, other biota) or a critical concen-	sdw	= in soil drainage water
		sw	= in surface water

Table 5.18: Symbols and abbreviations used in the calculation of critical loads of heavy metals

Symbols	Short explanation	Basic units
CL (M)	critical load of a metal (M)	[g ha ⁻¹ a ⁻¹]
M_u	metal net uptake in harvestable parts of plants (under critical load conditions)	[g ha ⁻¹ a ⁻¹]
M_w	weathering rate of a metal	[g ha ⁻¹ a ⁻¹]
$M_{le(crit)}$	critical leaching flux of a metal with drainage water	[g ha ⁻¹ a ⁻¹]
$M_{ret(crit)}$	net retention of a metal in the aquatic system at critical load	[g ha ⁻¹ a ⁻¹]
$M_{lo(crit)}$	critical lateral outflow of a metal from the aquatic system	[g ha ⁻¹ a ⁻¹]
Y_{ha}	yield of harvestable biomass	[kg dw ha ⁻¹ a ⁻¹]
Z_b	depth of the upper, biologically active soil layer (topsoil)	[m]
z	depth of the rooting zone	[m]
$Q_{le,zb}$	leaching flux of water from the topsoil	[m a ⁻¹]
$Q_{le,z}$	leaching flux of water from the rooting zone	[m a ⁻¹]
Q_{lo}	lateral outflow flux of water from the aquatic system	[m a ⁻¹]
$P/E_i/E_s/E_t$	symbols for water fluxes (water balance equation): Precipitation/ interception evaporation / soil evaporation / (plant) transpiration, resp.	[m a ⁻¹]
$f_{Mu,zb}$	fraction of metal net uptake within the topsoil	[-]
$f_{Mu,z}$	fraction of metal net uptake within the entire rooting zone	[-]
$f_{Et,zb}$	fraction of water uptake by plants within the topsoil	[-]
f_f	fractionation or transfer factor describing the Hg contamination of organic matter in solution relative to that in solids	[-]
A_l	lake area	[ha]
A_c	catchment area	[ha]
TF_{HgSite}	site-specific transfer function linking fish Hg to atmospheric Hg	[l kg ⁻¹ fw]
TF_{HgRun}	transfer function referring to the transfer of atmospheric Hg to fish flesh via runoff in a reference watershed at steady state	[l kg ⁻¹ fw]
TF_{HgBio}	organism-specific transfer function addressing Hg partitioning within food webs	[-]
$[M]_{ha}$	metal content in harvestable biomass	[mg kg ⁻¹ dw]
$[M]_{re}$	reactive content of a metal in soil	[mg kg ⁻¹]
$[M]_{AR}, [M]_{HF}, [M]_{EDTA}, [M]_{HNO_3}$	concentration of a metal in soil, extracted with Aqua Regia, HF, EDTA, HNO ₃ respectively.	[mg kg ⁻¹]
$[M]_{dis,sdw}$ or $[M]_{dis,sw}$	total dissolved metal concentration in soil drainage water, or in surface water, respectively	[mg m ⁻³]
$[M]_{tot,sdw}$ or $[M]_{tot,sw}$	total metal concentration in soil drainage water, or in surface water, including both dissolved metal and metal in suspended particles	[mg m ⁻³]

[M] _{free,sdw} or [M] _{free,sw}	concentration of free metal ion in soil drainage water, or in surface water, respectively	[mg m ⁻³]
[M] _{DIC,sdw}	concentration of metal bound to dissolved inorganic complexes in soil drainage water	[mg m ⁻³]
[M] _{DOM,sdw}	concentration of metal bound to dissolved organic matter in soil drainage water	[mg m ⁻³]
[M] _{SPM,sdw} or [M] _{SPM,sw}	concentration of metal bound to suspended particulate matter in soil drainage water, or in surface water, respectively	[mg kg ⁻¹]
[Hg] _{OM}	concentration of Hg, normalised for [OM] _s	[mg (kg OM) ⁻¹]
[Hg] _{Pike}	Hg concentration in the flesh of 1-kg pike	[mg kg ⁻¹ fw]
[Hg] _{Bio}	Hg concentration in biota, e.g. fish flesh	[mg kg ⁻¹ fw]
[Hg] _{Prec}	Hg concentration in precipitation	[ng l ⁻¹]
[clay]	clay content of the soil	[(kg clay) kg ⁻¹] or [%]
[OM] _s	organic matter content of the soil	[(kg OM) kg ⁻¹] or [%]
[DOM] _{sdw} or [DOC] _{sdw}	concentration of dissolved organic matter, or dissolved organic carbon, respectively, in soil drainage water	[g m ⁻³] or [mg l ⁻¹]
[TOC] _{sw}	concentration of total organic carbon in surface water	[g m ⁻³] or [mg l ⁻¹]
[TP] _{sw}	concentration of total phosphorus in surface water	[µg l ⁻¹] or [mg l ⁻¹]
[SPM] _{sdw} or [SPM] _{sw}	concentration of suspended particulate matter in soil drainage water, or in surface water, respectively	(kg m ⁻³)
pH _{sdw} or pH _{sw}	pH value in soil drainage water, or in surface water	[-]

5.5.1.4 Stand-still approach versus calculation of critical limit exceedance

The harmonised methodological basis for a first preliminary calculation and mapping of critical loads of *Cd* and *Pb* related to ecotoxicological effects (Hettelingh et al. 2002), was based on a guidance document (De Vries et al. 2002). In this document a stand-still approach, which aims at avoiding any (further) accumulation of heavy metals in the soil, was also included as an alternative to the effect-based approach. This method is, however, not included in this manual since it implies the continued addition of metals on historically polluted soils with high leaching rates. The current leaching may then already imply significant effects, both on terrestrial as well as aquatic ecosystems receiving the drainage water from the surrounding soils, and is thus not per se acceptable in the long term. Furthermore, it does lead to critical load exceedance at soils which strongly adsorb heavy metals, whereas the effect does occur through the soil solution.

Instead, it is suggested to calculate critical concentrations of metals in the soil, the soil drainage water or the surface water based on the critical limits and compare these to the present soil or water metal concentrations to assess the critical limit exceedance in the present situation. This implies that one has to map the present metal concentrations in the country (expressed as total or reactive soil contents, total dissolved concentrations or even free ion concentrations). Such a comparison can be seen as an intermediate step for dynamic models for heavy metals. If the present soil metal content exceeds the critical concentration (limit), the metal input has to be less than the critical load to reach the critical concentration at a defined time period. In the reverse case, the metal input can be larger than the critical load for a defined time period not exceeding during that period the critical concentration. However, only keeping the critical load will not lead to exceedance of the critical limit in the long run. More information on how to calculate the critical concentration is given in the background document.

5.5.2 Terrestrial ecosystems

5.5.2.1 Simple steady-state mass balance model and related input data

5.5.2.1.1 Steady-state mass balance model

The method to calculate critical loads of heavy metals for terrestrial ecosystems is focusing in particular on the upper soil layer. The critical load of a metal can be calculated as the sum of tolerable outputs from this considered soil layer by harvest and leaching minus the natural inputs by weathering release (De Vries and Bakker, 1998). Because weathering causes only a minor flux of metals in topsoils, while uncertainties of such calculations are very high, the model was further simplified by assuming that weathering is negligible within the topsoil outside ore-rich areas. As mentioned in the introduction of this chapter, the calculation of weathering rates is recommended to identify areas, where the natural input exceeds tolerable outputs; and such sites can be excluded from the database, subject to decision by the National Focal Centres.

The described approach implies that the critical load equals the net uptake by forest growth or agricultural products plus an acceptable metal leaching rate:

$$(5.88) \quad CL(M) = M_u + M_{le(crit)}$$

where:

$CL(M)$ = critical load of a heavy metal
 M ($g \text{ ha}^{-1} \text{ a}^{-1}$)

M_u = metal net uptake in harvestable parts of plants under critical load conditions ($g \text{ ha}^{-1} \text{ a}^{-1}$)

$M_{le(crit)}$ = critical leaching flux of heavy metal M from the considered soil layer ($g \text{ ha}^{-1} \text{ a}^{-1}$), whereby only the vertical drainage flux is considered

The notation has been related to the critical load equations for acidity and nutrient nitrogen: M stands for flux of a heavy metal and

can be substituted by the chemical symbol of the individual metal (Cd , Pb , Hg) under consideration. The critical metal leaching $M_{le(crit)}$ refers to the total vertical leaching rate, including dissolved, colloidal and particulate (metal) species in the drainage water. For a critical load, the critical metal leaching is based on a critical (toxic) metal concentration in soil or the (free ion or total) metal concentration in soil water.

In mass balance models for Hg , re-emission (volatilization) of deposited Hg occurs as an additional flux. This flux can, however, be ignored when calculating critical loads of Hg , because this re-emission is treated as part of the atmospheric net deposition in the modelling by EMEP MSC-E (Ryaboshapko et al. 1999, Ilyin et al. 2001). Therefore, in order to avoid double consideration in the calculation of critical load exceedances, it should be excluded from the critical loads model.

Appropriate and consistent calculation of critical loads for terrestrial ecosystems requires a consistent definition of the topsoil compartment and its boundaries. The depth can be variable. Relevant boundaries have been derived considering on one hand the expected probability of adverse impacts on the main target groups of organisms (plants, soil invertebrates, soil microbiota), or ground water quality, and on the other hand the occurrence and location of relevant metal fluxes within the soil profile:

-For Pb and Cd it is assumed that ecotoxicological effects as well as the main proportion of uptake by plants occur in (from) the organic layer (O horizon) and the humus rich (top)soil horizons (A_h , A_p). Therefore the depth of the biological active topsoil (z_b) should be considered for arable land, grassland, and forests as far as the critical load calculations are addressing ecotoxicological effects, or the protection of food/fodder quality, respectively. For forest soils covered by an organic layer, the critical loads for both the organic layer, and the upper mineral horizon should be calculated separately. In these

cases the most sensitive of both layers should be presented in the critical loads map. For all terrestrial ecosystems the maximum depth of the topsoil (z_b) to be considered is the lower boundary of the uppermost mineral horizon (in most soil classification systems called the A-horizon).

Default values of z_b are:

for forests: 0.1 m (O and/or A_h horizon)
 grassland: 0.1 m (A_h horizon)
 arable: 0.3 m (A_p horizon, plough layer)

-Regarding Hg , the critical receptor in terrestrial ecosystems is the organic topsoil (mor or humus layer) of forest soils (O -horizon excluding litter, which is sometimes divided into L, F and H horizons), where microbial processes are suspected to be affected. For calculating the critical load of Hg in forests, the topsoil is therefore defined as the humus layer, excluding underlying mineral soil layers.

Note, that for calculations of critical loads with respect to protection of groundwater quality the entire soil column has to be included. However, it is preliminarily not planned within the critical loads work to model the whole pathway of the metal flux with drainage water, considering the binding capacity of layers between rooting zone and upper groundwater. Therefore, for simplification the critical leaching of metals from the viewpoint of ground water protection is calculated by multiplying the drainage water flux below the rooting zone (soil depth = z) with the critical limit for drinking water (see 5.5.2.2.2).

5.5.2.1.2 Heavy metal removal from the topsoil by net growth and harvest of plants

For critical load calculations, the removal of heavy metals refers to a future steady-state level where critical limits in the ecosystem compartments are just reached (critical loads conditions). The calculation of a critical removal of metals on the basis of a

critical concentration for soil solution is hardly practicable since for many metals there are no clear relationships between concentrations in soil solution (or even free metal ions) and the content of the metals in harvestable part of the plants. Reasons are amongst others the plant specific exclusion of metals from root uptake or accumulation in specific tissues (detoxification). An exception is the transfer of Cd from soil to wheat grains, used to calculate critical loads related to food quality criteria (see 5.5.2.2.1).

Therefore a simplified approach is proposed to describe the tolerable removal of heavy metals by biomass net uptake. The average yield (or growth increment) of harvestable biomass is multiplied with the heavy metal content in harvestable plant parts and with a factor to account for the fraction of metal uptake from the relevant soil layer relative to the uptake from the total rooting zone (eq. 5.89):

$$(5.89) \quad M_u = f_{Mu} \cdot Y_{ha} \cdot [M]_{ha}$$

where:

M_u = metal net uptake in harvestable parts of plants under critical load conditions ($g \text{ ha}^{-1} \text{ a}^{-1}$) (see eq. 5.88),
 f_{Mu} = fraction of metal net uptake within the considered soil depth (z_b or z), accounting also for metal uptake due to deposition on vegetation surfaces (-); in calculations of critical loads to protect groundwater, $f_{Mu} = 1$, otherwise f_{Mu} is a value between 0 and 1
 Y_{ha} = yield of harvestable biomass (dry weight) ($kg \text{ ha}^{-1} \text{ a}^{-1}$),
 $[M]_{ha}$ = metal content of the harvestable parts of the plants ($g \text{ kg}^{-1} \text{ dw}$), including also metals deposited on vegetation surfaces (when the metal content is given in $mg \text{ kg}^{-1} \text{ dw}$, the value has to be divided by 1000).

As a default approximation, a root uptake factor ($f_{Mu,zb}$) of 1 can be used for all ecosys-

5 Mapping Critical Loads

tem types, assuming that most uptake of nutrients and pollutants occurs in the top soil. In forests values around 80 % have been reported for uptake from the humus layer alone (based on lead isotopes in Scots pine, Bindler et al. 2003). Thus, for calculations referring to the humus layer, $f_{Mu,zb}$ may be 0.8, but, if the top of the underlying mineral soil is included in the calculations, $f_{Mu,zb}$ is likely to approach 1, also in forests. If $f_{Mu,zb}$ is 1, the uptake from the upper horizon is equal to that of the entire rooting depth (assumed to be limited to the depth where 90 % of the root biomass is distributed). This implies that there is no difference in the uptake calculation of critical loads related to ecotoxicological effects and in view of ground water protection. More detailed values of $f_{Mu,zb}$ may be used, if information is available.

Data on yields for forests can in principle be obtained from the database of critical loads of acidity and nutrient nitrogen. Data on yields in agro-ecosystems are available from related statistics of the countries. The spatial pattern can be derived using information on land use as well as on soil quality and climate.

To get data on metal contents in harvestable biomass, studies from relatively unpolluted areas should be used. Median values (or averages) of metals contents in plants from such databases do in general not exceed quality criteria for food and fodder crops or phyto-toxic contents, respectively. Related fluxes can therefore be considered as tolerable. As far as appropriate national data are not available, the default values or ranges in Table 5.19 can be used for orientation, e.g. the average of a range.

If critical loads related to quality criteria of food or fodder are to be calculated, the critical concentrations in the harvestable plant parts should be multiplied with the yields (net crop removal), considering for arable land the coverage by the crops of interest, in order to calculate the tolerable output of metals by biomass harvest.

If contents are available for different harvested parts of the plants (e.g. stem and bark), a mass weighted mean should be used. Beware that only the net uptake is calculated. For instance, for agricultural land the amount of metals in stalks or the leaves of beets remaining on the field should not be considered. The removal of heavy metals in

Table 5.19: Ranges of mean values (averages, medians) of contents of *Pb*, *Cd*, and *Hg* in biomass for various species (harvestable parts)

L and use	Species	Metal content in harvestable plant parts, $[M]_{ha}$ [$mg\ kg^{-1}\ dw$]		
		Pb	Cd	Hg
Grassland	mixed grassland species	1.0 - 3.0	0.05 - 0.25	0.01-0.1
Arable land	wheat (grains)	0.1	0.08	0.01
	other cereals (grains)	0.1 - 0.3	0.02 - 0.06	0.01
	potato	0.73	0.23	0.02
	sugar beet	1.0	0.25	0.02
	maize	3.8	0.2	0.04
Coniferous forest	spruce, pine, fir, douglas,			
	Central Europe	0.5- 10	0.1 - 0.5	0.01-0.05*
	Northern Europe	0.1/0.2**	0.02/0.04**	0.004/0.008**
Deciduous forest	oak, beech, birch, poplar	0.5 - 10	0.05 - 0.5	

*) *Hg* in spruce stems \approx 10-20% of needle content (Schuetze and Nagel 1998)

***) Northern Sweden (Alriksson et al. 2002 and unpublished), for spruce stems without/with bark
Other data sources: De Vries and Bakker (1998), Nagel et al. (2000), Jacobsen et al. (2002)

this case is the product of the yield of grains/beets and the mean contents in these parts of the plants. For forest ecosystems, only the net increment should be considered, but not the uptake into needles, leaves, etc., which also remain in the system.

In ecosystems with appreciable precipitation surplus or with a very limited growth, the removal of metals by harvest may often be very low compared to metal losses by leaching at critical load. In these cases the uptake calculation do not deserve high efforts. Instead, it is better to concentrate on sophisticated calculations for the critical leaching rate.

5.5.2.1.3 Critical leaching of heavy metals from the soil

The critical leaching flux of a heavy metal from the regarded soil layer can be calculated according to the equation:

$$(5.90) \quad M_{le(crit)} = c_{le} \cdot Q_{le} \cdot [M]_{tot,sdw(crit)}$$

where:

- $M_{le(crit)}$ = critical leaching flux of heavy metal from the topsoil ($g \text{ ha}^{-1} \text{ a}^{-1}$) (see eq. 5.88)
- Q_{le} = flux of drainage water leaching from the regarded soil layer defined as above ($m \text{ a}^{-1}$).
- $[M]_{tot,sdw(crit)}$ = critical total concentration of heavy metal in the soil drainage water ($mg \text{ m}^{-3}$) (derived from critical limits, see 5.5.2.2)
- c_{le} = $10 \text{ g mg}^{-1} \text{ m}^2 \text{ ha}^{-1}$, factor for appropriate conversion of flux units

Flux of drainage water

In order to calculate critical loads in view of groundwater protection the data on precipitation surplus from the database on critical loads of acidity and nutrient nitrogen can be used. Deviating from this, the proportion of transpiration removing water from the upper

horizons (O , and/or A_h, A_p) has to be accounted for by using a scaling (root uptake) factor when critical loads with respect to ecotoxicological effects or to food/fodder quality are addressed.

The drainage water flux leaching from the topsoil at the bottom of the topsoil ($Q_{le,zb}$) at steady state can be calculated according to:

$$(5.91a) \quad Q_{le,zb} = P - E_i - E_s - f_{Et,zb} \cdot E_t$$

where:

- P = precipitation ($m \text{ a}^{-1}$)
- E_i = interception evaporation ($m \text{ a}^{-1}$)
- E_s = actual soil evaporation within the topsoil defined as above ($m \text{ a}^{-1}$)
- E_t = actual plant transpiration ($m \text{ a}^{-1}$)
- $f_{Et,zb}$ = scaling or root uptake factor, fraction of water uptake within the topsoil (-)

This approach is based on the assumption that soil evaporation (E_s) only takes place down to the depth z_b . Interception evaporation can be calculated as a function of the precipitation (De Vries et al. 1991). For sites without detailed water balance data, the annual mean water percolation Q_{le} can also be determined by the long-term mean annual temperature (mainly determining the potential evapotranspiration, E_{pot}) and precipitation (mainly influencing the actual evapotranspiration, E_{act}) according to:

$$(5.91b) \quad Q_{le,zb} = P_m - f_{E,zb} \cdot (P_m^{-2} + (e^{(0.063 \cdot T_m)} \cdot E_{m,pot})^{-2})^{-1/2}$$

where:

- P_m = annual mean precipitation ($m \text{ a}^{-1}$, data adjusted for common measurement bias)
- T_m = annual mean air temperature ($^{\circ}C$)
- $E_{m,pot}$ = annual mean potential evapotranspiration in humid areas at $T_m = 0^{\circ}C$; $E_{m,pot} \approx 0.35 \text{ m a}^{-1}$ in forests, possibly less in other terrestrial ecosystems.

$f_{E,zb}$ = Fraction of total annual mean evapotranspiration above z_b (-);
 $f_{E,zb} \approx 0.8$ for the organic top soil layer of forests.

For forested areas, this relationship is supported by data not only on river runoff but also on soil percolation (e.g. based on Michalzik et al. 2001), which together suggest that about 80% or more of the total evapotranspiration takes place above or within the organic top soil layer. Thus, the mean water flux from the organic top layer (Q) can easily be estimated from annual means of precipitation (P) and air temperature (T), which are two traditional climate normals available in traditional climate maps (see Background document):

In European forest regions, $Q_{le,zb}$ is typically $0.1-0.6 \text{ m a}^{-1}$, but may reach $>2 \text{ m a}^{-1}$ in coastal mountain regions. The standard parameter uncertainty is on the order of $\pm 0.1 \text{ m a}^{-1}$ (i.e. about $\pm 30\%$) at the landscape scale. Depending on climate, Q_{le} can account for 10 to 90% of P in temperate-boreal forests, but is usually close to half. In very dry regions the percentage of Q_{le} in P can become very low. With eq. 5.91b, Q_{le} almost never drops below 0.1 m^{-1} in Europe (considering EMEP-50 km grid square means). For eq. 5.91a, a suggested minimum value is 5 % of the precipitation. This seems a reasonable lower value since there are always periods during the year with downward percolation and a situation of no leaching hardly (or never) occurs on a yearly basis. The use of monthly water balances is not advocated as the effect of all seasonal variations is not included in the critical limits, since these represent annual or long-term means, in line with the critical load approach for acidity.

Critical total dissolved or total concentrations of heavy metals in soil drainage water

Information on the derivation of critical total dissolved concentrations of heavy metals in soil drainage water, $[M]_{dis,sw(crit)}$, either directly, through transfer functions (plant -

soil solution) or through $[M]_{free,sw(crit)}$ is given in the next section (5.5.2.2), with background information on used approaches in the Annexes 1-3. The critical total dissolved metal concentrations related to ecotoxicological effects in soils require some specific considerations. These critical total metal concentrations in soil solution are determined as the sum of the critical concentration of the free metal ion M^{2+} , $[M]_{free,sw(crit)}$, and the metals bound to dissolved inorganic complexes $[M]_{DIC,sw}$ such as MOH^+ , HCO_3^+ , MCl^+ , and to dissolved organic matter, $[M]_{DOM,sw}$, according to:

(5.92)

$$[M]_{dis,sw(crit)} = [M]_{free,sw(crit)} + [M]_{DIC,sw} + [M]_{DOM,sw} \cdot [DOM]_{sw}$$

where:

$[M]_{dis,sw(crit)}$ = critical total dissolved metal concentration in soil drainage water (mg m^{-3})

$[M]_{free,sw(crit)}$ = critical free metal ion concentration in soil drainage water (mg m^{-3})

$[M]_{DIC,sw}$ = concentration of metal bound to dissolved inorganic complexes in soil drainage water (mg m^{-3})

$[M]_{DOM,sw}$ = concentration of metal bound to dissolved organic matter in soil drainage water (mg.kg^{-1})

$[DOM]_{sw}$ = concentration of dissolved organic matter in soil drainage water (kg m^{-3})

Geochemical equilibrium partitioning of the heavy metal between the different fractions is assumed. Further, the water draining from the soil also contains metals bound to suspended particulate matter, $[M]_{SPM,sw}$, according to:

(5.93)

$$[M]_{tot,sw(crit)} = [M]_{dis,sw(crit)} + [M]_{SPM,sw} \cdot [SPM]_{sw}$$

where:

$[M]_{tot,sw(crit)}$ = critical total metal concentration in soil drainage water (mg m^{-3})

$[SPM]_{sdw}$ = concentration of suspended particulate matter in soil drainage water ($kg\ m^{-3}$)

In the calculations, we suggest the particulate fraction to be neglected to get comparable values of critical concentrations for the different effects pathways (see Section 5.5.2.2.3). In this manual, the description of methods is adapted to the use of the critical total dissolved metal concentrations, $[M]_{dis,sdw(crit)}$, being equal to total metal concentrations in soil solution, implicitly assuming that the concentration of metals bound to suspended particulate matter is negligible ($[SPM]_{sdw} = 0$), i.e. $[M]_{dis,sdw(crit)}$ equals $[M]_{tot,sdw(crit)}$.

5.5.2.2 Critical dissolved metal concentrations derived from critical limits in terrestrial ecosystems

Critical total concentrations of the heavy metals *Cd*, *Pb* and *Hg* in the soil solution, $[M]_{dis,sdw(crit)}$, depend on the target to be protected. These values have to be derived from critical limits (see Table 5.17):

- Critical metal contents in plants (*Cd*, *Pb*, *Hg*) in view of human health or animal health effects through intake of plant products.
- Critical metal concentrations in ground water (*Cd*, *Pb*, *Hg*) in view of human health effects through intake of drinking water.
- Critical concentrations of free metal ions in soil solution (*Cd*, *Pb*) in view of ecotoxicological effects on soil micro-organisms, plants and invertebrates.
- Critical metal contents in the soil (*Hg*) in view of ecotoxicological effects on soil micro-organisms and invertebrates in the forest humus layer.

The critical total dissolved concentration of a heavy metal in the soil drainage water ($[M]_{dis,sdw(crit)}$) includes both the free metal ions and the metals bound to dissolved inorganic and organic complexes (eq. 5.92).

The derivation of the critical total dissolved concentrations to be applied in eq. 5.90 is explained below.

5.5.2.2.1 Critical dissolved concentrations of *Cd*, *Pb* and *Hg* in view of critical plant metal contents

Starting from the idea to derive critical total *Cd*, *Pb* and *Hg* concentrations in soil solution related to human health effects on the basis of critical limits for plant metal contents (food quality criteria) for food crops on arable land De Vries et al. (2003) provided an overview on selected soil-plant relationships of *Cd*, *Pb* and *Hg*. It shows that only for *Cd* significant relationships (R^2 of ≥ 0.5) are available.

Cadmium

Starting with a critical *Cd* content in plant one may derive a critical dissolved metal concentration by a plant – soil solution relationship. Such a relationship was derived by applying a regression of *Cd* contents in wheat in the Netherlands to calculated soil solution concentrations, that were derived by using measured total soil contents and soil properties and application of a transfer function, relating total concentrations in solution to the soil metal content (Romkens et al. 2004). By applying such a function, regression relationships were derived for *Cd* in plant (wheat grains) as a function of *Cd* in soil solution and vice versa as described in Table 5.20. The best estimate of a critical *Cd* concentration might be the mean of both estimates.

The EU regulation (EG) No.466/2001 uses a limit for *Cd* of $0.2\ mg\ kg^{-1}$ fresh weight in wheat grains. This limit was derived with the principle “As Low As Reasonably Achievable” (ALARA) and is therefore not based on effects. There are however many indications that from the viewpoint of protection of human health, the critical limit of $0.1\ mg\ kg^{-1}$ fresh weight, which was used in the EU before 2001, is more appropriate (for these arguments see De Vries et al. 2003, De Vries et al. 2004a,b). Table 5.20 provides

Table 5.20. Values for the intercept (int) and the parameter a in the regression relationships relating Cd in plant (wheat grains) as a function of Cd in soil solution and vice versa. The table also gives the percentage variation explained (R^2), the standard error of the result (se) and the resulting critical total dissolved Cd concentration when applying a critical Cd content in wheat of 0.1 mg kg^{-1} fresh weight (0.12 mg kg^{-1} dry weight) and in brackets the value when applying the limit of 0.2 mg kg^{-1} fresh weight (EG No 466/2001).

Relationship	Intercept	a	R^2	se	$\log[\text{Cd}]_{\text{dis, sdw(crit)}} [\text{mmol.l}^{-1}]$	$[\text{Cd}]_{\text{dis, sdw(crit)}} [\text{mg.m}^{-3}]$
$\text{Cd}_{\text{Plant}} - \text{Cd}_{\text{solution}}^1$	1.05	0.39	0.62	0.25	-5.03 (-4.26)	1.05 (6.16)
$\text{Cd}_{\text{solution}} - \text{Cd}_{\text{plant}}^2$	-3.82	1.57	0.62	0.50	-5.28 (-4.81)	0.59 (1.75)

$$^1 \log(\text{Cd plant}) = \text{Int} + a * \log(\text{Cd soil solution})$$

$$^2 \log(\text{Cd soil solution}) = \text{Int} + a * \log(\text{Cd plant})$$

the parameters for the transfer functions as well as results based on the critical limit of 0.1 mg kg^{-1} fresh weight (results for the EU limit of 0.2 mg kg^{-1} fresh weight is given in brackets). If the mean of both results of transfer function application is used, the resulting critical total concentration is approximately 0.8 mg m^{-3} (or 4 mg m^{-3}). The most conservative estimate equals approximately 0.6 mg m^{-3} (or 1.75 mg m^{-3}).

A more sophisticated and consistent way would be to

- first derive a critical “pseudo” total soil metal content, by applying soil – plant relationships in the inverse way (derive a critical total soil content from a critical plant content)
- then apply a transfer function relating “pseudo” total metal contents to reactive metal contents (Annex 1, eq. A1.3).
- followed by a transfer function relating the free ion metal activity in solution to the reactive metal content (Annex 1, eq. A1.4 or eq. A1.5).
- followed by a calculation of total concentrations from free metal ion activities with a chemical speciation model (i.e. the W6S-MTC2 model, Section 5.5.2.2.3).

Please note that the current version of W6S-MTC2 is designed to calculate $M_{(\text{sdw})\text{crit}}$ based only on the critical limits relating to ecotoxicological effects and not to food quality.

Lead and mercury

For Pb and Hg in food crops, back calculation to soil content is not possible, because there are no relationships between content of soil and contents in plants for those metals. For Pb and Hg, direct uptake from the atmosphere by plants has to be considered. Methods for such calculations, based on data from De Temmerman and de Witte (2003a,b) are provided in Annex 5 of the background document (De Vries et al. 2004b).

5.5.2.2.2 Critical dissolved concentrations of Cd, Pb and Hg aiming at ground water protection

The critical total Cd, Pb and Hg concentration in soil solution related to human health effects can also be based on quality criteria (critical limits) for drinking water (WHO 2004) for all terrestrial ecosystems (see Table 5.17). In line with the decisions of the Expert Meeting on Critical Limits (2002, in Berlin) the protection of ground water for potential use as drinking water resource should also be addressed in critical load calculations. The Technical Guidance Document for Risk Assessment (<http://ecb.jrc.it>) suggests in chapter 3.1.3 that in the first instance the concentration in soil pore water can be used as an estimate of the concentration in ground water. The WHO guideline includes the following quality criteria for Cd, Pb and Hg in view of drinking water quality:

Pb: 10 mg m^{-3}

Cd: 3 mg m^{-3}

Hg: 1 mg m^{-3}

These values can directly be included as $[M]_{dis, sdw(crit)}$ in the critical load calculation.

5.5.2.2.3 Critical dissolved concentrations of Cd and Pb related to ecotoxicological effects

Critical limits related to the ecotoxicological effects of Cd and Pb are related to impacts on soil micro-organisms, plants and invertebrates for both agricultural land (arable land, grassland) and non-agricultural land (forests, natural non-forested ecosystems; see Table 5.17). The critical concentrations used in this manual are based on the following approach:

- Use of ecotoxicological data (NOEC and LOEC data) for the soil metal content using experiments with information on soil properties (clay and organic matter content and soil pH) as well;
- Calculation of critical free metal ion concentrations (critical limits) in soil solution on the basis of the ecotoxicological soil data (NOECs and LOECs) and soil properties, using transfer functions relating the reactive soil metal content to the free metal ion concentration;
- Calculation of the critical total dissolved metal concentrations $[M]_{dis, sdw(crit)}$ from critical limits for free metal ion concentrations using a chemical speciation model.

Calculation of critical free metal ion concentrations from critical soil reactive metal contents

Soil toxicity data collated and accepted under the terms of current EU Risk Assessment procedures (Draft Risk Assessment Report Cd (July 2003) see <http://ecb.jrc.it>, Voluntary Risk Assessment for Pb), were used. The data covered chronic population-level effects on soil plants, soil-dwelling invertebrates and microbial processes. The toxicity endpoints were quoted mainly in terms of an added metal dose. In using added doses, the assumption is made that the added metal is entirely in reactive forms over the course of the toxicity experiment.

The transfer functions for the calculation of free metal ion concentration from reactive soil metal content, used in the derivation of free ion critical limit functions, are given in Annex 1. Soil properties needed in this function are organic matter and soil solution pH. In the derivation, soil pH values measured by chemical extraction (by H₂O, KCl or CaCl₂) were used to estimate soil solution pH by application of regressions given in Annex 10 of the background document (De Vries et al. 2004b), assuming that the pH in soil solution equals pH_{sdw} . EU Risk Assessment procedures do not require the organic matter content of the soil to be specified for data to be accepted. However, such data were not usable for the calculation of critical free metal ion concentrations from critical soil metal contents, since the used transfer functions do require these data (see Annex 1) and were thus removed from the databases.

The bioavailability of metals does not only depend on the free metal ion concentration but also on the concentration of other cations, particularly H⁺. This was taken into account in deriving critical limits as a function of the pH in soil drainage water (pH_{sdw}). The derived critical limit functions were:

$$(5.94) \quad \log[Cd]_{free, sdw(crit)} = -0.32 \cdot pH_{sdw} - 6.34$$

$$(5.95) \quad \log[Pb]_{free, sdw(crit)} = -0.91 \cdot pH_{sdw} - 3.80$$

More information on the approach and the toxicity data is given in Lofts et al. (2004) and in De Vries et al. (2004a). A summary can be found in the background document (De Vries et al. 2004b).

Calculation of total dissolved metal concentrations from free metal ion concentrations

To calculate critical loads for soils from the critical limit functions, it is necessary to know the total concentration of metal in soil

5 Mapping Critical Loads

drainage water that corresponds to the free ion critical limit. In Annex 2, an overview is given of the calculation procedure using the WHAM model. Results thus obtained with this model for an assumed standard CO_2 pressure of 15 times the atmospheric pressure of 0.3 mbar (4.5 mbar) are given in Tables 5.21 and 5.22. WHAM includes also the fraction of suspended particulate matter, which strictly is not part of the soil solution. The total concentration is therefore related to soil drainage water. When $[SPM]_{sdw} = 0$, the value of $[M]_{tot, sdw(crit)}$ equals that of $[M]_{dis, sdw(crit)}$ (see eq. 5.93). For reasons of consistency with the other approaches (see before), in which the critical value refers to $[M]_{dis, sdw(crit)}$, it is advocated to apply the results with $[SPM]_{sdw} = 0$. Furthermore, there are high uncertainties in the data on SPM in soil solution. Table 5.21 furthermore shows that in most cases, the impact of suspended

particulate matter on the total Cd concentration in soil drainage water (even at a concentration of 50 mg l^{-1}) is small, but for Pb it can be large (Table 5.22).

Use of pH and DOC values to be considered in the calculation of critical metal concentrations

Some parameters in the critical load calculation depend on the status of the soil, in particular the acidification status (pH) and the concentration of DOC (see also the tables 5.21 and 5.22). In the following recommendations are provided, which status of soil conditions should be considered, when $M_{dis, sdw(crit)}$ is derived from critical limits for free metal ion concentrations, as presented in the tables 5.21 and 5.22.

Table 5.21: Look-up table to derive values of the total critical Cd concentrations in soil drainage water $[Cd]_{tot, sdw(crit)}$ at a CO_2 pressure that equals 15 times the CO_2 pressure of the air

OM	SPM	DOC	$[Cd]_{tot, sdw(crit)}$ (mg.m^{-3}), being $[Cd]_{dis, sdw(crit)}$ (mg.m^{-3}) at SPM=0									
			pH	pH	pH	pH	pH	pH	pH	pH	pH	pH
%dw	mg.l^{-1}	mg.l^{-1}	3.5	4.0	4.5	5.0	5.5	6.0	6.5	7.0	7.5	8.0
10	0	0	4.04	2.79	1.92	1.34	0.94	0.68	0.51	0.43	0.47	0.75
10	0	5	4.04	2.80	1.93	1.38	1.04	1.08	0.91	0.66	0.61	0.80
10	0	15	4.04	2.81	1.97	1.47	1.23	1.83	1.68	1.13	0.88	0.91
10	0	50	4.05	2.86	2.12	1.80	1.89	4.08	4.03	2.74	1.85	1.30
10	0	100	4.07	2.94	2.36	2.29	2.80	6.76	6.86	4.94	3.22	1.85
10	50	0	4.06	2.82	1.95	1.38	1.00	0.76	0.61	0.57	0.67	1.02
10	50	5	4.06	2.82	1.96	1.42	1.10	1.16	1.02	0.81	0.80	1.07
10	50	15	4.06	2.84	2.00	1.51	1.29	1.91	1.79	1.28	1.08	1.18
10	50	50	4.07	2.89	2.15	1.85	1.94	4.15	4.14	2.88	2.05	1.57
10	50	100	4.08	2.96	2.39	2.33	2.85	6.84	6.97	5.08	3.42	2.12
50	0	0	3.98	2.74	1.91	1.34	0.94	0.68	0.51	0.43	0.47	0.75
50	0	5	4.02	2.81	2.02	1.52	1.26	1.09	0.91	0.66	0.61	0.80
50	0	15	4.11	2.94	2.24	1.89	1.85	1.86	1.68	1.13	0.88	0.91
50	0	50	4.45	3.48	3.01	3.06	3.69	4.16	4.03	2.74	1.85	1.30
50	0	100	5.06	4.29	4.07	4.59	5.96	6.89	6.86	4.94	3.22	1.85
50	50	0	4.03	2.81	2.00	1.45	1.11	0.90	0.81	0.84	1.03	1.51
50	50	5	4.07	2.87	2.10	1.64	1.42	1.31	1.21	1.08	1.17	1.57
50	50	15	4.16	3.00	2.32	2.01	2.01	2.08	1.98	1.54	1.44	1.68
50	50	50	4.50	3.54	3.09	3.18	3.85	4.38	4.33	3.15	2.41	2.06
50	50	100	5.11	4.35	4.16	4.71	6.12	7.11	7.16	5.35	3.78	2.61

Table 5.22: Look-up table to derive values of the total critical Pb concentrations in soil drainage water $[Pb]_{tot,sdw(crit)}$ at a CO_2 pressure that equals 15 times the CO_2 pressure of the air

			[Pb] _{tot,sdw(crit)} (mg.m ⁻³), being [Pb] _{dis,ssdw(crit)} (mg.m ⁻³) at SPM=0									
OM	SPM	DOC	pH	pH	pH	pH	pH	pH	pH	pH	pH	pH
%dw	mg.l ⁻¹	mg.l ⁻¹	3.5	4.0	4.5	5.0	5.5	6.0	6.5	7.0	7.5	8.0
10	0	0	34.72	11.41	3.83	1.32	0.46	0.17	0.08	0.09	0.23	0.72
10	0	5	34.80	11.55	4.02	1.57	0.77	0.86	1.12	1.29	1.36	1.64
10	0	15	34.96	11.83	4.42	2.09	1.38	2.18	3.16	3.67	3.61	3.47
10	0	50	35.52	12.82	5.83	3.92	3.42	6.25	10.04	11.87	11.47	9.89
10	0	100	36.33	14.25	7.92	6.51	6.21	11.39	19.36	23.30	22.68	19.07
10	50	0	37.33	14.50	7.43	5.53	5.41	5.98	6.88	8.08	9.60	11.71
10	50	5	37.41	14.64	7.62	5.79	5.72	6.66	7.92	9.27	10.73	12.63
10	50	15	37.57	14.92	8.02	6.31	6.33	7.98	9.97	11.66	12.98	14.46
10	50	50	38.13	15.91	9.43	8.14	8.37	12.05	16.84	19.86	20.84	20.89
10	50	100	38.94	17.34	11.52	10.74	11.16	17.19	26.17	31.29	32.05	30.06
50	0	0	32.85	11.08	3.80	1.31	0.46	0.17	0.08	0.09	0.23	0.72
50	0	5	34.36	12.59	5.32	2.74	1.63	0.89	1.12	1.29	1.36	1.64
50	0	15	37.41	15.65	8.37	5.51	3.80	2.25	3.16	3.67	3.61	3.47
50	0	50	48.44	26.65	18.69	14.44	10.52	6.45	10.04	11.87	11.47	9.89
50	0	100	65.13	42.22	32.86	26.13	18.94	11.76	19.36	23.30	22.68	19.07
50	50	0	39.22	18.51	12.51	11.53	12.45	14.27	16.57	19.45	22.94	27.36
50	50	5	40.73	20.03	14.03	12.96	13.63	14.95	17.61	20.64	24.06	28.27
50	50	15	43.78	23.08	17.07	15.74	15.78	16.30	19.66	23.03	26.31	30.11
50	50	50	54.80	34.07	27.42	24.65	22.51	20.51	26.54	31.24	34.18	36.53
50	50	100	71.49	49.66	41.61	36.34	30.92	25.82	35.86	42.66	45.38	45.70

pH values: In principle the *pH* at steady state conditions assuming Gothenburg Protocol implementation, can best be taken as a basis. This may cause problems, as it has to be determined using dynamic models. Instead the *pH* at the critical acid load can be used. This *pH* is easier to calculate but it may strongly deviate from the *pH* at steady state assuming Gothenburg Protocol implementation. Furthermore, the calculation of the critical load *pH* is rather uncertain depending on arbitrary choices to be made. Therefore the use of the critical load *pH* is not

recommended.

Assuming that it is likely that present *pH* is (almost) equal to future *pH* at steady state (under Göteborg Protocol implementation conditions), the present *pH* is advised to use for pragmatic reasons. Because the present *pH* in soil solution is not always available, but rather measured as *pH* in water or in salt extracts, regression functions to relate several *pH* measurements to soil solution *pH* were derived. Relations are given in Table 5.22, assuming no effect of soil type on the

Table 5.23: Results of linear regression analyses of the *pH* in soil solution against *pH-H₂O*, *pH-CaCl₂* and *pH-KCl*

Explaining	N	Slope (α) ¹⁾	Intercept (β) ¹⁾	se _{Yest}	R ² adj
Explaining variable	N	Slope (α) ¹⁾	Intercept (β) ¹⁾	se _{Yest}	R ² adj
pH-H ₂ O	1145	1.0462	-0.2847	0.453	0.84
pH-KCl	905	0.9692	0.6233	0.491	0.80

¹⁾ All coefficients are significant at $p > 0,999$

relationship. These relations can be used to calculate the soil solution pH which is needed in the critical load calculations and also in the transfer functions relating reactive metal contents to free metal ion concentrations.

More detailed information is given in Annex 10 in the background document (De Vries et al. 2004b). This includes relationships as a function of soil type. Ranges in the present and steady-state critical soil pH for various combinations of land use, soil type and soil depth are also provided there.

DOC concentrations: The concentration of dissolved organic matter (*DOM*) in soils is nowadays frequently determined in climate-related studies. Concentrations of *DOM* are usually determined by analysis of carbon (*DOC*) which accounts for half of the weight of soil organic matter ($DOM = 2 \times DOC$). However, long-term data on soil solutions are rarely available at sufficient density for mapping region-specific means and variability's, and may need to be estimated from studies elsewhere. Ranges in *DOC* values for major forest types and soil layers, by means of the 5-, 50- and 95 percentiles, are presented in Annex 11 of the background document (De Vries et al. 2004b) on the basis of *DOC* values from approximately 120 Intensive Monitoring plots in Europe. In general, the results show a clear decrease in *DOC* concentrations going from the humus layer (median value of 40 mg l^{-1}) into the mineral subsoil. Furthermore, the values are slightly higher in coniferous forest compared to deciduous forests.

Relationships of *DOC* concentrations with vegetation type, hydrology, growth conditions or soil properties may be expected, which would be useful to improve estimates for different sites and regions. The data for the mineral soil (De Vries et al. 2004b) were thus used to derive relationships with available site characteristics and soil data that may affect the *DOC* concentrations, including the type of forest, (coniferous or deciduous forests), texture class (indication for soil type), temperature, pH and the contents of *C* and *N*, including the *C/N* ratio. Results thus obtained are given in

the background document. The results show a good relationship with the site and soil characteristics in the subsoil (below 30cm) but the relationships were much worse in the topsoil (above 30cm). In the topsoil there was a clear positive relationship with *C/N* ratio and temperature, while the correlated values of the individual *C* and *N* concentrations were negatively and positively related to *DOC*, respectively. The relationships are, however, too weak to be very useful. This is in line with the limited number of studies in the literature, from which no significant relationship could be discerned (Michalzik et al. 2001).

Based on the available data the following default values for calculating critical loads of *Pb* and *Cd*, or critical levels of atmospheric *Hg* pollution, respectively, are suggested (see background document, Annex 11):

Forest organic layer (O horizon):

$$[DOC]_{sdw} = 35 \text{ mg l}^{-1} \quad ([DOM]_{sdw} = 70 \text{ mg l}^{-1}).$$

Forest mineral topsoil (0-10 cm):

$$[DOC]_{sdw} = 20 \text{ mg l}^{-1} \quad ([DOM]_{sdw} = 40 \text{ mg l}^{-1}).$$

Grass land (0-10) cm:

$$[DOC]_{sdw} = 15 \text{ mg l}^{-1} \quad ([DOM]_{sdw} = 30 \text{ mg l}^{-1}).$$

Arable land (0-30) cm:

$$[DOC]_{sdw} = 10 \text{ mg l}^{-1} \quad ([DOM]_{sdw} = 20 \text{ mg l}^{-1}).$$

5.5.2.2.4 Critical dissolved concentrations of *Hg* related to ecotoxicological effects in soils

Critical limit for the soil: With respect to *Hg*, critical limits refer only to effects on soil micro-organisms and invertebrates in the humus layer of forests. The suggested critical limit for *Hg* is that the concentration in the humus layer (O-horizon) of forest soils after normalization with respect to the organic matter content should not exceed $0.5 \text{ mg kg (org)}^{-1}$ (Meili et al. 2003a). Because of the strong association of *Hg* with organic matter leaving virtually no free ions, the exposure of biota to *Hg* is controlled by the

competition between biotic and other organic ligands, and the contamination of all types of organic matter is determined by the supply of organic matter relative to the supply of *Hg* at a given site (Meili 1991a, 1997, cf. biodilution). Therefore, the critical limit for *Hg* in soils is set for the organically bound *Hg* rather than for the free ion concentration, also in solution.

Critical total mercury concentrations in soil solution can be calculated by using a transfer function for *Hg* from soil to soil solution, while assuming a similar critical *Hg/org* ratio in the solid phase and in the liquid phase, at least in oxic environments where binding to sulphides is negligible. Various reasons supporting this are given in Meili (1991a, 1997, 2003b), De Vries et al. (2003), and Åkerblom et al. (2004).

Transfer function for mercury: The critical leaching of *Hg* from the humus layer ($M_{le(crit)}$ in eq. 5.88) is related to the mobility and *Hg* content of dissolved organic matter because of the strong affinity of *Hg* for living and dead organic matter and the resulting lack of competition by inorganic ligands in this layer (e.g. Meili 1991, 1997). Because of the strong association of *Hg* with organic matter leaving virtually no free ions (apparently far less than one per km² of topsoil, based on Skyllberg et al. 2003), the biogeochemical turnover of *Hg* is controlled by the competition between biotic and other organic ligands. Therefore, *Hg/OM* ratios are a useful tool for calculating critical limits and loads and associated transfer functions (Meili et al. 2003a). This is the basis of the transfer function to derive total *Hg* concentrations in percolating (top)soil water ($[M]_{dis,sdw(crit)}$ in eq. 5.90, $mg\ m^{-3}$) as follows:

$$(5.96) \quad [Hg]_{dis,sdw(crit)} = [Hg]_{OM(crit)} \cdot f_f \cdot [DOM]_{sdw} \cdot c_{sdw}$$

where

$[Hg]_{dis,sdw(crit)}$ = critical total *Hg* concentration in soil drainage water ($mg\ m^{-3}$)

$[Hg]_{OM(crit)}$ = critical limit for *Hg* concentration in solid organic matter (*OM*), or the *Hg/OM* ratio in organic (top)soils ($[Hg]_{OM(crit)} = 0.5\ mg\ (kg\ OM)^{-1}$).

f_f = fractionation ratio, describing the *Hg* contamination of organic matter in solution (*DOM*) relative to that in solids (*OM*) (-),

$[DOM]_{sdw}$ = concentration of dissolved organic matter in soil drainage water ($g\ m^{-3}$),

c_{sdw} = $10^{-3}\ kg\ g^{-1}$, factor for appropriate conversion of mass units.

The scale-invariant fractionation or transfer factor f_f describes the *Hg* partitioning between organic matter in solids and organic matter in solution and is defined as the ratio between the *Hg* content of *DOM* and that of *OM* (Meili et al. 2003a, Meili et al. 2003b). Preliminary studies in Sweden suggest that the *Hg* concentration in *DOM* is of similar magnitude as that in *OM*, and that 1 may be used as a default value for f_f until deviations from unity prove to be significant (Åkerblom et al. 2004).

Critical concentration for the soil drainage water: Based on the *Hg* limit of $0.5\ mg\ kg^{-1}\ OM$ and a *DOM* concentration of $70\ mg\ l^{-1}$ ($DOC = 35\ mg\ l^{-1}$), the critical steady state concentration of total *Hg* in soil drainage water is $35\ ng\ l^{-1}$ or $0.035\ \mu g\ l^{-1}$ (see eq. 5.96). This concentration is consistent with that derived by a different approach at the watershed scale (Meili et al. 2003a) and is similar to high-end values presently observed in soil solutions and surface freshwaters (Meili, 1997; Meili et al. 2003b; Åkerblom et al. 2004). Note that this ecosystem limit for soil water is much lower than the drinking water limit above, but still higher than that for surface freshwaters where *Hg* limits for fish consumption usually are exceeded at surface water concentrations of $1\text{--}5\ ng\ l^{-1}$.

5.5.3. Aquatic ecosystems

5.5.3.1 Critical loads of cadmium and lead

5.5.3.1.1 Simple steady-state mass balance model and related input data

In principle, the simple steady-state mass balance approach can be used for *Cd*, *Pb* and *Hg* but it has been decided to restrict the approach in first instance to *Cd* and *Pb* and use a different, precipitation based approach for *Hg*, as described in Section 5.5.3.2.

Steady-state mass balance model in stream waters

As with terrestrial ecosystems, the critical load of *Cd* and *Pb* for freshwaters is the acceptable total load of anthropogenic heavy metal inputs corresponding to the sum of tolerable outputs from the catchment by harvest and outflow, minus the natural inputs by weathering release in the catchment but adding the retention in the surface water (De Vries et al. 1998). There is no need to consider net release in catchment soils, if the net weathering (weathering minus occlusion) is negligible. Since the estimation of net release in soils includes high uncertainties, it is preliminarily assumed to be negligible.

In the initial manual on the calculation of critical loads of heavy metals for aquatic ecosystems (De Vries et al. 1998), the default method presented to calculate critical loads of heavy metals for soils included in-lake metal retention, including all relevant metal fluxes, namely sedimentation, resuspension and exchange processes in the lake (infiltration, diffusion and bioirrigation), while assuming a steady state situation (DeVries et al.1998). To keep the approach as simple as possible, and also to stay as close as possible to the simple mass balance approach for nitrogen and acidity, this model can be simplified by neglecting weathering in the catchment and lumping transient exchange processes at the sediment-water interface and the net effect of sedimentation and resuspension in one retention term

according to De Vries et al. (1998):

$$(5.97) \quad CL(M) = M_u + M_{ret(crit)} \cdot \frac{A_l}{A_c} + M_{lo(crit)}$$

where:

M_u	= removal of heavy metal by biomass harvesting or net uptake in the catchment ($g \text{ ha}^{-1} \text{ a}^{-1}$)
$M_{ret(crit)}$	= net retention of heavy metal in the lake at critical load ($g \text{ ha}^{-1} \text{ a}^{-1}$)
$M_{lo(crit)}$	= critical lateral outflow of heavy metal from the whole catchment ($g \text{ ha}^{-1} \text{ a}^{-1}$)
A_l	= lake area (ha)
A_c	= catchment area (ha)

When critical loads of *Cd* and *Pb* for stream waters are calculated, there is no need to consider net retention, leading to the following critical load calculation:

$$(5.98) \quad CL(M) = M_u + M_{lo(crit)}$$

Because the estimation of net retention for lakes includes high uncertainties, it is recommendable to calculate preliminarily aquatic critical loads for stream waters only, for which the retention in surface water is negligible. It furthermore leads to the lowest critical loads and thus implies the protection of lakes as well. Finally, when calculating critical loads for lakes, one may also assume that net retention of metals in lakes is negligible, implying the assumption that the overall release or retention of metals in a catchment, including the lake sediment, is negligible.

Heavy metal removal by net uptake

The assessment of these data is comparable for those in terrestrial ecosystems (see eq. 5.89), but now the uptake or release refers to the complete catchment. This implies that no further reduction factors need to be applied to relate the uptake in the

root zone/catchment to the mineral topsoil. The equation for net uptake is thus equal to eq. 5.89 with f_{Mu} being equal to 1.

Critical output of heavy metals from the aquatic system

The critical lateral outflow can be described as the product of the lateral outflow flux of water and the critical limit for the total concentration of the heavy metal in the surface water according to:

$$(5.99) \quad M_{lo(crit)} = 10 \cdot Q_{lo} \cdot [M]_{tot,sw(crit)}$$

where:

- Q_{lo} = lateral outflow flux of water from the whole catchment area ($m^3 a^{-1}$)
- $[M]_{tot,sw(crit)}$ = critical limit for the total concentration (dissolved and in suspended particles) of heavy metal in surface water ($mg m^{-3}$)

Q_{lo} , which sometimes is denoted as the hydraulic load in the literature can be derived for a lake on the basis of the flow from the aquatic system, Q ($m^3 a^{-1}$) divided by the catchment area (m^2). The total concentration of metals can be calculated as:

$$(5.100) \quad [M]_{tot,sw(crit)} = [M]_{dis,sw(crit)} + [M]_{SPM,sw(crit)} \cdot [SPM]_{sw}$$

where:

- $[M]_{dis,sw(crit)}$ = critical dissolved concentration of a heavy metal in surface water ($mg m^{-3}$)
- $[M]_{SPM,sw(crit)}$ = critical total content of a heavy metal in suspended particles ($mg kg^{-1}$)
- $[SPM]_{sw}$ = concentration of suspended particulate matter in surface water ($kg m^{-3}$)

Data on the lateral outflow of lakes can be derived from the *S&N* critical loads

database. The critical load depends on the critical limit used. In the initial manual for aquatic ecosystems (De Vries et al. 1998), it was argued that critical limits referring to the free metal ion activity in surface water are most appropriate. This idea has been further developed by Lofts et al. (unpublished data), but has not been adopted here, for reasons which will be given in 5.5.3.1.2. Instead, critical limits referring to total dissolved metal concentrations have been adopted. It is necessary to include a solid-solution transfer function (see Annex 1) to calculate the critical metal concentration in suspended particles and hence the critical total aqueous metal concentration.

Information on how to estimate the critical net in-lake retention when calculating critical metal loads for lakes is given in the background document to this manual (De Vries et al. 2004b). Like for terrestrial ecosystems it is recommendable to calculate weathering rates (here at least for a depth of 1 m) to account for the influence of natural processes in comparison to atmospheric deposition in order to evaluate critical loads and critical limits exceedances. Information on how to calculate weathering within the catchment is given in Annex 6 of the background document.

5.5.3.1.2 Critical total dissolved cadmium and lead concentrations in aquatic ecosystems

Critical limits for total dissolved concentrations

Analysis of aquatic ecotoxicological data by Lofts et al. (unpublished) suggested overlap between aquatic and terrestrial toxic endpoint concentrations at a given *pH*. Hence it was suggested that common critical limits be applied for both soils and freshwaters, by using the critical limit functions derived in 5.5.2.2 for toxic effects on the soil ecosystem. However, although there is no theoretical reason why the sensitivities of soil and water organisms to metals should not be similar (assuming that uptake of the free ion from the aqueous phase is the

significant mechanism leading to toxicity) this approach has not been adopted for the following reasons:

1. The aquatic toxicity data for *Cd* covered a more restricted *pH* range than for the terrestrial toxicity data (*pH* 6.9 to 8.7 compared to *pH* 3.2 to 7.9). Therefore, although overlap of points was seen within the *pH* range covered by the aquatic toxicity data, no data were available to validate the theory of overlap below *pH* 6.9.
2. Observed overlapping of points for *Pb* was less than for any of the metals studied (*Cu* and *Zn* in addition to *Cd* and *Pb*). Most of the aquatic toxicity data gave free *Pb* endpoints higher than those observed for soils.

For these reasons, it was decided not to use the free ion approach for aquatic critical limits and instead to express the critical limits as the total dissolved metal (mg m^{-3}). A summary of preliminary effect-based critical limits is given in Table 5.24. The values for *Cd* are based on the EU Risk Assessment Report for *Cd* (Risk assessment Cadmium metal CAS-No. 7440-43-9) The values for *Pb* are based on Crommentuijn et al. (1997) for the value suggested for use in the 2004 call for data, and on a substance data sheet on *Pb* and its compounds (2003) for the value to be used when updated Annex 3 is available. The reason of needing an update of Annex 3 is described below. The suggested substitute for Annex 3 is provided in Annex 12 of the background

document (DeVries et al. 2004b) including detailed calculation examples. The values are all related to ecotoxicological effects. There are also critical limits related to secondary poisoning, but these values are not yet recommended for use because they do require further substantiation and discussion.

The value of 0.38 mg m^{-3} , taken from EU Risk Assessment Report for *Cd*, is based on the 5-percentile cut-off value of chronic toxicity data from 168 reliable tests on single species and 9 multi-species studies. An assessment factor of 2 is further introduced in the report, leading to a critical limit of 0.19 mg m^{-3} , but this approach was not accepted in this manual. For *Cd*, a relationship with water hardness has also been found. In the EU Risk Assessment Report. Recently, it was also accepted to take the influence of hardness on the toxicity of cadmium into account, using 3 hardness classes (with hardness *H* in $\text{mg CaCO}_3 \text{ l}^{-1}$) according to 0.16 mg m^{-3} if $H < 100$, 0.30 mg m^{-3} if $100 < H < 200$ and 0.50 mg m^{-3} if $H > 200$, using no assessment factor (see also the background document to the manual).

For *Pb*, the critical limit of 11 mg m^{-3} is based on Crommentuijn et al. (1997), whereas the value of 5 mg m^{-3} (range of $2.1\text{-}9.3 \text{ mg m}^{-3}$) is based on the 5-percentile cut-off value of chronic toxicity data, calculated with the method of Aldenberg & Jaworska, using 3 data sets of selected (i) freshwater and saltwater NOECs/EC10s (30 values), (ii)

Table 5.24: Recommended critical limits for dissolved *Cd* and *Pb* concentrations surface waters

Metal	Critical dissolved concentration (mg m^{-3})	
	Value to be used now	Value to be used when updated Annex 3 is available
Cd	0.38^1	0.16 if $H < 100^2$ 0.30 if $100 < H < 200$ and 0.50 if $H > 200$
Pb	11	5

¹ A comparable critical limit is suggested in the RAR on *Cd* for the protection of top predators, namely 0.26 mg m^{-3} . This value is based on a critical limit for the intake of *Cd* of $160 \mu\text{g Cd/kg}$ food (wet weight) of the predator, being the quality standard for biota tissue with respect to secondary poisoning. However, this value is yet considered too uncertain to be used in the critical load calculations

² *H* = hardness in $\text{mg CaCO}_3 \text{ l}^{-1}$

freshwater NOECs/EC10s (19 values) and (iii) saltwater NOECs/EC10s (11 values). In the substance data sheet on *Pb*, an assessment factor of 3 is further introduced, but this approach was not accepted in this manual. At a workshop of ICP Waters on heavy metals, 2002, in Lillehammer (Skjelkvale and Ulstein, 2002) a range of 1 - 11 $mg\ m^{-3}$ was suggested in dependence on water chemistry, with low values referring to clear softwaters. The critical limit of 5 $mg\ m^{-3}$ is in the middle of this range and thus consistent. A much lower critical limit is suggested in substance data sheet on *Pb* for the protection of human health using a critical limit of 200 $\mu g\ Pb\ kg^{-1}$ muscle meat of fish (food standard set by Commission Regulation (EC) No. 466/2001) and the protection of predators in freshwater and saltwater environments from secondary poisoning (near 0.4 $\mu g\ Pb\ l^{-1}$). However, this value is yet considered to uncertain to be used in the critical load calculations.

Although not presently used, a preliminary critical limit for *Hg* can be found in the substance data sheet on *Hg* and its compounds (2003). As with *Pb*, this value is based on the 5-percentile cut-off value of chronic toxicity data, using 3 data sets of selected (i) freshwater and saltwater, (ii) freshwater and (iii) saltwater, leading to a value of 0.142 $mg\ m^{-3}$ (90 percentile range of 0.056 - 0.281 $mg\ m^{-3}$). In the substance data sheet on *Hg*, an assessment factor of 4 is further introduced, but this approach was not accepted in this manual. A reliable quality standard to protect top predators from secondary poisoning can not be given, but the value is much lower than those for ecotoxicological effects. The value of 0.035 $mg\ m^{-3}$ presented earlier for soils is likely to be an upper limit for secondary poisoning.

Calculation of critical limits for total aqueous concentrations

In order to calculate critical loads of metals for freshwater ecosystems it is necessary to know the total aqueous concentration at the critical limit, i.e. the concentration of dissolved metal and of metal bound to

suspended particulate matter (*SPM*). There are various possible approaches to derive adsorbed metal contents on suspended particles ($[M]_{SPM_{sw}}$) from total dissolved metal concentrations in surface water ($[M]_{tot,sw}$). The simplest approach is an empirical linear approach (K_d -value) relating both contents and concentrations, while accounting for the impact of major properties of the suspended particles influencing the sorption relationship. However, K_d values for a given metal may vary substantially from place to place and so the K_d approach is not appropriate when calculating metal contents on suspended particles from a large number of different locations.

An alternative approach, which uses as far as possible data and models used elsewhere in this manual, is to take a two-stage approach:

1. Calculate the critical free ion concentration from the critical dissolved metal concentration.
2. Calculate the critical particle-bound metal from the critical free ion.
3. Sum the critical particle-bound and dissolved metal to obtain the critical total metal.

Step 1 uses a complexation model (e.g. WHAM) to calculate the critical free ion concentration from the critical dissolved metal concentration. Step 2 uses a transfer function to calculate the particle-bound metal from the free ion. This transfer function is given in Annex 2. The calculation of the critical total aqueous concentration is presented in Annex 3.

In Annex 3, the procedure given applies only to the values of 0.38 $mg\ m^{-3}$ for *Cd* and 11 $mg\ m^{-3}$ for *Pb*. Use of different values (for *Cd* as a function of hardness and for *Pb* 5 instead of 11) implies a rerun of the WHAM model. This will be done and these values can be used, as soon as the updated Annex 3 is adopted.

Surface water chemistry data

Data needed to calculate the total dissolved metal concentration are the concentration of suspended particles in the water compartment, $[SPM]_{sw}$, the pH and DOC concentrations of surface water. The concentration of SPM in the surface water ($kg\ m^{-3}$ or $g\ l^{-1}$) depends on the turbulence of the water, which in turn depends on the geological setting (incl. land use) and water flow velocity (i.e. wind speed for lakes). The concentration of suspended particles may thus vary considerably and generally ranges from 1 to $100\ g\ m^{-3}$. The average concentration for Dutch surface waters, for example, is $30\ g\ m^{-3}$, and for a dataset of lowland UK rivers ($n = 2490$) it is $30.6\ g\ m^{-3}$ with a range of <0.1 to $890\ g\ m^{-3}$, while Scandinavian waters typically show much lower values.

pH and DOC values for lakes largely depend on the landscape surrounding the lakes including the parent material (its sensitivity to acid inputs). Typical DOC values for clear water lakes are below $5\ mg\ l^{-1}$, whereas for humic lakes, values can be higher than $50\ mg\ l^{-1}$. Values for the pH generally vary between 5 and 7. Both pH and DOC are standard measurements in lake surveys and a wealth of data can be derived from those surveys.

When calculating in-lake retention in deriving critical loads for lakes, data on characteristics such as the lake and catchment area and the net retention rate are needed. For more information we refer to the background document (De Vries et al. 2004b) and an earlier manual (De Vries et al. 1998).

5.5.3.2 Critical levels of mercury in precipitation

Critical loads of atmospheric pollution for aquatic ecosystems (lakes and rivers) may be approached by a mass balance approach involving a wide variety of processes both within the water column and in the surrounding watershed. Alternatively, the steady state

partitioning of pollutants in a constant environment can be formulated without any need for mass balance considerations or detailed understanding of ecosystem processes. This can be achieved by linking critical receptors such as fish directly to the main immissions through transfer functions (TF) describing the relationship of their Hg concentrations at steady state, as described below.

5.5.3.2.1 Derivation of critical levels of mercury in precipitation referring to a standard fish

Basic concept

Hg concentrations in fish show a wide variation, about 30-fold both within and among sites (Meili 1997). A standardized value for a given site (lake or river) can be obtained by referring to a commonly caught piscivorous fish with a total body weight of 1 kg, in particular pike (*Esox lucius*). Using a 1-kg pike as a standard receptor, the mean Hg concentration in fish flesh can be related to the mean Hg concentration in precipitation at a given site as follows:

(5.101)

$$[Hg]_{Pike} = c_{bp} \cdot [Hg]_{Prec} \cdot TF_{HgSite}$$

where:

$[Hg]_{Pike}$ = Hg concentration in the flesh of 1-kg pike ($mg\ kg^{-1}\ fw$)

$[Hg]_{Prec}$ = Hg concentration in precipitation ($ng\ l^{-1}$)

TF_{HgSite} = site-specific transfer function ($l\ kg^{-1}\ fw$) referring to the transfer of atmospheric Hg to fish flesh in a watershed at steady state

c_{bp} = $10^{-6}\ mg\ ng^{-1}$, factor for appropriate conversion of units.

The critical level of atmospheric pollution ($[Hg]_{Prec(crit)}$) can thus be calculated as follows:

(5.102)

$$[Hg]_{Prec(crit)} = \frac{[Hg]_{Pike(crit)}}{(TF_{HgSite} \cdot c_{bp})}$$

where:

$[Hg]_{Pike(crit)}$ = critical *Hg* concentration in the flesh of 1-kg pike
(0.3 mg kg⁻¹ fw)

$[Hg]_{Prec(crit)}$ = critical *Hg* concentration in precipitation (ng l⁻¹)

c_{bp} = 10⁻⁶ mg ng⁻¹, factor for appropriate conversion of flux units.

Regarding the critical limit for mercury in pike of 0.3 mg kg⁻¹ fw, we refer to the background document of the manual (De Vries et al. 2004b).

The transfer function TF_{HgSite}

TF_{HgSite} addresses the wide variation of *Hg* concentrations among ecosystems in response to a given atmospheric *Hg* input at steady state. It accounts for a variety of complex processes including both terrestrial and aquatic aspects related to the biogeochemistry of *Hg* in lakes and rivers (Meili et al. 2003a), thus accounting for both fluxes and transformations of *Hg* (e.g. sorption, volatilization, net methylation, bioavailability, biodilution, biomagnification). For mapping of watershed sensitivity, TF_{HgSite} is preferably expressed as a function of basic physical-chemical parameters. *Hg* concentrations in fish are generally highest in nutrient-poor softwaters in acidic watersheds rich in wetlands (e.g. Verta et al. 1986, Håkanson et al. 1988, Meili 1991a, 1994, 1996a, 1997). Such differences can be described by empirical relationships to address regional and local differences in watershed biogeochemistry, based on variables for which data are commonly available (e.g. from other studies under CLRTAP), such as surface

water *pH* or concentrations of organic carbon or nutrients (the latter being of particular relevance for mercury). Two alternative formulations capturing part of the large variation in TF_{HgSite} are:

(5.103a)

$$TF_{HgSite} \approx \frac{TF_{HgRun} \cdot ([TOC]_{sw} + 1)}{(400 [TP]_{sw} + 6)}$$

(5.103b)

$$TF_{HgSite} \approx TF_{HgRun} \cdot e^{-\frac{(pH_{sw} - 6)}{2}}$$

where:

$[TOC]_{sw}$ = concentration of total organic carbon in surface water (mg l⁻¹)

$[TP]_{sw}$ = concentration of total phosphorus in surface water (mg l⁻¹)

pH_{sw} = *pH* in surface water

TF_{HgRun} = transfer function (l kg⁻¹ fw) referring to the transfer of atmospheric *Hg* to fish flesh via runoff in a reference watershed at steady state.

The first formulation (16a) is most appropriate and should be used when concentrations of total organic carbon and total phosphorus in surface water are available, which is often the case from routine monitoring of surface waters. The alternative formulation based on *pH* alone (16b) is less adequate but can be used if data access is limited.

TF_{HgRun} can be quantified from adequate data sets in various ways (see Annex 13 of the background document, De Vries et al. 2004b). If such data are not available, a value of 250 000 l kg⁻¹ fw can be used for TF_{HgRun} referring to the standard fish (1 kg, in particular pike, *Esox lucius*) at steady state (Meili et al. 2003a, cf. Verta et al. 1986, Meili 1991a). An important aspect to consider when quantifying TF_{HgRun} (or other steady state parameters) from field data is that present environmental *Hg* concentrations are not in steady state with the present level of atmospheric pollution.

5 Mapping Critical Loads

5.5.3.2.2 Derivation of critical levels of mercury in precipitation referring to other organisms

Basic concept

The *Hg* concentration in any fish or other organism, serving as food for humans and fish-based wildlife such as birds and mammals, can be related to the *Hg* concentration in 1-kg pike according to:

$$(5.104) \quad [Hg]_{Bio} = [Hg]_{Pike} \cdot TF_{HgBio}$$

where:

$[Hg]_{Bio}$ = *Hg* concentration in any biota, e.g. fish flesh (*mg kg⁻¹ fw*)

TF_{HgBio} = organism-specific transfer function addressing the typical *Hg* partitioning within food webs (-)

The critical level of atmospheric pollution ($[Hg]_{Prec(crit)}$) can thus be calculated from a combination of eq. 5.102 and eq. 5.104 as follows:

$$(5.105) \quad [Hg]_{Prec(crit)} = \frac{[Hg]_{Bio(crit)}}{(TF_{HgBio} \cdot TF_{HgSite} \cdot c_{bp})}$$

where:

$[Hg]_{Bio(crit)}$ = critical *Hg* concentration in any biota, e.g. fish flesh (*mg kg⁻¹ fw*)

c_{bp} = see above

TF_{HgBio} is useful for two purposes:

(1) to estimate values for 1-kg pike for sites/regions in which only mercury concentrations in other organisms are available, (2) to convert critical load maps referring to 1-kg pike into maps for other target organisms of local/regional interest.

The transfer function TF_{HgBio}

TF_{HgBio} addresses the wide variation of *Hg* concentrations among organisms within

food webs, by describing the typical deviation from the standard fish. Among commonly available variables, body weight is the most powerful single predictor of fish *Hg* levels, also across species. The variation in TF_{HgBio} can be described as follows:

$$(5.106) \quad TF_{HgBio} \approx f_{HgY} + f_{HgW} W^{2/3}$$

where:

f_{HgY} = value for very young fish and other small animals (-); $f_{HgY} \approx 0.13$

f_{HgW} = species-specific slope coefficient (-); $f_{HgW} \approx 0.2 \dots 2$ (Table 5.25)

W = total body fresh weight (*kg fw*)

For many freshwater fish used for human consumption, this will generate estimates of mean *Hg* concentrations at a given fish size that differ less than 2-fold from observed means. Species-specific slope coefficients (f_{HgW}) for some common freshwater fish are given in Table 5.25 for the typical case that the value for very young fish and other small animals (f_{HgY}) can be maintained at 0.13. For any fish species (e.g. for unexplored sites or for unknown future fish populations), a first approximation differing less than 3-fold from observed size-class means can be made based on body weight alone, using the parameter for the standard fish, pike ($f_{HgW} = 0.87$, Table 5.25). If fish weight data are not available, total body weight (W in kg) can be estimated from total body length by applying a species-specific shape factor (f_{LW} , Table 5.25) according to:

$$(5.107) \quad W \approx f_{LW} \cdot L^{3.1}$$

where:

L = length of the fish (cm)

Table 5.25: Coefficients for size conversion (f_{LW}) and normalization of Hg concentrations (f_{HgW}) in freshwater fish, some standard fish weights (W) for consumption and the related value for TF_{HgBio}

Fish taxa			f_{LW}	f_{HgW}	W	TF_{HgBio}
pike	<i>Esox lucius</i>	Esocidae	$3.8 \cdot 10^{-6}$	0.87	1.0	1.0
pike-perch, zander	<i>Stizostedion lucioperca</i>	Percidae	$6.4 \cdot 10^{-6}$	1.2	1.0	1.3
perch	<i>Perca fluviatilis</i>	Percidae	$7.9 \cdot 10^{-6}$	1.9	0.3	1.0
trout	<i>Salmo trutta</i>	Salmonidae	$7.2 \cdot 10^{-6}$	0.4	0.3	0.3
Arctic char	<i>Salvelinus alpinus</i>	Salmonidae	$6.8 \cdot 10^{-6}$	0.7	0.3	0.4
whitefish	<i>Coregonus spp.</i>	Coregonidae	$6 \cdot 10^{-6}$	<0.4...>2		
burbot	<i>Lota lota</i>	Lotidae	$5 \cdot 10^{-6}$	0.9	0.3	0.5
bream	<i>Abramis brama</i>	Cyprinidae	$8 \cdot 10^{-6}$	0.25	0.3	0.2
roach	<i>Rutilus rutilus</i>	Cyprinidae	$6.8 \cdot 10^{-6}$	0.6...1.2		

Table 5.25 is meant as a reference that can be expanded and adapted for local use, based on additional field data from systems where several coexisting species have been analyzed. Note that for compatibility of transfer functions and for inter-regional comparisons, the value of TF_{HgBio} refers to a 1-kg pike, which should be maintained as a reference receptor with a value of $TF_{HgBio} = 1$.

5.5.4. Limitations in the present approach and possible future refinements

In general the uncertainties in measurement as well as in modelling are higher with respect to trace elements than for main nutrient elements. In particular the following uncertainties of the models should be mentioned:

- The steady-state of metal inputs and outputs on the level of the critical limit is a theoretical situation. In dependence of the actual status of a site (or area) it may take years to centuries (e.g. for calcareous soils) to reach this steady-state. This should be considered, when critical loads and their exceedances are to be interpreted. To consider the processes of metal accumulation or loss from soils over time, dynamic approaches would be needed. Although such models are already suggested, they are not yet considered here, because they still need further sophistication. There is some inconsistency between the calculation of the critical leaching and the tolerable removal of the

metals with biomass, because types of critical limits and their mode of use are different for both fluxes.

- The uptake of heavy metals by plants is not constant over time but varies strongly with changes in pollution and is at present likely lower than indicated above at steady state at the level of critical concentrations,
- Possible effects of thinning of the metal concentration due to high mass fluxes of biomass harvest (high yields) are not considered due to missing knowledge,
- The delivery of heavy metals to the available pools of soils and surface waters is excluded from the mass balance equation due to high uncertainties of the available calculation approach. However since the same approach is used to identify sites with high natural inputs it may happen that one site is excluded, while another site with an insignificant lower weathering rate will stay in the database,
- The approaches taken to calculate critical limits for ecotoxicological effects are different for terrestrial and aquatic ecosystems. Given the likelihood that terrestrial and freshwater organisms (with the exception of surface-dwelling soil invertebrates such as snails) are exposed to metal in a similar manner (i.e. via the solution phase), a common approach to deriving critical limits, if not common values or functions for the limits, is scientifically desirable,

- The critical limit derivation includes several uncertainties, as e.g. differences between results from laboratory or field, which are (deviating e.g. from OECD methodologies) not taken into account by the use of "uncertainty factors",
- Organisms can be affected by different pathways, this could only partly considered here,
- The vertical flux of metals bound to particulate matter suspended in the drainage water, may be remarkable in certain soils, this holds in particular for *Pb*. It was, however, not recommended to consider this, in order to be consistent with other parts of the manual,
- The seasonal variation of soil parameters such as *pH*, *DOC* cannot be accounted for in the models.

References

- Achermann B, Bobbink R (eds) (2003) Empirical Critical Loads for Nitrogen. Environmental Documentation No. 164, Swiss Agency for the Environment, Forests and Landscape (SAEFL), Berne Switzerland, 327 pp.
- Aherne J, Kelly-Quinn M, Farrell EP (2002) A survey of lakes in the Republic of Ireland: Hydrochemical characteristics and acid sensitivity. *Ambio* 31: 452-459.
- Aherne J, Curtis CJ (2003) Critical loads of acidity for Irish lakes. *Aquatic Sciences* 65: 21-35.
- Aherne J, Posch M, Dillon PJ, Henriksen A (2004) Critical loads of acidity for surface waters in south-central Ontario, Canada: Regional application of the First-order Acidity Balance (FAB) model. *Water, Air and Soil Pollution: Focus* 4: 25-36.
- Åkerblom S, Meili M, Bringmark L, Johansson K (2004). Determination of the fractionation factor (ff) in forest soil describing the Hg content of organic matter in solution relative to that in solids based on field data from Sweden. Background Document on Critical Loads of Heavy Metals, UN/ECE-CLRTAP-ICP Modelling and Mapping, 6 p. (<http://www.icpmapping.com>, http://www.oekodata.com/pub/mapping/workshops/ws_potsdam/Akerblom.pdf).
- Ariksson A, Eriksson H, Karlton E, Lind T, Olsson M (2002) Carbon pools and sequestration in soil and trees in Sweden, based on data from national soil and forest inventories. In: M Olsson (ed): Land Use Strategies for Reducing Net Greenhouse Gas Emissions (LUSTRA), Progress Report 1999-2002, pp. 30-36. Swedish University of Agricultural Sciences, Uppsala, Sweden
- Baker LA, Brezonik PL (1988) Dynamic model of in-lake alkalinity generation. *Water Resources Research* 24: 65-74.
- Batterbee RW, Allot TEH, Juggins S, Kreiser AM (1995) Estimating the base critical load: The diatom model. In: CLAG (1995) *op. cit.*, pp.3-6.
- Berendse F, Beltman B, Bobbink R, Kwant M, Schmitz MB (1987) Primary production and nutrient availability in wet heathland ecosystems. *Acta Oec./Oecol. Plant.* 8: 265-276.
- Bindler R, Renberg I, Klaminder J, Emteryd O (2004). Tree rings as Pb pollution archives? A comparison of $^{206}\text{Pb}/^{207}\text{Pb}$ isotope ratios in pine and other environmental media. *Sci. Total Environ.* 319: 173-183.
- Bobbink R, Boxman D, Fremstad E, Heil G, Houdijk A, Roelofs J (1992) Critical loads for nitrogen eutrophication of terrestrial and wetland ecosystems based upon changes in vegetation and fauna. In: Grennfelt and Thörnelöf (1992), *op. cit.*, pp. 111-159.
- Bobbink R, Hornung M, Roelofs JGM (1996) Empirical nitrogen critical loads for natural and semi-natural ecosystems. In: UBA (1996) *op. cit.*, Annex III (54 pp).
- Bobbink R, Hornung M, Roelofs JGM (1998) The effects of air-borne pollutants on species diversity in natural and semi-natural European vegetation. *Journal of Ecology* 86: 717-738.
- Bobbink R, Ashmore M, Braun S, Flückiger W, Van den Wyngaert IJJ (2003) Empirical nitrogen critical loads for natural and semi-natural ecosystems: 2002 update. In: Achermann and Bobbink (2003), *op. cit.*, pp 43-170.
- Boggero A, Barbieri A, De Jong J, Marchetto A, Mosello R (1998) Chemistry and critical loads of Alpine lakes in Canton Ticino (southern central Alps). *Aquatic Science* 60: 300-315.
- Bolt GH, Bruggenwert MGM (eds) (1976) Soil Chemistry. Part A. Basic Elements. Elsevier, Amsterdam, The Netherlands, 281 pp.
- Bouten W, De Vre FM, Verstraten JM, Duysings JJHM (1984) Carbon dioxide in the soil atmosphere: simulation model parameter estimation from field measurements. In: E Eriksson (ed): Hydrochemical

- Balances of Freshwater Systems. IAHS-AISH 150, Uppsala, Sweden, pp. 23-30.
- Brakke DF, Henriksen A, Norton SA (1989) Estimated background concentrations of sulfate in dilute lakes. *Water Resources Bulletin* 25(2): 247-253.
- Brakke DF, Henriksen A, Norton SA (1990) A variable F-factor to explain changes in base cation concentrations as a function of strong acid deposition. *Verh. Internat. Verein. Limnol.* 24: 146-149.
- Breeuwsma A, Chardon JP, Kragt JF, De Vries W (1991) Pedotransfer functions for denitrification. Final Report of the project 'Nitrate in Soils', DG XII, European Community, Brussels, pp. 207-215.
- Brook GA, Folkoff ME, Box EO (1983) A world model of carbon dioxide. *Earth Surface Processes and Landforms* 8: 79-88.
- Burman R, Pochop LO (1994) *Evaporation, Evapotranspiration and Climatic Data*. Developments in Atmospheric Science 22, Elsevier, Amsterdam, 278 pp.
- CLAG (Critical Loads Advisory Group) (1995) Critical loads of acid deposition for United Kingdom freshwaters. ITE Edinburgh/Department of the Environment, London, United Kingdom, 80 pp.
- Crommentuijn T, Polder MD, Van de Plassche EJ (1997) Maximum permissible concentrations and negligible concentrations for metals, taking background concentrations into account. Report 601501 001, National Institute for Public Health and the Environment, Bilthoven, The Netherlands, 157 pp.
- Cronan CS, Walker WJ, Bloom PR (1986) Predicting aqueous aluminium concentrations in natural waters. *Nature* 324: 140-143.
- Davies CE, Moss D (2002) EUNIS habitat classification, Final Report. CEH Monks Wood, United Kingdom.
- De Temmerman L, de Witte T (2003a). Biologisch onderzoek van de verontreiniging van het milieu door zware metalen te Hoboken groeiseizoen 2001. Internal report Centrum voor onderzoek in diergeneeskunde en agrochemie C.O.D.A, Tervuren.
- De Temmerman L, de Witte T (2003b) Biologisch onderzoek van de verontreiniging van het milieu door kwik en chloriden te Tessenderlo en van kwik te Berendrecht. Internal report Centrum voor onderzoek in diergeneeskunde en agrochemie C.O.D.A, Tervuren. EG No. 466/2001: COMMISSION REGULATION (EC) No 466/2001 of 8 March 2001 setting maximum levels for certain contaminants in foodstuffs, Official Journal of the European Commission No. L 77;
- De Vries W (1988) Critical deposition levels for nitrogen and sulphur on Dutch forest ecosystems. *Water, Air and Soil Pollution* 42: 221-239.
- De Vries W, Hol A, Tjalma S, Voogd JC (1990) Literature study on the amounts and residence times of elements in forest ecosystems (in Dutch). Rapport 94, DLO Winand Staring Centre, Wageningen, The Netherlands, 205 pp.
- De Vries W (1991) Methodologies for the assessment and mapping of critical loads and of the impact of abatement strategies on forest soils. Report 46, DLO Winand Staring Centre, Wageningen, The Netherlands, 109 pp.
- De Vries W, Posch M, Reinds GJ, Kämäri J (1993) Critical loads and their exceedance on forest soils in Europe. Report 58 (revised version), DLO Winand Staring Centre, Wageningen, The Netherlands, 116 pp.
- De Vries W (1994) Soil response to acid deposition at different regional scales. PhD thesis, Agricultural University Wageningen, Wageningen, The Netherlands, 487 pp.
- De Vries W, Reinds GJ, Posch M (1994) Assessment of critical loads and their exceedances on European forests using a one-layer steady-state model. *Water, Air and Soil Pollution* 72: 357-394.
- De Vries W, Bakker DJ (1998) Manual for calculating critical loads of heavy metals

- for terrestrial ecosystems. Guidelines for critical limits, calculation methods and input data. DLO Winand Staring Centre, Report 166, Wageningen, The Netherlands, 144 pp.
- De Vries W, Bakker DJ, Sverdrup HU (1998) Manual for calculating critical loads of heavy metals for aquatic ecosystems. Guidelines for critical limits, calculation methods and input data. DLO Winand Staring Centre, Report 165, Wageningen, The Netherlands, 91 pp.
- De Vries W, Posch M (2003) Derivation of cation exchange constants for sand loess, clay and peat soils on the basis of field measurements in the Netherlands. Alterra-Rapport 701, Alterra Green World Research, Wageningen, The Netherlands, 50 pp.
- De Vries W, Reinds GJ, Posch M, Sanz MJ, Krause GHM, Calatayud V, Renaud JP, Dupouey JL, Sterba H, Vel EM, Dobbertin M, Gundersen P, Voogd JCH (2003) Intensive Monitoring of Forest Ecosystems in Europe. Technical Report 2003, EC-UNECE, Brussels and Geneva, 161 pp.
- De Vries W, Schütze G, Lofts S, Meili M, Römkens PFAM, Farret R, De Temmerman L, Jakubowski M (2003) Critical limits for cadmium, lead and mercury related to ecotoxicological effects on soil organisms, aquatic organisms, plants, animals and humans. In: Schütze et al. (2003) *op. cit.*, pp. 29 - 78
- De Vries W, Lofts S, Tipping E., Meili M., Groenenberg JE, Schütze G (2004a). Critical limits for cadmium, lead, copper, zinc and mercury related to ecotoxicological effects on terrestrial and aquatic organisms. *Water, Air and Soil Pollution* (in prep)
- De Vries W, Schütze G, Lofts S, Tipping E, Meili M, Groenenberg JE, Römkens PFAM (2004b). Calculation of critical loads for cadmium, lead and mercury. Background document to Mapping Manual Chapter 5.5, ..pp, www.icpmapping.org
- Dillon PJ, Molot LA (1990) The role of ammonium and nitrate retention in the acidification of lakes and forested catchments. *Biogeochemistry* 11: 23-43.
- Driscoll CT, Lehtinen MD, Sullivan TJ (1994) Modeling the acid-base chemistry of organic solutes in Adirondack, New York, lakes. *Water Resources Research* 30: 297-306.
- Duan L, Hao J, Xie S, Du K (2000) Critical loads of acidity for surface waters in China. *Science of the Total Environment* 246: 1-10.
- Dutch J, Ineson P (1990) Denitrification of an upland forest site. *Forestry* 63: 363-377.
- Eurosoil (1999) Metadata: Soil Geographical Data Base of Europe v.3.2.8.0. Joint Research Centre, Ispra, Italy.
- FAO (1981) FAO-Unesco Soil Map of the World, 1:5.000.000; Volume V Europe, Unesco-Paris, 199 pp.
- Farret R (2003) General Methodology. In: Schütze et al. (2003) *op. cit.*, pp. 103-107.
- Grennfelt P, Thörnelöf E (eds) (1992) Critical Loads for Nitrogen. *Nord* 92:41. Nordic Council of Ministers, Copenhagen, 428 pp.
- Groenenberg JE, Römkens PFAM, Tipping E, Pampura T, De Vries W (2004) Transfer functions for the solid solution partitioning of *Cd*, *Cu*, *Pb* and *Zn* – Review, synthesis of datasets, derivation and validation. (in prep.)
- Gunn J, Trudgill ST (1982) Carbon dioxide production and concentrations in the soil atmosphere: a case study from New Zealand volcanic ash soils. *Catena* 9: 81-94.
- Håkanson L, Nilsson Å, Andersson T (1988) Mercury in fish in Swedish lakes. *Environmental Pollution* 49: 145-162.
- Hall J, Bull K, Bradley I, Curtis C, Freer-Smith P, Hornung M, Howard D, Langan S, Loveland P, Reynolds B, Ulyett J, Warr T (1998) Status of UK critical loads and exceedances. Part 1: Critical loads and critical load maps. Report prepared under DETR/NERC Contract EPG1/3/116. <http://critloads.ceh.ac.uk>

- Hall J, Ulliyett J, Heywood E, Broughton R, Fawehinmi J & UK experts (2003) Status of UK critical loads: critical loads methods, data and maps. Report prepared under Defra/NERC contract EPG 1/3/185. <http://critloads.ceh.ac.uk>
- Hall J, Ashmore M, Curtis C, Doherty C, Langan S, Skeffington R (2001) UN/ECE expert workshop: Chemical criteria and critical limits. In: Posch et al. (2001) *op. cit.*, pp. 67-71.
- Hall J, Davies C, Moss D (2003) Harmonisation of ecosystem definitions using the EUNIS habitat classification. In: Achermann and Bobbink (2003) *op. cit.*, pp 171-195.
- Henriksen A (1984) Changes in base cation concentrations due to freshwater acidification. *Verh. Internat. Verein. Limnol.* 22: 692-698.
- Henriksen A, Lien L, Traaen TS, Sevaldrud IS, Brakke DF (1988) Lake acidification in Norway - Present and predicted chemical status. *Ambio* 17: 259-266.
- Henriksen A, Lien L, Rosseland BO, Traaen TS, Sevaldrud IS (1989) Lake acidification in Norway - Present and predicted fish status. *Ambio* 18: 314-321.
- Henriksen A, Kämäri J, Posch M, Wilander A (1992) Critical loads of acidity: Nordic surface waters. *Ambio* 21: 356-363.
- Henriksen A, Forsius M, Kämäri J, Posch M, Wilander A (1993) Exceedance of critical loads for lakes in Finland, Norway and Sweden: Reduction requirements for nitrogen and sulfur deposition. Acid Rain Research Report 32/1993, Norwegian Institute for Water Research, Oslo, Norway, 46 pp.
- Henriksen A, Posch M, Hultberg H, Lien L (1995) Critical loads of acidity for surface waters – Can the ANC_{limit} be considered variable? *Water, Air and Soil Pollution* 85: 2419-2424.
- Henriksen A, Posch M (2001) Steady-state models for calculating critical loads of acidity for surface waters. *Water, Air and Soil Pollution: Focus* 1: 375-398.
- Henriksen A, Dillon PJ (2001) Critical load of acidity in south-central Ontario, Canada: I. Application of the Steady-State Water Chemistry (SSWC) model. Acid Rain Research Report 52/01, Norwegian Institute for Water Research, Oslo, Norway, 31 pp.
- Henriksen A, Dillon PJ, Aherne J (2002) Critical loads of acidity for surface waters in south-central Ontario, Canada: Regional applications of the Steady-State Water Chemistry (SSWC) model. *Canadian Journal of Fisheries and Aquatic Sciences* 59: 1287-1295.
- Hettelingh J-P, Slootweg J, Posch M, Dutchak S, Ilyin I (2002) Preliminary modelling and mapping of critical loads of cadmium and lead in Europe. Report 259101011, CCE & EMEP MSC-East, RIVM, Bilthoven, The Netherlands, 127 pp.
- Hindar A, Posch M, Henriksen A, Gunn J, Snucins E (2000) Development and application of the FAB model to calculate critical loads of S and N for lakes in the Killarney Provincial Park (Ontario, Canada). Report SNO 4202-2000, Norwegian Institute for Water Research, Oslo, Norway, 40 pp.
- Hindar A, Posch M, Henriksen A (2001) Effects of in-lake retention of nitrogen on critical load calculations. *Water, Air and Soil Pollution* 130: 1403-1408.
- Hornung M, Sutton MA, Wilson RB (eds) (1995) Mapping and Modelling of Critical Loads for Nitrogen: A Workshop Report. Proceedings of the Grange-over-Sands Workshop 24-26 October 1994. Institute for Terrestrial Ecology, United Kingdom, 207 pp.
- Hornung M, Bull KR, Cresser M, Hall J, Langan SJ, Loveland P, Smith C (1995) An empirical map of critical loads of acidity for soils in Great Britain. *Environmental Pollution* 90: 301-310.
- Ilyin I, Ryaboshapko A, Afinogenova O, Berg T, Hjellbrekke AG (2001) Evaluation of transboundary transport of heavy metals in 1999. Trend analysis. EMEP Report 3/2001, EMEP Meteorological Synthesizing Centre - East, Moscow.

- Jacobsen C, Rademacher P, Meesenburg H, Meiwes KJ (2002) Gehalte chemischer Elemente in Baumkompartimenten, Niedersächsische Forstliche Versuchsanstalt Göttingen, im Auftrag des Bundesministeriums für Verbraucherschutz, Ernährung und Landwirtschaft (BMVEL), Bonn, 80 pp.
- Johansson M, Tarvainen T (1997) Estimation of weathering rates for critical load calculations in Finland. *Environmental Geology* 29(3/4): 158-164.
- Johnson DW, Cole DW, Gessel SP (1979) Acid precipitation and soil sulfate adsorption properties in a tropical and in a temperate forest soil. *Biotropica* 11: 38-42.
- Johnson DW, Henderson GS, Huff DD, Lindberg SE, Richter DD, Shriner DS, Todd DE, Turner J (1982) Cycling of organic and inorganic sulphur in a chestnut oak forest. *Oecologia* 54: 141-148.
- Johnson DW (1984) Sulfur cycling in forests. *Biogeochemistry* 1: 29-43.
- Joki-Heiskala P, Johansson M, Holmberg M, Mattson T, Forsius M, Kortelainen P, Hallin L (2003) Long-term base cation balances of forest mineral soils in Finland. *Water, Air and Soil Pollution* 150: 255-273.
- Kaste Ø, Dillon PJ (2003) Inorganic nitrogen retention in acid-sensitive lakes in southern Norway and southern Ontario, Canada – a comparison of mass balance data with and empirical N retention model. *Hydrological Processes* 17: 2393-2407.
- Kelly CA, Rudd JWM, Hesslein RH, Schindler DW, Dillon PJ, Driscoll CT, Gherini SA, Hecky RE (1987) Prediction of biological acid neutralization in acid-sensitive lakes. *Biogeochemistry* 3: 129-140.
- Kimmins JP, Binkley D, Chatarpaul L, De Catanzaro J (1985) Biogeochemistry of temperate forest ecosystems: Literature on inventories and dynamics of biomass and nutrients. Information Report PI-X-47E/F, Petawawa National Forestry Institute, Canada, 227 pp.
- Larssen T, Høgåsen T (2003) Critical loads and critical load exceedances in Norway (in Norwegian with English Appendix). NIVA Report 4722-2003, Norwegian Institute for Water Research, Oslo, Norway, 23 pp.
- Lien L, Raddum GG, Fjellheim A, Henriksen A (1996) A critical limit for acid neutralizing capacity in Norwegian surface waters, based on new analyses of fish and invertebrate responses. *The Science of the Total Environment* 177: 173193.
- Lofts S, Spurgeon DJ, Svendsen C, Tipping E (2003) Soil critical limits for *Cu*, *Zn*, *Cd* and *Pb*: a new free ion-based approach, *Env. Science and Technology*, accepted).
- Lydersen E, Larssen T, Fjeld E (2004) The influence of TOC on the relationship between Acid Neutralizing Capacity (ANC) and fish status in Norwegian lakes. *The Science of the Total Environment* (in press).
- Meili M (1991a) The coupling of mercury and organic matter in the biogeochemical cycle – towards a mechanistic model for the boreal forest zone. *Water, Air and Soil Pollution* 56: 333-347.
- Meili M (1991b) Mercury in boreal forest lake ecosystems. *Acta Universitatis Upsaliensis* 336, Chapter 8.
- Meili M (1994) Aqueous and biotic mercury concentrations in boreal lakes: model predictions and observations. In: CJ Watras and JW Huckabee (eds) *Mercury Pollution: Integration and Synthesis*. CRC Press, Lewis Publishers Inc., Boca Raton FL, Chapter 1.8, pp. 99-106.
- Meili M, Malm O, Guimarães JRD, Forsberg BR, Padovani CR (1996a) Mercury concentrations in tropical (Amazon) and boreal freshwater fish: natural spatial variability and pollution effects. 4th International Conference on Mercury as a Global Pollutant, Hamburg, Germany, 4–8 Aug. 1996. Book of Abstracts, GKSS, p. 403.
- Meili M (1997) Mercury in lakes and rivers. *Metal Ions in Biological Systems* 34: 21-51.
- Meili M, Bishop K, Bringmark L, Johansson K, Munthe J, Sverdrup H, De Vries W

- (2003a) Critical levels of atmospheric pollution: criteria and concepts for operational modelling of mercury in forest and lake ecosystems. *The Science of the Total Environment* 304: 83-106.
- Meili M, Åkerblom S, Bringmark L, Johansson K, Munthe J (2003b) Critical loads and limits of heavy metals in ecosystems: Some Swedish contributions to European modelling efforts, Background document presented at the Editorial Meeting of the Expert Panel on Critical Loads of Heavy Metals under UNECE-CLRTAP-ICP Modelling and Mapping, Paris, 9–10 April 2003, 22 pp. http://www.icpmapping.com/workshops/ws_berlin/sweden.pdf.
- Michalzik B, Kalbitz K, Park JH, Solinger S, Matzner E (2001) Fluxes and concentrations of dissolved organic carbon and nitrogen – a synthesis for temperate forests. *Biogeochemistry* 52: 173-205.
- Moiseenko T (1994). Acidification and critical load in surface waters: Kola, Northern Russia. *Ambio* 23: 418-424.
- Monteith JL, Unsworth M (1990) *Principles of Environmental Physics* (2nd edition). Arnold, London, 291 pp.
- Mulder J, Stein A (1994) The solubility of aluminum in acidic forest soils: long-term changes due to acid deposition. *Geochimica et Cosmochimica Acta* 58: 85-94.
- Nagel H-D, Gregor H-D (eds) (1999) *Ökologische Belastungsgrenzen – Critical Loads & Levels* (in German). Springer, Berlin, 259 pp.
- Nagel H-D, Becker R, Eitner H, Kunze F, Schlutow A, Schütze G (2000) Kartierung von Critical Loads für den Eintrag von Säure und eutrophierenden Stickstoff in Waldökosysteme und naturnahe waldfreie Ökosysteme zur Unterstützung von UNECE-Protokollen, Abschlussbericht zum Forschungsprojekt 297 73 011 im Auftrag des Umweltbundesamtes Berlin.
- NEG/ECP (2001) Protocol for Assessment and Mapping of Forest Sensitivity to Atmospheric S and N Deposition, prepared by the NEG/ECP Forest Mapping Group, New England Governors/Eastern Canadian Premiers, 'Acid Rain Action Plan 2001, Action Item 4: Forest Mapping Research Project', 79 pp.
- Nilsson J, Grennfelt P (eds) (1988) Critical Loads for Sulphur and Nitrogen. Environmental Report 1988:15 (*Nord* 1988:97), Nordic Council of Ministers, Copenhagen, 418 pp.
- Oliver BG, Thurman EM, Malcolm RL (1983) The contribution of humic substances to the acidity of colored natural waters. *Geochimica et Cosmochimica Acta* 47: 2031-2035.
- Olsson M, Rosén K, Melekrud P-A (1993) Regional modelling of base cation losses from Swedish forest soils due to whole-tree harvesting. *Applied Geochemistry*, Suppl. Issue No.2, pp. 189-194.
- Paces T (1983) Rate constants of dissolution derived from the measurements of mass balance in hydrological catchments. *Geochimica et Cosmochimica Acta* 47: 1855-1863.
- Posch M, Forsius M, Kämäri J (1993) Critical loads of sulfur and nitrogen for lakes I: Model description and estimation of uncertainty. *Water, Air and Soil Pollution* 66: 173-192.
- Posch M, Hettelingh J-P, Sverdrup HU, Bull K, De Vries W (1993) Guidelines for the computation and mapping of critical loads and exceedances of sulphur and nitrogen in Europe. In: RJ Downing, J-P Hettelingh, PAM de Smet (eds) Calculation and Mapping of Critical Loads in Europe. CCE Status Report 1993, RIVM Report 259101003, Bilthoven, The Netherlands, pp. 25-38. See also www.rivm.nl/cce
- Posch M, Kämäri J, Forsius M, Henriksen A, Wilander A (1997) Exceedance of critical loads for lakes in Finland, Norway and Sweden: Reduction requirements for acidifying nitrogen and sulfur deposition. *Environmental Management* 21(2): 291-304.
- Posch M (2000) Critical loads of acidity: Possible modifications. In: M Holmberg

- (ed) Critical Loads Calculations: Developments and Tentative Applications. TemaNord 2000:566, Nordic Council of Ministers, Copenhagen, pp.8-19.
- Posch M, De Smet PAM, Hettelingh J-P, Downing RJ (eds) (2001) Modelling and Mapping of Critical Thresholds in Europe. CCE Status Report 2001, RIVM Report 259101010, Bilthoven, Netherlands, iv+188 pp. See also www.rivm.nl/cce
- Posch M, Hettelingh J-P, Slootweg J (eds) (2003a) Manual for dynamic modelling of soil response to atmospheric deposition. RIVM Report 259101012, Bilthoven, The Netherlands, 69 pp. See also www.rivm.nl/cce
- Posch M, Reinds GJ, Slootweg J (2003b) The European background database. In: M Posch, J-P Hettelingh, J Slootweg, RJ Downing (eds) Modelling and Mapping of Critical Thresholds in Europe. CCE Status Report 2003, RIVM Report 259101013, Bilthoven, The Netherlands, pp. 37-44. See also www.rivm.nl/cce
- Reinds GJ, Posch M, De Vries W (2001) A semi-empirical dynamic soil acidification model for use in spatially explicit integrated assessment models for Europe. Alterra Report 084, Alterra Green World Research, Wageningen, The Netherlands, 55 pp.
- Reuss JO (1983) Implications of the calcium-aluminum exchange system for the effect of acid precipitation on soils. *Journal of Environmental Quality* 12(4): 591-595.
- Reuss JO, Johnson DW (1986) *Acid Deposition and the Acidification of Soils and Waters*. Ecological Studies 59, Springer, New York, 119 pp.
- Römkens PFAM, Groenenberg JE, Bril J, De Vries W (2001) Derivation of partition relationships to calculate *Cd*, *Cu*, *Pb*, *Ni* and *Zn* solubility and activity in soil solutions: an overview of experimental results. Summary of an Alterra Report.
- Rosén K (1990) The critical load of nitrogen to Swedish forest ecosystems. Department of Forest Soils, Swedish University of Agricultural Sciences, Uppsala, Sweden, 15 pp.
- Rosén K, Gundersen P, Tegnhammar L, Johansson M, Frogner T (1992) Nitrogen enrichment in Nordic forest ecosystems – The concept of critical loads. *Ambio* 21: 364-368.
- Ryaboshapko A, Ilyin I, Gusev A, Afinogenova O, Berg T, Hjellbrekke AG 1999: Monitoring and modelling of lead, cadmium and mercury transboundary transport in the atmosphere of Europe. EMEP Report 3/99, Meteorological Synthesizing Centre - East, Moscow.
- Santore RC, Driscoll CT, Aloji M (1995) A model of soil organic matter and its function in temperate forest soil development. In: WW McFee, JM Kelly (eds) *Carbon Forms and Functions in Forest Soils*. Soil Science Society of America, Madison, Wisconsin, pp.275-298.
- Sauvé S, McBride M, Hendershot W et al. (1998). Soil solution speciation of lead(II): effects of organic matter and *pH* *Soil Sci. Soc. Am. J.* , 62, 618 - 621
- Sauvé S, Norvell W, McBride, Hendershot W (2000). Speciation and complexation of cadmium in extracted soil solutions *Environ. Sci. Technol.*, 34, 291 – 296
- Schütze G, Nagel H-D (1998) Kriterien für die Erarbeitung von Immissionsminderungszielen zum Schutz der Böden und Abschätzung der langfristigen räumlichen Auswirkungen anthropogener Stoffeinträge auf die Bodenfunktionen, Abschlußbericht UBA-FKZ 104 02 825, in UBA-Texte 19/98, Umweltbundesamt, Berlin.
- Schütze G, Lorenz U, Spranger T (2003) Expert meeting on critical limits for heavy metals and methods for their application, 2–4 December 2002 in Berlin, Proceedings, UBA Texte 47/2003, Umweltbundesamt, Berlin.
- SEPA (2000) Environmental quality criteria: lakes and running waters. Swedish Environmental Protection Agency, Report 5050, 102 pp.
- Skjelkvåle BL, Ulstein M (2002) Proceedings from the workshop on heavy metals (*Pb*, *Cd*, *Hg*) in surface waters: Monitoring and

- biological impact. 18–20 March 2002, Lillehammer, Norway, ICP Waters Report 67/2002, Norwegian Institute for Water Research, NIVA, Oslo.
- Skyllberg U, Qian J, Frech W, Xia K, Bleam WF, (2003). Distribution of mercury, methyl mercury and organic sulphur species in soil, soil solution and stream of a boreal forest catchment. *Biogeochemistry* 64: 53–76.
- Sogn TA, Stuanes AO, Abrahamsen G (1999) The capacity of forest soil to absorb anthropogenic N. *Ambio* 28: 346-349.
- Steenvorden J (1984) Influence of changes in water management on water quality (in Dutch). Report 1554, Institute for Land and Water Management, Wageningen, The Netherlands.
- Sverdrup H, Warfvinge P (1988) Weathering of primary silicate minerals in the natural soil environment in relation to a chemical weathering model. *Water, Air and Soil Pollution* 38: 387-408.
- Sverdrup HU (1990) *The Kinetics of Base Cation Release due to Chemical Weathering*. Lund University Press, Lund, Sweden, 246 pp.
- Sverdrup H, De Vries W, Henriksen A (1990) Mapping Critical Loads. Environmental Report 1990:14 (NORD 1990:98), Nordic Council of Ministers, Copenhagen, 124 pp.
- Sverdrup H, Ineson P (1993) Kinetics of denitrification in forest soils. *Compuscript*, 18 pp.
- Sverdrup H, Warfvinge P (1993) The effect of soil acidification on the growth of trees, grass and herbs as expressed by the (Ca+Mg+K)/Al ratio. Reports in Ecology and Environmental Engineering 2, Lund University, Lund, Sweden, 177 pp.
- Sverdrup H, De Vries W (1994) Calculating critical loads for acidity with the simple mass balance method. *Water, Air and Soil Pollution* 72: 143-162.
- Technical Guidance Document on Risk Assessment in support of Commission Regulation (EC) No 1488/94 on Risk Assessment for existing substances, TGD
- European Chemicals Bureau, Institute for Health and Consumer Protection, European Commission Joint Research Centre
- Tippling E (1994) WHAM – A chemical equilibrium model and computer code for waters, sediments, and soils incorporating a discrete site/electrostatic model of ion-binding by humic substances. *Computers & Geosciences* 20(6): 973-1023.
- Tippling E (1998) Humic ion-binding Model IV: an improved description of the interactions of protons and metal ions with humic substances. *Aquatic Geochemistry* 4: 3-48.
- Tippling E, Lofts S, Smith EJ, Shotbolt L, Ashmore MR, Spurgeon D, Svendsen C (2003a) Information and proposed methodology for determining critical loads of cadmium and lead; a UK contribution. Background document presented at the Editorial Meeting of the Expert Panel on Critical Loads of Heavy Metals under ICP Modelling and Mapping, Paris, 9–10 April 2003.
- Tippling E, Rieuwerts J, Pan G, Ashmore MR, Lofts S, Hill MTR, Farrago ME, Thornton I (2003b) The solid-solution partitioning of heavy metals (*Cu, Zn, Cd, Pb*) in upland soils of England and Wales. *Environmental Pollution* 125: 213-225.
- UBA (1996) Manual on Methodologies and Criteria for Mapping Critical Levels/Loads and Geographical Areas where they are exceeded. UNECE Convention on Long-range Transboundary Air Pollution, Federal Environmental Agency, Berlin.
- UNECE (1995) Calculation of critical loads of nitrogen as a nutrient. Summary report on the development of a library of default values. Document EB.AIR/WG.1/R.108, United Nations Economic Commission for Europe, Geneva, 7 pp.
- UNECE (2001) Workshop on chemical criteria and critical limits. Document EB.AIR/WG.1/2001/13, United Nations Economic Commission for Europe, Geneva, 8 pp.

- Ulrich B, Sumner ME (eds) (1991) *Soil Acidity*. Springer, Berlin, 224 pp.
- Utermann J, Duewel O, Gaebler H-E, Hindel R (2000) Beziehung zwischen Totalgehalten und königswasser-extrahierbaren Gehalten von Schwermetallen in Böden. In: Rosenkranz D, Einsele G, Bachmann G, Harreß M (Eds): *Handbuch Bodenschutz, Loseblattsammlung*, Erich Schmidt-Verlag, Berlin, Kennzahl 1600.
- Van Dam D (1990) Atmospheric deposition and nutrient cycling in chalk grassland. PhD Thesis, University of Utrecht, Utrecht, The Netherlands, 119 pp.
- Van der Salm C, Köhlenberg L, De Vries W (1998) Assessment of weathering rates in Dutch loess and river-clay soils at *pH* 3.5, using laboratory experiments. *Geoderma* 85: 41-62.
- Van der Salm C, De Vries W (2001) A review of the calculation procedure for critical acid loads for terrestrial ecosystems. *The Science of the Total Environment* 271: 11-25.
- Verta M, Rekolainen S, Mannio J, Surma-Aho K (1986) The origin and level of mercury in Finnish forest lakes. Finnish National Board of Waters, Helsinki, Publications of the Water Research Institute 65: 21-31.
- Walther B (1998) Development of a process-based model to derive methane emissions from natural wetlands for climate studies. Dissertation im Fachbereich Geowissenschaften der Universität Hamburg, Examensarbeit Nr. 60, Max-Planck-Institut für Meteorologie, Hamburg.
- Warfvinge P, Sverdrup H (1992) Calculating critical loads of acid deposition with PRO-FILE - A steady-state soil chemistry model. *Water, Air and Soil Pollution* 63: 119-143. See also www2.chemeng.lth.se
- Warfvinge P, Sverdrup H (1995) Critical loads of acidity to Swedish forest soils. Reports in Ecology and Environmental Engineering 5, Lund University, Lund, Sweden, 104 pp.
- Weng LP, Temminghoff EJM, Lofts S, Tipping E, Van Riemsdijk WH (2002) Environ. Complexation with dissolved organic matter and solubility control of metals in a sandy soil. *Sci. Technol.* 36, 4804-4810
- WHO (2000) *Air Quality Guidelines for Europe, Second Edition*. WHO Regional Publications, European Series, No. 91. World Health Organisation, Regional Office for Europe, Copenhagen, 273 pp.
- WHO (2004): *Guidelines for Drinking Water Quality - Third Edition, Vol. 1 - Recommendations*, World Health Organisation, Geneva.
- Wilander A (1994) Estimation of background sulphate concentrations in natural surface waters in Sweden. *Water Air and Soil Pollution* 75: 371-387.
- Witkamp M (1966) Decomposition of leaf litter in relation to environment, microflora, and microbial respiration. *Ecology* 47(2): 194-201.
- Wright RF, Lie MC (eds) (2002) Workshop on models for biological recovery from acidification in a changing climate, 9-11 September 2002 in Grimstad, Norway. Acid Rain Research Report 55/02, Norwegian Institute for Water Research (NIVA), Oslo, Norway, 42 pp.
- Závodský D, Babiaková G, Mitosinková M, Pukančíková K, Roneák P, Bodis D, Rapant S, Mindás J, Skvarenina J, Cambel B, Rehák S, Wathne BM, Henriksen A, Sverdrup H, Tørseth K, Semb A, Aamlid D (1995) Mapping critical level/loads for the Slovak Republic. Acid Rain Research Report 37/1995. Norwegian Institute for Water Research (NIVA), Oslo, Norway, 74 pp.

Annex 1: Transfer functions for lead and cadmium for the conversion of metal concentrations in different soil phases

Need of transfer functions in deriving critical dissolved metal concentrations

In principle, transfer functions are not needed in performing a critical load calculation. Transfer functions have been used to derive critical limits for free metal ion concentrations from NOEC data, referring to reactive soil metal contents. When applying critical limits for free metal ion concentrations, related to ecotoxicological effects, no transfer function is needed any more, since $[M]_{(sdw)crit}$ can be obtained directly, either by reference to the look up tables or by use of the W6S-MTC2 program (see Section 5.5.2.2.3). In case of ground water protection, total dissolved critical concentrations can be used directly (see Section 5.5.2.2.2). In the case of using critical limits referring to the metal content in plants, an empirical relationship can be used to derive total dissolved critical concentrations in soil solution, at least for *Cd* (See Table 4).

Using the more sophisticated and consistent way to derive soil solution concentrations from critical plant contents does however require transfer functions according to the following:

- first derive a critical “pseudo” total soil metal content, by applying soil–plant relationships in the inverse way (derive a critical total soil content from a critical plant content)
- then apply a transfer function relating pseudo- total metal contents to reactive metal contents (Annex 1, eq. A1.3).
- followed by a transfer function relating the free ion metal activity in solution to the reactive metal content (Annex 1, eq. A1.4 or eq. A1.5).

Furthermore, all the transfer functions listed

below are needed for the calculation of a critical soil limit (from a given critical limit function for the soil solution) and to compare this to the present soil metal content to assess the critical limit exceedance in the present situation. This requires a map of the present soil metal content in the country. Inversely, one may calculate the present dissolved metal concentration from the present soil metal content, using the transfer functions described below and compare this to the critical limit function for the soil solution (see section 5.5.1.4).

Transfer functions to calculate pseudo-total from total contents of Cd and Pb

In some countries true total metal concentrations are measured, whereas most or nearly all countries use “pseudo-total” concentrations. Utermann et al. (2000) provided transfer functions to calculate *pseudo-total* contents of heavy metals (here aqua regia extract $[M]_{AR}$) from total contents (here $[M]_{HF}$), according to:

(A1.1)

$$\log_{10}[M]_{AR} = a_0 + a_1 \cdot \log_{10}[M]_{HF}$$

where:

$[M]_{HF}$ = total content of heavy metal *M* in soil, provided as *HF*-extraction ($mg\ kg^{-1}$)

$[M]_{AR}$ = *pseudo-total* content of heavy metal *M* in soil provided as Aqua Regia extraction ($mg\ kg^{-1}$)

Values for a_0 and a_1 are given in Tables A1.1 and A1.2. The correlations are depending on metal and substrate. In general, total and *pseudo-total* contents are very similar. For back-calculations of total contents from *pseudo-total* contents, different functions are to be used (see background document, De Vries et al 2004b, Annex 7). These functions are not provided here, since those calculations are not needed in the present calculation of critical loads.

5 Mapping Critical Loads

Table A1.1: Relationship between cadmium (*Cd*) content in soils extractable by aqua regia (*AR*) and total contents in dependence on the parent material.

parent material	a ₀	a ₁	n	R ²	range of validity Cd (HF) (mg kg ⁻¹)	
basic and intermediate igneous rock	0.13	1.41	25	0,94	0,25	1,12
boulder clay	0.09	1.38	26	0.91	0.07	0.39
limestone	-0.15	1.24	25	0.91	0.26	1.86
loess or loessic loam	-0.15	1.26	25	0.91	0.07	0.88
marl stone	-0.05	1.24	25	0.93	0.10	0.98
sand	-0.02	1.26	37	0.89	0.04	0.65
sandy loess	0.29	1.78	36	0.82	0.06	0.29
acid igneous and metamorphic rock	-0.09	1.08	25	0.80	0.09	0.63
quartzitic sand stones and conglomerates	-0.11	1.23	25	0.81	0.07	0.60
clay stone, hard argillaceous and silty slates	-0.05	1.33	25	0.96	0.14	1.88
all parent materials	-0.12	1.19	274	0.91	0.04	1.88

Table A1.2: Relationship between lead (*Pb*) content in soils extractable by aqua regia (*AR*) and total contents extractable by *HF* in dependence on the parent material.

parent material	a ₀	a ₁	n	R ²	range of validity Pb (HF) (mg kg ⁻¹)	
basic and intermediate igneous rock	-0.20	1.11	25	0.97	5.6	113.6
boulder clay	-0.54	1.32	26	0.95	8.3	49.5
limestone	-0.02	0.99	22	0.88	24.8	132.7
loess or loessic loam	-0.42	1.22	24	0.91	15.1	91.8
marl stone	-0.03	0.95	25	0.94	5.5	124.0
sand	-0.54	1.31	49	0.91	2.7	76.7
sandy loess	-0.72?	1.46	43	0.97	6.0	75.9
acid igneous and metamorphic rock	-0.84	1.44	25	0.84	14.6	106.1
quartzitic sand stones and conglomerates	-0.55	1.28	25	0.88	12.6	109.2
clay stone, hard argillaceous and silty slates	-0.11	1.05	25	0.98	13.9	270.3
all parent materials	-0.45	1.24	289	0.95	2.7	270.3

Transfer functions to calculate reactive contents from pseudo-total contents of *Cd* and *Pb*

The reactive metal concentration $[M]_{re}$ (mol kg⁻¹) can be related to the pseudo-total concentration extracted with Aqua Regia $[M]_{AR}$ (mol kg⁻¹) according to:

$$(A1.3) \quad \log[M]_{re} = \beta_0 + \beta_1 \cdot \log[M]_{AR} + \beta_2 \cdot \log(\%[OM]_s) + \beta_3 \cdot \log(\%[clay])$$

Regression relations were derived from a Dutch dataset containing 630 soil samples which were both extracted with 0.43 Mol l⁻¹ HNO₃ and Aqua Regia. The dataset consists of large variety of soil types with a wide variety in soil properties such as the organic matter and clay content. The dataset comprises both polluted and unpolluted soils. Results are shown in Table A1.3 and suggest that reactive contents typically are more than half of pseudo-total contents.

Table A1.2: Relationship between lead (*Pb*) content in soils extractable by aqua regia (*AR*) and total contents extractable by *HF* in dependence on the parent material.

Metal	β_0	β_1	β_2	β_3	R^2	se-yest ¹⁾
Cd	0.225	1.075	0.006	-0.020	0.82	0.26
Pb	0.063	1.042	0.024	-0.122	0.88	0.17

¹⁾ The standard error of the y-estimate on a logarithmic basis

Transfer functions to calculate free *Cd* and *Pb* ion concentrations from reactive *Cd* and *Pb* contents used in the derivation of critical limits for free *Cd* and *Pb* ion concentrations

Critical concentrations of soil metal are frequently higher than ambient soil concentrations. Therefore, a transfer function should if possible be calibrated over a range of soil metal concentrations which is the whole range of critical receptor concentrations observed. This is relevant since the derived critical limit functions are dependent upon the transfer functions.

For calibration of direct transfer functions for *Cd* and *Pb*, data were drawn from four sources:

- Sauvé et al. (1998). Soil metal and labile *Pb* in *Pb*-contaminated soils of various origins. Free *Pb* concentrations were estimated by measurement of labile *Pb* using differential pulse anodic stripping voltammetry (DPASV) and speciation calculations.
- Sauvé et al. (2000). Soil metal and labile *Cd* in *Cd*-contaminated soils of various origins. Free *Cd* concentrations were estimated by measurement of labile *Cd* using differential pulse anodic stripping voltammetry (DPASV) and speciation calculations.
- Weng et al. (2002). Soil metal and free ion concentrations in sandy Dutch soils.

Free *Cd* and *Pb* concentrations were estimated by the Donnan membrane technique.

-Tipping et al. (2003a). Soil metal and free ion concentrations in UK upland soils. Free *Cd* and *Pb* were estimated by using the WHAM6 speciation model (Tipping, 1998) to speciate the soil solution.

The data were fitted to the following transfer function (termed as c-Q relationship:

$$(A1.4) \quad \log[M]_{\text{free, sdw}} = a + b \cdot \log[OM]_s + c \cdot \text{pH}_{\text{sdw}} + m \cdot \log[M]_{\text{re}}$$

where:

- $[M]_{\text{free, sdw}}$ = the free metal ion concentration (mol l^{-1})
- $[M]_{\text{re}}$ = the reactive metal content in the solid phase (mol l^{-1})
- $[OM]_s$ = organic matter (%)
- pH_{sdw} = soil drainage water *pH*

Calculated values of the parameters are given in Table A1.4.

Table A1.4: Values for the regression coefficients for the free ion concentration - reactive metal content relationship (eq. A1.4) and statistical measures R^2 and $se(Y)$ based on results of studies carried out in Canada, the Netherlands and the UK. Values in brackets are the standard errors for the coefficients.

Metal	a	b	c	m	R^2	se(Y)
		(OM) _s	(pH) _{sdw}	($\log[M]_{\text{re}}$)		
Cd	-0.08 (0.65)	-0.60 (0.08)	-0.53 (0.03)	0.60 (0.06)	0.624	0.53
Pb	4.32 (0.49)	-0.69 (0.07)	-1.02 (0.03)	1.05 (0.06)	0.854	0.60

5 Mapping Critical Loads

Transfer functions to calculate reactive Cd and Pb contents from free Cd and Pb ion concentrations used in the derivation of critical Cd and Pb contents on suspended particles in aquatic ecosystems

This transfer function (termed as Q-c relationship) has been derived using the same soil data set used to calculate the transfer function relating the free ion to the soil reactive metal (See Table A1.4). The expression for the Q-c relation is:

$$(A1.5) \quad \log[M]_{re} = a + b \cdot \log[OM]_s + c \cdot pH_{sw} + m \cdot \log[M]_{free,sw}$$

where:

$[M]_{free,sw}$ = the free metal ion concentration in surface water ($mol\ l^{-1}$)

$[M]_{re}$ = the reactive metal content in the solid phase ($mol\ l^{-1}$)

$[OM]_s$ = organic matter (%), here the organic matter content of the suspended particles

pH_{sw} = the pH of the surface water

Calculated values of the parameters are given in Table A1.5.

Use of transfer functions in the manual

The direct transfer function for the calculation of the free ion concentration from the soil reactive metal content (the c-Q relation) is used for the calculation of the pH -dependent critical limit functions (see Section 5.5.2.2.3), in order to express the endpoint metal dose in toxicity experiments as the free ion concentration. The transfer function for the calculation of the soil reactive metal content from the free metal ion concentration (the Q-c relation) is used to calculate the critical SPM -bound metal ($[M]_{SPM(crit)}$) in surface waters (see Section 5.5.2.2.3 and Annex 2).

Table A1.5: Values for the regression coefficients for the reactive metal content - free ion concentration relationship (eq. 8) and statistical measures R^2 and $se(Y)$ based on results of studies carried out in Canada, the Netherlands and the UK. Values in brackets are the standard errors for the coefficients.

Metal	a	b ($[OM]_s$)	c (pH_{sw})	m ($\log[M]_{free,sw}$)	R^2	$se(Y)$
Cd	-6.42 (0.41)	0.64 (0.07)	0.45 (0.04)	0.58 (0.06)	0.507	0.52
Pb	-5.42 (0.21)	0.55 (0.06)	0.70 (0.03)	0.61 (0.03)	0.698	0.45

Annex 2: Calculation of total metal concentration from free metal ion concentrations using the WHAM model

The metal in soil drainage water comprises the following metal species

Metal species	Symbol
Metal free ion M^{2+}	$[M]_{free, sdw}$
Inorganic complexes MOH^+ , $MHCO_3^+$, MCl^+ etc	$[M]_{DIC, sdw}$
Metal bound to DOM	$[M]_{DOM, sdw}$
Metal bound to SPM	$[M]_{SPM, sdw}$

Here, DOM is dissolved organic matter, and SPM is suspended particulate matter. The total concentration of metal in soil drainage water does not refer simply to dissolved components ($[M]_{free, sdw}$, $[M]_{DIC, sdw}$, and $[M]_{DOM, sdw}$), but also includes $[M]_{SPM, sdw}$. Data on SPM concentration in soil drainage waters may be scarce, and in many cases the contribution of SPM to the metal leaching is only small. Thus this flux can be neglected preliminarily. The calculation model includes, however, the possibility of metal being leached from the soil in association with particulates.

Given the activity or concentration of M^{2+} , the concentrations of the other metal species can be estimated by applying an equilibrium speciation model. The calculation has to take into account the dependence of the metal speciation on pH and competitive effects due to major cationic species of Mg , Al , Ca and Fe . For this purpose a custom version of the Windermere Humic Aqueous Model version 6 (WHAM6; Tipping 1998) speciation model, termed W6S MTC2, has been produced. A more detailed description of the model calculation steps is given in the background document (De Vries et al. 2004b). NFCs may calculate critical dissolved metal concentrations from the free ion concentration by one of three methods:

1. Linear interpolation in the look-up tables (chapter 5.5.2.2.3). The look-up tables list critical dissolved metal concentrations (calculated using W6S-MTC2) for various combinations of pH , concentrations of soil organic matter, dissolved organic carbon ($[DOC]_{sdw}$) and suspended particulate matter (SPM) and partial CO_2 pressure (pCO_2).
2. Sending suitably formatted files to the Centre for Ecology & Hydrology (CEH), Lancaster, Ed Tipping (ET@CEH.AC.UK), who will perform the computations with W6S-MTC2. Instructions for preparing suitably formatted files for this purpose are given below.
3. Using the W6S-MTC2 program themselves. Instructions for use are given with the program, which can be obtained by contacting Ed Tipping (see above).

NFCs that wish values of $M_{tot, sdw(crit)}$ to be calculated by should submit files to the CEH Lancaster, Ed Tipping (ET@CEH.AC.UK). The data should simply be entered into an Excel workbook, under the following headings.

code	pH	% OM	pCO ₂	DOC	SPM
------	----	------	------------------	-----	-----

<i>code</i>	the user's identifier of the site
<i>pH</i>	soil solution <i>pH</i>
<i>% OM</i>	the soil organic matter content
<i>pCO₂</i>	the soil <i>pCO₂</i> expressed as a multiple of the atmospheric value
<i>DOC</i>	concentration of dissolved organic carbon in $mg\ l^{-1}$
<i>SPM</i>	concentration of suspended particulate matter in $mg\ l^{-1}$.

- Please see the background document (Annex 8 and 9) regarding the selection of pH and pCO_2 values. If data on DOC concentration are not available, a standard value of $20\ mg\ l^{-1}$ will be assumed.

5 Mapping Critical Loads

- If data on pCO_2 are not available, a value of 15 x atmospheric will be assumed.
- If data on SPM are not available, a value of zero will be assumed.

Please note that it is necessary to recalculate values of soil pH (measured in KCl , $CaCl_2$, H_2O) to soil solution pH , as mentioned in the main text, before applying the look-up tables or creating input files for W6S-MTC2.

Annex 3: Calculation of the critical total aqueous concentration from the critical dissolved concentration using the WHAM model

The calculation of the critical total aqueous concentration comprises the following steps:

1. Estimate the critical free metal ion concentration from the critical dissolved concentration.
2. Calculate the metal bound per unit mass of *SPM*.
3. Sum the total dissolved and particulate concentrations.

Step 1

The free ion concentrations are calculated using WHAM6, for waters of different *pH*, *DOC* and *pCO₂*, making the same assumptions as are used for calculating total metal from free-ion critical limits (for the Look Up Tables). In the calculations the critical dissolved concentrations used were 0.38 *mg m⁻³* for *Cd* and 11 *mg m⁻³* for *Pb*. Note that, here, all waters are assumed to be “normal” with respect to dissolved *Al* (i.e. acid bog-waters are not included).

The free ion activities calculated with WHAM6 can be expressed in terms of multiple regression equations at different *pH* values. Thus;

$$(A3.1) \quad \log [M^{2+}] = A \log_{10} [DOC]_{sw} + B \log_{10} pCO_2 + C$$

where:

$[DOC]_{sw}$ is in *mg l⁻¹* and *pCO₂* is a multiple of the atmospheric *pCO₂*. The regression coefficients are given in Tables A3.1 and A3.2. Linear interpolation can be performed to obtain coefficients for intermediate *pH* values.

Table A3.1: Regression coefficients for estimating free *Cd²⁺* concentrations

pH	A	B	C
4	-0.006	-0.0001	-8.50
5	-0.075	-0.0006	-8.48
6	-0.402	0.0396	-8.49
7	-0.559	0.2171	-8.62
8	-0.304	-0.0881	-8.74
9	-0.014	-0.7092	-9.52

Table A3.2: Regression coefficients for estimating free *Pb²⁺* concentrations

pH	A	B	C
4	-0.028	0.0000	-7.31
5	-0.339	0.0004	-7.29
6	-0.869	0.0591	-7.68
7	-1.113	0.2572	-8.77
8	-1.040	0.3491	-9.78
9	-0.222	-1.2027	-11.00

Step 2

The critical *SPM*-bound metal ($[M]_{SPM,sw(crit)}$, *mol g⁻¹*) is calculated using the Q-c relations derived in Annex 1, eq. A1.5 (Table A1.5). Before proceeding to Step 3 $[M]_{SPM,sw(crit)}$ must be converted to units of *mg kg⁻¹*:

$$(A3.2a) \quad [Cd]_{SPM,sw(crit)} (mg \text{ kg}^{-1}) = [Cd]_{SPM,sw(crit)} (mol \text{ g}^{-1}) \times (1.124 \times 10^8)$$

$$(A3.2b) \quad [Pb]_{SPM,sw(crit)} (mg \text{ kg}^{-1}) = [Pb]_{SPM,sw(crit)} (mol \text{ g}^{-1}) \times (2.072 \times 10^8)$$

Step 3

The total aqueous metal at the critical limit is given by:

$$(A3.3) \quad [M]_{tot, sw(crit)} = [M]_{dis,sw(crit)} + [M]_{SPM,sw(crit)} \times [SPM]_{sw}$$

where:

$[M]_{dis,sw(crit)}$ is the critical dissolved concentration (*mg m⁻³* or *μg l⁻¹*) (Table 10), $[M]_{SPM,sw(crit)}$ is the critical concentration

bound to *SPM* calculated in Step 2 ($mg\ kg^{-1}$), and $[SPM]_{sw}$ is the concentration of *SPM* in the surface water ($kg\ m^{-3}$ or $g\ l^{-1}$).

Calculation examples

For a water of *pH* 6 with $[DOC] = 8\ mg\ l^{-1}$ a pCO_2 four times the atmospheric value and $[SPM]_{sw} = 0.050\ g\ l^{-1}$ ($50\ mg\ l^{-1}$) with 20% organic matter content:

(A3.4)

$$\begin{aligned} [Cd]_{tot, sw(crit)} &= 0.38\ \mu g\ l^{-1} + 0.057\ \mu g\ l^{-1} \\ &= 0.44\ \mu g\ l^{-1} \end{aligned}$$

and

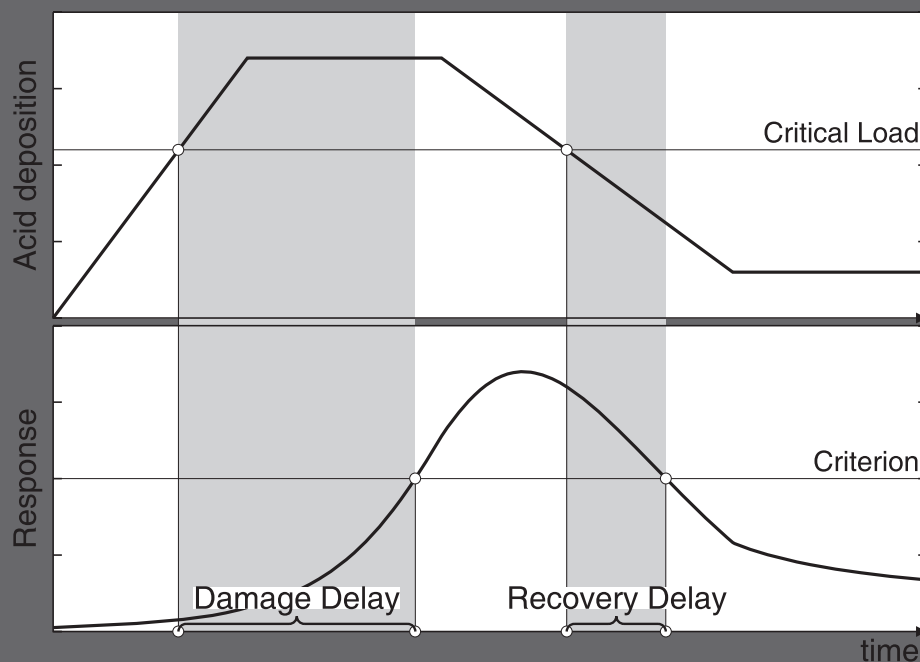
(A3.5)

$$\begin{aligned} [Pb]_{tot, sw(crit)} &= 11\ \mu g\ l^{-1} + 23.7\ \mu g\ l^{-1} \\ &= 33.7\ \mu g\ l^{-1} \end{aligned}$$

using the critical limits listed in Table 7 for the critical limits recommended for the call for data 2004.

An update of this annex will be made soon by applying critical *Cd* limits as a function of water hardness and applying a critical *Pb* limit of $5\ mg\ m^{-3}$.

Mapping Manual 2004



Chapter 6 is an updated version of the Manual for Dynamic Modelling of Soil Response to Atmospheric Deposition, compiled and published by the Coordination Center of Effects in 2003. It has been re-edited by M. Posch and benefited from suggestions made by J. Aherne (Trent University, Ontario, Canada).

6.1 Introduction

Dynamic modelling is the logical extension of critical loads. Critical loads are based on a steady-state concept, they are the constant depositions an ecosystem can tolerate in the long run, i.e., after it has equilibrated with these depositions. However, many ecosystems are not in equilibrium with present or projected depositions, since there are processes ('buffer mechanisms') at work, which delay the reaching of an equilibrium (steady state) for years, decades or even centuries. By definition, critical loads do not provide any information on these time scales. Dynamic models are needed to assess time delays of recovery in regions where critical loads cease being exceeded and time delays of damage in regions where critical loads continue to be exceeded.

The purpose of this Chapter is to explain the use (and constraints) of dynamic modelling in support of the effects-oriented work under the LRTAP Convention. This Chapter is a shortened and updated version of a 'Dynamic Modelling Manual' published earlier by the CCE (Posch et al. 2003).

For the sake of simplicity and in order to avoid the somewhat vague term 'ecosystem', we refer in the sequel to non-calcareous (forest) soils. However, most of the considerations hold for surface water systems as well, since their water quality is strongly influenced by properties of and processes in catchment soils. A separate report dealing with the dynamic modelling of surface waters on a regional scale has been prepared under the auspices of the ICP Waters (Jenkins et al. 2002).

6.1.1 Why dynamic modelling?

In the causal chain from deposition of strong acids to damage to key indicator organisms there are two major links that can give rise to delays. Biogeochemical processes can delay the chemical response in soil, and biological processes can further delay the response of indicator organisms, such as damage to trees in forest ecosystems. The static models to determine critical loads

consider only the steady-state condition, in which the chemical and biological response to a (new) (constant) deposition is complete. Dynamic models, on the other hand, attempt to estimate the time required for a new (steady) state to be achieved.

With critical loads, i.e. in the steady-state situation, only two cases can be distinguished when comparing them to deposition: (1) the deposition is below critical load(s), i.e. does not exceed critical loads, and (2) the deposition is greater than critical load(s), i.e. there is critical load exceedance. In the first case there is no (apparent) problem, i.e. no reduction in deposition is deemed necessary. In the second case there is, by definition, an increased risk of damage to the ecosystem. Thus a critical load serves as a warning as long as there is exceedance, since it states that deposition should be reduced. However, it is often assumed that reducing deposition to (or below) critical loads immediately removes the risk of 'harmful effects', i.e. the chemical criterion (e.g. the Al/Bc -ratio¹) that links the critical load to the (biological) effect(s), immediately attains a non-critical ('safe') value, and that there is immediate biological recovery as well. But the reaction of soils, especially their solid phase, to changes in deposition is delayed by (finite) buffers, the most important being the cation exchange capacity (CEC). These buffer mechanisms can delay the attainment of a critical chemical parameter, and it might take decades or even centuries, before an equilibrium (steady state) is reached. These finite buffers are not included in the critical load formulation, since they do not influence the steady state, but only the time to reach it. Therefore, dynamic models are needed to estimate the times involved in attaining a certain chemical state in response to deposition scenarios, e.g. the consequences of 'gap closures' in emission reduction negotiations. In addition to the delay in chemical recovery, there is likely to be a further delay before the 'original' biological state is reached, i.e. even if the chemical criterion is met (e.g. $Al/Bc < 1$), it will take time before biological recovery is achieved.

¹ In Chapter 5 (and elsewhere) the Bc/Al -ratio is used. However, this ratio becomes infinite when the Al concentration approaches zero. To avoid this inconvenience, its inverse, the Al/Bc -ratio, is used here.

Figure 6.1 summarises the possible development of a (soil) chemical and biological variable in response to a 'typical' temporal deposition pattern. Five stages can be distinguished:

Stage 1: Deposition was and is below the critical load (CL) and the chemical and biological variables do not violate their respective criteria. As long as deposition stays below the CL , this is the 'ideal' situation.

Stage 2: Deposition is above the CL , but (chemical and) biological criteria are not violated because there is a time delay before this happens. No damage is likely to occur at this stage, therefore, despite exceedance of the CL . The time between the first exceedance of the CL and the first violation of the biological criterion (the first occurrence of actual damage) is termed the *Damage Delay Time* ($DDT=t_3-t_1$).

Stage 3: The deposition is above the CL and both the chemical and biological criteria are violated. Measures (emission reductions) have to be taken to avoid a (further) deterioration of the ecosystem status.

Stage 4: Deposition is below the CL , but the (chemical and) biological criteria are

still violated and thus recovery has not yet occurred. The time between the first non-exceedance of the CL and the subsequent non-violation of both criteria is termed the *Recovery Delay Time* ($RDT=t_6-t_4$).

Stage 5: Deposition is below the CL and both criteria are no longer violated. This stage is similar to Stage 1 and only at this stage can the ecosystem be considered to have recovered.

Stages 2 and 4 can be subdivided into two sub-stages each: Chemical delay times ($DDT_c=t_2-t_1$ and $RDT_c=t_5-t_4$; dark grey in Figure 6.1) and (additional) biological delay times ($DDT_b=t_3-t_2$ and $RDT_b=t_6-t_5$; light grey). Very often, due to the lack of operational biological response models, damage and recovery delay times mostly refer to chemical recovery alone and this is used as a surrogate for overall recovery. It is also important to note that recovery does not follow the same, (inverse) path of damage, since there is a so-called hysteresis in these natural systems (see, e.g., Warfvinge et al. 1992).

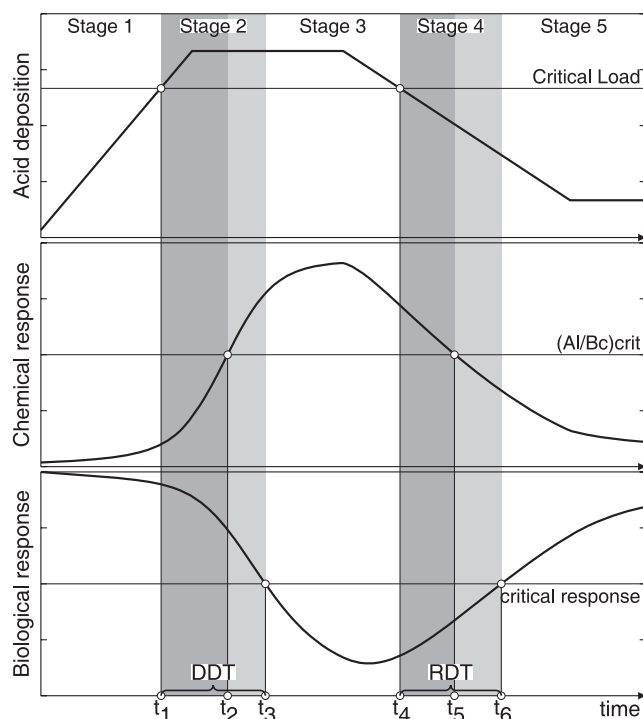


Figure 6.1: 'Typical' past and future development of the acid deposition effects on a soil chemical variable (AI/Bc-ratio) and the corresponding biological response in comparison to the critical values of those variables and the critical load derived from them. The delay between the (non)exceedance of the critical load, the (non)violation of the critical chemical criterion and the crossing of the critical biological response is indicated in grey shades, highlighting the *Damage Delay Time* (DDT) and the *Recovery Delay Time* (RDT) of the system.

6.1.2 Constraints for dynamic modelling under the LRTAP Convention

Steady-state models (critical loads) have been used to negotiate emission reductions in Europe. In this context, an emission reduction is judged successful if non-exceedance of critical loads is attained. To gain insight into the time delay between the attainment of non-exceedance and actual chemical (and biological) recovery, dynamic models are needed. Thus if dynamic models are to be used to assess recovery under the LRTAP Convention, they should be compatible with the steady-state models used for calculating critical loads. In other words, when critical loads are used as input to the dynamic model, the (chemical) parameter chosen as the criterion in the critical load calculation has to attain the critical value (after the dynamic simulation has reached steady state). But this also means that concepts and equations used in the dynamic model have to be an extension of the concepts and equations employed in deriving the steady-state model. For example, if critical loads are calculated with the Simple Mass Balance (SMB) model (see Chapter 5), this model should be the steady-state version of the dynamic model used (e.g., the VSD model, see below).

Due to a lack of (additional) data, it may be impossible to run dynamic models on all sites in a country for which critical loads have been calculated. The selection of the subset of sites, at which dynamic models are applied, has to be representative enough to allow comparison with results obtained with critical loads.

6.2 Basic Concepts and Equations

Dynamic models of acidification are based on the same principles as steady-state models: The charge balance of the ions in the soil solution, mass balances of the various ions, and equilibrium equations. However, whereas in steady-state models only infinite sources and sinks are considered (such as base cation weathering), the inclusion of the

finite sources and sinks of major ions into dynamic models is crucial, since they determine the long-term (slow) changes in soil (solution) chemistry. The three most important processes involving finite buffers and time-dependent sources/sinks are cation exchange, nitrogen retention and sulphate adsorption.

A short description of the models mentioned in this section, such as VSD, MAGIC, SAFE and SMART, can be found in Section 6.3.

6.2.1 Charge and mass balances

As mentioned above, we consider as 'ecosystem' non-calcareous forest soils, although most of the considerations hold also for non-calcareous soils covered by (semi-)natural vegetation. Since we are interested in applications on a large regional scale (for which data are scarce) and long time horizons (decades to centuries with a time step of one year), we make the same simplifying assumption as for the SMB model (see Chapter 5). We assume that the soil is a single homogeneous compartment and its depth is equal to the root zone. This implies that internal soil processes (such as weathering and uptake) are evenly distributed over the soil profile, and all physico-chemical constants are assumed uniform in the whole profile. Furthermore we assume the simplest possible hydrology: The water leaving the root zone is equal to precipitation minus evapotranspiration; more precisely, percolation is constant through the soil profile and occurs only vertically.

As for the SMB model, the starting point is the charge balance of the major ions in the soil water, leaching from the root zone (cf. eq.5.9):

$$(6.1) \quad \begin{aligned} SO_{4,le} + NO_{3,le} - NH_{4,le} - BC_{le} + Cl_{le} &= H_{le} \\ + Al_{le} - HCO_{3,le} - RCOO_{le} &= -ANC_{le} \end{aligned}$$

where $BC = Ca + Mg + K + Na$ and $RCOO$ stands for the sum of organic anions. Eq. 6.1 also defines the acid neutralising capacity, ANC .

The leaching term is given by $X_{le} = Q \cdot [X]$ where $[X]$ is the soil solution concentration (eq/m³) of ion X and Q (m/yr) is the water leaving the root zone.

The concentrations $[X]$ of an ion in the soil compartment, and thus its leaching X_{le} , are either obtained from equilibrium equations with $[H]$, such as $[Al]$, $[HCO_3]$ and $[RCOO]$ (see eqs. 5.42, 5.43 and 5.45), or from mass balance equations. The latter describe the change over time of the total amount of ion X per unit area in the soil matrix/soil solution, X_{tot} (eq/m²):

$$(6.2) \quad \frac{d}{dt} X_{tot} = X_{in} - X_{le}$$

where X_{in} (eq/m²/yr) is the net input of ion X (sources minus sinks, except leaching).

With the simplifying assumptions used in the derivation of the SMB model, the net input of sulphate and chloride is given by their respective deposition:

$$(6.3) \quad SO_{4,in} = S_{dep} \quad \text{and} \quad Cl_{in} = Cl_{dep}$$

For base cations the net input is given by (Bc=Ca+Mg+K):

$$(6.4) \quad BC_{in} = BC_{dep} + BC_w - BC_u$$

where the subscripts *dep*, *w* and *u* stand for deposition, weathering and net uptake, respectively. Note, that S adsorption and cation exchange reactions are not included here, they are included in X_{tot} and described by equilibrium equations (see below). For nitrate and ammonium the net input is given by:

$$(6.5) \quad NO_{3,in} = NO_{x,dep} + NH_{4,ni} - NO_{3,i} - NO_{3,u} - NO_{3,de}$$

$$(6.6) \quad NH_{4,in} = NH_{3,dep} - NH_{4,ni} - NH_{4,i} - NH_{4,u}$$

where the subscripts *ni*, *i* and *de* stand for nitrification, net immobilisation and denitrification, respectively. In the case of complete nitrification one has $NH_{4,in} = 0$ and the net input of nitrogen is given by:

$$(6.7) \quad NO_{3,in} = N_{in} = N_{dep} - N_i - N_u - N_{de}$$

6.2.2 From steady state (critical loads) to dynamic models

Steady state means there is no change over time in the total amounts of ions involved, i.e. (see eq.6.2):

$$(6.8) \quad \frac{d}{dt} X_{tot} = 0 \quad \Rightarrow \quad X_{le} = X_{in}$$

From eq.6.7 the critical load of nutrient nitrogen, $CL_{nut}(N)$, is obtained by specifying an acceptable N -leaching, $N_{le,acc}$. By specifying a critical leaching of ANC , $ANC_{le,crit}$, and inserting eqs. 6.3, 6.4 and 6.7 into the charge balance (eq. 6.1), one obtains the equation describing the *critical load function* of S and N acidity, from which the three quantities $CL_{max}(S)$, $CL_{min}(N)$ and $CL_{max}(N)$ can be derived (see Chapter 5).

To obtain time-dependent solutions of the mass balance equations, the term X_{tot} in eq. 6.2, i.e. the total amount (per unit area) of ion X in the soil matrix/soil solution system has to be specified. For ions, which do not interact with the soil matrix, X_{tot} is given by the amount of ion X in solution alone:

$$(6.9) \quad X_{tot} = \Theta \cdot z \cdot [X]$$

where z (m) is the soil depth under consideration (root zone) and Q (m³/m³) is the (annual average) volumetric water content of the soil

compartment. The above equation holds for chloride. For every base cation Y participating in cation exchange, Y_{tot} is given by:

$$(6.10) \\ Y_{tot} = \Theta \cdot z \cdot [Y] + \rho \cdot z \cdot CEC \cdot E_Y$$

where ρ is the soil bulk density (g/cm³), CEC the cation exchange capacity (meq/kg) and E_Y is the exchangeable fraction of ion Y .

The (long-term) changes of the soil N pool are mostly caused by net immobilisation, and N_{tot} is given by:

$$(6.11) \\ N_{tot} = \Theta \cdot z \cdot [N] + \rho \cdot z \cdot N_{pool}$$

If there is no ad/desorption of sulphate, $SO_{4,tot}$ is given by eq. 6.9. If sulphate adsorption cannot be neglected, it is given by:

$$(6.12) \\ SO_{4,tot} = \Theta \cdot z \cdot [SO_4] + \rho \cdot z \cdot SO_{4,ad}$$

When the rate of Al leaching is greater than the rate of Al mobilisation by weathering of primary minerals, the remaining part of Al has to be supplied from readily available Al pools, such as Al hydroxides. This causes depletion of these minerals, which might induce an increase in Fe buffering which in turn leads to a decrease in the availability of phosphate (De Vries 1994). Furthermore, the decrease of those pools in podzolic sandy soils may cause a loss in the structure of those soils. The amount of aluminium is in most models assumed to be infinite and thus no mass balance for Al is considered. The SMART model, however, includes an Al balance, and the terms in eq. 6.2 are $Al_{in}=Al_w$, and Al_{tot} is given by:

$$(6.13) \\ Al_{tot} = \Theta \cdot z \cdot [Al] + \rho \cdot z \cdot CEC \cdot E_{Al} \\ + \rho \cdot z \cdot Al_{ox}$$

where Al_{ox} (meq/kg) is the amount of oxalate

extractable Al , the pool of readily available Al in the soil.

Inserting these expressions into eq. 6.2 and observing that $X_{le}=Q \cdot [X]$, one obtains differential equations for the temporal development of the concentration of the different ions. Only in the simplest cases can these equations be solved analytically. In general, the mass balance equations are discretised and solved numerically, with the solution algorithm depending on the model builders' preferences.

6.2.3 Finite buffers

Finite buffers of elements in the soil are not included in the derivation of critical loads, since they do not influence the steady state. However, when investigating the state soils over time as a function of changing deposition patterns, these finite buffers govern the long-term (slow) changes in soil (solution) chemistry. In the following we describe the most important ones in turn.

6.2.3.1 Cation exchange

Generally, the solid phase particles of a soil carry an excess of cations at their surface layer. Since electro-neutrality has to be maintained, these cations cannot be removed from the soil, but they can be exchanged against other cations, e.g. those in the soil solution. This process is known as cation exchange; and every soil (layer) is characterised by the total amount of exchangeable cations per unit mass (weight), the so-called cation exchange capacity (CEC , measured in meq/kg). If X and Y are two cations with charges m and n , then the general form of the equations used to describe the exchange between the liquid-phase concentrations (or activities) $[X]$ and $[Y]$ and the equivalent fractions E_X and E_Y at the exchange complex is

$$(6.14) \\ \frac{E_X^i}{E_Y^j} = K_{XY} \cdot \frac{[X^{m+}]^n}{[Y^{n+}]^m}$$

where K_{XY} is the so-called exchange (or selectivity) constant, a soil-dependent quantity. Depending on the powers i and j different models of cation exchange can be distinguished: For $i=n$ and $j=m$ one obtains the Gaines-Thomas exchange equations, whereas for $i=j=mn$, after taking the mn -th root, the Gapon exchange equations are obtained.

The number of exchangeable cations considered depends on the purpose and complexity of the model. For example, Reuss (1983) considered only the exchange between Al and Ca (or divalent base cations). In general, if the exchange between N ions is considered, $N-1$, exchange equations (and constants) are required, all the other $(N-1)(N-2)/2$ relationships and constants can be easily derived from them. In the VSD, SMART and SAFE model the exchange between aluminium, divalent base cations and protons is considered. The exchange of protons is important, if the cation exchange capacity (CEC) is measured at high pH -values ($pH=6.5$). In the case of the $Bc-Al-H$ system, the Gaines-Thomas equations read:

(6.15)

$$\frac{E_{Al}^2}{E_{Bc}^3} = K_{AlBc} \cdot \frac{[Al^{3+}]^2}{[Bc^{2+}]^3} \quad \text{and} \quad \frac{E_H^2}{E_{Bc}} = K_{HBc} \cdot \frac{[H^+]^2}{[Bc^{2+}]}$$

where $Bc=Ca+Mg+K$, with K treated as divalent. The equation for the exchange of protons against Al can be obtained from eqs. 6.15 by division:

(6.16)

$$\frac{E_H^3}{E_{Al}} = K_{HAL} \cdot \frac{[H^+]^3}{[Al^{3+}]} \quad \text{with} \quad K_{HAL} = \sqrt{K_{HBc}^3 / K_{AlBc}}$$

The corresponding Gapon exchange equations read:

(6.17)

$$\frac{E_{Al}}{E_{Bc}} = k_{AlBc} \cdot \frac{[Al^{3+}]^{1/3}}{[Bc^{2+}]^{1/2}} \quad \text{and} \quad \frac{E_H}{E_{Bc}} = k_{HBc} \cdot \frac{[H^+]}{[Bc^{2+}]^{1/2}}$$

Again, the $H-Al$ exchange can be obtained by division (with $k_{HAL}=k_{HBc}/k_{AlBc}$). Charge

balance requires that the exchangeable fractions add up to one:

(6.18)

$$E_{Bc} + E_{Al} + E_H = 1$$

The sum of the fractions of exchangeable base cations (here E_{Bc}) is called the *base saturation* of the soil; and it is the time development of the base saturation, which is of interest in dynamic modelling. In the above formulations the exchange of Na , NH_4 (which can be important in high NH_4 deposition areas) and heavy metals is neglected (or subsumed in the proton fraction).

Care has to be exercised when comparing models, since different sets of exchange equations are used in different models. Whereas eqs. 6.15 are used in the SMART model (but with $Ca+Mg$ instead of Bc , K -exchange being ignored in the current version), the SAFE model employs the Gapon exchange equations (eqs. 6.17), however with exchange constants $k'_{XY}=1/k_{XY}$. In the MAGIC model the exchange of Al with all four base cations is modelled separately with Gaines-Thomas equations, without explicitly considering H -exchange.

6.2.3.2 Nitrogen immobilisation

In the calculation of critical loads the (acceptable, sustainable) long-term *net* immobilisation (i.e. the difference between immobilisation and mineralisation) is assumed to be constant. However, it is well known, that the amount of N immobilised is (at present) in many cases larger than this long-term value. Thus a submodel describing the nitrogen dynamics in the soil is part of most dynamic models. For example, the MAKEDEP model, which is part of the SAFE model system (but can also be used as a stand-alone routine) describes the N -dynamics in the soil as a function of forest growth and deposition.

According to Dise et al. (1998) and Gundersen et al. (1998) the forest floor C/N -ratios may be used to assess risk for nitrate leaching. Gundersen et al. (1998)

suggested threshold values of >30, 25 to 30, and <25 to separate low, moderate, and high nitrate leaching risk, respectively. This information has been used in several models, such as SMART and MAGIC to calculate nitrogen immobilisation as a fraction of the net N input, linearly depending on the C/N -ratio in the mineral topsoil.

In addition to the long-term constant net immobilisation, $N_{i,acc}$, the net amount of N immobilised is a linear function of the actual C/N -ratio, CN_t , between a prescribed maximum, CN_{max} , and a minimum C/N -ratio, CN_{min} :

$$(6.19) \quad N_{i,t} = \begin{cases} N_{in,t} & \text{for } CN_t \geq CN_{max} \\ \frac{CN_t - CN_{min}}{CN_{max} - CN_{min}} \cdot N_{in,t} & \text{for } CN_{min} < CN_t < CN_{max} \\ 0 & \text{for } CN_t \leq CN_{min} \end{cases}$$

where $N_{in,t}$ is the available N (e.g., $N_{in,t} = N_{dep,t} - N_{u,t} - N_{i,acc}$). At every time step the amount of immobilised N is added to the amount of N in the top soil, which in turn is used to update the C/N -ratio. The total amount immobilised at every time step is then $N_i = N_{i,acc} + N_{i,t}$. The above equation states that when the C/N -ratio reaches the minimum value, the annual amount of N immobilised equals the acceptable value $N_{i,acc}$ (see Figure 6.2). This formulation is compatible with the critical load formulation for $t \rightarrow \infty$.

6.2.3.3 Sulphate adsorption

The amount of sulphate adsorbed, $SO_{4,ad}$ (meq/kg), is often assumed to be in equilibri-

um with the solution concentration and is typically described by a Langmuir isotherm (e.g., Cosby et al. 1986):

$$(6.20) \quad SO_{4,ad} = \frac{[SO_4]}{S_{1/2} + [SO_4]} \cdot S_{max}$$

where S_{max} is the maximum adsorption capacity of sulphur in the soil (meq/kg) and $S_{1/2}$ the half-saturation concentration (eq/m³).

6.2.4 From soils to surface waters

The processes discussed so far are assumed to occur in the soil solution while it is in contact with the soil matrix. To calculate surface water concentrations it is assumed that the water leaves the soil matrix and is exposed to the atmosphere (Cosby et al. 1985, Reuss and Johnson 1986). When this occurs, excess CO_2 in the water degasses. This shifts the carbonate-bicarbonate equilibria and changes the pH (see eq. 5.43). Surface water concentrations are thus calculated by resolving the system of equations presented above at a lower partial pressure of CO_2 (e.g. mean p_{CO_2} of $8 \cdot 10^{-4}$ atm for 37 lakes, Cole et al. 1994) while ignoring exchange reactions, nitrogen immobilisation and sulphate adsorption. Since exchanges with the soil matrix are precluded, the concentration of the base cations and the strong acid anions (SO_4 , NO_3 and Cl) will not change as the soil water becomes surface water. As such, ANC is conservative (see eq. 6.1).

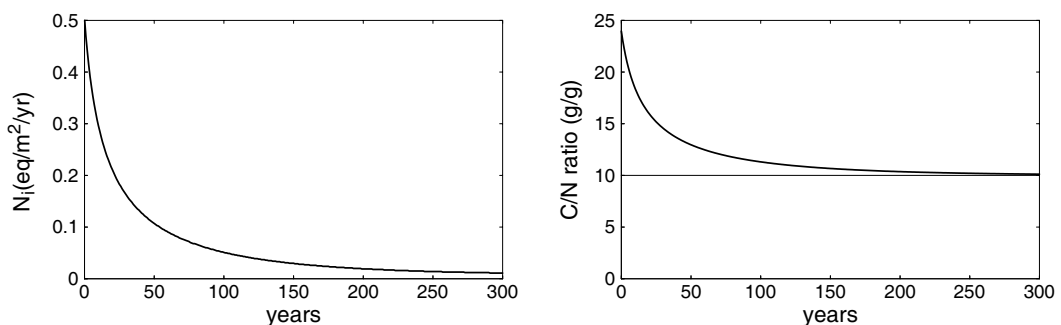


Figure 6.2: Amount of N immobilised (left) and resulting C/N -ratio in the topsoil (right) for a constant net input of N of 1 eq/m²/yr (initial $C_{pool} = 4000$ gC/m², $N_{i,acc} = 1$ kg/ha/yr).

6.2.5 Biological response models

Just as there are delays between changes in acid deposition and changes in surface (or soil) water chemistry, there are delays between changes in chemistry and the biological response. Because the goal in recovery is to restore good or healthy population of key indicator organisms, the time lag in response is the sum of the delays in chemical and biological response (see Figure 6.1). Thus dynamic models for biological response are needed; and in the following a summary is provided of existing models and ideas.

6.2.5.1 Terrestrial ecosystems

A major drawback of most dynamic soil acidification models is the neglect of biotic interactions. For example, vegetation changes are mainly triggered by a change in N cycling (N mineralisation; Berendse et al. 1987). Furthermore the enhancement of diseases by elevated N inputs, such as heather beetle outbreaks, may stimulate vegetation changes. Consequently, dynamic soil-vegetation models, which include such processes, have a better scientific basis for the assessment of critical and target N loads. Examples of such models are CALLUNA (Heil and Bobbink 1993) and ERICA (Berendse 1988). The model CALLUNA integrates N processes by atmospheric deposition, accumulation and sod removal, with heather beetle outbreaks and competition between species, to establish the critical N load in lowland dry-heathlands (Heil and Bobbink 1993). The wet-heathland model ERICA incorporates the competitive relationships between the species *Erica* and *Molinia*, the litter production from both species, and nitrogen fluxes by accumulation, mineralisation, leaching, atmospheric deposition and sheep grazing. At present there are also several forest-soil models that do calculate forest growth impacts in response to atmospheric deposition and other environmental aspects, such as meteorological changes (precipitation, temperature) and changes in CO_2 concentration. Examples are the models NAP (Van Oene 1992), ForSVA (Oja et al. 1995) and Hybrid (Friend et al. 1997).

To date, biological dose/response models related to impacts on species diversity in terrestrial ecosystems did not focus on time-dynamic aspects. Instead, statistical models have been developed to assess the relationship between the species diversity of the ecosystem and abiotic aspects related to acidification and eutrophication. An example is the vegetation model MOVE (Latour and Reiling 1993), that predicts the occurrence probability of plant species in response to scenarios for acidification, eutrophication and desiccation. Input to the model comes from the output of the soil model SMART2 (Kros et al. 1995), being an extension of SMART. The SMART2 model predicts changes in abiotic soil factors indicating acidification (pH), eutrophication (N availability) and desiccation (moisture content) in response to scenarios for acid deposition and groundwater abstraction, including the impact of nutrient cycling (litterfall, mineralisation and uptake). MOVE predicts the occurrence probability of ca 700 species as a function of three abiotic soil factors, including nitrogen availability, using regression relationships. Since combined samples of vegetation and environmental variables are rare, the indication values of plant species by Ellenberg (1985) are used to assess the abiotic soil conditions. Deduction of values for the abiotic soil factors from the vegetation guarantees ecological relevance. Combined samples of vegetation with environmental variables are used exclusively to calibrate Ellenberg indication values with quantitative values of the abiotic soil factors. A calibration of these indication values to quantitative values of the abiotic soil factors is necessary to link the soil module to the vegetation module.

A comparable statistical model is the NTM model (Wamelink et al. 2003, Schouwenberg et al. 2000), that was developed to predict the potential conservation value of natural areas. Normally conservation values are calculated on the basis of plant species or vegetation types. As with MOVE, NTM has the possibility to link the vegetation and the site conditions by using plant ecological indicator values. NTM uses a matrix of the habitats of plant species defined on the basis of

moisture, acidity and nutrient availability. The model was calibrated using a set of 160,252 vegetation relevees. A value index per plant species was defined on the basis of rarity, decline and international importance. This index was used to determine a conservation value for each relevee. The value per relevee was then assigned to each species in the relevee and regressed on the Ellenberg indicator values for moisture, acidity and nutrient availability (Ellenberg 1985) using a statistical method (P-splines). The model has these three Ellenberg indication values as input for the prediction of the potential conservation value. A potential conservation value is calculated for a combination of the abiotic conditions and vegetation structure (ecotope). Therefore four vegetation types are accounted for, each represented by a submodel of NTM: heathland, grassland, deciduous forest and pine-forest. Use of those models in dynamic modelling assessments is valuable to gain more insight in the effect of deposition scenarios on terrestrial ecosystems.

6.2.5.2 Aquatic ecosystems

As with terrestrial ecosystems, biological dose/response models for surface waters have not generally focussed on the time-dynamic aspects. For example, the relationship between lake *ANC* and brown trout population status in Norwegian lakes used to derive the critical limit for surface waters is based on synoptic (once in time) surveys of *ANC* and fish status in a large number of lakes. Similarly the invertebrate indices (Raddum 1999) and diatom response models (Allot et al. 1995, Battarbee et al. 1996) do not incorporate time-dynamic aspects. Additional information on dose/response comes from traditional laboratory studies of toxicity (chronic and acute) and reproductive success.

Information on response times for various organisms comes from studies of recovery following episodes of pollution, for example, salmon population following chemical spill in a river. For salmon full recovery of the population apparently requires about 10 years after the water chemistry has been restored.

There are currently no available time-dynamic process-oriented biological response models for effects of acidification on aquatic and terrestrial organisms, communities or ecosystems. Such models are necessary for a full assessment of the length of time required for recovery of damage from acidification.

There are several types of evidence that can be used to empirically estimate the time delays in biological recovery. The whole-lake acidification and recovery experiments conducted at the Experimental Lakes Area (ELA), north-western Ontario, Canada, provide such information at realistic spatial and temporal scales. These experiments demonstrate considerable lag times between achievement of acceptable water quality following decrease in acid inputs, and achievement of acceptable biological status. The delay times for various organisms are at least several years. In the case of several fish species irreversible changes may have occurred (Hann and Turner 2000, Mills et al. 2000).

A second source of information on biological recovery comes from liming studies. Over the years such studies have produced extensive empirical evidence on rate of response of individual species as well as communities following liming. There has been little focus, however, on the processes involved.

Finally there is recent documentation of recovery in several regions at which acid deposition has decreased in the 1980s and 1990s. Lakes close to the large point-source of sulphur emissions at Sudbury, Ontario, Canada, show clear signs of chemical and biological recovery in response to substantial decreases in emissions beginning in the late 1970s (Keller and Gunn 1995). Lakes in the nearby Killarney Provincial Park (Ontario, Canada) also show clear signs of biological recovery during the past 20 years (Snucins et al. 2001). Here there are several biological factors that influence the rate of biological recovery such as:

- (1) fish species composition and density
- (2) dispersal factors such as distance to intact population and ability to disperse

- (3) existence of resting eggs (for such organisms such as zooplankton)
- (4) existence of precluding species – i.e. the niche is filled.

Recently, a workshop held under the auspices of the UNECE reviewed the current knowledge on models for biological recovery in surface waters (see Wright and Lie 2002).

Future work on biological response models must also include consideration of the frequency and severity of harmful episodes, such as *pH* shocks during spring snowmelt, or acidity and aluminium pulses due to storms with high seasalt inputs. These links between episodic water chemistry and biological response at all levels (organisms, community, and ecosystem) are poorly quantified and thus not yet ready to be incorporated into process-oriented models.

6.3 Available Dynamic Models

In the previous sections the basic processes involved in soil acidification have been summarised and expressed in mathematical form, with emphasis on slow (long-term) processes. The resulting equations, or generalisations and variants thereof, together with appropriate solution algorithms and input-output routines have over the past 15 years been packaged into soil acidification models, mostly known by their (more or less fancy) acronyms.

There is no shortage of soil (acidification) models, but most of them are not designed for regional applications. A comparison of 16 models can be found in a special issue of the journal 'Ecological Modelling' (Tiktak and Van Grinsven 1995). These models emphasise either soil chemistry (such as SMART, SAFE and MAGIC) or the interaction with the forest (growth). There are very few truly integrated forest-soil models. An example is the forest model series ForM-S (Oja et al. 1995), which is implemented not in a 'conventional' Fortran code, but is realised in the high-level modelling software STELLA.

The following selection is biased towards models which have been (widely) used and which are simple enough to be applied on a (large) regional scale. Only a short description of the models is given, but details can

be found in the references cited. It should be emphasised that the term 'model' used here refers, in general, to a model system, i.e. a set of (linked) software (and databases) which consists of pre-processors for input data (preparation) and calibration, post-processors for the model output, and – in general the smallest part – the actual model itself.

An overview of the various models is given in Table 6.1 and a short description below. The first three models are soil models of increasing complexity, whereas the MAGIC model is

Table 6.1: Overview of dynamic models that have been (widely) applied on a regional scale.

Model	Essential process descriptions	Layers	Essential model inputs	Contact
VSD	ANC charge balance Mass balances for BC and N (complete nitrification assumed)	One	CL input data + CEC, base saturation C/N-ratio	M Posch
SMART	VSD model + SO ₄ sorption Mass balances for CaCO ₃ and Al Separate mass balances for NH ₄ and NO ₃ , nitrification Complexation of Al with DOC	One	VSD model + <i>S</i> _{max} and <i>S</i> _{1/2} Ca-carbonate, <i>Al</i> _{ox} nitrification fraction, pK values	W de Vries
SAFE	VSD model + Separate weathering calculation, Element cycling by litterfall, Root decay, Mineralisation and root uptake	Several	VSD model + Input data for PROFILE, litterfall rate, parameters describing mineralisation and root uptake	H Sverdrup
MAGIC	VSD model + SO ₄ sorption, Al speciation/complexation, Aquatic chemistry	Several (mostly one)	VSD model + <i>S</i> _{max} and <i>S</i> _{1/2} pK values for several Al reactions parameters for aquatic chemistry	RF Wright

generally applied at the catchment level. Application on the catchment level, instead on a single (forest) plot, has implications for the derivation of input data. For example, weathering rates have to represent the average weathering of the whole catchment, data that is difficult to obtain from soil parameters. Thus in MAGIC catchment weathering is calibrated from water quality data.

6.3.1 The VSD model

The basic equations presented in section 6.2 have been used to construct a **Very Simple Dynamic (VSD)** soil acidification model. The VSD model is designed as the simplest extension of the SMB model for critical loads. It only includes cation exchange and *N* immobilisation, and a mass balance for cations and nitrogen as described above, in addition to the equations included in the SMB model. It resembles the model presented by Reuss (1980) which, however, does not consider nitrogen processes.

In the VSD model, the various ecosystem processes have been limited to a few key processes. Processes that are *not* taken into account, are: (i) canopy interactions, (ii) nutrient cycling processes, (iii) *N* fixation and NH_4 adsorption, (iv) interactions (adsorption, uptake, immobilisation and reduction) of SO_4 , (v) formation and protonation of organic anions, (*R*COO) and (vi) complexation of *Al* with *OH*, SO_4 and *R*COO.

The VSD model consists of a set of mass balance equations, describing the soil input-output relationships, and a set of equations describing the rate-limited and equilibrium soil processes, as described in section 6.2. The soil solution chemistry in VSD depends solely on the net element input from the atmosphere (deposition minus net uptake minus net immobilisation) and the geochemical interaction in the soil (CO_2 equilibria, weathering of carbonates and silicates, and cation exchange). Soil interactions are described by simple rate-limited (zero-order) reactions (e.g. uptake and silicate weathering) or by equilibrium reactions (e.g. cation exchange). It models the exchange of *Al*, *H*

and $Ca+Mg+K$ with Gaines-Thomas or Gapon equations. Solute transport is described by assuming complete mixing of the element input within one homogeneous soil compartment with a constant density and a fixed depth. Since VSD is a single layer soil model neglecting vertical heterogeneity, it predicts the concentration of the soil water leaving this layer (the rootzone). The annual water flux percolating from this layer is taken equal to the annual precipitation excess. The

time step of the model is one year, i.e. seasonal variations are not considered. The model is available from the CCE website (www.rivm.nl/cce); and a detailed description will be found in Posch and Reinds (2005).

6.3.2 The SMART model

The SMART model (**S**imulation **M**odel for **A**cidification's **R**egional **T**rends) is similar to the VSD model, but somewhat extended and is described in De Vries et al. (1989) and Posch et al. (1993). As with the VSD model, the SMART model consists of a set of mass balance equations, describing the soil input-output relationships, and a set of equations describing the rate-limited and equilibrium soil processes. It includes most of the assumptions and simplifications given for the VSD model; and justifications for them can be found in De Vries et al. (1989). SMART models the exchange of *Al*, *H* and divalent base cations using Gaines-Thomas equations. Additionally, sulphate adsorption is modelled using a Langmuir equation (as in MAGIC) and organic acids can be described as mono-, di- or tri-protic. Furthermore, it includes a balance for carbonate and *Al*; thus allowing the calculation from calcareous soils to completely acidified soils that do not have an *Al* buffer left. In this respect, SMART is based on the concept of buffer ranges expounded by Ulrich (1981). Recently a description of the complexation of aluminium with organic acids has been included. The SMART model has been developed with regional applications in mind, and an early example of an application to Europe can be found in De Vries et al. (1994).

6.3.3 The SAFE model

The SAFE (**S**oil **A**cidification in **F**orest **E**cosystems) model has been developed at the University of Lund (Warfvinge et al. 1993) and a recent description of the model can be found in Alveteg (1998) and Alveteg and Sverdrup (2002). The main differences to the SMART and MAGIC models are: (a) weathering of base cations is not a model input, but it is modelled with the PROFILE (sub-)model, using soil mineralogy as input (Warfvinge and Sverdrup 1992); (b) SAFE is oriented to soil profiles in which water is assumed to move vertically through several soil layers (usually 4), (c) Cation exchange between *Al*, *H* and (divalent) base cations is modelled with Gapon exchange reactions, and the exchange between soil matrix and the soil solution is diffusion limited. The standard version of SAFE does not include sulphate adsorption although a version, in which sulphate adsorption is dependent on sulphate concentration and *pH* has recently been developed (Martinson et al. 2003).

The SAFE model has been applied to many sites and more recently also regional applications have been carried out for Sweden (Alveteg and Sverdrup 2002) and Switzerland (SAEFL 1998, Kurz et al. 1998, Alveteg et al. 1998).

6.3.4 The MAGIC model

MAGIC (**M**odel of **A**cidification of **G**round-water **I**n **C**atchments) is a lumped-parameter model of intermediate complexity, developed to predict the long-term effects of acidic deposition on soils and surface water chemistry (Cosby et al. 1985a,b,c, 1986). The model simulates soil solution chemistry and surface water chemistry to predict the monthly and annual average concentrations of the major ions in lakes and streams. MAGIC represents the catchment with aggregated, uniform soil compartments (one or two) and a surface water compartment that can be either a lake or a stream. MAGIC consists of (1) a section in which the concentrations of major ions are assumed to be governed by simultaneous reactions involving sulphate adsorption, cation exchange, dissolution-precipitation-speciation of

aluminium and dissolution-speciation of inorganic and organic carbon, and (2) a mass balance section in which the flux of major ions to and from the soil is assumed to be controlled by atmospheric inputs, chemical weathering inputs, net uptake in biomass and losses to runoff. At the heart of MAGIC is the size of the pool of exchangeable base cations in the soil. As the fluxes to and from this pool change over time owing to changes in atmospheric deposition, the chemical equilibria between soil and soil solution shift to give changes in surface water chemistry. The degree and rate of change in surface water acidity thus depend both on flux factors and the inherent characteristics of the affected soils.

The soil layers can be arranged vertically or horizontally to represent important vertical or horizontal flowpaths through the soils. If a lake is simulated, seasonal stratification of the lake can be implemented. Time steps are monthly or yearly. Time series inputs to the model include annual or monthly estimates of: (1) deposition (wet plus dry) of ions from the atmosphere; (2) discharge volumes and flow routing within the catchment; (3) biological production, removal and transformation of ions; (4) internal sources and sinks of ions from weathering or precipitation reactions; and (5) climate data. Constant parameters in the model include physical and chemical characteristics of the soils and surface waters, and thermodynamic constants. The model is calibrated using observed values of surface water and soil chemistry for a specified period.

MAGIC has been modified and extended several times from the original version of 1984. In particular organic acids have been added to the model (version 5; Cosby et al. 1995a) and most recently nitrogen processes have been added (version 7; Cosby et al. 2001).

The MAGIC model has been extensively applied and tested over a 15-year period at many sites and in many regions around the world. Overall, the model has proven to be robust, reliable and useful in a variety of scientific and managerial activities.

6.4 Input Data and Model Calibration

Running a dynamic model is usually the least time- or resource-consuming step in an assessment. It takes more time to interpret model output, but most time-consuming is the acquisition and preparation of input data. Rarely can laboratory or literature data be directly used as model inputs. They have to be pre-processed and interpreted, often with the help of other models. Especially for regional applications not all model inputs are available (or directly usable) from measurements at sites, and interpolations and transfer functions have to be derived and used to obtain the necessary input data. When acquiring data from different sources of information, it is important to keep a record of the 'pedigree', i.e. the entire chain of information, assumptions and (mental) models used to produce a certain number. Also the uncertainty of the data should be assessed, recorded and communicated.

As with critical loads, for the policy support of the effects-oriented work under the LRTAP Convention output of dynamic models will most usefully represent not a particular site, but a larger area, e.g. a forest instead of a single tree stand. Therefore, certain variables should be 'smoothed' to represent that larger area. For example, (projected) growth uptake of nutrients (nitrogen and base cations) should reflect the (projected) average uptake of the forest over that area, and not the succession of harvest and re-growth at a particular spot.

6.4.1 Input data

The input data required to run dynamic models depend on the model, but essentially all of them need the following (minimum) data, which can be roughly grouped into in- and output fluxes, and soil properties. Note that this grouping of the input data depends on the model considered. For example, weathering has to be specified as a (constant) input flux in the SMART and MAGIC model, whereas in the

SAFE model it is internally computed from soil properties and depends on the state of the soil (e.g. the pH). Some of the input data are also needed in the SMB model to calculate critical loads, and are described in Chapter 5. This chapter thus focuses on additional data and parameters needed to run dynamic models. The most important soil parameters are the cation exchange capacity (CEC), the base saturation and the exchange (or selectivity) constants describing cation exchange, as well as parameters describing nitrogen retention and sulphate ad/desorption, since these parameters determine the long-term behaviour (recovery) of soils.

Ideally, all input data are directly derived from measurements. This is usually not feasible for regional applications, in which case input data have to be derived from relationships (transfer functions) with basic (map) information. In this chapter we provide information on the input data needed for running the VSD model and thus, by extension, also other models. Descriptions and technical details of the input data for those models can be found in Posch et al. (1993) for the SMART model, in Cosby et al. (1985a) for the MAGIC model and in Alveteg and Sverdrup (2002) for the SAFE model.

In most of the (pedo-)transfer functions presented here, soils – or rather soil groups – are characterised by a few properties, mostly organic carbon and clay content of the mineral soil (see also Figure 6.3). The organic carbon content, C_{org} , can be estimated as 0.5 or 0.4 times the organic matter content in the humus or mineral soil layer, resp. If $C_{org} > 15\%$, a soil is considered a *peat* soil. Mineral soils are called *sand* (or sandy soil) here, if the clay content is below 18% (coarse textured soils; see also Table 5.6), otherwise it is called a *clay* (or clayey/loamy soil). Loess soils are soils with more than 50% *silt*, i.e. $clay + sand < 50\%$ (since $clay + silt + sand = 100\%$).

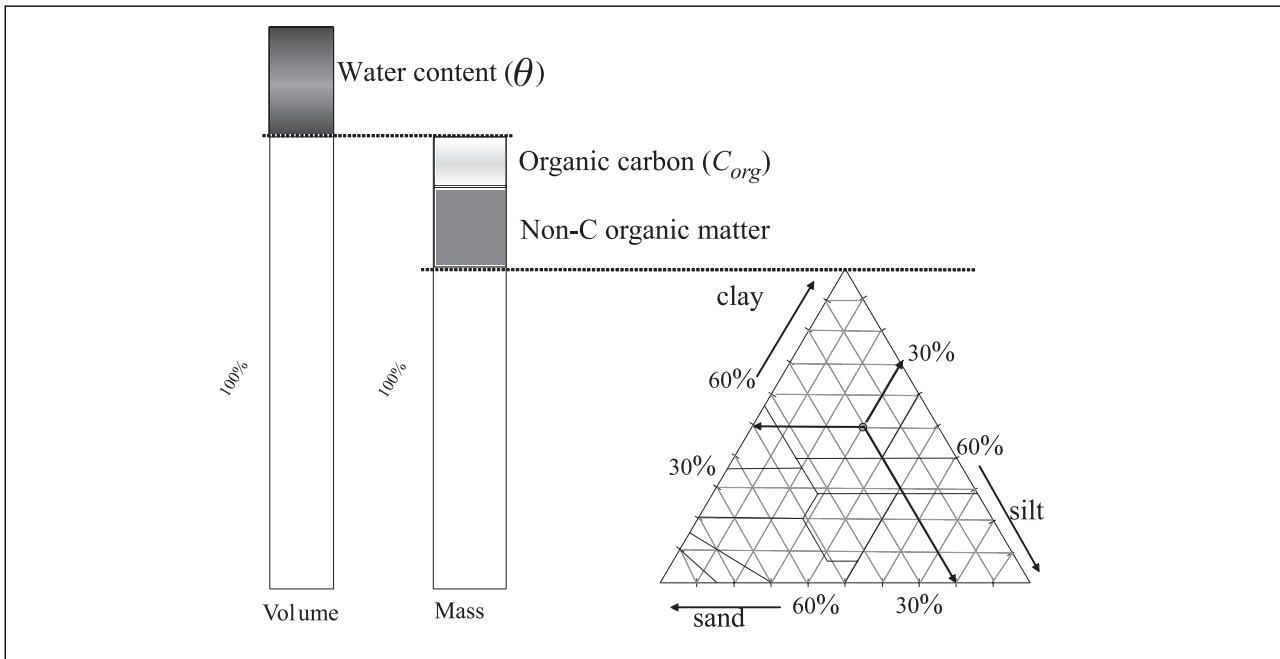


Figure 6.3: Illustration of the basic composition of a soil profile: soil water, organic matter (organic carbon) and the mineral soil, characterised by its *clay*, *silt* and *sand* fraction ($clay + silt + sand = 100\%$).

6.4.1.1 Averaging soil properties

For single layer soil models, such as VSD, SMART or MAGIC, the profile averages of certain soil parameters are required, and in the sequel formulae for the average bulk density, cation exchange capacity and base saturation are derived.

For a given soil profile it is assumed that there are measurements of bulk density ρ_l (g/cm³), cation exchange capacity CEC_l (meq/kg) and base saturation $E_{BC,l}$ for n (homogeneous) soil horizons with thickness z_l ($l=1, \dots, n$). Obviously, the total thickness (soil depth) z is given by:

$$(6.21) \quad z = \sum_{l=1}^n z_l$$

The mean bulk density ρ of the profile is derived from mass conservation (per unit area):

$$(6.22) \quad \rho = \frac{1}{z} \sum_{l=1}^n z_l \cdot \rho_l$$

The average cation exchange capacity CEC has to be calculated in such a way that the total number of exchange sites (per unit area) is given by $z \cdot \rho \cdot CEC$. This implies the following formula for the profile average cation exchange capacity:

$$(6.23) \quad CEC = \frac{1}{z \cdot \rho} \sum_{l=1}^n z_l \cdot \rho_l \cdot CEC_l$$

And for the profile average base saturation E_{BC} one then gets:

$$(6.24) \quad E_{BC} = \frac{1}{z \cdot \rho \cdot CEC} \sum_{l=1}^n z_l \cdot \rho_l \cdot CEC_l \cdot E_{BC,l}$$

Note that for aquatic ecosystems, these parameters have to be averaged over the terrestrial catchment area as well.

6.4.1.2 Data also used for critical load calculations

In this section we describe those input data which are also used in critical load calculations (see Chapter 5) and for details the reader is referred to that Chapter, especially

sections 5.3.1.3 and 5.3.2.3. Whereas for critical loads and exceedance calculations data are needed at a specific point in time (or at steady-state), their past and future temporal development is needed for dynamic modelling.

Deposition:

Non-anthropogenic (steady-state) base cation and chloride deposition are incorporated into the definition of the critical load of acidity. For dynamic models times series of past and future depositions are needed. However, at present there are no projections available for these elements on a European scale. Thus in most model applications (average) present base cation and chloride depositions are assumed to hold also in the future (and past).

Sulphur and nitrogen depositions enter only the exceedance calculations of critical loads. In contrast, their temporal development is the driving force of every dynamic model. Time series for the period 1880-1990 of *S* and *N* deposition on the EMEP-150 grid have been recently computed using published estimates of historical emissions (Schöpp et al. 2003) and 12-year average transfer matrices derived from the EMEP/MSC-W lagrangian atmospheric transport model. Scenarios for future sulphur and nitrogen deposition are provided by integrated assessment modellers, based on atmospheric transport modelling by EMEP.

In case the deposition model provides only grid average values, a local deposition (adjustment) model could compute the local deposition from the grid average values, especially for forest soils, where the actual (larger) deposition depends on the type and age of trees (via the 'filtering' of deposition by the canopy). An example of such a model is the MAKEDEP model, which is also part of the SAFE model system (Alveteg and Sverdrup 2002).

Uptake:

Long-term average values of the net growth-uptake of nitrogen and base cations by forests are also needed to calculate critical

loads; and data sources and calculation procedures are given in Chapter 5. In simple dynamic models these processes are described as a function of actual and projected forest growth. To this end, additional information on forest age and growth rates is needed, and the amount of data needed depends largely on whether the full nutrient cycle is modelled or whether only net sources and sinks are considered.

Considering net removal by forest growth, as in the VSD, SMART and MAGIC models, the yield (forest growth) at a certain age can be derived from yield tables for the considered tree species. The element contents in stems (and possibly branches) should be the same as used in the critical load calculations (see, e.g., Table 5.2). If the nutrient cycle is modelled, as in the SAFE model, data are needed on litterfall rates, root turnover rates, including the nutrient contents in litter (leaves/needles falling from the tree), and fine roots. Such data are highly dependent on tree species and site conditions. Compilations of such data can be found in De Vries et al. (1990) and Jacobsen et al. (2002).

Water flux and soil moisture:

Water flux data that are needed in one-layer models are limited to the precipitation surplus leaving the root zone (see Chapter 5), whereas multi-layer models require water fluxes for each soil layer down to the bottom of the root zone. For simple dynamic models, water fluxes could be calculated by a separate hydrological model, running on a daily or monthly time step with aggregation to annual values afterwards. An example of such a model is WATBAL (Starr 1999), which is a capacity-type water balance model for forested stands/plots running on a monthly time step and based on the following water balance equation:

$$(6.25) \quad Q = P - ET \pm \Delta SM$$

where: Q = precipitation surplus, P = precipitation, ET = evapotranspiration and $\pm \Delta SM$ = changes in soil moisture content. WATBAL

uses relatively simple input data, which is either directly available (e.g., monthly precipitation and air temperature) or which can be derived from other data using transfer functions (e.g., soil available water capacity).

In any dynamic model, which includes a mass balance for elements, also information on the soil moisture content is needed. This is also output from a hydrological model (see *SM* in eq. 6.25) or has to be estimated from other site properties. An approximate annual average soil moisture content θ (m^3/m^3) can be obtained as a function of the clay content (see Brady 1974):

(6.26)

$$\theta = \min\{0.04 + 0.0077 \cdot \text{clay}, 0.27\}$$

i.e., for clay contents above 30% a constant value of 0.27 is assumed. It should be noted that most models are quite insensitive to the value of θ .

Base cation weathering:

The various possibilities to assess weathering rates of base cations, which are a key input also to critical load calculations, are discussed and cited in Chapter 5.

Mineralisation and (de-)nitrification:

Rate constants (and possibly additional parameters) for mineralisation, nitrification and denitrification are needed in detailed models, but simple models mostly use factors between zero and one, which compute nitrification and denitrification as fraction of the (net) input of nitrogen.

As in the calculation of critical loads (SMB model), in the VSD model complete nitrification is assumed (nitrification fraction equals 1.0), and denitrification fractions can be found in Table 5.3. Mineralisation is not considered explicitly, but included in the net immobilisation calculations.

For the complete soil profile, the nitrification fraction in forest soils varies mostly between 0.75 and 1.0. This is based on measurements of NH_4/NO_3 ratios below the rootzone of highly acidic Dutch forests with very high

NH_4 inputs in the early nineties, which were nearly always less than 0.25 (De Vries et al. 1995). Generally, 50% of the NH_4 input is nitrified above the mineral soil in the humus layer (Tietema et al. 1990). Actually, the nitrification fraction includes the effect of both nitrification and preferential ammonium uptake.

Al-H equilibrium:

The constants needed to quantify the equilibrium between $[\text{Al}]$ and $[\text{H}]$ in the soil solution are discussed and presented in Chapter 5 (Table 5.9), since they are also needed for critical load calculations. For models including the complexation of *Al* with organic anions, such as MAGIC and SMART, relevant parameters can be found, e.g., in Driscoll et al. (1994).

6.4.1.3 Data needed to simulate cation exchange

In all dynamic soil models, cation exchange is a crucial process (see section 6.2.3.1). Data needed to allow exchange calculations are:

- The pool of exchangeable cations, being the product of layer thickness, bulk density, cation exchange capacity (*CEC*) and exchangeable cation fractions
- Cation exchange constants (selectivity coefficients)

Preferably these data are taken from measurements. Such measurements are generally made for several soil horizons. For single-layer models, such as VSD, these data have to be properly averaged over the entire soil depth (rooting zone; see eqs. 6.21 - 6.24).

In the absence of measurements, the various data needed to derive the pool of exchangeable cations for major forest soil types can be derived by extrapolation of point data, using transfer functions between bulk density, *CEC* and base saturation and basic land and soil characteristics, such as soil type, soil horizon, organic matter content, soil texture, etc.

Soil bulk density:

If no measurements are available, the soil bulk density ρ (g/cm³) can be estimated from the following transfer function:

(6.27)

$$\rho = \begin{cases} 1 / (0.625 + 0.05 \cdot C_{org} + 0.0015 \cdot clay) & \text{for } C_{org} \leq 5\% \\ 1.55 - 0.0814 \cdot C_{org} & \text{for } 5\% < C_{org} < 15\% \\ 0.725 - 0.337 \cdot \log_{10} C_{org} & \text{for } C_{org} \geq 15\% \end{cases}$$

where C_{org} is the organic carbon content and $clay$ the clay content (both in %). The top equation for mineral soils is based on data by Hoekstra and Poelman (1982), the bottom equation for peat(y) soils is derived from Van Wallenburg (1988) and the central equation is a linear interpolation (for $clay=0$) between the two (Reinds et al. 2001).

Cation exchange capacity (CEC):

The value of the CEC depends on the soil pH at which the measurements are made. Consequently, there is a difference between unbuffered CEC values, measured at the actual soil pH and buffered values measured at a standard pH , such as 6.5 or 8.2. In the VSD (and many other) models the exchange constants are related to a CEC that is measured in a buffered solution in order to standardise to a single pH value (e.g.,

$pH=6.5$, as upper limit of non-calcareous soils). The actual CEC can be calculated from pH , clay and organic carbon content according to (after Helling et al. 1964):

(6.28)

$$CEC(pH) = (0.44 \cdot pH + 3.0) \cdot clay + (5.1 \cdot pH - 5.9) \cdot C_{org}$$

where CEC is the cation exchange capacity (meq/kg), $clay$ is the clay content (%) and C_{org} the organic carbon content (%). The pH in this equation should be as close as possible to the measured soil solution pH . For sandy soils the clay content can be set to zero in eq. 6.28. Typical average clay contents as a function of the texture class, presented on the FAO soil classification (FAO 1981), are given in Table 6.2. Values for C_{org} range from 0.1% for arenosols (Qc) to 50% for peat soils (Od).

Table 6.2: Average clay contents and typical base saturation as a function of soil texture classes (see Table 5.12).

Texture class	Name	Definition	average clay content (%)	typical base saturation (%)
1	coarse	clay < 18% and sand \geq 65%	6	5
2	medium	clay < 35% and sand \geq 15%; but clay \geq 18% if sand \geq 65%	20	15
3	medium fine	clay < 35% and sand < 15%	20	20
4	fine	35% \leq clay < 60%	45	50
5	very fine	clay \geq 60%	75	50
9	organic soils	Soil types O	5	10-70

Computing $CEC(pH_{measured})$, i.e. the CEC from eq. 6.28, using measured (site-specific) C_{org} , clay and pH does not always match the measured CEC , $CEC_{measured}$, and thus computing CEC at $pH=6.5$, $CEC(6.5)$, would not be consistent with it. Nevertheless, eq. 6.28 can be used to *scale* the measured CEC to a value at $pH=6.5$, i.e. the value needed for modelling, in the following manner:

(6.29)

$$CEC_{pH=6.5} = CEC_{measured} \cdot \frac{CEC(6.5)}{CEC(pH_{measured})}$$

This method of scaling measured data with the ratio (or difference) of model output is widely used in global change work to obtain, e.g., climate-changed (meteorological) data consistent with observations.

Exchangeable base cation fraction (base saturation):

In most models, a lumped expression is used for the exchange of cations, distinguishing only between H , Al and base cations (VSD, SMART and SAFE). As with the clay content, data for the exchangeable cation fractions, or in some cases only the base saturation, can be based on information on national soil information systems, or in absence of these, on the FAO soil map of Europe (FAO 1981). Base saturation data vary from 5-25% in relatively acid forest soils to more than 50% in well buffered soils. A very crude indication of the base saturation as a function of the texture class of soils is given in the last column of Table 6.2. This relationship is based on data from forest soils given in FAO (1981) and in Gardiner (1987). A higher texture class reflects a higher clay content implying an increase in weathering rate, which implies a higher base saturation. For organic soils the base saturation is put equal to 70% for eutric histosols (Oe) and 10% for dystic histosols (Od).

Ideally, only measured CEC and exchangeable cation data are used. However, when data on the initial base saturation of soils are not available for regional (national) model applications, one may derive them from a relationship with environmental factors.

Such an exercise was carried out using a European database with approximately 5300 soil chemistry data for the organic layer and the forest topsoil (0-20 cm) collected on a systematic 16×16 km² grid (ICP Forest level-I grid; Vanmechelen et al. 1997). The regression relationship for the estimated base saturation E_{BC} (expressed as a fraction with values between 0 and 1) is:

(6.30a)

$$E_{BC} = \frac{1}{1 + e^{-B}} \quad \text{with}$$

(6.30b)

$$B = a_0 + a_1(\text{soil group}) + a_2(\text{treespecies}) + a_3 \cdot \text{altitude} \\ + a_4 \cdot \ln(\text{age}) + a_5 \cdot \text{temperature} + a_6 \cdot (\text{temperature})^2 \\ + a_7 \cdot \ln(\text{precipitation}) + \sum_{k=8}^{k=11} a_k \cdot \ln(\text{deposition}_k) \\ + \sum_{k=12}^{k=15} a_k \cdot \ln(\text{deposition fraction}_k)$$

where 'ln' is the natural logarithm, $\ln(x) = \ln(x/(1-x))$, and the a_k 's are the regression coefficients. The regression analysis was carried out using a so-called Select-procedure. This procedure combines qualitative predictor variables, such as tree species and/or soil type, with quantitative variables and it combines forward selection, starting with a model including one predictor variable, and backward elimination, starting with a model including all predictor variables. The 'best' model was based on a combination of the percentage of explained variance, that should be high and the number of predictor variables that should be low. More information on the procedure is given in Klap et al. (2004). Results of the analyses are given in Table 6.3. The explained variance for base saturation was approx. 45%.

Note: When data are not available, one may also calculate base saturation as the maximum of (i) a relation with environmental factors as given above and (ii) an equilibrium with present deposition levels of SO_4 , NO_3 , NH_4 and BC . Especially in southern Europe, where acid deposition is relatively low and base cation input is high, the base saturation in equilibrium with the present load can be higher than the value computed according to eq. 6.30.

Table 6.3: Coefficients for estimating base saturation and the C/N-ratio in the mineral topsoil (0-20 cm) and the organic layer (after Klap et al. 2004; Note: (a) the star denotes sea-salt corrected depositions, (b) depositions <0.1 should be set to 0.1 to avoid underflow in the equations).

Predictor variable	Base saturation (mineral topsoil)	C/N-ratio (organic layer)	C/N-ratio (mineral topsoil)	Coefficients in eqs.6.30 and 6.31
Constant	3.198	3.115	1.310	a_0
<i>Soil group:</i>				
sandy soils	0	0	0	a_1
loamy/clayey soils	0.297	-0.807	-0.279	a_1
peat soils	0.534	-0.025	-0.312	a_1
<i>Tree species:</i>				
pine	0	0	0	a_2
spruce	-0.113	-0.158	-0.093	a_2
oak	0.856	-0.265	-0.218	a_2
beech	0.591	-0.301	-0.218	a_2
<i>Site conditions:</i>				
Altitude [m]	-0.00014	-0.00008	-0.000136	a_3
Age [yr]	0	0.025	0.096	a_4
<i>Meteorology:</i>				
Temperature [°C]	0	-0.0078	-0.041	a_5
Temperature ² [°C ²]	0	0.00095	0.0014	a_6
Precipitation [mm/yr]	0	0.178	0.194	a_7
<i>Deposition:</i>				
Na [eq/ha/yr]	-0.223	0	0.080	a_8
<i>N-tot (=NO_y+NH₂) [eq/ha/yr]:</i>				
sandy soils	0	-0.150	-0.019	a_9
loamy/clayey soils	0	-0.032	0	a_9
peat soils	0	-0.136	0	a_9
Acid (=SO _x *+N-tot) [eq/ha/yr]	-1.025	0	0	a_{10}
Bc* (=Ca*+Mg*+K*) [eq/ha/yr]	0.676	0	0	a_{11}
<i>Deposition fractions:</i>				
<i>NH₂ / Acid [-]:</i>				
sandy soils	0	0	0	a_{12}
loamy/clayey soils	-0.494	0	0	a_{12}
peat soils	-0.896	0	0	a_{12}
NH ₂ / N-tot [-]	0	0.102	0.120	a_{13}
Ca* / Bc* [-]	1.211	0	0	a_{14}
Mg* / Bc* [-]	0.567	0	0	a_{15}

Exchange constants (selectivity coefficients):

In many exchange models the cations are lumped to *H*, *Al* and base cations (as in VSD, SMART and SAFE), but in MAGIC every base cation (*Ca*, *Mg*, *K*, *Na*) is modelled separately. Furthermore, cation exchange in SMART and MAGIC is based upon Gaines-Thomas equations, in SAFE it is described by Gapon exchange reactions, whereas in the VSD model the user can choose between the two. Exchange constants can be derived from the simultaneous measurement of the major cations (*H*, *Al*, *Ca*, *Mg*, *K* and *Na*) at the adsorption complex and in the soil solution.

Using more than 800 such measurements from Dutch soils, extensive tables of

exchange constants have been derived for sand, loess, clay and peat soils, together with their standard deviations and correlations for all combinations of *H*, *Al* and base cations (De Vries and Posch 2003). The data show the high affinity of the complex for protons compared to all other monovalent cations, and that the relative contributions of *K*, *Na* and *NH₄* on the adsorption complex are very low. Results for the logarithms (\log_{10}) of the exchange constants used in the VSD model, both for the 'Gaines-Thomas mode' and the 'Gapon mode', together with their standard deviation ('stddev') are given in Tables 6.4 to 6.7. For a conversion to other units see Annex III.

Table 6.4: Mean and standard deviation of logarithmic **Gaines-Thomas** exchange constants of H against $Ca+Mg+K$ as a function of soil depth for sand, loess, clay and peat soils (mol/l)⁻¹.

Layer (cm)	Sand		Loess		Clay		Peat	
	Mean	stddev	Mean	stddev	Mean	stddev	Mean	stddev
0-10	5.338	0.759	5.322	0.692	6.740	1.464	4.754	0.502
10-30	6.060	0.729	5.434	0.620	6.007	0.740	4.685	0.573
30-60	6.297	0.656	-	-	6.754	0.344	5.307	1.051
60-100	6.204	0.242	5.541	0.579	7.185	-	5.386	1.636
0-30	5.236	0.614	5.386	0.606	6.728	1.373	4.615	0.439
0-60	5.863	0.495	-	-	6.887	1.423	4.651	0.562

Table 6.5: Mean and standard deviation of logarithmic **Gaines-Thomas** exchange constants of Al against $Ca+Mg+K$ as a function of soil depth for sand, loess, clay and peat soils (mol/l).

Layer (cm)	Sand		Loess		Clay		Peat	
	Mean	stddev	Mean	stddev	Mean	stddev	Mean	stddev
0-10	2.269	1.493	1.021	1.147	1.280	1.845	0.835	1.204
10-30	3.914	1.607	1.257	0.939	-0.680	1.152	0.703	0.968
30-60	4.175	1.969	-	-	-3.070	0.298	0.567	1.474
60-100	2.988	0.763	1.652	1.082	-2.860	-	0.969	1.777
0-30	2.306	1.082	0.878	1.079	0.391	1.555	0.978	0.805
0-60	2.858	1.121	-	-	-0.973	1.230	0.666	0.846

Table 6.6: Mean and standard deviation of logarithmic **Gapon** exchange constants of H against $Ca+Mg+K$ as a function of soil depth for sand, loess, clay and peat soils (mol/l)^{-1/2}.

Layer (cm)	Sand		Loess		Clay		Peat	
	Mean	stddev	Mean	stddev	Mean	stddev	Mean	stddev
0-10	3.178	0.309	3.138	0.268	3.684	0.568	2.818	0.199
10-30	3.527	0.271	3.240	0.221	3.287	0.282	2.739	0.175
30-60	3.662	0.334	-	-	3.521	0.212	2.944	0.382
60-100	3.866	0.125	3.232	0.251	3.676	-	3.027	0.672
0-30	3.253	0.311	3.170	0.206	3.620	0.530	2.773	0.190
0-60	3.289	0.340	-	-	3.604	0.654	2.694	0.170

Table 6.7: Mean and standard deviation of logarithmic **Gapon** exchange constants of Al against $Ca+Mg+K$ as a function of soil depth for sand, loess, clay and peat soils (mol/l)^{1/6}.

Layer (cm)	Sand		Loess		Clay		Peat	
	Mean	stddev	Mean	stddev	Mean	stddev	Mean	stddev
0-10	0.306	0.440	0.190	0.546	-0.312	0.738	-0.373	0.350
10-30	0.693	0.517	0.382	0.663	-0.463	0.431	-0.444	0.255
30-60	0.819	0.527	-	-	-1.476	0.093	-0.740	0.336
60-100	1.114	0.121	0.390	0.591	-1.795	-	-0.867	0.401
0-30	0.607	0.472	0.221	0.647	-0.609	0.731	-0.247	0.404
0-60	0.199	0.633	-	-	-1.054	0.362	-0.551	0.210

It should be noted that exchange constants vary widely and are unknown for most sites. Therefore, in most models (SAFE, MAGIC, but also VSD) they are calibrated against measurements of base saturation (and soil solution concentrations).

6.4.1.4 Data needed for balances of nitrogen, sulphate and aluminium

C/N-ratio:

Data for the C/N -ratio generally vary between 15 in rich soils where humification has been high to 40 in soils with low N inputs and less humification. Values can also be obtained from results of a regression analysis similar to that of the base saturation according to:

(6.31)

$$\begin{aligned} \ln(\text{C/N - ratio}) = & a_0 + a_1(\text{soil group}) + a_2(\text{tree species}) + a_3 \cdot \text{altitude} + a_4 \cdot \ln(\text{age}) \\ & + a_5 \cdot \text{temperature} + a_6 \cdot (\text{temperature})^2 + a_7 \cdot \ln(\text{precipitation}) \\ & + \sum_{k=8}^{k=11} a_k \cdot \ln(\text{deposition}_k) + \sum_{k=12}^{k=15} a_k \cdot \ln(\text{deposition fraction}_k) \end{aligned}$$

where 'ln' is the natural logarithm and $\ln(x) = \ln(x/(1-x))$. Results of the analysis, which was performed with the same data sets as described in the section on base saturation, are given in Table 6.3; and more information on the procedure is given in Klap et al. (2004).

Sulphate sorption capacity and half-saturation constant:

Values for the maximum sorption capacity for sulphate, S_{max} , can be related to the content of oxalate extractable Al (meq kg⁻¹) according to (Johnson and Todd 1983):

(6.32)

$$S_{max} = 0.02 \cdot Al_{ox}$$

Estimates for the oxalate extractable Al content are given below. Adsorption or half-saturation constants for sulphate, $S_{1/2}$, can be derived from literature information (e.g. Singh and Johnson 1986, Foster et al. 1986). A reasonable average value is 1.0 eq/m³.

Al-hydroxide content:

Data for the oxalate extractable Al content (the content of readily available Al-hydroxide) are often available in national soil information systems, such as the soil information system of the Netherlands. In sandy soils the Al-hydroxide content (in meq/kg) mostly varies between 100-200 for A-horizons, between 200-350 for B-horizons and between 50-150 for C-horizons (parent material, De Vries 1991).

6.4.2 Model calibration

If all input parameters, initial conditions and driving forces were known, the chosen model would describe the future develop

ment of the soil chemical status for any given deposition scenario. However, in most cases several of the parameters are poorly known, and thus many models, i.e. the badly known parameters in the model, have to be 'calibrated'. The method of calibration varies with the model and/or the application.

In standard applications of both the MAGIC and SAFE model it is assumed that in pre-acidification times (say 1850) the input of ions is in equilibrium (steady state) with the soil (solution) chemistry. Furthermore it is assumed that the deposition history of all (eight) ions is known (properly reconstructed).

In SAFE, weathering rates and uptake/net removal of *N* and base cations are computed within the model (see above). Only simulated (present) base saturation is matched with observations (in every soil layer) by adjusting the cation exchange selectivity coefficient(s). Matching simulated and observed soil solution concentrations is not part of the standard calibration procedure.

The calibration of MAGIC is a sequential process whereby firstly the input and output of those ions assumed to act conservatively in the catchment are balanced (usually only *Cl*). Next, the anion concentrations in surface waters are matched by adjusting catchment net retention (of *N*) and soil adsorption (of *S*) if appropriate. Thirdly, the four individual major base cation concentration in the stream and on the soil solid phase (expressed as a percentage of cation exchange capacity) are matched by adjusting the cation exchange selectivity coefficients and the base cation weathering rates. Finally, surface water *pH*, *Al* and organic anion concentrations are matched by adjusting the aluminium solubility

coefficient and total organic acid concentration in surface water.

Both in MAGIC and SAFE automatic calibration routines are an important part of the overall model system. For the SMART model no such automatic model calibration routine is presently available. For the VSD model the same calibration routine as used in SAFE has been implemented, and details can be found in Posch and Reinds (2005) and in the help-file of the 'VSD-Studio' software (available at www.rivm.nl/cce).

6.5 Model Calculations and Presentation of Model Results

As stated above, the most demanding part is not the actual running of a model, but the derivation and preparation of input data (files) and the model initialisation/calibration. However, especially for regional applications, i.e. runs for many sites, additional work is required to embed the model – often designed for single site applications – into a suitable (data base) framework which allows the efficient handling of model inputs and outputs.

6.5.1 Use of dynamic models in integrated assessment

Most usefully, for the review of the Gothenburg Protocol, a link should be established between the dynamic models and integrated assessment (models). In the following several modes of interaction with integrated assessment (IA) models are identified.

Scenario analyses:

Deposition scenario output from IA models are used by the 'effects community' (ICPs) as input to dynamic models to analyse their impact on (European) soils and surface waters, and the results (recovery times etc.) are reported back.

Presently available dynamic models are well suited for this task. The question is how to summarise the resulting information on a

European scale. Also, the 'turn-around time' of such an analysis, i.e. the time between obtaining deposition scenarios and reporting back dynamic model results, may be long, as it could involve the work of several subsidiary bodies under the LRTAP Convention.

Response functions:

Response functions are pre-processed dynamic model runs for a large number of plausible future deposition patterns from which the results for every (reasonable) deposition scenario can be obtained by interpolation. Such response functions encapsulate a site's temporal behaviour to reach a certain (chemical) state and linking them to IA models allows to evaluate the site's response to a broad range of deposition patterns.

An example is shown in Figure 6.4: It shows the isolines of years ('recovery isochrones') in which $AI/Bc=1$ is attained for the first time for a given combination of percent deposition reduction (vertical axis) and implementation year (horizontal axis). The reductions are expressed as percentage of the deposition in 2010 after implementation of the Gothenburg Protocol and the implementation year refers to the full implementation of that additional reduction. For example, a 44% reduction of the 2010 deposition, fully implemented by the year 2020 will result in a (chemical) recovery by the year 2040 (dashed line in Figure 6.4). Note that for this example site no recovery is possible, unless deposition is reduced more than 18% of the 2010 level.

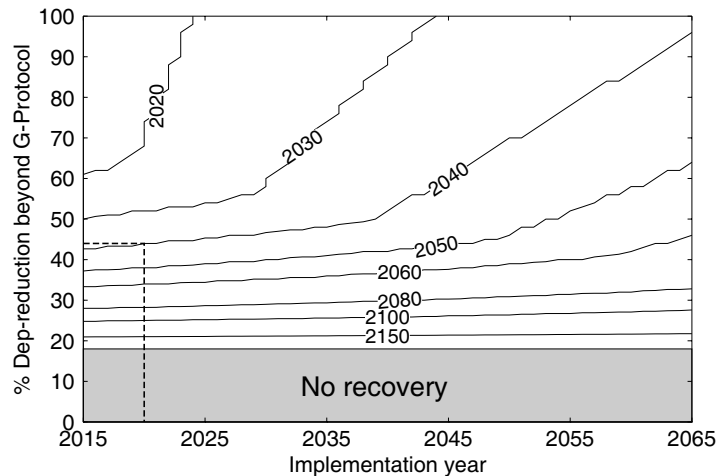


Figure 6.4: Example of ‘recovery isochrones’ for a single site. The vertical axis gives the additional reduction in acidifying deposition *after* the implementation of the Gothenburg Protocol in 2010 (expressed as percentage of the 2010 level) and the horizontal axis the year at which this additional reductions are fully implemented. The isolines are labelled with the first year at which $Al/Bc=1$ is attained for a given combination of percent reduction and implementation year.

Considering how critical loads have been used in IA during the negotiations of protocols, it is unlikely that there will be a wide variation in the implementation year of a new reduction agreement (generally 5-10 years after a protocol enters into force). Thus, for a fixed implementation year the question will be: What is the maximum deposition allowed to achieve recovery, i.e., reach (and sustain!) a desired chemical state (e.g. $Al/Bc=1$) in a prescribed year? Such a

deposition is called a **target load** and, in the case of a single pollutant, target loads can, in principle, be read from information as presented in Figure 6.4. In Figure 6.5 target loads (expressed as percent deposition reductions from the 2010 level) are shown explicitly as function of the target year for the (fixed) implementation year 2020. In the case of a single pollutant, this is the type of information to be linked to IA models.

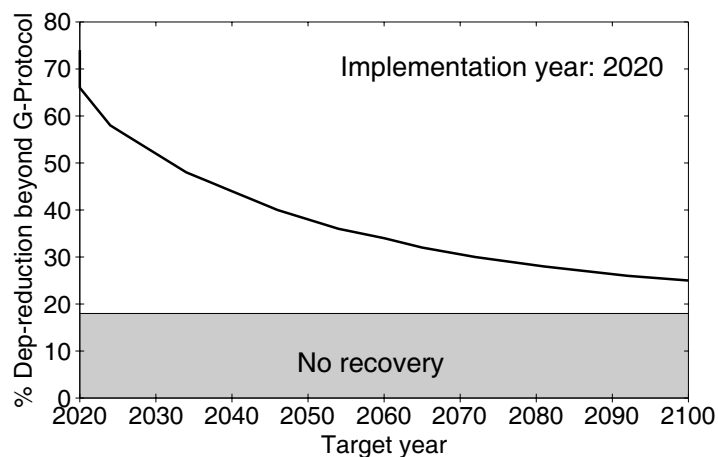


Figure 6.5: Required deposition reductions (target loads) for a site as a function of the target year, i.e. the year in which recovery is achieved (see also Figure 6.4). The implementation year of the reductions is 2020. Note that for reductions above 74% the recovery happens already before the implementation year.

However, in the case of acidity, both N and S deposition determine the soil chemical state and it will not be possible to obtain unique pairs of N and S deposition to reach a prescribed target (similar to critical load functions for acidity). Thus, target loads functions have to be derived with dynamic models for a series of target years and agreed upon implementation years. These target load functions, or suitable statistics derived from them, are passed on to the IA modellers who evaluate their feasibility of achievement (in terms of costs and technological abatement options available).

The determination of response functions, such a target loads, requires no changes to existing models *per se*, but rather additional work, since dynamic soil model have to run many times and/or 'backwards', i.e. in an iterative mode. A further discussion of the problems and possible pitfalls in the computation of target loads is provided in the next section (see also Jenkins et al. 2003).

Integrated dynamic model:

The 'most intimate' link would be the integration of a dynamic model into an IA model (e.g. RAINS). In this way it could be an integral part of all scenario analyses and optimisation runs. Widely used models, such as MAGIC, SAFE and SMART, are not easily

incorporated into IA models, and they might be still too complex to be used in optimisation runs. Alternatively, a very simple dynamic model could be incorporated into an IA model, capturing the essential, long-term features of dynamic soil models. This would be comparable to the process that led to the simple ozone model included in RAINS, which was derived from the complex photo-oxidant model of EMEP. However, even this would require a major effort, not the least of which is the creation of a European database to run the model.

6.5.2 Target load calculations

As outlined above, target loads, or target load functions in the case of acidification, are a way to link dynamic models with integrated assessment models, not least due to their similarity with critical load functions (see Chapter 5). If a target load exists, there exists also an infinite variety of deposition paths to reach that target load. To bring order into this multitude and to make results comparable, we define a target load as a deposition path characterised by three numbers (years): (i) the protocol year, (ii) the implementation year, and (iii) the target year (see Figure 6.6). If needed, these terms are preceded by the term 'dynamic modelling' ('DM') to distinguish them from similar terms used in IA circles.

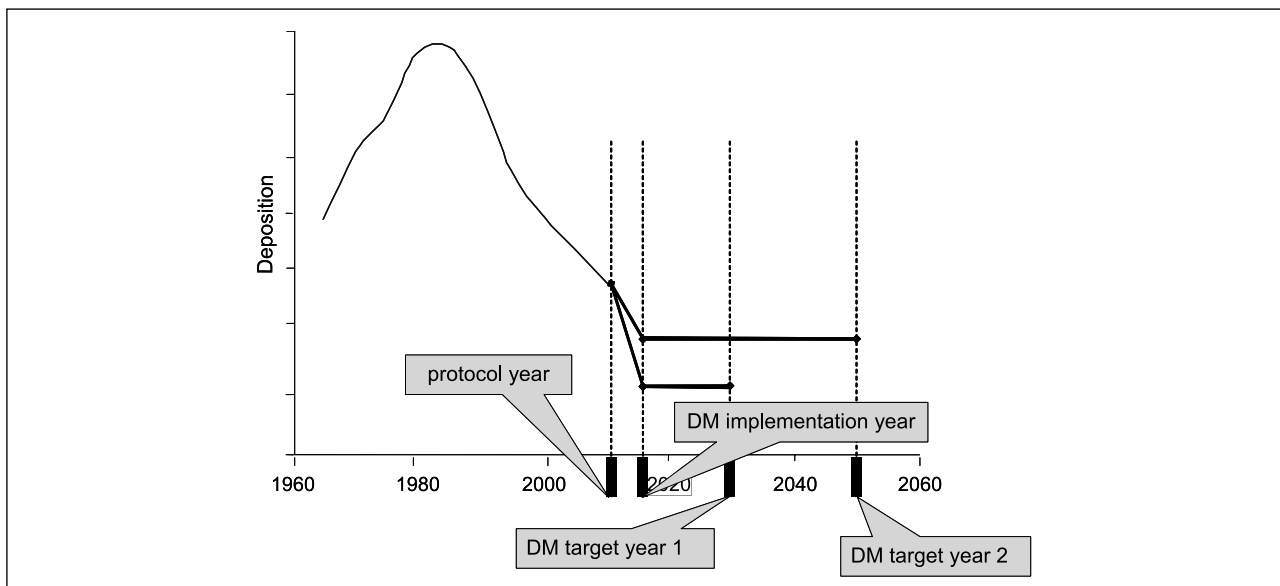


Figure 6.6: Deposition paths for calculating target loads by dynamic models (DM) are characterised by three key years. (i) The year up to which the (historic) deposition is fixed (**protocol year**); (ii) the year in which the emission reductions leading to a target load are fully implemented (**DM implementation year**); and (iii) the years in which the chemical criterion is to be achieved (**DM target years**).

In contrast to scenario analyses, the computation of target loads is not straightforward. After specifying the target year and the year of implementation of the (yet unknown) target load, the dynamic model has to be run iteratively until the deposition (= target load) is found which is required to reach the desired chemical status in the specified target year. The following examples demonstrate the different cases that can arise when calculating target loads and what can happen when doing such calculations 'blindly'. For simplicity we use a single pollutant (deposition), but the conclusions hold for target load functions as well.

As an example, Figure 6.7 shows the deposition history (left) and the resulting molar Al/Bc -ratio (right) as simulated (by the VSD

model) for three different soils, solely distinguished by their CEC (40, 60 and 80 meq/kg). In two cases the Al/Bc -ratio in the year 2010 is above the critical value (=1), while for $CEC=80$ it stayed below it during the past. To investigate the future behaviour of the soils, we let the deposition drop to the critical load (which is independent of the CEC) during the 'implementation period' (marked by two vertical lines in Figure 6.7). Obviously, for $CEC=80$, the Al/Bc -ratio stays below one, whereas for $CEC=60$ it drops below one within the first decade and then slowly rises again towards the critical value. For $CEC=40$, the Al/Bc -ratio stays well above the critical value, approaching it asymptotically over time. In all three cases the approach to the critical value is very slow.

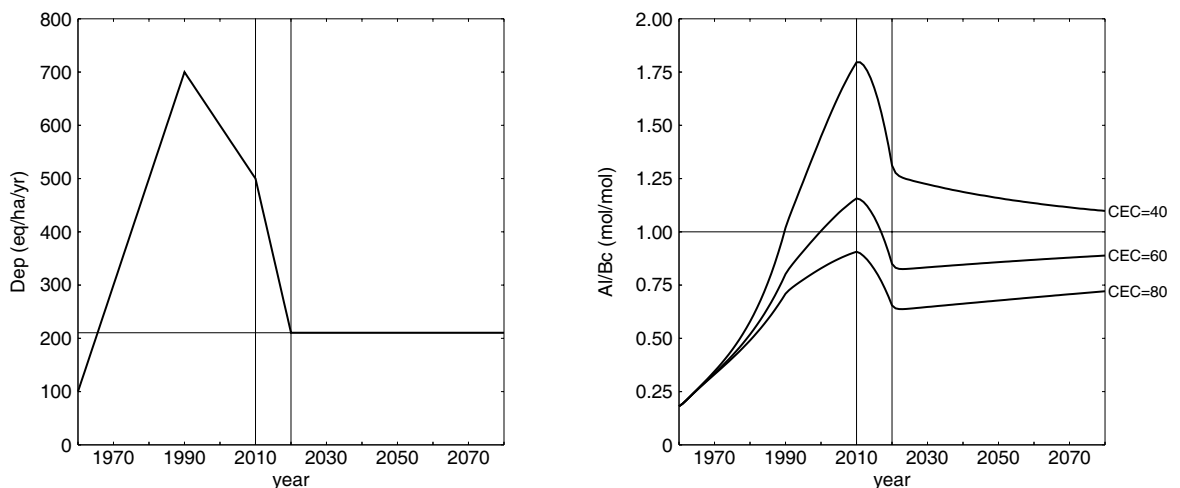


Figure 6.7: Temporal development of acidifying deposition (left) and corresponding molar Al/Bc -ratio (right) for 3 soils varying in CEC . The two vertical lines separate 50 years of 'history', 10 years (2010-2020) of implementation, and the future. Also shown are the critical load and the critical value $(Al/Bc)_{crit}=1$ as thin horizontal lines. The deposition drops to the critical load within the implementation period and the Al/Bc -ratios (slowly) approach the critical value.

Next we look at target load calculations for these three soils. Figure 6.8 shows the results of target load calculations for 40 years, i.e. achieving $(Al/Bc)_{crit}=1$ in the year 2050. For $CEC=40$ meq/kg the target load is smaller than the critical load, as one would expect. For $CEC=60$ and 80, however, the computed target loads are higher than the critical load. As Figure 6.8 illustrates, this

does not make sense: After reaching the critical limit, these two soils deteriorate and the Al/Bc -ratio gets larger and larger. Since target loads are supposed to protect also after the target year, we stipulate that *whenever a calculated target load is higher than the critical load, it has to be set equal to the critical load*.

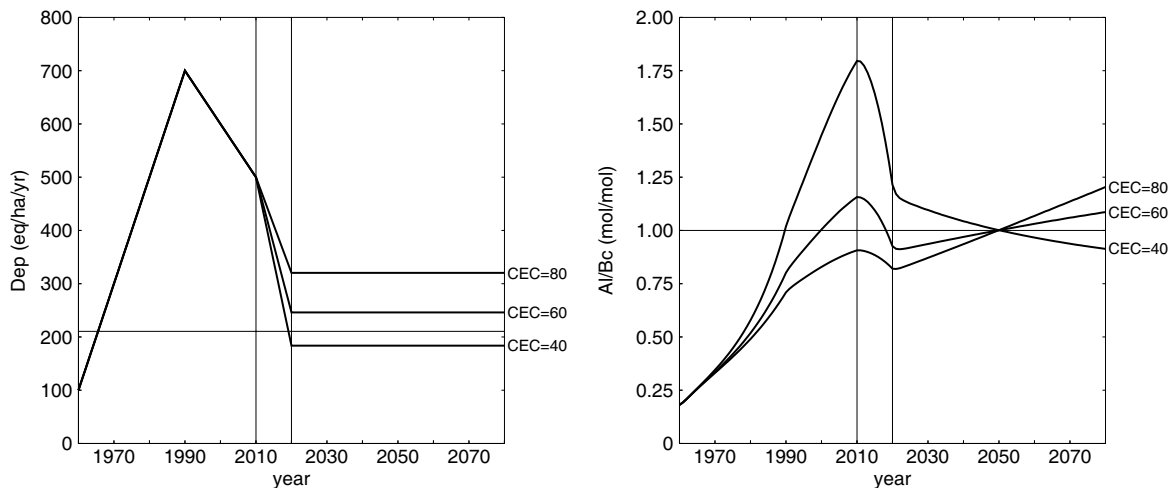


Figure 6.8: Target loads (with 2050 as target year) for three soils and the resulting Al/Bc -ratio (left). Note that for $CEC=60$ and 80 the target load is higher than the critical load, even when $(Al/Bc)_{crit} < 1$ at present (for $CEC=80$)! Clearly, in such cases target load calculations don't make sense.

In the light of the above considerations we define that **a target load is the deposition for which a pre-defined chemical or biological status is reached in the target year and maintained (or improved) thereafter.**

In view of this, the steps to be considered for calculating a target load are shown in the flow chart in Figure 6.9. The first check at

every site is, whether the critical load (CL) is exceeded in the reference year (2010 in our case). If the answer is 'yes' (as for the soils with $CEC=40$ and 60 in Figure 6.7), the next step is to run the dynamic model with the deposition equal to the critical load. If in the target year the chemical criterion is no longer violated (e.g. $Al/Bc \leq 1$), the target load equals the critical load ($TL=CL$).

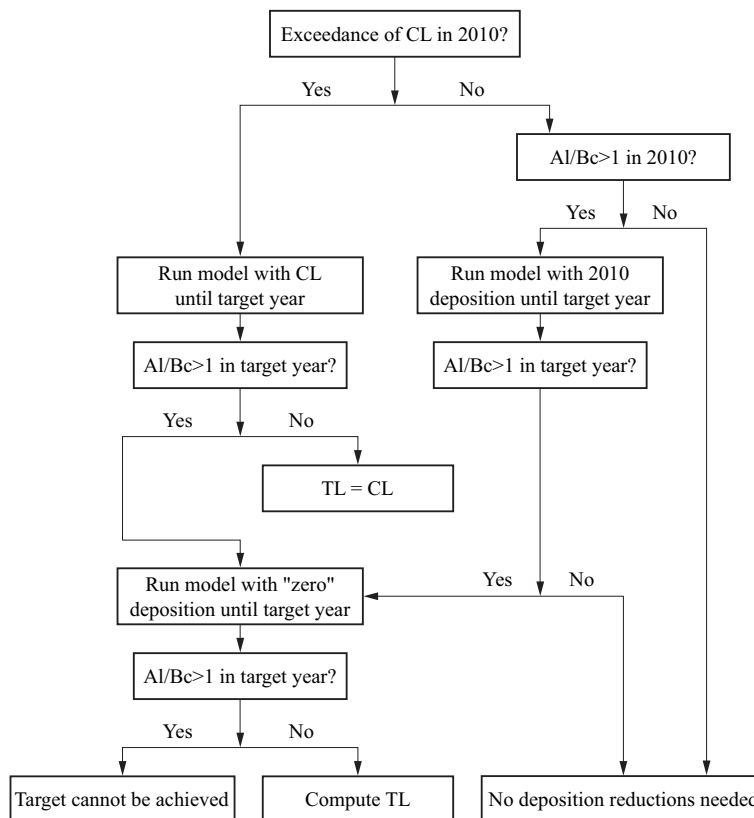


Figure 6.9: Flow chart of the procedure to calculate a target load, avoiding the pitfalls mentioned in the text (e.g. computing a target load that allows violation of the criterion after the target year).

If, after running the model with the critical load as deposition, the criterion is still violated in the target year, the model has to be run with “zero” deposition until the specified target year. “Zero” deposition means a deposition small enough as not to contribute to acidification (or eutrophication). In the case of nitrogen this would mean that N_{dep} is set equal to $CL_{min}(N)$, thus avoiding problems, e.g. negatively influencing forest growth in case of zero N deposition.

If, after running the model with “zero” deposition, the criterion is still violated in the target year, then the target cannot be met in that year. In such a case recovery can only be achieved in a later year. Otherwise, a target load exists and has to be calculated; its value lies somewhere between zero and the critical load.

If the critical load is not (or no longer) exceeded in 2010 (as for the soil with $CEC=80$ in Figure 6.7), this does *not* mean that the risk of damage to the ecosystem is already averted – it only means that *eventually*, maybe after a very long time, the chemical criterion is no longer violated. Only if, in addition, the chemical criterion is not violated in 2010, no further emission reductions are required for that ecosystem. Also, if the model is run with the 2010 deposition until the target year and the criterion is no longer violated in that year, no further emission reductions are required.

In the implementation of the above procedure one could skip the step in which the model is run with the critical load as deposition (in case of exceedance in 2010) and immediately start with target load calculations (if a target load exists). And only afterwards check if this target load is greater than the CL (and set it equal to the CL) (see the soil with $CEC=60$ in Figure 6.8). However, in view of the fact that TL calculations require iterative model runs, and also to avoid surprises due to round-off errors, it makes good sense to include that intermediate step.

An issue requiring attention in all target load calculations is the assumptions about finite nitrogen buffers. If it is, e.g., assumed that a soil can immobilise N for (say) the next 50 years more than assumed in the critical load calculations, then target loads can be higher than the critical load. This might cause confusion and demands careful explanations.

The above considerations hold also in the case of two pollutants, such as S and N in the case of acidification. The results is then not a single value for a target load, but a so-called **target load function** consisting of all pairs of deposition (N_{dep}, S_{dep}) for which the target is achieved in the selected year. This concept is very similar to the critical load function (see Chapter 5). In Figure 6.10 examples of target load functions are shown or a set of target years.

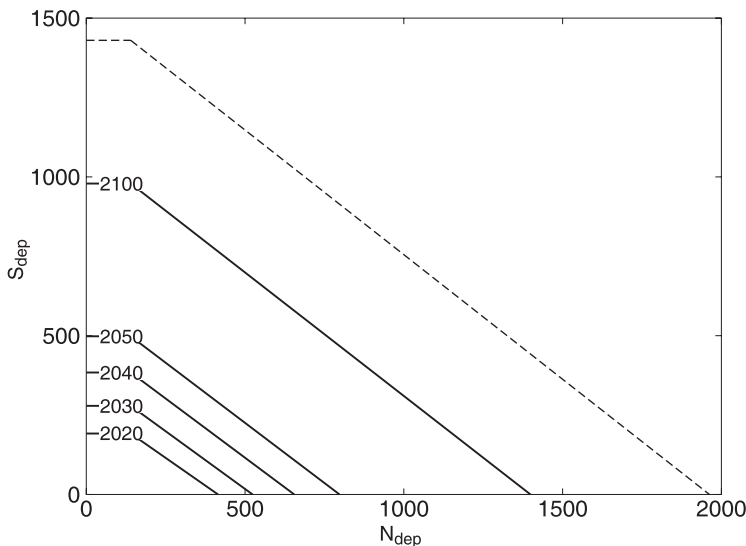


Figure 6.10: Example of target load functions for a site for five different target years. Also shown is the critical load function of the site (dashed line). Note that any meaningful target load function has to lie below the critical load function, i.e. require stricter deposition reductions than achieving critical loads.

When summarising target load calculations for ecosystems in a grid square (or region) it is important not only to report sites for which target load (functions) could be derived, but all cases (and their areas), i.e. the sites for which (i) no further deposition reductions are necessary, (ii) a target load has been calculated, and (iii) no target load exists (for the given target year). Note that in case (i), the 2010 deposition has necessarily to be below (or equal to) the critical load.

6.5.3 Presentation of model results

For single site applications of dynamic models the obvious way to present model output are graphs of the *temporal development of*

the most relevant *soil chemical variables*, such as base saturation or the concentrations of ions in the soil solution (e.g. *Al/Bc-ratio*), in response to given deposition scenarios. In regional (European) applications, however, this kind of information has to be summarised. This can be done in several ways, e.g., by displaying the temporal development of selected percentiles of the distribution of the variable(s) of interest (see Figure 6.11). Another way is to show a sequence of maps displaying the variable of interest in (say) five-year intervals ('map movies'). These and other options are discussed and illustrated in Evans et al. (2001), Jenkins et al. (2002) and Moldan et al. (2003).

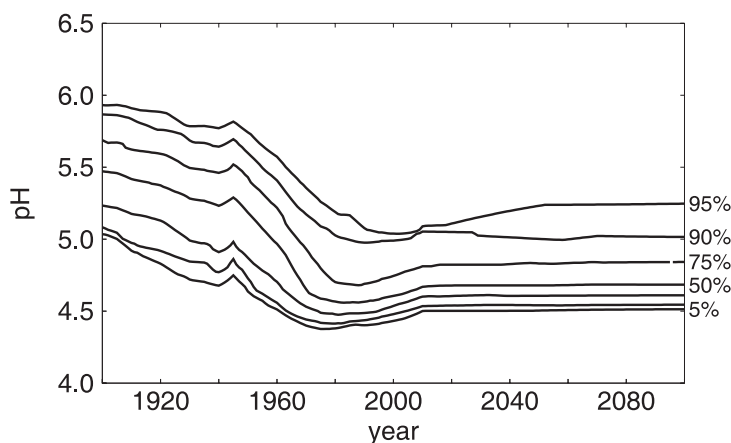


Figure 6.11: Example of percentile traces of a regional dynamic model output. From it seven percentiles (5, 10, 25, 50, 75, 90 and 95%) can be read for every time step.

Maps can represent single sites only if their number does not become too large. If the number of sites reaches the thousands, statistical descriptors (means, percentiles) have to be used to represent the model output. For example, for a given target year the percentage of ecosystems in a grid square for which the target is achieved under a given deposition scenario can be displayed in a map format, very much in the same way as protection percentages (derived from protection isolines) have been displayed for critical load exceedances. Procedures for calculating percentiles and 'target load' isolines can be found in Chapter 8.

References

- Allott TEH, Battarbee RW, Curtis C, Kreiser AM, Juggins S, Harriman R (1995) An empirical model of critical acidity loads for surface waters based on palaeolimnological data. In: Hornung M, Sutton MA, Wilson RB (eds) *Mapping and Modelling of Critical Loads for Nitrogen: A Workshop Report*. Institute of Terrestrial Ecology, Penicuik, United Kingdom, pp.50-54.
- Alveteg M (1998) Dynamics of forest soil chemistry. PhD thesis, Reports in Ecology and Environmental Engineering 3:1998, Department of Chemical Engineering II, Lund University, Lund, Sweden, 81 pp.+appendices.
- Alveteg M, Sverdrup H, Kurz D (1998) Integrated assessment of soil chemical status. 1. Integration of existing models and derivation of a regional database for Switzerland. *Water, Air and Soil Pollution* 105: 1-9.
- Alveteg M, Sverdrup H (2002) Manual for regional assessments using the SAFE model (draft version 8 April 2002). Department of Chemical Engineering II, Lund University, Lund, Sweden. See also www2.chemeng.lth.se
- Battarbee RW, Allott TEH, Juggins S, Kreiser AM, Curtis C, Harriman R (1996) Critical loads of acidity to surface waters – an empirical diatom-based palaeolimnological model. *Ambio* 25: 366-369.
- Berendse F, Beltman B, Bobbink R, Kwant M, Schmitz MB (1987) Primary production and nutrient availability in wet heathland ecosystems. *Acta Oec./Oecol. Plant.* 8: 265-276.
- Berendse F (1988) The nutrient balance of vegetation on dry sandy soils in the context of eutrophication via the air. Part 1: A simulation model as an aid for the management of wet heathlands (in Dutch). Centre for Agrobiological Research, Wageningen, The Netherlands, 51 pp.
- Brady NC (1974) *The Nature and Properties of Soils* (8th edition). MacMillan, New York, 693 pp.
- Cole JJ, Caraco NF, Kling GW, Kratz TK (1994) Carbon dioxide supersaturation in the surface waters of lakes. *Science* 265: 1568-1570.
- Cosby BJ, Hornberger GM, Galloway JN, Wright RF (1985a) Modeling the effects of acid deposition: Assessment of a lumped parameter model of soil water and streamwater chemistry. *Water Resources Research* 21(1): 51-63.
- Cosby BJ, Wright RF, Hornberger GM, Galloway JN (1985b) Modeling the effects of acid deposition: Estimation of long-term water quality responses in a small forested catchment. *Water Resources Research* 21(11): 1591-1601.
- Cosby BJ, Hornberger GM, Galloway JN, Wright RF (1985c) Time scales of catchment acidification: A quantitative model for estimating freshwater acidification. *Environmental Science & Technology* 19:1144-1149.
- Cosby BJ, Hornberger GM, Wright RF, Galloway JN (1986) Modeling the effects of acid deposition: Control of long-term sulfate dynamics by soil sulfate adsorption. *Water Resources Research* 22(8): 1283-1291.

- Cosby BJ, Ferrier RC, Jenkins A, Wright RF (2001) Modelling the effects of acid deposition: refinements, adjustments and inclusion of nitrogen dynamics in the MAGIC model. *Hydrology and Earth System Sciences* 5(3): 499-517.
- De Vries W, Posch M, Kämäri J (1989) Simulation of the long-term soil response to acid deposition in various buffer ranges. *Water, Air and Soil Pollution* 48: 349-390.
- De Vries W, Hol A, Tjalma S, Voogd JC (1990) Stores and residence times of elements in a forest ecosystem: a literature study (in Dutch). DLO-Staring Centrum, Rapport 94, Wageningen, The Netherlands, 205 pp.
- De Vries W (1991) Methodologies for the assessment and mapping of critical loads and the impact of abatement strategies on forest soils. DLO Winand Staring Centre for Integrated Land, Soil and Water Research, Report 46, Wageningen, The Netherlands, 109 pp.
- De Vries W, Reinds GJ, Posch M, Kämäri J (1994) Simulation of soil response to acidic deposition scenarios in Europe. *Water, Air and Soil Pollution* 78: 215-246.
- De Vries W (1994) Soil response to acid deposition at different regional scales. Field and laboratory data, critical loads and model predictions. PhD Thesis, Agricultural University, Wageningen, The Netherlands, 487 pp.
- De Vries W, Van Grinsven JJM, Van Breemen N, Leeters EEJM, Jansen PC (1995) Impacts of acid atmospheric deposition on concentrations and fluxes of solutes in Dutch forest soils. *Geoderma* 67: 17-43.
- De Vries W, Posch M (2003) Derivation of cation exchange constants for sand loess, clay and peat soils on the basis of field measurements in the Netherlands. Alterra-rapport 701, Alterra Green World Research, Wageningen, The Netherlands, 50 pp.
- Dise NB, Matzner E, Gundersen P (1998) Synthesis of nitrogen pools and fluxes from European forest ecosystems. *Water, Air and Soil Pollution* 105: 143-154.
- Driscoll CT, Lehtinen MD, Sullivan TJ (1994) Modeling the acid-base chemistry of organic solutes in Adirondack, New York, lakes. *Water Resources Research* 30: 297-306.
- Ellenberg H (1985) Veränderungen der Flora Mitteleuropas unter dem Einfluss von Düngung und Immissionen. *Schweizerische Zeitschrift für das Forstwesen* 136: 19-39.
- Evans C, Jenkins A, Helliwell R, Ferrier R, Collins R (2001) Freshwater Acidification and Recovery in the United Kingdom. Centre for Ecology and Hydrology, Wallingford, United Kingdom, 80 pp.
- FAO (1981) FAO Unesco Soil Map of the World, 1:5,000,000. Volume V Europe. Unesco, Paris 1981, 199 pp.
- Friend AD, Stevens AK, Knox RG, Channel MGR (1997) A process-based terrestrial biosphere model of ecosystem dynamics (Hybrid v3.0). *Ecological Modelling* 95: 249-287.
- Foster NW, Morrison IK, Nicolson JA (1986) Acid deposition and ion leaching from a podzolic soil under hardwood forest. *Water, Air and Soil Pollution* 31: 879-889.
- Gardiner MJ (1987) Representative data for major soil units in the EEC soil map. An Foras Taluntais, Ireland. Internal Report, 486 pp.
- Gundersen P, Callesen I, De Vries W (1998) Nitrate leaching in forest ecosystems is controlled by forest floor C/N ratio. *Environmental Pollution* 102: 403-407.
- Hann BJ, Turner MA (2000) Littoral microcrustacea in Lake 302S in the Experimental Lakes Area of Canada: acidification and recovery. *Freshwater Biology* 43: 133-146.
- Heil GW, Bobbink R (1993) 'CALLUNA' a simulation model for evaluation of impacts of atmospheric nitrogen deposition on dry heathlands. *Ecological Modelling* 68: 161-182.
- Helling CS, Chesters G, Corey RB (1964) Contribution of organic matter and clay to soil cation exchange capacity as affected by the pH of the saturating solution. *Soil*

- Sci. Soc. Am. J.* 28: 517-520.
- Hoekstra C, Poelman JNB (1982) Density of soils measured at the most common soil types in the Netherlands (in Dutch). Report 1582, Soil Survey Institute, Wageningen, The Netherlands, 47 pp.
- Jacobsen C, Rademacher P, Meesenburg H, Meiwes KJ (2002) Element contents in tree compartments – Literature study and data collection (in German). Report, Niedersächsische Forstliche Versuchsanstalt, Göttingen, Germany, 80 pp.
- Jenkins A, Larssen T, Moldan F, Posch M, Wright RF (2002) Dynamic modelling of surface waters: Impact of emission reduction – possibilities and limitations. ICP-Waters Report 70/2002, Norwegian Institute for Water Research (NIVA), Oslo, Norway, 42 pp.
- Jenkins A, Cosby BJ, Ferrier RC, Larssen T, Posch M (2003) Assessing emission reduction targets with dynamic models: deriving target load functions for use in integrated assessment. *Hydrology and Earth System Sciences* 7(4): 609-617.
- Johnson DW, Todd DE (1983) Relationships among iron, aluminium, carbon, and sulfate in a variety of forest soils. *Soil Sci. Soc. Am. J.* 47: 792-800.
- Keller W, Gunn JM (1995) Lake water quality improvements and recovering aquatic communities. In: Gunn JM (ed), *Restoration and Recovery of an Industrial Region*, Springer Verlag, New York, pp.67-80.
- Klap JM, Brus DJ, De Vries W, Reinds GJ (2004) Assessment of site-specific estimates of critical deposition levels for nitrogen and acidity in European forest ecosystems using measured and interpolated soil chemistry. (in prep).
- Kros J, Reinds GJ, De Vries W, Latour JB, Bollen M (1995) Modelling of soil acidity and nitrogen availability in natural ecosystems in response to changes in acid deposition and hydrology. Report 95, DLO Winand Staring Centre, Wageningen, The Netherlands, 90 pp.
- Kurz D, Alveteg M, Sverdrup H, (1998) Integrated assessment of soil chemical status. 2. Application of a regionalized model to 622 forested sites in Switzerland. *Water, Air and Soil Pollution* 105: 11-20.
- Latour JB, Reiling R (1993) A multiple stress model for vegetation (MOVE): a tool for scenario studies and standard setting. *Science of the Total Environment Supplement* 93: 1513-1526.
- Martinson L, Alveteg M, Warfvinge P (2003) Parameterization and evaluation of sulfate adsorption in a dynamic soil chemistry model. *Environmental Pollution* 124(1): 119-125.
- Mills KH, Chalanchuk SM, Allan DJ (2000) Recovery of fish populations in Lake 223 from experimental acidification. *Can. J. Fish. Aquat. Sci.* 57: 192-204.
- Moldan F, Beier C, Holmberg M, Kronnäs V, Larssen T, Wright RF (2003) Dynamic modelling of soil and water acidification: Display and presentation of results for policy purposes. Acid Rain Research Report 56/03, Norwegian Institute for Water Research (NIVA), Oslo, Norway, 62 pp.
- Oja T, Yin X, Arp PA (1995) The forest modelling series ForM-S: applications to the Solling spruce site. *Ecological Modelling* 83: 207-217.
- Posch M, Reinds GJ, De Vries W (1993) SMART – A Simulation Model for Acidification's Regional Trends: Model description and user manual. Mimeograph Series of the National Board of Waters and the Environment 477, Helsinki, Finland, 43 pp.
- Posch M, Hettelingh J-P, Slootweg J (eds) (2003) Manual for dynamic modelling of soil response to atmospheric deposition. RIVM Report 259101012, Bilthoven, The Netherlands, 69 pp. See also www.rivm.nl/cce
- Posch M, Reinds GJ (2005) VSD - User Manual of the Very Simple Dynamic soil acidification model. Coordination Center for Effects, RIVM, Bilthoven, The Netherlands (in preparation).

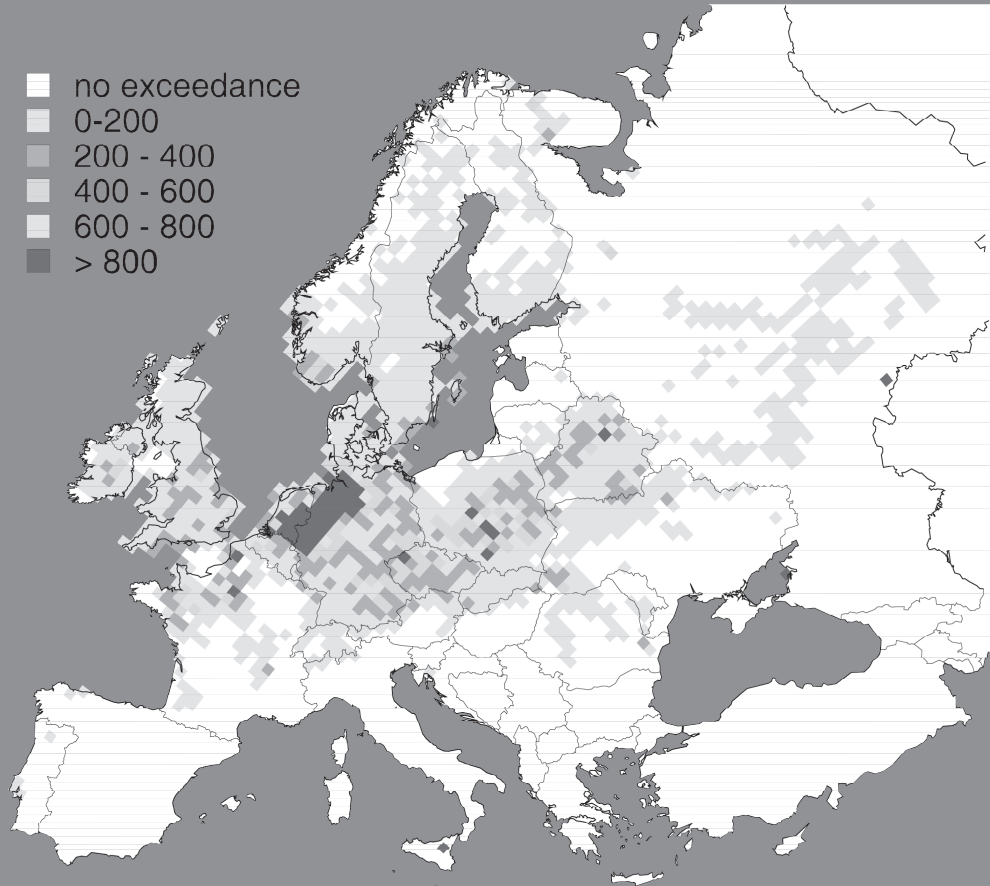
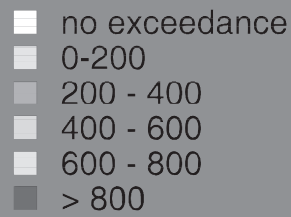
- Raddum GG (1999) Large scale monitoring of invertebrates: Aims, possibilities and acidification indexes. In: GG Raddum, BO Rosseland, J Bowman (eds) Workshop on Biological Assessment and Monitoring; Evaluation and Models. ICP-Waters Report 50/99, Norwegian Institute for Water Research, Oslo, Norway, pp.7-16.
- Reinds GJ, Posch M, De Vries W (2001) A semi-empirical dynamic soil acidification model for use in spatially explicit integrated assessment models for Europe. Alterra Report 084, Alterra Green World Research, Wageningen, The Netherlands, 55 pp.
- Reuss JO (1980) Simulation of soil nutrient losses due to rainfall acidity. *Ecological Modelling* 11: 15-38.
- Reuss JO (1983) Implications of the calcium-aluminum exchange system for the effect of acid precipitation on soils. *Journal of Environmental Quality* 12(4): 591-595.
- Reuss JO, Johnson DW (1986) *Acid Deposition and the Acidification of Soils and Waters*. Ecological Studies 59, Springer, New York, 119 pp.
- SAEFL (1998) Acidification of Swiss forest soils - Development of a regional dynamic assessment. Environmental Documentation No.89, (Swiss Agency for the Environment, Forest and Landscape), Berne, Switzerland, 115 pp
- Schöpp W, Posch M, Mylona S, Johansson M (2003) Long-term development of acid deposition (1880-2030) in sensitive freshwater regions in Europe. *Hydrology and Earth System Sciences* 7(4): 436-446.
- Schouwenberg EPAG, Houweling H, Jansen MJW, Kros J, Mol-Dijkstra JP (2000) Uncertainty propagation in model chains: a case study in nature conservancy. Alterra Report 001, Alterra Green World Research, Wageningen, The Netherlands, 90 pp.
- Singh BR, Johnson DW (1986) Sulfate content and adsorption in soils of two forested watersheds in southern Norway. *Water, Air and Soil Pollution* 31: 847-856.
- Snucins S, Gunn JM, Keller W, Dixit S, Hindar A, Henriksen A (2001) Effects of regional reductions in sulphur deposition on the chemical and biological recovery of lakes within Killarney Park, Ontario, Canada. *Journal of Environmental Monitoring and Assessment* 67: 179-194.
- Starr M (1999) WATBAL: A model for estimating monthly water balance components, including soil water fluxes. In: S Kleemola, M Forsius (eds) 8th Annual Report, UNECE ICP Integrated Monitoring, Finnish Environment Institute, Helsinki, Finland. *The Finnish Environment* 325: 31-35.
- Tietema A, Duysings JJHM, Verstraten JM, Westerveld JW (1990) Estimation of actual nitrification rates in an acid forest soil. In: AF Harrison, P Ineson, OW Heal (eds) *Nutrient cycling in terrestrial ecosystems; Field methods, application and interpretation*. Elsevier Applied Science, London and New York, pp.190-197.
- Tiktak A, Van Grinsven JJM (1995) Review of sixteen forest-soil-atmosphere models. *Ecological Modelling* 83: 35-53.
- Ulrich B (1981) Ökologische Gruppierung von Böden nach ihrem chemischen Bodenzustand. *Z. Pflanzenernähr. Bodenk.* 144: 289-305.
- Vanmechelen L, Groenemans R, Van Ranst E (1997) Forest soil condition in Europe. Results of a large-scale soil survey. EC-UN/ECE, Brussels, Geneva, 261 pp.
- Van Oene H (1992) Acid deposition and forest nutrient imbalances: a modelling approach. *Water, Air and Soil Pollution* 63: 33-50.
- Van Wallenburg C (1988) The density of peaty soils (in Dutch). Internal Report, Soil Survey Institute, Wageningen, The Netherlands, 5 pp.
- Wamelink GWW, Ter Braak CJF, Van Dobben HF (2003) Changes in large-scale patterns of plant biodiversity predicted from environmental economic scenarios. *Landscape Ecology* 18: 513-527.
- Warfvinge P, Sverdrup H (1992) Calculating critical loads of acid deposition with PROFILE - A steady-state soil chemistry model. *Water, Air and Soil Pollution* 63: 119-143.

Warfvinge P, Holmberg M, Posch M, Wright RF (1992) The use of dynamic models to set target loads. *Ambio* 21: 369-376.

Warfvinge P, Falkengren-Grerup U, Sverdrup H, Andersen B (1993) Modelling long-term cation supply in acidified forest stands. *Environmental Pollution* 80: 209-221.

Wright RF, Lie MC (eds) (2002) Workshop on models for biological recovery from acidification in a changing climate, 9-11 September 2002 in Grimstad, Norway. Acid Rain Research Report 55/02, Norwegian Institute for Water Research (NIVA), Oslo, Norway, 42 pp.

Mapping Manual 2004



This chapter has been compiled by M. Posch, mostly from material scattered in CCE Status Reports. J. Aherne (Canada) read it critically and provided the linguistic information on 'acid rain' and 'exceedance'

In this Chapter the calculation of exceedances, i.e., the comparison of critical load/levels with depositions/concentrations, is described. In Section 7.1 the basic definition of an exceedance is given, including some historical remarks on the origin and use of the word 'exceedance'. In Section 7.2 the concept of a conditional critical load of S and N is introduced, which allows to treat these two acidifying pollutants separately, and thus also straight-forward exceedance calculations. In Section 7.3 the exceedance of critical loads of acidity is defined, which involves two pollutants simultaneously, in Section 7.4 the exceedances of surface water critical loads are considered, and in Section 7.5 the relationship between depositions and target loads are briefly touched. Most of the material presented here is taken from Posch et al. (1997, 1999).

The word 'exceedance' is defined as "the amount by which something, especially a pollutant, exceeds a standard or permissible measurement" (The American Heritage Dictionary of the English Language, Fourth Edition 2000) and is a generally accepted term within the air pollution discipline. Nevertheless, the term 'critical load excess' is preferred by some (English) speakers due to the apparent coining of 'exceedance' during the development of the critical load concept. Interestingly, the Oxford English Dictionary (OED) database has an example of 'exceedance' from 1836 (Quinion 2004) - 36 years *before* Robert Angus Smith is credited with coining of the term 'acid rain' (Smith 1872). However, the term 'acid rain' (in French) had already been used in 1845 by Ducros in a scientific journal article (Ducros 1845).

7.1 Basic Definitions

Critical loads and levels are derived to characterise the vulnerability of ecosystem (parts, components) in terms of a deposition or concentration. If the critical load of pollutant X at a given location is smaller than the deposition of X at that location, it is said that

the critical load is exceeded and the difference is called **exceedance**. In mathematical terms, the exceedance Ex of the critical load $CL(X)$ is given as:

$$(7.1) \quad Ex(X_{dep}) = X_{dep} - CL(X)$$

where X_{dep} is the deposition of pollutant X . In the case of the critical level, the comparison is with the respective concentration quantity. If the critical load is greater than or equal to the deposition, one says that it is not exceeded or there is non-exceedance of the critical load.

An exceedance defined by eq. 7.1 can obtain positive, negative or zero value. Since it is in most cases sufficient to know that there is non-exceedance, without being interested in the magnitude of non-exceedance, the exceedance can be also defined as:

$$(7.2) \quad Ex(X_{dep}) = \max \{0, X_{dep} - CL(X)\} \\ = \begin{cases} X_{dep} - CL(X) & X_{dep} > CL(X) \\ 0 & X_{dep} \leq CL(X) \end{cases}$$

An example of the application of this basic equation is the exceedance of the critical load of nutrient N (see Chapter 5.3.1), which is given by:

$$(7.3) \quad Ex_{nut}(N_{dep}) = N_{dep} - CL_{nut}(N)$$

It should be noted that exceedances differ fundamentally from critical loads, as they are time-dependent. One can speak of *the* critical load of X for an ecosystem, but not of *the* exceedance of it. For exceedances the time for which they have been calculated has to be reported, since - especially in integrated assessment - it is exceedances due to (past or future) *anthropogenic* depositions that are of interest.

Of course, the time-invariance of critical loads and levels has its limitations, certainly

when considering a geological time frame. But also during shorter time periods, such as decades or centuries, one can anticipate changes in the magnitude of critical loads due to global (climate) change, which influences the processes from which critical loads are derived. An example of a study of the (first-order) influence of temperature and precipitation changes on critical loads of acidity and nutrient N in Europe can be found in Posch (2002).

The exceedance of a critical load is often misinterpreted as the amount of excess leaching, i.e., the amount leached above the critical/acceptable leaching. This is in general *not* the case as exemplified by the exceedance of the critical load of nutrient N . The excess leaching due to the deposition N_{dep} , Ex_{le} , is given as:

$$(7.4) \quad Ex_{le}(N_{dep}) = N_{le} - N_{le,acc}$$

Inserting the mass balance of N and the deposition-dependent denitrification one obtains for the excess leaching (eqs.5.2-5.5):

$$(7.5) \quad \begin{aligned} Ex_{le}(N_{dep}) &= (1 - f_{de}) \cdot (N_{dep} - CL_{nut}(N)) \\ &= (1 - f_{de}) \cdot EX_{nut}(N_{dep}) \end{aligned}$$

which shows that a deposition reduction of 1 eq/ha/yr reduces the leaching of N by only $1-f_{de}$ eq/ha/yr. Only in the simplest case, in which all terms of the mass balances are independent of depositions, equals the

change in leaching the change in deposition.

7.2 Conditional Critical Loads of N and S

The non-uniqueness of the critical loads of S and N acidity makes both their implementation into integrated assessment models and their communication to decision makers more difficult. However, if one is interested in reductions of only one of the two pollutants, a unique critical load can be derived, and thus also a unique exceedance according to eq. 7.1 can be calculated.

If emission reductions deal with nitrogen only, a unique critical load of N for a fixed sulphur deposition S_{dep} can be derived from the critical load function. We call it the conditional critical load of nitrogen, $CL(N|S_{dep})$, and it is computed as:

$$(7.6) \quad CL(N|S_{dep}) = \begin{cases} CL_{min}(N) & \text{if } S_{dep} \geq CL_{max}(S) \\ CL_{max}(N) - \alpha \cdot S_{dep} & \text{if } S_{dep} < CL_{max}(S) \end{cases}$$

with

$$(7.7) \quad \alpha = \frac{CL_{max}(N) - CL_{min}(N)}{CL_{max}(S)}$$

In Figure 7.1a the procedure for calculating $CL(N|S_{dep})$ is depicted graphically.

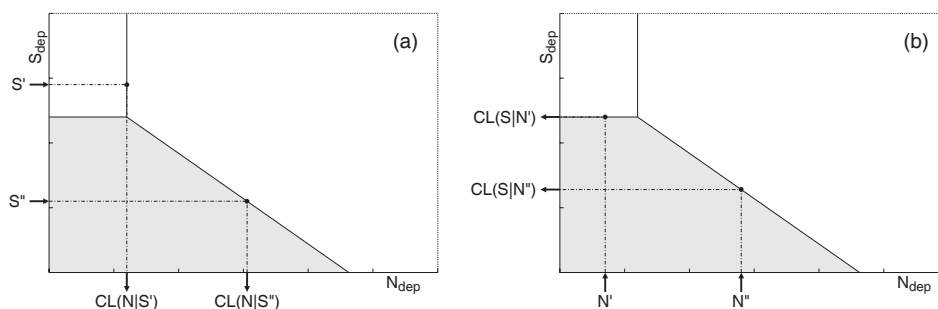


Figure 7.1: Examples of computing (a) conditional critical loads of N for different S deposition values S' and S'' , and (b) conditional critical loads of S for different N deposition values N' and N'' .

In an analogous manner a conditional critical load of sulphur, $CL(N|S_{dep})$, for a fixed nitrogen deposition N_{dep} can be computed as:

$$(7.8) \quad CL(S|N_{dep}) = \begin{cases} 0 & \text{if } N_{dep} \geq CL_{max}(N) \\ \frac{CL_{max}(N) - N_{dep}}{\alpha} & \text{if } CL_{min}(N) < N_{dep} < CL_{max}(N) \\ CL_{max}(S) & \text{if } N_{dep} \leq CL_{min}(N) \end{cases}$$

where α is given by eq. 7.7. The procedure for calculating $CL(N|S_{dep})$ is depicted graphically in Figure 7.1b. Setting $N_{dep} = CL_{nut}(N)$, the resulting conditional critical load has been termed **minimum critical load of sulphur**: $CL_{min}(S) = CL(S|CL_{nut}(N))$.

Eq. 7.8 would have been the consistent procedure for calculating critical loads of S used in the negotiations of the 1994 Oslo Protocol; however, critical loads for nitrogen - $CL_{min}(N)$ and $CL_{max}(N)$ - were not available then.

When using conditional critical loads, the following caveats should be kept in mind:

- (a) A conditional critical load can be considered a true critical load only when the chosen deposition of the other pollutant is kept constant.
- (b) If the conditional critical loads of both pollutants are considered simultaneously, care has to be exercised. It is not necessary to reduce the exceedances of both, but only one of

them to reach non-exceedance for both pollutants; recalculating the conditional critical load of the other pollutant results (in general) in non-exceedance. However, if $S_{dep} > CL_{max}(S)$ or $N_{dep} > CL_{max}(N)$, depositions have to be reduced at least to their respective maximum critical load values, irrespective of the conditional critical loads.

7.3 Two Pollutants

As has been shown in Chapter 5.3, there is no unique critical load of S and N acidity, and all deposition pairs (N_{dep}, S_{dep}) lying on the critical load function lead to the critical leaching on ANC (see eq. 5.19 and Figure 5.1). Whereas non-exceedance is easily defined (as long as its amount is not important), there is no unique exceedance of acidity critical loads. This is illustrated in Figure 7.1a: Let the point E denote the (current) deposition of N and S . By reducing N_{dep} substantially, one reaches the point Z1 and thus non-exceedance without reducing S_{dep} ; on the other hand one can reach non-exceedance by only reducing S_{dep} (by a smaller amount) until reaching Z3; finally, with a reduction of both N_{dep} and S_{dep} , one can reach non-exceedance as well (e.g. point Z2).

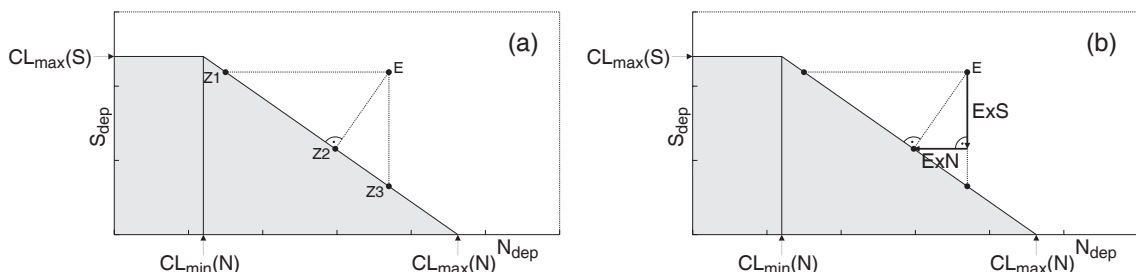


Figure 7.2: Critical load function for S and acidifying N (thick line; see Figure 5.1). The grey-shaded area below the critical load function defines deposition pairs (N_{dep}, S_{dep}) for which there is non-exceedance. (a) The points E and Z1-Z3 show that there is no unique exceedance; (b) the quantities involved in the definition of an exceedance (see text for further explanations).

7 Exceedance Calculations

Intuitively, the reduction required in N and S deposition to reach point $Z2$ (see Figure 7.2b), i.e., the shortest distance to the critical load function, seems a good measure for exceedance. Thus we *define* the exceedance for a given pair of depositions (N_{dep}, S_{dep}) as the sum of the N and S deposition reductions required to reach the critical load function by the 'shortest' path. Figure 7.3 depicts the five cases that can arise:

- (a) the deposition falls on or below the critical load function (Region 0). In this case the exceedance is defined as zero (non-exceedance);
- (b) the deposition falls into Region 1 (e.g. point $E1$). In this case the line perpendicular to the critical load function would yield a negative S_{dep} , and thus

every exceedance in this region is defined as the sum of N and S deposition reduction needed to reach point $Z1$;

- (c) the deposition falls into Region 2 (e.g. point $E2$): this is the 'regular' case, the exceedance is given by the sum of N and S deposition reduction, $ExN + ExS$, required to reach the point $Z2$, such that the line $E2-Z2$ is perpendicular to the critical load function;
- (d) Region 3: every exceedance is defined as the sum of N and S deposition reduction needed to reach point $Z3$;
- (e) Region 4: the exceedance is simply defined as $S_{dep} - CL_{max}(S)$.

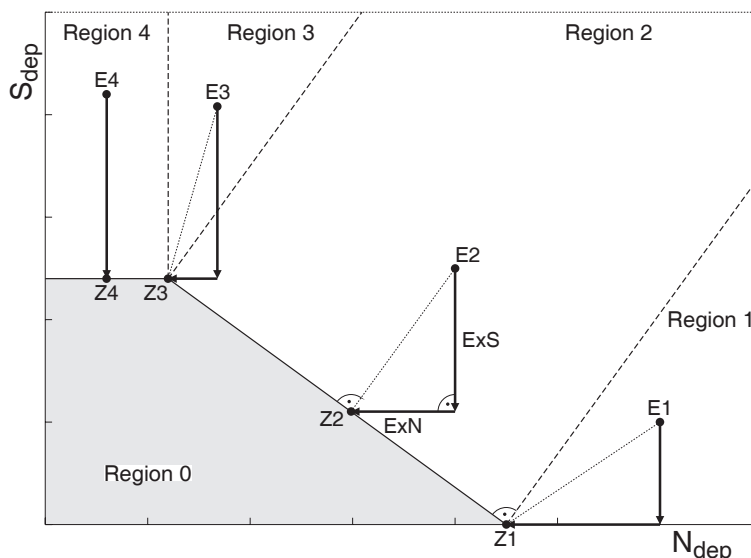


Figure 7.3: Illustration of the different cases for calculating the exceedance for a given critical load function.

The exceedance function can be described by the following equation; note the point $Z2$ on the critical load function obtained by drawing a perpendicular line through a point

in Region 2 (see Figure 7.3) is denoted by (N_0, S_0) :

(7.9)

$$Ex(N_{dep}, S_{dep}) = \begin{cases} 0 & \text{if } (N_{dep}, S_{dep}) \in \text{Region 0} \\ N_{dep} - CL_{max}(N) + S_{dep} & \text{if } (N_{dep}, S_{dep}) \in \text{Region 1} \\ N_{dep} - N_0 + S_{dep} - S_0 & \text{if } (N_{dep}, S_{dep}) \in \text{Region 2} \\ N_{dep} - CL_{min}(N) + S_{dep} - CL_{max}(S) & \text{if } (N_{dep}, S_{dep}) \in \text{Region 3} \\ S_{dep} - CL_{max}(S) & \text{if } (N_{dep}, S_{dep}) \in \text{Region 4} \end{cases}$$

The function thus defined fulfils the criteria of a meaningful exceedance function: it is zero, if there is no exceedance of critical loads, positive when there is exceedance, and increasing in value when the point (N_{dep}, S_{dep}) moves away from the critical load function.

The computation of the exceedance function requires the estimation of the coordinates of the point Z2 on the critical load function. If (x_1, y_1) and (x_2, y_2) are two arbitrary points of a straight line g and (x_e, y_e) another point (not on that line), then the coordinates (x_0, y_0) of the point obtained by intersecting the line passing through (x_e, y_e) and perpendicular to g (called the 'foot' or 'foot of the perpendicular') are given by:

(7.10a)

$$x_0 = (d_1 s + d_2 v) / d^2 \quad \text{and}$$

$$y_0 = (d_2 s - d_1 v) / d^2$$

with
(7.10b)

$$d_1 = x_2 - x_1, \quad d_2 = y_2 - y_1,$$

$$d^2 = d_1^2 + d_2^2$$

and
(7.10c)

$$s = x_e d_1 + y_e d_2,$$

$$v = x_1 d_2 - y_1 d_1 = x_1 y_2 - y_1 x_2$$

Applying these equations to

$(x_1, y_1) = (CL_{min}(N), CL_{max}(S))$,
 $(x_2, y_2) = (CL_{max}(N), 0)$ and $(x_e, y_e) = (N_{dep}, S_{dep})$ one obtains the point $(x_0, y_0) = (N_0, S_0)$ (Z2 in Figure 7.3). The final difficulty in computing the $Ex(N_{dep}, S_{dep})$ is to determine into which of the regions (Region 0 through Region 4 in Figure 7.3) a given pair of deposition (N_{dep}, S_{dep}) falls. Without going into the details of the geometrical considerations, a FORTRAN subroutine is listed below, which returns the number of the region as well as ExN and ExS :

```

subroutine exceed (CLmaxS, CLminN, CLmaxN, depN, depS, ExN, ExS, ireg)
!
! Returns the exceedances ExN and ExS (Ex=ExN+ExS) for N and S
! depositions depN and depS and the critical load function given by
! CLmaxS, CLminN and CLmaxN.
! The 'region' in which (depN, depS) lies, is returned in ireg.
!
integer(4)          ireg
real(4)             CLmaxS, CLminN, CLmaxN, depN, depS, ExN, ExS
!
ExN = -1.
ExS = -1.
if (CLmaxS < 0. .or. CLminN < 0. .or. CLmaxN < 0.) return ! error
d1 = CLmaxN-CLminN
dnn = depN-CLminN
dxn = depN-CLmaxN
dxs = depS-CLmaxS
if (depS <= CLmaxS .and. depN <= CLmaxN .and.
& CLmaxS*dxn <= -d1*depS) then ! non-exceedance
    ireg = 0
    ExN = 0.
    ExS = 0.
else if (depN <= CLminN) then
    ireg = 4
    ExN = 0.
    ExS = dxs
else if (dxn*d1 >= depS*CLmaxS) then
    ireg = 1
    ExN = dxn
    ExS = depS

```

7 Exceedance Calculations

```
else if (CLmaxS*dxs >= d1*dnn) then
  ireg = 3
  ExN = dnn
  ExS = dxs
else
  ireg = 2
  d2 = -CLmaxS
  dd = d1*d1+d2*d2
  s = depN*d1+depS*d2
  v = -CLmaxS*CLmaxN
  x0 = (d1*s+d2*v)/dd
  y0 = (d2*s-d1*v)/dd
  ExN = depN-x0
  ExS = depS-y0
end if

return

end subroutine exceed
```

For a given critical load function an exceedance can be defined for every pair of depositions (N_{dep}, S_{dep}) as outlined above. Connecting points in the (N_{dep}, S_{dep}) plane which have identical values of the

exceedance function, results in **exceedance isolines** as illustrated Figure 7.4. The 'kinks' in the isolines when passing from one exceedance region to a neighbouring one can be clearly discerned.

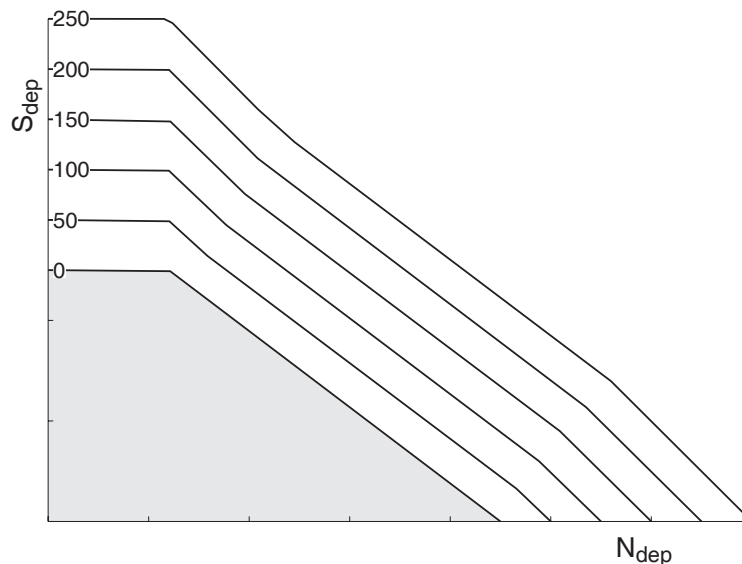


Figure 7.4: Exceedance isolines for a given critical load function. The line labelled "0" corresponds to the critical load function and delimits the grey-shaded area of zero exceedance.

7.4 Surface Waters

Since exceedance calculations for the critical loads for surface waters require special considerations due to the peculiarities of (some of) the models, they are treated here separately. The three critical load models mentioned are described in Chapter 5.4.

7.4.1 The SSWC model

In the SSWC model sulphate is assumed to be a mobile anion (i.e. leaching equals deposition), whereas nitrogen is assumed to a large extent to be retained in the catchment by various processes. Therefore, only the so-called present-day exceedance can be calculated from the leaching of N , N_{le} , which is determined from the sum of the measured concentrations of nitrate and ammonia in the runoff. This present exceedance of the critical load of acidity is defined as (Henriksen and Posch 2001):

(7.11)

$$Ex(A) = S_{dep} + N_{le} - CL(A)$$

where $CL(A)$ is the critical load of acidity as computed with eq. 5.50. No N deposition data are required for this exceedance calculation; however, $Ex(A)$ quantifies only the exceedance at present rates of retention of N in the catchment. Only in the FAB model (see below) are nitrogen processes modelled explicitly, and thus only that model can be used for comparing the effects of different N deposition scenarios. In the above derivation we assumed that base cation deposition and net uptake did not change over time. If there is increased base cation deposition due to human activities or a change in the net uptake due to changes in management practices, this has to be taken into account in the exceedance calculations by subtracting that anthropogenic $BC_{dep}^* - BC_u$ from $S_{dep}^* + N_{le}$.

7.4.2 The empirical diatom model

For this empirical model the exceedance of the critical load of acidity is given by:

(7.12)

$$Ex(A) = S_{dep} + f_N \cdot N_{dep} - CL(A)$$

where f_N is the fraction of the nitrogen deposition contributing to acidification (see eq. 5.66).

7.4.3 The FAB model

Since in the FAB model a critical load function for surface waters is derived from the in the same way as in the SMB model for soils, the same considerations hold as given in Section 7.2. Again there is no unique exceedance for a given pair of depositions (N_{dep}, S_{dep}), but an exceedance can be **defined** in an analogous manner as for the soil critical load function (see also Henriksen and Posch 2001).

7.5 Target Loads

In the previous sections the excess of depositions over critical loads has been defined as exceedance. In the case of target loads or target load functions the same quantities as defined above can be calculated, but if they are positive, we talk about the **non-achievement** of the target load; if it is zero or negative, we say the target (load) for a given year has been achieved.

References

Ducros M (1845) Observation d'une pluie acid. *Journale de la Pharmacologie Chimique* 3: 273-277.

Henriksen A Posch M (2001) Steady-state models for calculating critical loads of acidity for surface waters. *Water, Air and Soil Pollution: Focus* 1: 375-398.

Posch M, Hettelingh J-P, De Smet PAM, Downing RJ (eds) (1997) Calculation and mapping of critical thresholds in Europe. Status Report 1997, Coordination Center for Effects, RIVM Report 259101007, Bilthoven, Netherlands, iv+163 pp. www.rivm.nl/cce

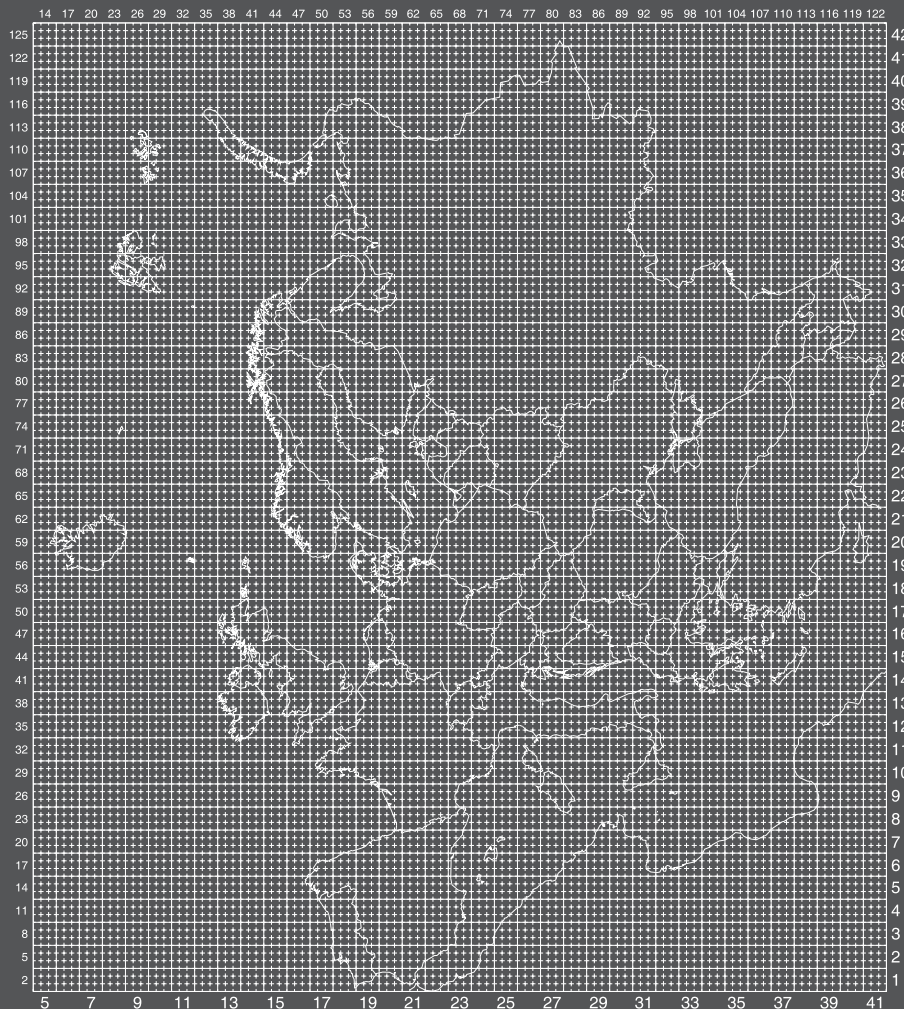
Posch M De Smet PAM, Hettelingh J-P, Downing RJ (eds) (1999) Calculation and mapping of critical thresholds in Europe. Status Report 1999, Coordination Center for Effects, RIVM Report 259101009, Bilthoven, Netherlands, iv+165 pp. www.rivm.nl/cce

Posch M (2002) Impacts of climate change on critical loads and their exceedances in Europe. *Environmental Science and Policy* 5(4): 307-317.

Quinion M (2004) "The example I quoted [on www.worldwidewords.org] is known to the compilers of the OED (who will be writing an entry for 'exceedance' at some point) from their in-house database of unpublished citations. They didn't provide me with a full citation, only with the date" (personal communication to Julian Aherne in July 2004).

Smith RA (1872) *Air and Rain: The Beginnings of a Chemical Climatology*. Longmans, Green & Co., London, 600 pp.

Mapping Manual 2004



This Chapter has been compiled by M. Posch, using material from the previous version of the Manual and various CCE Status Reports.

In this Chapter procedures are discussed which can be used for summarising and presenting results of critical load and exceedance calculations and on a regional scale, in particular on the EMEP grid. The material presented here is a summary of the material from CCE Status Reports (see Posch et al. 1995, 1997, 1999). In Section 8.1 the EMEP grid is defined, in Section 8.2 the methods for the calculation of percentiles (in one and two dimensions) are presented, and in Section 8.3 the (average) accumulated exceedance is defined.

8.1 The EMEP grid

To make critical loads usable and useful for the work under the LRTAP Convention, one has to be able to compare them to deposition estimates. Deposition of sulphur and nitrogen compounds have earlier been reported by EMEP on a 150 x 150 km² grid covering (most of) Europe, but in recent years depositions have also become available on a 50 x 50 km² grid. Both are special cases of the so-called polar stereographic projection, which is described in the following.

8.1.1 The polar stereographic projection

In the polar stereographic projection each point on the Earth's sphere is projected from the South Pole onto a plane perpendicular to the Earth's axis and intersecting the Earth at a fixed latitude ϕ_0 . (See Figure A-1 in the CCE Status Report 2001, p. 182.) Consequently, the coordinates x and y are obtained from the geographical longitude λ and latitude ϕ (in radians) by the following equations:

$$(8.1) \quad x = x_p + M \cdot \tan\left(\frac{\pi}{4} - \frac{\phi}{2}\right) \cdot \sin(\lambda - \lambda_0)$$

and

$$(8.2) \quad y = y_p - M \cdot \tan\left(\frac{\pi}{4} - \frac{\phi}{2}\right) \cdot \cos(\lambda - \lambda_0)$$

where (x_p, y_p) are the coordinates of the North Pole; λ_0 is a rotation angle, i.e. the longitude parallel to the y -axis; and M is the scaling of the x - y coordinates. In the above definition the x -values increase and the y -values decrease when moving towards the equator. For a given unit length (grid size) d in the x - y plane the scaling factor M is given by

$$(8.3) \quad M = \frac{R}{d} \cdot (1 + \sin \phi_0)$$

where R (= 6370 km) is the radius of the Earth. The inverse transformation, i.e. longitude and latitude as function of x and y , is given by

$$(8.4) \quad \lambda = \lambda_0 + \arctan\left(\frac{x - x_p}{y_p - y}\right)$$

and

$$(8.5) \quad \phi = \frac{\pi}{2} - 2 \cdot \arctan(r / M)$$

with

$$r = \sqrt{(x - x_p)^2 + (y - y_p)^2}$$

The *arctan* in eq. 8.5 gives the correct longitude for quadrant 4 ($x > x_p$ and $y < y_p$) and quadrant 3 ($x < x_p$ and $y < y_p$); π (=180°) has to be added for quadrant 1 ($x > x_p$ and $y > y_p$) and subtracted for quadrant 2 ($x < x_p$ and $y > y_p$). Note that quadrant 4 is the one covering (most of) Europe.

Every stereographic projection is a so-called conformal projection, i.e. an angle on the sphere remains the same in the projection

plane, and vice versa. However, the stereographic projection distorts areas (even locally), i.e. it is not an equal-area projection (see below).

We define a **grid cell** (i,j) as a square in the x - y plane with side length d (see eq. 8.3) and centre point as the integral part of x and y , i.e.

$$(8.6) \quad i = \text{nint}(x) \quad \text{and} \quad j = \text{nint}(y)$$

where 'nint' is the nearest integer (rounding function). Consequently, the four corners of the grid cell have coordinates $(i \pm 1/2, j \pm 1/2)$.

8.1.2 The EMEP grid

The 50x50 km² grid (EMEP50 grid):

The eulerian dispersion model of EMEP/ MSC-W produces concentration and deposition fields on a 50 x 50 km² grid with the parameters (see also www.emep.int):

$$(8.7) \quad d = 50 \text{ km}, \quad (x_p, y_p) = (8, 110),$$
$$\phi_0 = \frac{\pi}{3} = 60^\circ \text{ N}, \quad \lambda_0 = -32^\circ \text{ (i.e. } 32^\circ \text{ W)}$$

yielding $M=237.7314\dots$

The 150x150 km² grid (EMEP150 grid):

The coordinate system used by EMEP/ MSC-W for the (old) lagrangian long-range transport model is defined by the following parameters (Saltbones and Dovland 1986):

$$(8.8) \quad d = 150 \text{ km}, \quad (x_p, y_p) = (3, 37),$$
$$\phi_0 = \frac{\pi}{3} = 60^\circ \text{ N}, \quad \lambda_0 = -32^\circ \text{ (i.e. } 32^\circ \text{ W)}$$

which yields $M=79.2438\dots$

An EMEP150 grid cell (i,j) contains $3 \times 3 = 9$ EMEP50 grid cells (m,n) with all combina-

tions of the indices $m=3i-2, 3i-1, 3i$ and $n=3j-2, 3j-1, 3j$. The part of the two EMEP grid systems covering Europe is shown in Figure 8.1.

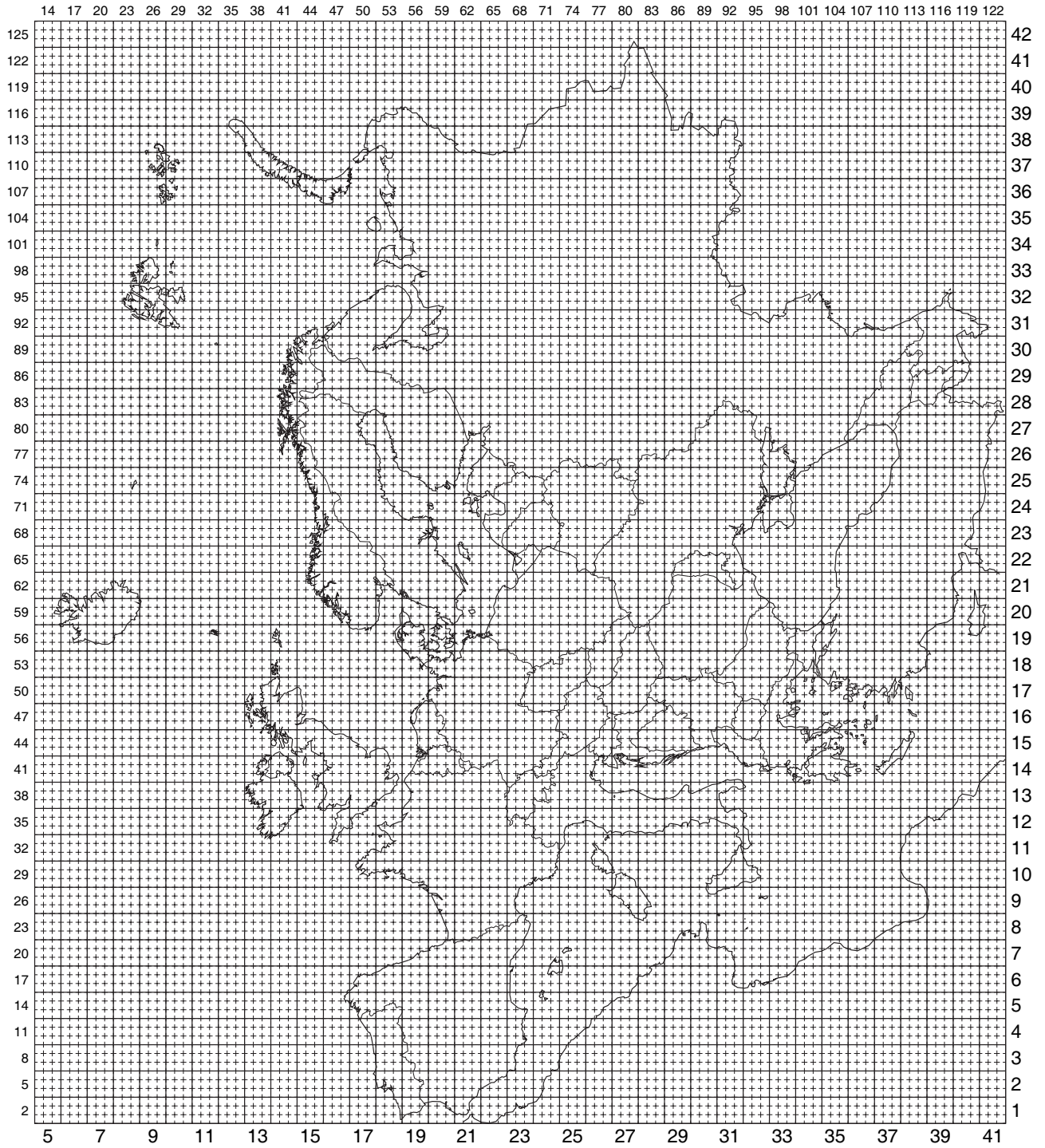


Figure 8.1: The EMEP150 grid (solid lines) and EMEP50 grid (dashed lines). The numbers at the bottom and to the right are EMEP150 grid indices; those at the top and to the left are EMEP50 grid indices (every third).

8 General Mapping Issues

To convert a point (*xlon,ylat*), given in degrees of longitude and latitude, into EMEP coordinates (*emepi,emepj*) the following FORTRAN subroutine can be used:

```
subroutine llemp (xlon,ylat,par,emepi,emepj)
!
! This subroutine computes for a point (xlon,ylat), where xlon is the
! longitude (<0 west of Greenwich) and ylat is the latitude in degrees,
! its EMEP coordinates (emepi,emepj) with parameters given in par().
!
! par(1) ... size of grid cell (km)
! (par(2),par(3)) = (xp,yp) ... EMEP coordinates of the North Pole
!
real(4)          xlon, ylat, par(*), emepi, emepj
!
data Rearth /6370./      ! radius of spherical Earth (km)
data xlon0 /-32./       ! = lambda_0
data drm /1.8660254/    ! = 1+sin(pi/3) = 1+sqrt(3)/2
data pi180 /0.017453293/ ! = pi/180
data pi360 /0.008726646/ ! = pi/360
!
em = (Rearth/par(1))*drm
tp = tan((90.-ylat)*pi360)
rlamp = (xlon-xlon0)*pi180
emepi = par(2)+em*tp*sin(rlamp)
emepj = par(3)-em*tp*cos(rlamp)
!
!                               return
end subroutine llemp
```

EMEP50 coordinates are obtained by calling the above subroutine with *par(1)=50*, *par(2)=8* and *par(3)=110*; and EMEP150 coordinates are obtained with *par(1)=150*, *par(2)=3* and *par(3)=37*. Conversely, the EMEP coordinates of a point can be converted into its longitude and latitude with the following subroutine:

```
subroutine emep11 (emepi,emepj,par,xlon,ylat)
!
! This subroutine computes for a point (emepi,emepj) in the EMEP
! coordinate system, defined by the parameters in par(), its
! longitude xlon and latitude ylat in degrees.
!
! par(1) ... size of grid cell (km)
! (par(2),par(3)) = (xp,yp) ... EMEP coordinates of the North Pole
!
real(4)          emepi, emepj, par(*), xlon, ylat
!
data Rearth /6370./      ! radius of spherical Earth (km)
data xlon0 /-32./       ! = lambda_0
data drm /1.8660254/    ! = 1+sin(pi/3) = 1+sqrt(3)/2
data pi180 /57.2957795/ ! = 180/pi
data pi360 /114.591559/ ! = 360/pi
!
emi = par(1)/(Rearth*drm) ! = 1/M
ex = emepi-par(2)
ey = par(3)-emepj
if (ex == 0. .and. ey == 0.) then ! North Pole
  xlon = xlon0 ! or whatever
else
  xlon = xlon0+pi180*atan2(ex,ey)
endif
endif
r = sqrt(ex*ex+ey*ey)
ylat = 90.-pi360*atan(r*emi)
!
!                               return
end subroutine emep11
```

8.1.3 The area of an EMEP grid cell

As mentioned above, the stereographic projection does not preserve areas, e.g. a 50 x 50 km² EMEP grid cell is 2,500 km² only in the projection plane, but never on the globe. The area A of an EMEP grid cell with lower-left corner (x_1, y_1) and upper-right corner (x_2, y_2) is given by:

$$(8.9) \quad A(x_1, y_1, x_2, y_2) = 2R^2 \left\{ I(u_2, v_2) - I(u_1, v_2) - I(u_2, v_1) + I(u_1, v_1) \right\}$$

where $u_1 = (x_1 - x_p)/M$, etc.; and $I(u, v)$ is the

double integral (see Posch et al. 1997 for details):

$$(8.10) \quad I(u, v) = \iint \frac{2dudv}{(1+u^2+v^2)^2} \\ = \frac{v}{\sqrt{1+v^2}} \cdot \arctan \frac{u}{\sqrt{1+v^2}} \\ + \frac{u}{\sqrt{1+u^2}} \cdot \arctan \frac{v}{\sqrt{1+u^2}}$$

These two equations allow the calculation of the area of the EMEP grid cell (i, j) by setting $(x_1, y_1) = (i-1/2, j-1/2)$ and $(x_2, y_2) = (i+1/2, j+1/2)$.

The following FORTRAN functions compute the area of an EMEP grid cell for arbitrary grid indices (i, j) , for the EMEP50 or the EMEP150 grid, depending on the parameters in $par()$ (see above):

```

      real function aremep (par,i,j)
      !
      ! Returns the area (in km2) of an ax-parallel cell with
      ! centerpoint (i,j) in the EMEP grid defined by par().
      !
      ! par(1) ... size of grid cell (km)
      ! (par(2),par(3)) = (xp,yp) ... EMEP coordinates of the North Pole
      !
      integer(4)      i, j
      real(4)         par(*)
      !
      external        femep
      !
      data Rearth /6370./      ! radius of spherical Earth (km)
      data drm /1.8660254/    ! = 1+sin(pi/3) = 1+sqrt(3)/2
      !
      x1 = real(i)-0.5
      y1 = real(j)-0.5
      emi = par(1)/(Rearth*drm) ! = 1/M
      u1 = (x1-par(2))*emi
      v1 = (y1-par(3))*emi
      u2 = u1+emi
      v2 = v1+emi
      ar0 = 2.*Rearth*Rearth
      aremep = ar0*(femep(u2,v2)-femep(u1,v2)-femep(u2,v1)+femep(u1,v1))
      return
    end function aremep
      !
      real function femep (u,v)
      !
      ! Function used in computing the area of an EMEP grid cell.
      !
      real(4)         u, v
      !
      ui = 1./sqrt(1.+u*u)
      vi = 1./sqrt(1.+v*v)
      femep = v*vi*atan(u*vi)+u*ui*atan(v*ui)
      return
    end function femep

```


The area distortion ratio α , i.e. the ratio between the area of a small rectangle in the EMEP grid and its corresponding area on the globe, is obtained by the following limit operation:

$$(8.11) \quad \alpha = \lim_{h,k \rightarrow 0} \frac{A(x, y, x+h, y+k)}{h \cdot k \cdot d^2} = \frac{R^2}{d^2 \cdot M^2} \cdot \frac{4}{(1 + (r/M)^2)}$$

where R , M , d and r are defined in eqs. 8.1–8.5. Using eqs. 8.3 and 8.5 and the identities $1/(1+\tan^2 z) = \cos^2 z$ and $2\cos^2(\pi/4 - z/2) = 1 + \sin z$, one arrives at the following expression for the area distortion ratio:

$$(8.12) \quad \alpha = \left(\frac{1 + \sin \phi}{1 + \sin \phi_0} \right)^2$$

which shows that the distortion ratio depends on the latitude ϕ only, and (small) areas are undistorted, i.e. $\alpha=1$, only at $\phi=\phi_0=60^\circ$.

8.2 Percentiles and Protection Isolines

In this section we first define and investigate different methods for calculating percentiles of a cumulative distribution function (cdf) given by a finite number of values. Then we generalise the concept of a percentile to the case in which the cdf is defined by a set of functions (critical load functions), resulting in the so-called percentile function (protection isoline).

8.2.1 Cumulative distribution function

Let us assume we have critical load values for n ecosystems. We sort these values in ascending order, resulting in a sequence $x_1 \leq x_2 \leq \dots \leq x_n$. Each value is accompanied

by a weight (area) A_i ($i=1, \dots, n$), characterizing the size (importance) of the respective ecosystem. From these we compute normalized weights w_i according to

$$(8.13) \quad w_i = A_i / \sum_{j=1}^n A_j, \quad i = 1, \dots, n$$

resulting in:

$$(8.14) \quad \sum_{i=1}^n w_i = 1$$

The cumulative distribution function (cdf) of these n critical load values is then defined by

$$(8.15) \quad F(x) = \begin{cases} 0 & \text{for } x < x_1 \\ W_k & \text{for } x_k \leq x < x_{k+1} \\ 1 & \text{for } x \geq x_n \end{cases}$$

with

$$(8.16) \quad W_k = \sum_{i=1}^k w_i, \quad k = 1, \dots, n$$

$F(x)$ is the probability of a critical load being smaller than (or equal to) x , i.e. $1-F(x)$ is the fraction of ecosystems protected. With this definition $F(x)$ has the mathematical properties of a cdf: F is a monotonously increasing right-continuous function with $F(-\infty)=0$ and $F(\infty)=1$. In Figure 8.2 an example of a cdf is shown; note that the function assumes only a finite number of values.

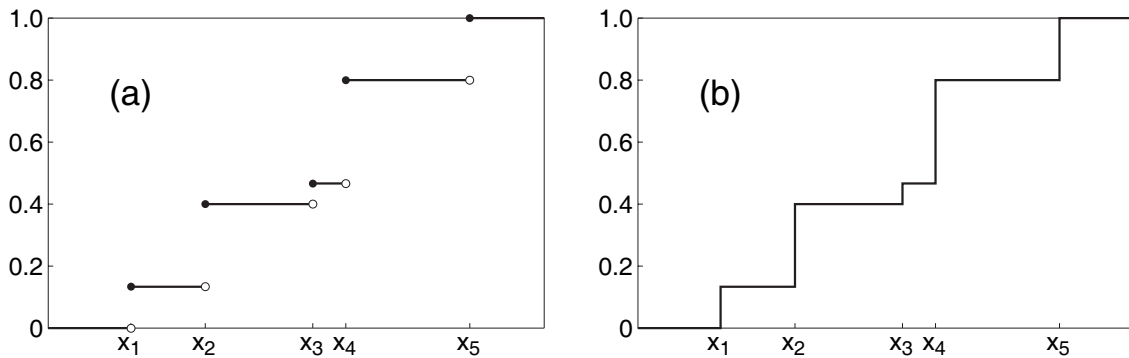


Figure 8.2: (a) Example of a cumulative distribution function for $n=5$ data points ($x_1 < x_2 < x_3 < x_4 < x_5$, with weights $w_1=2/15, w_2=4/15, w_3=5/15, w_4=1/15, w_5=3/15$). The filled (empty) circles indicate whether a point is part (not part) of the function. (b) The same cdf is drawn by connecting all points, the way a cdf is usually displayed.

8.2.2 Quantiles and percentiles

All ecosystems in a region (grid cell) are protected, if deposition stays below the smallest critical load values. However, to discard outliers and to account for uncertainties in the critical load calculations, but also to ensure that a sufficient percentage of ecosystems are protected, (low) percentiles of the cdf are compared to the deposition.

The q -th **quantile** ($0 \leq q \leq 1$) of a cdf F , denoted by x_q , is the value satisfying

$$(8.17) \quad F(x_q) = q$$

which means that x_q , viewed as a function of q , is the inverse of the cdf, i.e. $x_q = F^{-1}(q)$.

Percentiles are obtained by scaling quantiles to 100, i.e. the p -th percentile is the $(p/100)$ -th quantile. Other terms used are *median* for the 50-th percentile, lower and upper *quartile* for the 25-th and 75-th percentile, respectively. We suggest the term *pentile* for the 5-th percentile (from the Greek word *penta* for *five*). Note that the p -th percentile critical load protects $100-p$ percent of the ecosystems.

Computing quantiles, i.e. the inverse of a cdf given by a finite number of points poses a problem: due to the discrete nature of the cdf, a unique inverse simply does not exist. For many values of q no value x_q exists at all so that eq. 8.17 holds; and for the n values x_i such a value exists (i.e. $q = F(x_i)$), but the

resulting quantile is not unique – every value between x_i and x_{i+1} could be taken (see Figure 8.2). Therefore, the cdf is approximated (interpolated) by a function which allows solving eq. 8.17 for every q . There is neither a unique approximation, nor is there a single accepted way for calculating percentiles; e.g., Posch et al. (1993) discuss six methods for calculating percentiles. Note that commonly definitions are given for data with identical weights (i.e. $w_i = 1/n$), but the generalization to arbitrary weights is mostly straightforward. It should be also born in mind that the differences between different approximation methods vanish when the number of points becomes very large (and all weights small).

In the following we have a closer look at two types of quantile functions: (a) those derived from linearly interpolating the cdf, and (b) those using the empirical cdf. After defining their equations for arbitrary weights we discuss their advantages and disadvantages.

(a) Linear interpolation of the cdf:

In this case the quantile function is the inverse of the linearly interpolated cdf given by:

$$(8.18) \quad x_q = \begin{cases} x_1 & \text{for } q \leq w_1 = W_1 \\ x_k + (x_{k+1} - x_k) \cdot \frac{q - W_k}{W_{k+1}} & \text{for } W_k < q \leq W_{k+1} \\ & k = 1, \dots, n \end{cases}$$

where the W_k are defined in eq. 8.16. An example is shown in Figure 8.3a.

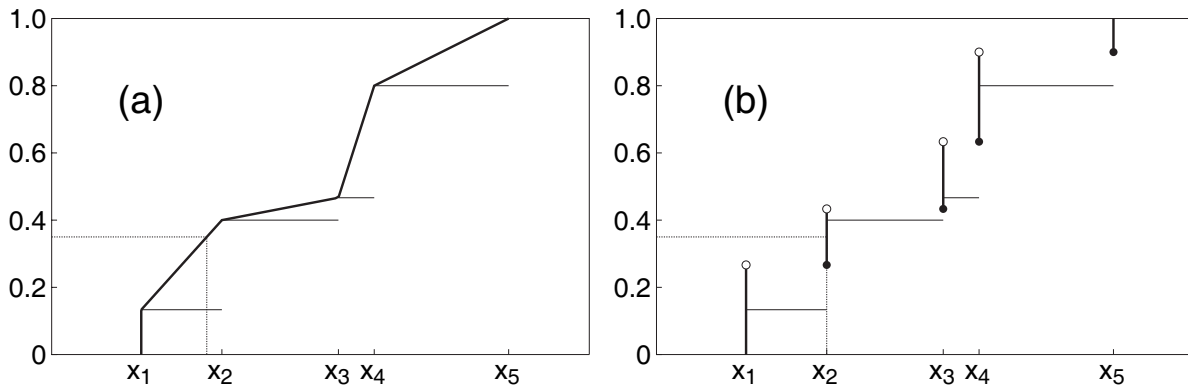


Figure 8.3: Examples of the two quantile functions discussed in the text. Values and weights are the same as in Figure 8.2. The filled (empty) circles indicate whether a point is part (not part) of the function. The thin horizontal lines indicate the cumulative distribution function. Note that for almost all values of q (e.g. $q=0.35$) the resulting quantile is smaller in (a) than in (b).

The advantage of this quantile function is that it is continuous, i.e. a small change in q leads to only a small change in the resulting quantile x_q . However, it has the following three disadvantages:

(i) In case of two (or more) identical data points the definition of the quantile function is not unique: for identical critical load values the shape of the interpolation

function depends on the order of the weights (see Figures 8.4a,a'). This could be resolved by sorting the weights of identical data points according to size (smallest first, as in Figures 8.4a.b). This minimizes the difference to the empirical distribution function (see below), but requires fairly complicated (and time-consuming) routines for the actual computations.

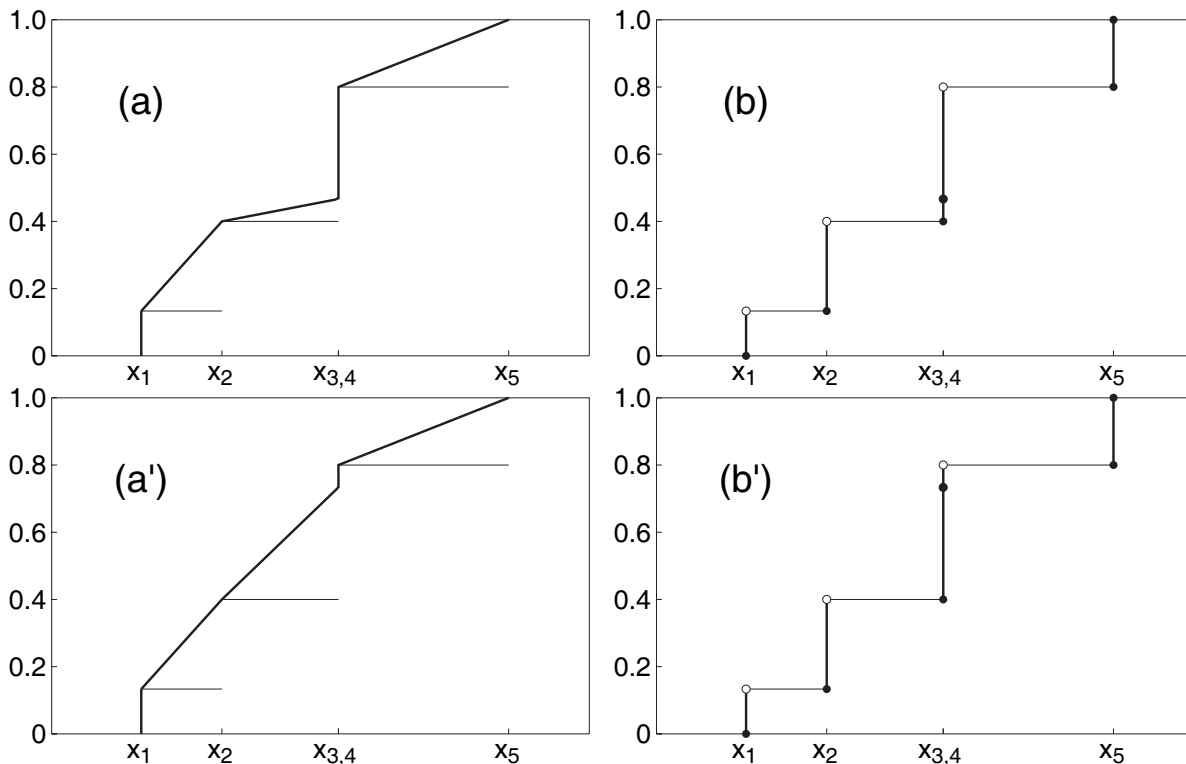


Figure 8.4: Examples of the two quantile functions discussed in the text. Values and weights are the same as in Figure 8.2, except that $x_3=x_4$ (compare Figure 8.3). Note, that for the linearly interpolated quantile function (a,a') its shape depends on the order of the weights for the identical values.

(ii) As mentioned above, a critical load x_q is selected to protect the $(1-q)$ -th fraction of the ecosystems within a given region (grid cell). However, for the linear interpolated quantile function certain choices of q result in x_q -values which are *below* the actual value needed to protect a fraction $1-q$ of the ecosystems (see example in Figure 8.3). This is fine for the ecosystems, but may lead to higher costs for abatement.

(iii) The computation of quantiles is not order-preserving when using linear interpolation. We say the order is preserved by a quantile function, if the following holds for two cdfs:

$$(8.19) \\ F_1(x) \leq F_2(x) \\ \text{for all } x \Rightarrow x_q^{(1)} \leq x_q^{(2)} \\ \text{for all } q$$

i.e. the smaller cdf leads to smaller quantiles. In Figure 8.5a an example is shown with two data sets for the same n ecosystems, x_1, \dots, x_n and y_1, \dots, y_n with common weights w_1, \dots, w_n and the property $x_i < y_i$ for $i=1, \dots, n$ (e.g. CL_{min} 's and CL_{max} 's). But for certain values of q it turns out that $x_q > y_q$ when computed by linear interpolation (Fig. 85.a).

(b) Empirical distribution function:
In this case the quantile function assumes only values defining the cdf:

$$(8.20) \\ x_q = \begin{cases} x_1 & \text{for } q < w_1 = W_1 \\ x_k & \text{for } W_{k-1} \leq q < W_k, k = 2, \dots, n-1 \\ x_n & \text{for } q \geq W_{n-1} \end{cases}$$

An example of this quantile function is shown in Figure 8.3b. The disadvantage of this quantile function is that it is not continuous, i.e. a very small change in q may lead to a significant change in the quantile x_q (jump from x_i to x_{i+1}).

However, none of the disadvantages of the linear interpolation holds for this function, but:

- (i) identical values do not lead to ambiguities (see Figures 8.4b,b'),
- (ii) the quantile x_q protects (at least) a fraction q of the ecosystems (see Figure 8.3b), and
- (iii) the computation of quantiles is order-preserving (see eq. 8.19 and Figure 8.5b).

It is especially property (iii) which makes the empirical distribution function the only viable choice for computing percentiles. The following FORTRAN subroutine computes the q -quantile of a given vector of data with a corresponding vector of weights. The data have to be sorted in ascending order, but the weights don't have to be normalised to one:

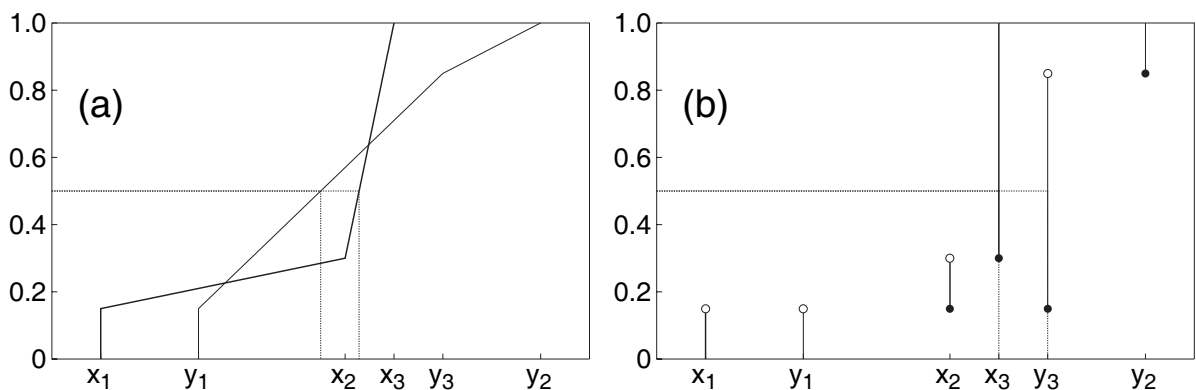


Figure 8.5: Example of two quantile functions for 3 values each (x_1, x_2, x_3 and y_1, y_2, y_3) and common weights w_1, w_2, w_3 and the property $x_i < y_i$ for $i=1,2,3$. However, in case (a) the median $x_{0.5}$ is greater than the median $y_{0.5}$.

```
subroutine qantilcw (q,num,vec,wei,xq)
!
! This subroutine computes the q-quantile xq of the num values in vec()
! - sorted in ascending order - with corresponding weights wei()
! from the empirical distribution function.
!
integer(4)      num
real(4)        q, vec(*), wei(*), xq
!
if (num == 0) stop 'Quantile of nothing?!'
if (q < 0. .or. q > 1.) stop 'q outside [0,1]!'
!
wsum = wei(1)
do k = 2,num
  wsum = wsum+wei(k)
  if (vec(k) < vec(k-1)) stop 'Data not sorted!'
end do
!
qw = q*wsum
sum = 0.
do k = 1,num
  sum = sum+wei(k)
  if (qw < sum) then
    xq = vec(k)
  end if
end do
xq = vec(num) ! if q=1
return
end subroutine qantilcw
```

8.2.3 Percentile functions and protection isolines

In this section we generalize of the concept of cumulative distribution function (cdf) and quantile (percentile) to the case when the data (e.g. critical loads) are given as a functions (rather than as single values), which is the case when considering two pollutants (e.g. sulphur and nitrogen in the case of acidification), leading to the so-called percentile function or (ecosystem) protection isoline.

In the following we assume that a (critical load) function is defined by a set of pairs of values (nodes) (x_j, y_j) , ($j=1, \dots, m$), and the function is given by connecting (x_1, y_1) with (x_2, y_2) etc., in this way generating a polygon in the x-y plane. We denote this polygon by:

$$(8.22) \quad f = [(x_1, y_1), \dots, (x_m, y_m)]$$

For the values x_j and y_j we assume that:

$$(8.23) \quad 0 = x_1 \leq x_2 \leq \dots \leq x_m$$

and

$$y_1 \geq y_2 \geq \dots \geq y_m = 0$$

i.e. the nodes on the polygon are numbered from left to right, starting on the y-axis and ending on the x-axis. Eq. 8.23 also ensures that the polygon is monotonically decreasing, when considered as a function of x or y . (Alternatively, the numbering could start on the x-axis, etc.). With the notation $(x, y) < f$ we mean that the point (x, y) lies below the polygon (i.e. critical loads are not exceeded).

Considering the critical load for S and N acidity the critical load function for an ecosystem is defined by 3 values, namely $CL_{min}(N)$, $CL_{max}(N)$ and $CL_{max}(S)$, and as a polygon with $m=3$ nodes it is written according to eq. 8.22 as:

(8.24)

$$CLF = \left[\left(0, CL_{max}(S) \right), \right. \\ \left. \left(CL_{min}(N), CL_{max}(S) \right), \right. \\ \left. \left(CL_{max}(N), 0 \right) \right]$$

where we assumed that the *N*-deposition is plotted along the x-axis and the *S*-deposition along the y-axis.

Now we assume that we have *n* critical load functions f_1, \dots, f_n with respective weights w_1, \dots, w_n ($\sum w_i = 1$). In general it will not be possible to sort these critical load functions, i.e. it is not possible to say that f_i is larger or smaller than f_j , because $CL_{max}(S)$ for f_i could be larger and $CL_{max}(N)$ smaller than the corresponding values for f_j (see Figure 8.6 for examples). Nevertheless, we can define a cumulative distribution function *F* in the following way:

(8.25)

$$F(x, y) = \sum_{(x,y) < f_i} w_i$$

meaning that for a given point (x,y) we sum all weights w_i for which $(x,y) < f_i$, i.e. for which there is no exceedance. Obviously $0 \leq F(x,y) \leq 1$, and *F* has also otherwise all properties of a (two-dimensional) cdf. A percentile *p* is now easily defined as the intersection of such a function with a

horizontal plane at height $q = p/100$. The result (projected onto the x-y plane) is a curve, more precisely a polygon which has the property defined in eq. 8.23. Let f_q be the quantile (percentile) function for a given *q*, then every point (x,y) , i.e. every pair of *N* and *S* deposition, with $(x,y) < f_q$ protects (at least) a fraction of $1-q$ of the ecosystems; and f_q is also called a (ecosystem) protection isoline. Note that protection isolines for the same set of polygons (critical load functions) do not intersect (although they might partly coincide), and for $r < s$ f_r lies below f_s .

Since an exact computation of a percentile function is hardly feasible (especially in case of a large number of critical load functions), we have to use an approximate method (see Figure 8.6): we draw rays through the origin of the x-y plane (i.e. lines with a constant *S*:*N* deposition ratio) and compute the intersections of these rays with all critical load functions (small circles in Figure 8.6a). For each ray the intersection points are sorted according to their distance from the origin and the chosen quantiles of these distances are calculated according to eq. 8.20. Finally, the resulting quantile values are connected to obtain the percentile functions (protection isolines). Obviously, the more rays are used in this procedure the more accurate are the protection isolines. As Figure 8.6b shows, a protection isoline need not be convex.

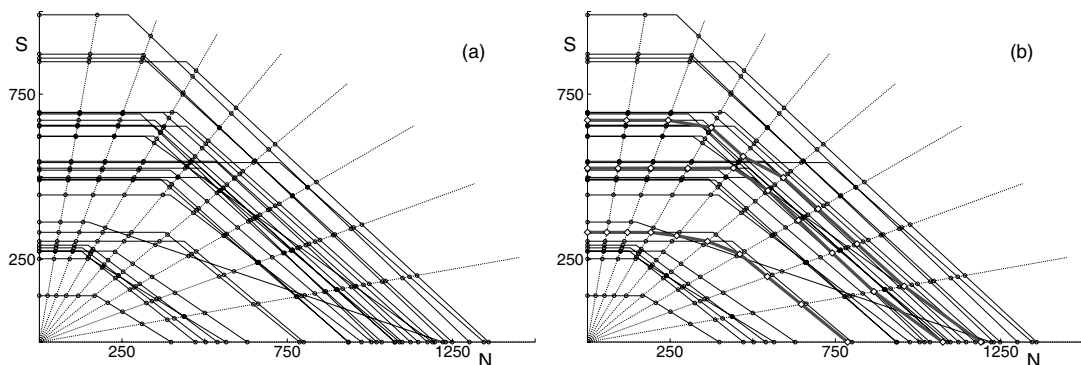


Figure 8.6: Computation of protection isolines: (a) set of critical load functions and intersection of these CL-functions with rays from the origin (small circles); (b) computing the percentiles ($q=0.25, 0.50$ and 0.75 in this case) along each ray (small diamonds) and connecting them to obtain the protection isolines (thick [red] lines).

8.3 The Average Accumulated Exceedance (AAE)

Above we showed how to summarise critical loads data with the help of cumulative distribution functions and protection isolines. Here we want to accomplish the same for exceedances computed for two pollutants, i.e. exceedances of critical load functions. Let $Ex_i(N_{dep}, S_{dep})$ be the exceedance for ecosystem i with area A_i as defined in Chapter 7, then we define the *accumulated exceedance* (AE) of n ecosystems on a region (grid cell) as:

(8.26)

$$AE(N_{dep}, S_{dep}) = \sum_{i=1}^n A_i Ex_i(N_{dep}, S_{dep})$$

For a given deposition, AE is total amount of acidity (in eq/yr) which is deposited in excess over the critical loads in the region in a given year. This function is thus strongly determined by the total ecosystem area in a grid cell. In order to minimise this dependence and to obtain a quantity which is directly comparable to depositions (in eq/ha/yr), we define the *average accumulated exceedance* (AAE) by dividing the AE function by the total ecosystem area:

(8.27)

$$AAE(N_{dep}, S_{dep}) = AE(N_{dep}, S_{dep}) / \sum_{i=1}^n A_i$$

Instead of the total ecosystem area, one could also think of dividing by another area, e.g. the area exceeded for a given (fixed) deposition scenario. However, re-calculating the AAE with new areas when depositions have changed can lead to inconsistencies: the new AAE could be larger, despite declining deposition – as can be shown with simple examples. In analogy to protection isolines, isolines of AAE can be calculated for a given region (grid cell).

8.4 Critical Load Exceedance and Gap Closure Methods

Except for the earliest protocols, integrated assessment modellers have used uniform *percentage* reductions of the excess deposition (so-called *gap closures*) to define emission reduction scenarios. In the following we summarize the different gap closure methods used and illustrate them for the case of a single pollutant. This section follows largely Posch et al. (2001).

In the 1994 Sulphur Protocol, only sulphur was considered as acidifying pollutant (N deposition was fixed; it determined, together with N uptake and immobilization, the sulphur fraction). Furthermore, taking into account the uncertainties in the CL calculations, it was decided to use the 5-th percentile of the critical load cdf in a grid cell as the only value representing the ecosystem sensitivity of that cell. And the exceedance was simply the difference between the (current) S deposition and that 5-th percentile critical load. This is illustrated in Figure 8.7a): Critical loads and deposition are plotted along the horizontal axis and the (relative) ecosystem area along the vertical axis. The thick solid and the thick broken lines are two examples of critical load cdfs (which have the same 5-th percentile critical load, indicated by 'CL'). 'D0' indicates the (present) deposition, which is higher than the CLs for 85% of the ecosystem area. The difference between 'D0' and 'CL' is the exceedance in that grid cell. It was decided to reduce the exceedance everywhere by a fixed percentage, i.e. to 'close the gap' between (present) deposition and (5-th percentile) critical load. In Figure 8.7a, a *deposition gap closure* of 60% is shown as an example. As can be seen, a fixed deposition gap closure can result in very different improvements in ecosystem protection percentages (55% vs. 22%), depending on the shape of the critical load cdf.

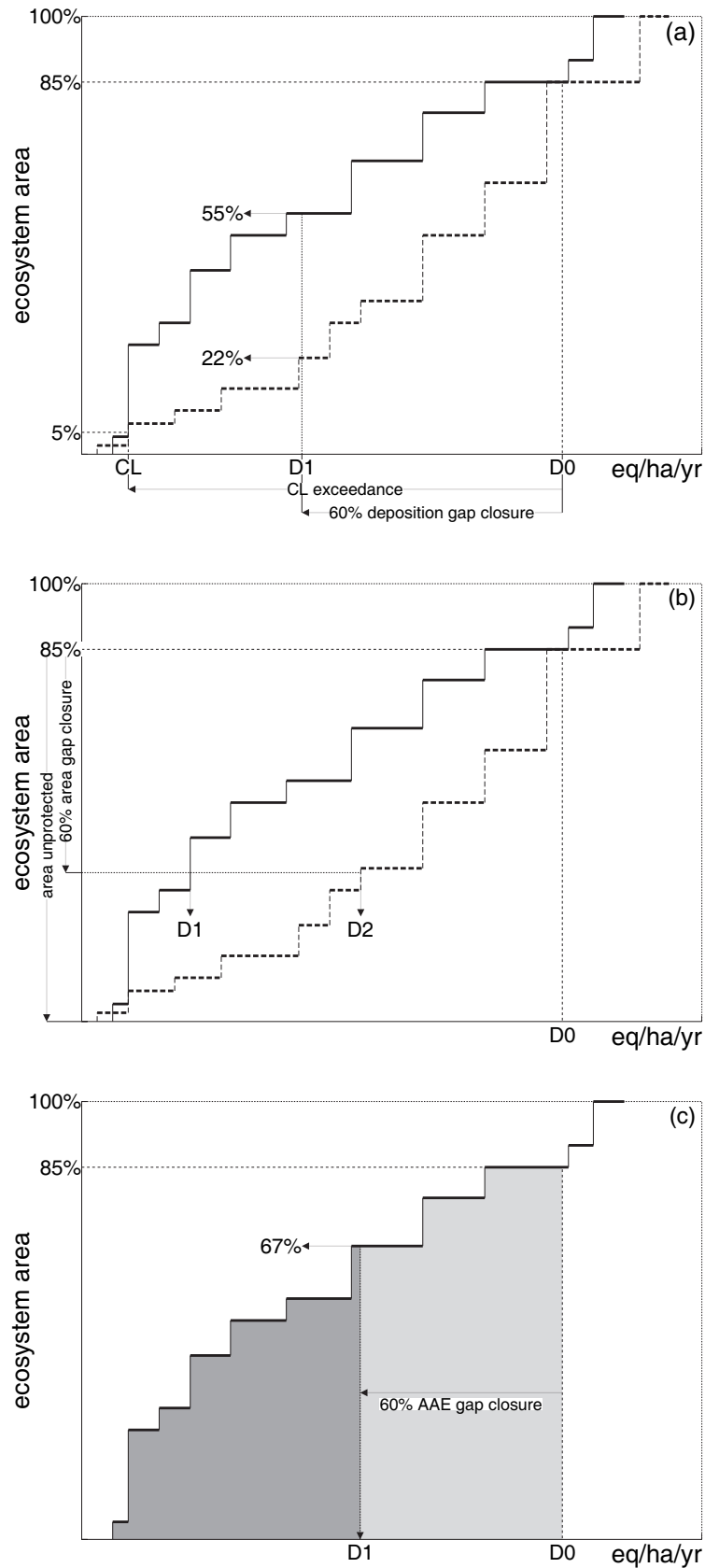


Figure 8.7: Cumulative distribution function (thick solid line) of critical loads and different methods of gap closure: (a) deposition gap closure, (b) ecosystem gap closure, and (c) accumulated exceedance (AE) gap closure. The thick dashed line in (a) and (b) depict another cdf, illustrating how different ecosystem protection follows from the same deposition gap closure (a), or how different deposition reductions are required to achieve the same protection level (b).

To take into account all critical loads within a grid cell (and not only the 5-th percentile), it was suggested to use an *ecosystem area gap closure* instead of the deposition gap closure. This is illustrated in Figure 8.7b: for a given deposition ' D_0 ' the ecosystem area unprotected, i.e. with deposition exceeding the critical loads can be read from the vertical axis. After agreeing to a certain (percent) reduction of the unprotected area (e.g. 60%), it is easy to compute for a given cdf the required deposition reduction (' D_1 ' and ' D_2 ' in Figure 8.7b). Another important reason to use the ecosystem area gap closure is that it can be easily generalized to two (or more) pollutants, which is not the case for a deposition-based exceedance. This generalization became necessary for the negotiations of the 1999 Gothenburg Protocol, as both N and S contribute to acidification. Critical load values have been replaced by critical load functions and percentiles replaced by ecosystem protection isolines (see above). However, the use of the area gap closure becomes problematic if only a few critical load values or functions are given for a grid cell. In such a case the cdf becomes highly discontinuous, and small changes in deposition may result in either no increase in the protected area at all or large jumps in the area protected.

To remedy the problem with the area gap closure caused by discontinuous cdfs, the accumulated exceedance (AE) concept has been introduced (see above). In the case of one pollutant, the AE is given as the area under the cdf of the critical loads (the entire grey-shaded area in Figure 8.7c). Deposition reductions are now negotiated in terms of an AE (or AAE) gap closure, also illustrated in Figure 8.7c: a 60% AE gap closure is achieved by a deposition ' D_1 ' which reduces the total grey area by 60%, resulting in the dark grey area; also the corresponding protection percentage (67%) can be easily derived. The greatest advantage of the AE and AAE is that it varies smoothly as deposition is varied, even for highly discontinuous cdfs, thus facilitating optimization calculations in integrated assessment. The advantages and disadvantages of the three gap closure methods described above are summarized in the following table.

	Advantages	Disadvantages
Deposition gap closure (used for the 1994 Sulphur Protocol)	<ul style="list-style-type: none"> • Easy to use even for discontinuous cdfs (e.g. grid cells with only one CL). 	<ul style="list-style-type: none"> • Takes only one CL value (e.g. 5th percentile) into account. • May result in no increase in protected area. • Difficult to define for two pollutants.
Ecosystem area gap closure (used for the EU Acidification Strategy)	<ul style="list-style-type: none"> • In line with the goals of CL use (maximum ecosystem protection). • Easy to apply to any number of pollutants. 	<ul style="list-style-type: none"> • Difficult (or even impossible) to define a gap closure for discontinuous cdfs (e.g. grid cells with only one CL).
Accumulated Exceedance (AE) gap closure (used for the 1999 Gothenburg Protocol)	<ul style="list-style-type: none"> • AE (and AAE) is a smooth and convex function of deposition even for discontinuous cdfs. 	<ul style="list-style-type: none"> • AE stretches the limits of the critical load definition.* • Exceedance definition not unique for two or more pollutants.

* It assumes a linear damage function. However, this feature could also be an advantage.

References

- Posch M, Kämäri J, Johansson M, Forsius M (1993) Displaying inter- and intra-regional variability of large-scale survey results. *Environmetrics* 4: 341-352.
- Posch M, De Smet PAM, Hettelingh J-P, Downing RJ (eds) (1995) Calculation and mapping of critical thresholds in Europe. Status Report 1995, Coordination Center for Effects, RIVM Report 259101004, Bilthoven, Netherlands, iv+198 pp. www.rivm.nl/cce
- Posch M, Hettelingh J-P, De Smet PAM, Downing RJ (eds) (1997) Calculation and mapping of critical thresholds in Europe. Status Report 1997, Coordination Center for Effects, RIVM Report 259101007, Bilthoven, Netherlands, iv+163 pp. www.rivm.nl/cce
- Posch M, De Smet PAM, Hettelingh J-P, Downing RJ (eds) (1999) Calculation and mapping of critical thresholds in Europe. Status Report 1999, Coordination Center for Effects, RIVM Report 259101009, Bilthoven, Netherlands, iv+165 pp. www.rivm.nl/cce
- Posch M, Hettelingh J-P, De Smet PAM (2001) Characterization of critical load exceedances in Europe. *Water, Air and Soil Pollution* 130: 1139-1144.
- Saltbones J, Dovland H (1986) Emissions of sulphur dioxide in Europe in 1980 and 1983. EMEP/CCC Report 1/86, Norwegian Institute for Air Research, Lillestrøm (now in Kjeller), Norway.